STUDIES

OF VIBRONIC EXCITON INTERACTIONS

BETWEEN PAIRS OF CHROMOPHORES

DANIEL FORNASIERO, Maître ès Sciences, AEA. (Grenoble)

Department of Physical and Inorganic Chemistry,

University of Adelaide.

Thesis presented for the degree of

Doctor of Philosophy

June, 1981

Summary

Vibronic exciton theory was applied to the circular dichroism spectra of two different dimeric systems: dinucleosides and dye-DNA complexes. The approach adopted necessitates an investigation into the electronic properties of the monomeric moieties of the dimer. Monomeric absorption and circular dichroism spectra were analysed in terms of their vibronic structures and were fitted to a progression involving a single harmonic vibrational mode.

A comparative study of adenosine and adenosine derivatives using absorption, circular dichroism and linear dichroism spectroscopy has revealed the composite nature of the near-ultraviolet X-band of adenosine. The parameters which characterize the spectrum of the two transitions present were obtained as was their respective polarization. A correlation between the relative circular dichroism intensities of the two transitions and the sugar-base torsion angle, ϕ_{CN}, of adenosine has been shown experimentally and confirmed by theory.

The temperature dependence of the absorption and circular dichroism of Adenylyl-(3'-5')-Adenosine and Deoxyadenylyl-(3'-5')-deoxyadenosine in aqueous solution was also studied. The experimental data were analysed in terms of a two-state equilibrium between one right-handed helical stacked conformation and one monomeric unstacked form. From these thermal denaturation data, apparent thermodynamic parameters, $\Delta H°$ and $\Delta S°$, were determined and found to be wavelength independent. In addition, the absorption and circular dichroism spectra of the stacked conformers were extrapolated and analysed using the vibronic exciton coupling

theory. From the results obtained, a geometrical model for deoxy- and ribodinucleoside has been proposed. The similarity in the values of the thermodynamic parameters and the exciton interaction parameters obtained using the two independent experimental techniques, on the one hand, and their agreements with recently published NMR results, on the other, leads to the conclusion that it is the same equilibrium which is monitored and emphasizes the reliability of the procedure used.

The interaction of DNA and Acridine Orange, Proflavine and 9-aminoacridine dyes, has been studied at several salt concentrations through the use of circular dichroism and absorption spectroscopy. The spectra were totally and satisfactorily interpreted in terms of only one electronic transition of the dye molecule, and by using a recent model of dye binding to DNA. It was shown that the experimental circular dichroism spectrum for any value of bound dye to DNA phosphate in the strong binding region, could be expressed in terms of a monomeric circular dichroism spectrum of intercalated and non-intercalated bound dyes and a dimeric circular dichroism spectrum arising from the vibronic exciton interactions between these dyes. Several important conclusions were drawn from the results obtained: The intercalation process is salt dependent, with the number of sites excluded next to an intercalated dye increasing with salt concentration; the dimerization process is little affected by the electrical environment in solution; the weak interaction found in the dimer is in agreement with the model used which postulated partial overlap between the two moieties in the dimer.

To the best of my knowledge and belief, this thesis contains no material previously published or written by another person, nor any material previously submitted for a degree or diploma at any university, except where due reference is made in the text.

D. Fornasiero

Acknowledgements

I wish to thank my supervisor, Dr. T. Kurucsev, for his encouragement and guidance; without his generous and unfailing support, this work would not have been possible.

I wish to express my gratitude to all those who have helped me and in particular Mr. G. Boehm, with whom I have had many interesting and fruitful discussions. I should also like to thank the typist for the typing of this thesis.

D. FORNASIERO

Department of Physical and
Inorganic Chemistry,
The University of Adelaide,
South Australia.

June, 1981.

Contents

CHAPTER I INTRODUCTION

1. CIRCULAR DICHROISM 1

1.1 Mechanism of Optical Activity 2

2. DEGENERATE COUPLED OSCILLATORS 4

2.1 Exciton Theory 4

2.2 Vibronic Exciton Theory 8

REFERENCES 14

CHAPTER II VIBRONIC EXCITON COUPLING IN DINUCLEOSIDES

3. INTRODUCTION 17

3.1 The Nucleic Acids and their Constituents 18

4. NUCLEOSIDES 20

4.1 Electronic Properties of Adenine 20

4.2 Analysis of the Optical Spectra 23

4.2.1 *Adenosine* 23

4.2.2 *Adenosine Derivatives* 24

4.2.3 *Polarisation of the Different Transitions* 27

4.3 Structure of the Nucleosides 28

4.3.1 *Configuration at the Asymmetric Carbon* 28

4.3.2 *Conformation of the Sugar Ring* 29

4.3.3 *Relative Orientation between Adenine Base and Ribose Group* 29

4.3.4 *Correlation between Torsion Angles and Circular Dichroism Spectra* 34

4.4 A Theoretical Approach 38

4.4.1 *A Simple Model* 38

4.4.2 *The Induced Moment in the Sugar* 39

	4.5	The Geometry of the Platinum-Adenosine Complex	41
	4.6	Guanosine	43
	4.7	Conclusion	46
5.	DINUCLEOSIDES		47
	5.1	Introduction	47
	5.2	Spectroscopic Methods and their Relation to Molecular Structure	47
	5.2.1	*Absorption Spectroscopy*	48
	5.2.2	*Circular Dichroism*	49
	5.2.3	*Nuclear Magnetic Resonance Spectroscopy*	50
	5.3	Conformational Model for Dinucleosides	50
	5.4	Conformational Dynamics	52
	5.4.1	*Choice of a Model*	52
	5.4.2	*The Two-State Model*	52
	5.4.3	*Its Theory*	53
	5.5	Analysis of the Temperature Dependent Spectra of APA	55
	5.5.1	*Effect of Temperature on the CD spectra of APA*	55
	5.5.2	*Effect of Temperature on the Absorption Spectra of APA*	57
	5.5.3	*Comparison with Previous Studies on APA*	58
	5.6	Analysis of the Temperature Dependent Spectra of dApdA	63
	5.6.1	*Effect of Temperature on the CD Spectra of dApdA*	63
	5.6.2	*Effect of Temperature on the Absorption Spectra of dApdA*	64
	5.6.3	*Comparison with Previous Studies on dApdA*	67

5.7 Differences between Deoxy- and Ribodinucleoside Phosphates 68

5.7.1 *Thermodynamic Differences* 68

5.7.2 *Conformational Differences* 68

5.8 The Two-State Model Opposed to a Multi-State Model 70

5.9 GPG Dinucleoside 72

5.10 Conclusion 75

REFERENCES 76

CHAPTER III INTERACTION BETWEEN DYES AND DNA

6. INTRODUCTION 87

6.1 Modes of Binding of Dyes to DNA 87

6.2 Heterogeneity of the Binding Sites 91

6.3 Spectroscopic Methods for the Study of the Dye-DNA Interaction 92

6.3.1 *Absorption Spectroscopy* 92

6.3.2 *Circular Dichroism* 96

7. THE ACRIDINE ORANGE AND PROFLAVINE-DNA COMPLEXES 99

7.1 The Electronic Properties of the AO and PF Dyes 99

7.2 The Armstrong, Kurucsev and Strauss Binding Model 101

7.3 The Circular Dichroism of the Acridine Orange-DNA Complex 106

7.4 The Circular Dichroism of the Proflavine-DNA Complex 111

7.5 Interpretation of the Results Obtained from the Binding Study 113

7.5.1 *Justification of the Method Used* 113

7.5.2 *The Intercalation Process* 117

7.5.3 *The Dimerization Process* 118

7.5.4 *The Geometry of the Dimeric Dye Bound to DNA* 119

7.5.5 *The Induced Circular Dichroism of the Intercalated Dye* 121

7.6 Conclusion 123

8. THE 9-AMINOACRIDINE-DNA COMPLEX 125

8.1 The Electronic Properties of the 9-aminoacridine Dye 125

8.2 The Binding of 9-AA to DNA seen through the Absorption Spectra 127

8.3 Results Obtained from the Analysis of the Circular Dichroism Spectra 129

8.4 Interpretation of the Results 130

9. CONCLUSION 134

APPENDICES

A. MATERIALS AND METHODS 145

A-1 Nucleosides and Dinucleosides 145

A-2 Dye-DNA Complexes 145

A-3 Preparation of Films 148

A-4 Temperature Studies 149

B. OPTICAL MEASUREMENTS 151

B-1 Linear Dichroism 151

B-2 Circular Dichroism 151

B-3 Ultra-Violet and Visible Absorption 153

C. COMPUTATIONAL METHODS 154

D. DERIVATION OF THE EXPRESSIONS OF THE DIPOLE STRENGTH AND THE ROTATIONAL STRENGTH 156

E. CALCULATION OF THE "GEOMETRIC-FACTOR" OF THE CD SPECTRUM OF ADENOSINE WITH THE USE OF THE COUPLED OSCILLATOR THEORY 159

F. ABBREVIATIONS 161

REFERENCES 162

CHAPTER I

Introduction

1. CIRCULAR DICHROISM

The phenomenon of optical activity has been known since the beginning of the 19th century but it is only in the last three decades that its potential use as a probe for molecular structure has been realised. The interest in optical activity has been only brought about by a better understanding of the phenomenon and also by dramatic advances in instrumentation. The widely used spectroscopic technique associated with the phenomenon of optical activity is circular dichroism (CD). Circular dichroism is defined as the difference in absorption between the left and the right circularly polarised light by a dissymmetric medium or molecule. From this, it follows that circular dichroism and ordinary absorption have much in common and are both associated with the same electronic transition or rearrangement of electronic charges in the molecule. In a molecule the redistribution of charges is, to a first approximation, localised within a particular functional group, the so-called chromophore. The rest of the molecule will have only a secondary effect on the electronic transition considered but, it is its dissymmetric character that will be reflected in circular dichroism. Just as ordinary absorption can be represented by the dipole strength, so circular dichroism can be represented by the rotational strength which is a measure of the area of the circular dichroism band. From quantum-mechanics, the rotational strength is also defined by

$$\mathcal{R} = \mathrm{Im}(\vec{\mu}.\vec{m}) \qquad (1.1)$$

where Im refers to the imaginary part of a complex quantity; $\vec{\mu}$ and $\vec{m}$ are, respectively, the electric and the magnetic

transition dipole moment.

The principal applications of circular dichroism have been in the domains of structure determination, analytical discrimination, in the detection of weak and hidden transition bands and finally in stereochemistry. However its high sensitivity to conformation has been mostly emphasized in biological systems where, in general, the complexity and the size of the molecules prevent a simple analysis by any other method.

The main intention of this thesis is to show that circular dichroism provides an essential tool in determining the molecular geometry of molecules on the condition that appropriate model and analysis methods are used.

1.1 Mechanism of Optical Activity

Although a lot of progress has been acquired during the last 20 years, the ab-initio calculations of optical activity are still not fully appropriate and any correlation between the sign of the circular dichroism spectrum and the conformation must be based on experimental data. Attempts were made to rationalise the amount of information available and this is why numerous empirical models or rules[1-14] were proposed to explain the many phenomena observed.

The dissymmetric molecule is composed of two independent groups which do not exchange electrons but interact through the Coulombic field existing between their respective charge distributions. The first group is the symmetric chromophore which absorbs energy and the second one consists of a dissymmetric molecular environment of substituents. From the developments of the theory of

optical activity, two simple limiting mechanisms of optical activity emerge.

In the first mechanism, the substituents perturb the chromophore, in other words the Coulombic field produced by the dissymmetric charge distribution of the substituents mixes the electric and magnetic transition dipole moments of the chromophore. This is the so-called one-electron theory or static coupling theory[3,8,10]. Included in this mechanism is the extensively used Octant rule which has provided important stereochemical information[20]. The coupled electric and magnetic transition dipole moments have a rotational strength of equal magnitude but different sign. The absorption and circular dichroism spectrum envelopes are similar.

In the second mechanism, called the dynamic coupling theory[4], the chromophore perturbs the substituents. The charge distribution of the chromophore transition dipole moment induces an electric dipole in the substituent group through the Coulomb potential existing between these two groups. The dynamic coupling theory can be sub-divided into two cases according to whether the considered transition in the chromophore is magnetic-dipole allowed as in the μ-m mechanism[11,16] or electric-dipole allowed as in the coupled oscillator theory[4]. The resulting circular dichroism spectrum for each transition will behave similarly to that observed in the one-electron mechanism. In this thesis, we will be mainly concerned with the coupled-oscillator mechanism and, in particular, its extension to the degenerate coupled-oscillator or exciton theory[17-19] in which the substituent group has become a light-absorbing group identical to the chromophore. It follows that the excited states of the whole molecule are degenerate.

2. DEGENERATE COUPLED OSCILLATORS

2.1 Exciton theory

The exciton concept was introduced by Frenkel[21] in 1931. Although the idea was first applied to molecular crystals, the exciton phenomenon has extended its range of application to a wide variety of problems[22-26] and, in particular has given promising results in the biological field[27-29]. Exciton has been associated with energy transfer in wave packets of excitation[21]. There is a rapid transfer of energy (10^{13} to 10^{15} sec^{-1})[27] by a radiationless process between the donor and the acceptor molecules during the excitation lifetime of the donor before the emission of a photon takes place. Long range interactions of up to 60Å has been shown to occur[24]. The nature of exciton interactions will be analysed through the study of dimeric aggregates.

The dimer model consists of two identical molecules A and B which are in a fixed spatial arrangement. There exists a symmetry operation which exchanges molecules A and B. The molecules are assumed to interact through a purely electronic mechanism.

If the coupling between the two molecules is weak, the total dimeric Hamiltonian can be separated as follows:

$$H = H^A + H^B + V^{AB} \qquad (2.1)$$

H^A and H^B represent the monomeric Hamiltonians and V^{AB} represents the interactions between the two moieties of the dimer. The ground state wave function, Ψ_o, for the dimer is written as $\Psi_o = \psi_N^A \psi_N^B$, whereas the excited state is degenerate because it can result on excitation within molecule A or within molecule B

$$\psi_a = \psi_M^A \psi_N^B \quad ; \quad \psi_b = \psi_N^A \psi_M^B \qquad (2.2)$$

The functions ψ^A and ψ^B refer to monomeric wave functions. The subscripts N and M stand for ground state and excited state respectively. The total wave function Ψ_M can be constructed as a linear combination of the unperturbed excited state functions ψ_a and ψ_b

$$\Psi_M^{\pm} = C^{\pm}(\psi_a \pm \psi_b) \tag{2.3}$$

where $C^{\pm}$ are normalizing factors. The secular determinant for the dimer is written as

$$\begin{vmatrix} H^{AA} - H^{00} - E & H^{AB} \\ H^{AB} & H^{BB} - H^{00} - E \end{vmatrix} = 0 \tag{2.4}$$

It follows that

$$\begin{aligned} H^{AA} &= (\psi_M^A\psi_N^B|H^A + H^B + V^{AB}|\psi_M^A\psi_N^B) \\ &= (\psi_M^A|H^A|\psi_M^A) + (\psi_N^B|H^B|\psi_N^B) + (\psi_M^A\psi_N^B|V^{AB}|\psi_M^A\psi_N^B) \end{aligned} \tag{2.5}$$

In equation (2.5) the first term $(\psi_M^A|H^A|\psi_M^A) = E_M^A$ represents the excited energy of the transition $\psi_M^A \leftarrow \psi_N^A$ of molecule A; the term $(\psi_N^B|H^B|\psi_N^B) = E_N^B$ represents the ground state energy of molecule B; the last term is the Coulombic interaction V_c between molecule A in the excited state and molecule B in the ground state. Following the usual procedure, the determinant in equation (2.4) is reduced to

$$\begin{vmatrix} \Delta E - V_c - E & V_{AB} \\ V_{AB} & \Delta E - V_c - E \end{vmatrix} = 0 \tag{2.6}$$

where $V_{AB} = (\psi_M^A\psi_N^B|H^{AB}|\psi_N^A\psi_M^B)$ (2.7)

represents the interchange of energy between the molecules A and B, the so-called resonance or exciton coupling energy; $\Delta E = E_M^A - E_N^A$ represents the energy of the transition $\psi_M^A \leftarrow \psi_N^A$.

From the above determinant we found the eigenvalues of the system

$$E^{\pm} = \Delta E - V_c \pm V_{AB} \tag{2.8}$$

The corresponding eigenfunctions for E^+ and E^- are:

$$\Psi_M^{\pm} = 2^{-1/2}(\psi_a \pm \psi_b) \tag{2.9}$$

The electric transition dipole moment for a transition $\Psi_M^{\pm} \leftarrow \Psi_o$ is given by

$$\vec{\mu}_M^{\pm} = (\Psi_M^{\pm}|\vec{\mu}|\Psi_o) \tag{2.10}$$

where $\vec{\mu}$ is the electric dipole operator. For the dimer considered, it takes the form

$$\vec{\mu}_M^{\pm} = e^{-1/2}(\vec{\mu}_A \pm \vec{\mu}_B) \tag{2.11}$$

The dipole strengths $\mathcal{D}^{\pm}$ characterize the absorption spectrum and are defined as

$$\mathcal{D}^{\pm} = |\vec{\mu}_M^{\pm}|^2 = \mu^2[1 \pm \sin\theta_B \cos(\phi_A - \phi_B)] \tag{2.12}$$

where θ, ϕ give the orientation of $\vec{\mu}$ in a spherical coordinate system. The axes of the right handed coordinate system are chosen so that $\vec{\mu}_A$ is in the x y plane and the distance vector separating the two coupled group A and B, defined by $\vec{R}_{AB} = \vec{R}_B - \vec{R}_A$, is along the x axis ($R = |\vec{R}_{AB}|$). The rotational strength $\mathcal{R}^{\pm}$ for a transition $\Psi_M^{\pm} \leftarrow \Psi_o$ is

$$\mathcal{R}^{\pm} = \mathrm{Im}(\vec{\mu}_M^{\pm} . \vec{m}_M^{\pm}) \tag{2.13}$$

$\vec{\mu}_M^{\pm}$ and $\vec{m}_M^{\pm}$ are the electric and the magnetic transition dipole moment respectively, and are defined as[4]

$$\vec{\mu}_M^{\pm} = (\Psi_o|\vec{\mu}|\Psi_M^{\pm}) \quad ; \quad \vec{m}_M^{\pm} = (\Psi_M^{\pm}|\vec{m}|\Psi_o) \tag{2.14}$$

The magnetic dipole operator[11,30,31] is given by

$$\vec{m} = \frac{e}{eMc}\{(\vec{R}_A \times \vec{p}_A) + \vec{m}_A + (\vec{R}_B \times \vec{p}_B) + \vec{m}_B\} \tag{2.15}$$

where $\vec{m}_A$ and $\vec{m}_B$ are intrinsic magnetic dipole operators

relative to their respective monomer center of gravity, $\vec{p}_A$ and $\vec{p}_B$ are momentum operators and $\vec{R}_A$ and $\vec{R}_B$ are the distance vectors from an arbitrary origin to the center of gravity of group A and B respectively. In the case of strong transitions and of optically inactive monomers, the intrinsic magnetic dipole operators can be neglected [11,30,31]. With the use of the formula $\vec{p}_A = (-2\pi i\frac{Mc}{e})\tilde{\nu}_o\vec{\mu}_A$, where $\tilde{\nu}_o$ is the frequency of transition in cm^{-1}, the magnetic transition dipole moment becomes

$$\vec{m}_M^{\pm} = 2^{-2/3} i\pi\tilde{\nu}_o \{(\vec{R}_{AB} \times \vec{\mu}_A) \mp (\vec{R}_{AB} \times \vec{\mu}_B)\} \qquad (2.16)$$

Using equations (2.11), (2.13), (2.15) and the fact that $(\Psi_o|\vec{\mu}|\Psi_M^{\pm}) = -(\Psi_M^{\pm}|\vec{\mu}|\Psi_o)$ the rotational strengths are given by

$$\mathcal{R}^{\pm} = \pm 2^{-1}\pi\tilde{\nu}_o(\vec{\mu}_A.\vec{R}_{AB} \times \vec{\mu}_B) = \pm 2^{-1}\pi\tilde{\nu}_o R\mu^2 \sin\phi_A\cos\theta_B \qquad (2.17)$$

It can be shown that the conservation laws for both dipole strength and rotational strength hold;

$$\mathcal{D}^+ + \mathcal{D}^- = 2\mu^2 \quad \text{and} \quad \mathcal{R}^+ + \mathcal{R}^- = 0 \qquad (2.18)$$

The spectrum of the dimer consists of two absorption bands, of energies E^+ and E^-, separated by the exciton coupling energy, V_{AB}. This last term can be calculated using the point-dipole formula

$$V_{AB} = \frac{1}{R^3}\left[\vec{\mu}_A\vec{\mu}_B - \frac{3(\vec{R}_{AB}.\vec{\mu}_A)(\vec{R}_{AB}.\vec{\mu}_B)}{R^2}\right]$$

$$V_{AB} = \frac{\mu^2}{R^3}[\sin\theta_2\cos(\phi_1-\phi_2) - 3\sin\theta_1\sin\theta_2\cos\theta_1\cos\theta_2] \qquad (2.19)$$

Although the point-dipole approximation can lead to errors in the absolute magnitude of V_{AB}, if the molecules A and B are in close proximity to each other, it will give nevertheless the sense of splitting. Figure 2.1 presents the optical properties for a given orientation of the monomeric transition moments in a dimer. At the top of figure 2.1, is represented

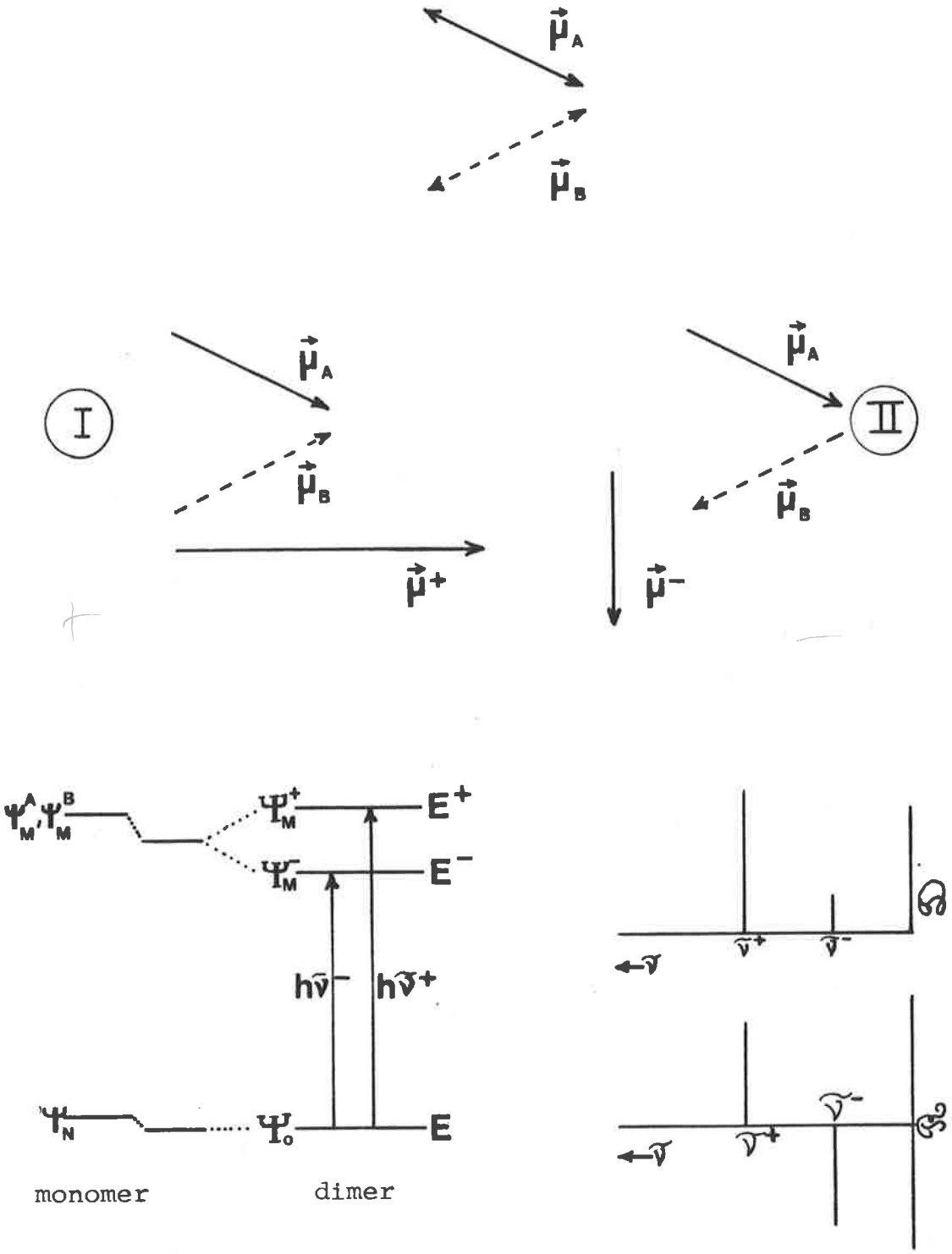

FIG.2.1 SCHEMATIC REPRESENTATION OF COUPLED OSCILLATORS. Top, orientation of the transition moments; center, the two possible combinations of the transition moments; bottom left, energy levels of the monomer and the dimer;bottom right, dipole and rotational strengths of the dimer. (see text).

Broken arrows rear and full arrows in front

the relative orientation of the electric transition dipole moments of the two molecules A and B. In the center are represented the two possible combinations of the monomeric transition moments (in-phase combination in I and out-of-phase combination in II) as well as the total electric transition dipole moments. We can see that $\vec{\mu}^{+}$ and $\vec{\mu}^{-}$ are polarised perpendicularly to each other. At the bottom left of figure 2.1 is to be found the schematic energy level diagram which shows the relative energy positions of the three wave functions, ψ_N, ψ_M^A and ψ_M^B, before exciton coupling, and the energy positions of the final wave functions, Ψ_o, Ψ_M^+ and Ψ_M^-, after exciton coupling. The dipole-dipole interaction is repulsive in I and attractive in II. Thus, the energy of the combination I is higher than that of combination II; accordingly, E^+ is higher than E^- ($\tilde{\nu}^+ > \tilde{\nu}^-$). At the bottom right of figure 2.1, the absorption frequencies, dipole strengths and rotational strengths are represented. The sign of the CD bands can be easily determined by looking at the torsion angle between the two monomeric transition moment arrows.[11] If we consider the total transition moment $\vec{\mu}^{\pm}$ as the axis of a cylinder and the two momomeric transition moments $\vec{\mu}_A$ and $\vec{\mu}_B$ as tangents to this cylinder, for the in-phase combination (I) $\vec{\mu}_A$ and $\vec{\mu}_B$ appear to wind around one another in a right handed sense, therefore the corresponding CD is positive. For the out-of-phase combination (II), the corresponding CD is negative.

2.2 Vibronic exciton theory

The exciton theory has been developed[32] almost exclusively in the fixed nuclei approximation (Born-Oppenheimer approximation[33]), in which the change in the position of the

nuclei during electronic excitation may be neglected. Although the exciton theory gives a rather good representation of the phenomenon occurring in the case of polymers[34,35] and indeed dimers[36-42], in particular when the transitions considered are strongly allowed, there have been several observations[43-46] that cannot be explained by this simple theory, even qualitatively, but require the inclusion of the vibrational motions. We can add, that, because most electronic band envelopes show a vibrational structure, molecular vibrations have to be taken into account in order to make a quantitative and detailed application of the exciton theory. Two limiting behaviour for the spectrum of a dimer have been found[47]. In the first one, the exciton coupling energy, V_{AB} is strong and much larger than the vibrational energy[48]. The shape of the vibronic levels is determined by electronic considerations. In the strong limit, the dimeric spectrum obeys the Born-Oppenheimer approximation[47,49]. In the second limit, the weak coupling, V_{AB} is small in comparison with the vibrational energy and the spectral changes are confined to vibrational details. Between these two limits the intermediate coupling, which covers the majority of cases, corresponds to the break down of the Born-Oppenheimer separability of the electronic and vibrational wave functions. The individual vibronic levels of the interacting molecules perturb one another; it follows that the general envelope pattern of the optical spectrum is rather confused[27].

However the inclusion of molecular vibrations in the exciton theory is not straightforward[50]. This explains the widespread interest for the development of the vibronic exciton theory around 1960.[38,43,48,49,51-54] Although more recent attempts have been made to improve the model[55-60],

the strength of the theory developed by Fulton and Gouterman[53,54] lies in its simplicity, completeness and practical application. This theory will be used in this thesis for the calculation of dimeric spectra. The theory refers to vibronic coupling, that is, the interactions between the vibrational and electronic motions in molecules. In addition to the assumptions previously made for our dimer model, it is assumed that each moiety behaves as an harmonic oscillator with only one fundamental vibrational mode Q; the relative motion of their centers of gravity is confined to a single degree of freedom, the variable distance between them. A further simplification needs to be made in order to successfully complete the mathematical development of the vibronic coupling theory: this is the crude adiabatic approximation in which the nuclear coordinates have been fixed at an equilibrium position Q_o. Therefore the electronic wave functions will depend solely on the electronic coordinates[50]. It follows that for non-interacting molecules, the vibrational wave functions are determined by the following vibrational Hamiltonians[53,54]

$$H^0 = (2M)^{-1}(P)^2 + \tfrac{1}{2}k(Q)^2 \qquad \text{in the ground state,}$$

$$\text{and } H' = (2M)^{-1}(P)^2 + \tfrac{1}{2}k(Q)^2 + lQ \text{ in the excited state.} \quad (2.20)$$

P and M are the momentum and effective mass of the nuclei respectively and k is the force constant for the vibrational mode Q. The only effect which electronic excitation has on the molecular vibration is that it produces a displacement of the equilibrium position, l, between the ground and excited states of the oscillator considered. When the two molecules interact, an exciton coupling energy, V_{AB} (see eqn. 2.7) is introduced into the Hamiltonians (2.20). Fulton and

Gouterman have shown that the following reduced Hamiltonians represent the solution to the vibronic problem[54].

$$h' = \tfrac{1}{2}[(p^+)^2 + (q^+)^2] + \lambda q^+$$
$$h^\pm = \tfrac{1}{2}[(p^-)^2 + (q^-)^2] + \lambda q^- \pm \varepsilon G \qquad (2.21)$$

where G is the symmetry operator between molecules A and B. The set of coordinates p^+, q^+ and p^-, q^- are associated with symmetric and antisymmetric (or in-phase and out-of-phase) modes of vibration[54]. ε which represents the energy separation between coupled states and λ which represents the nuclear displacement are dimensionless variables and are defined as[54]

$$\varepsilon = (\hbar w)^{-1} V_{AB} \quad \text{and} \quad \lambda = (2M\hbar w^3)^{-\frac{1}{2}} l \qquad (2.22)$$

The perturbation method[49,53] has shown that the eigenvalue equations associated with h' and $h^\pm$ depend on three limiting cases; the strong ($\varepsilon >> \lambda$), the intermediate ($\varepsilon \sim \lambda$) and the weak coupling ($\varepsilon << \lambda$). However, in this thesis, the more quantitative theory development of Fulton and Gouterman[54] or Merrifield[52] will be followed. It was found that the electric transition dipole moment for a transition $\Psi_{\mu\nu}^{\pm} \leftarrow \Psi_{oo}$ is

$$\vec{\mu}_{\mu\nu}^{\pm} = 2^{-\frac{1}{2}} b_{\mu o} c_{\nu o}^{\pm} (\vec{\mu}_A \pm \vec{\mu}_B) \qquad (2.23)$$

while the electric dipole strength is

$$\mathcal{D}_{\mu\nu}^{\pm} = |\vec{\mu}_{\mu\nu}^{\pm}|^2 = 2^{-1} |b_{\mu o} c_{\nu o}^{\pm}|^2 (\vec{\mu}_A \pm \vec{\mu}_B)^2 \qquad (2.24)$$

The μ and ν subscripts stand for symmetric and antisymmetric combinations of the vibration mode in the electronic excited state. $b_{\mu o}$ and $c_{\nu o}^{\pm}$ are vibrational wave function overlaps. Furthermore, the energy levels in the excited state, which correspond to $\Psi_{\mu\nu}^{+}$ and $\Psi_{\mu\nu}^{-}$, are separated by 2ε, regardless of λ[54].

Weigang[61], using the coupled oscillator model, extends the vibronic exciton theory to the calculation of the

circular dichroism spectrum of a dimer. The expression for the rotational strength is

$$\mathcal{R}_{\mu\nu}^{\pm} = \pm 2^{-1}\tilde{\nu}_o \pi |b_{\mu o} c_{\nu o}^{\pm}|^2 (\vec{\mu}_A . \vec{R}_{AB} \times \vec{\mu}_B) \qquad (2.25)$$

where all quantities have been defined in paragraph 2.1. From the expressions which defined the dipole (2.24) and the rotational strength (2.25) we can see that, although the same factor $|b_{\mu o} c_{\nu o}^{\pm}|^2$ governs the shape of the (+) and (-) components in both the absorption and the circular dichroism spectra, significant differences in the overall shape of these two kinds of spectrum can be found, due to the additive character of the (+) and (-) bands in absorption and their subtractive character in circular dichroism.

Theoretical absorption and CD spectra were calculated by means of the computer program EXCITON (appendix C). Gaussian bandshapes of the form shown in equation (C1) were superposed on each computed line spectra. The parameter λ was kept constant, as in[62]

$$\lambda = \sqrt{X}$$

where X is the ratio of the (1,0) to the (0,0) band intensities in the monomeric spectrum. For absorption, the exciton coupling parameter, ε, and the angle between the two moieties of the dimer were varied until the theoretical spectrum coincided with the experimental one. For circular dichroism, only ε was a variable parameter, while the angle between the two moieties was set to 90° in order to satisfy equation 2.18. We should point out that for the (+) component, the effect of increasing the value of ε does not result in a shift of a band of constant structure, as is frequently suggested, but rather a redistribution of intensity from lower to higher energy vibronic bands. For the (-) component, as ε increases, the

distribution of intensity remains practically constant and similar to that of the monomeric spectrum.

REFERENCES

1. H. Bethe, *Ann. Phys.*, 5, 133 (1929).
2. W. Kuhn and K. Bein, *Z. Phys. Chem.*, 24, 335 (1934).
3. E.U. Condon, W. Altar and H. Eyring, *J. Chem. Phys.*, 5, 753 (1937).
4. J.G. Kirkwood, *J. Chem. Phys.*, 5, 479 (1937).
5. W. Moffit, *J. Chem. Phys.*, 25, 1189 (1956).
6. W. Moffit and A. Moscowitz, *J. Chem. Phys.*, 30, 648 (1959).
7. A. Moscowitz, *Tetrahedron*, 13, 48 (1961).
8. W. Moffit, R.B. Woodward, A. Moscowitz, W. Klyne and C. Djerassi, *J. Am. Chem. Soc.*, 83, 4013 (1961).
9. G. Snatzke, *Tetrahedron*, 21, 413, 421, 439 (1965).
10. J.A. Schellman, *J. Chem. Phys.*, 44, 55 (1966).
11. J.A. Schellman, *Acc. Chem. Res.*, 1, 144 (1968).
12. E.G. Höhn and O.E. Weigang, Jr., *J. Chem. Phys.*, 48, 1127 (1968).
13. P.E. Schipper, *Mol. Phys.*, 29, 1705 (1975).
14. G. Snatzke, *Angew. Chem.*, 18, 363 (1979).
15. S.F. Mason, *Quart. Rev. Chem. Soc.*, 17, 20 (1963).
16. R.W. Woody and I. Tinoco, Jr., *J. Chem. Phys.*, 46, 4927 (1967).
17. A.S. Davydov, *Theory of Molecular Exciton*, McGraw-Hill, New York (1962).
18. W. Moffit, *J. Chem. Phys.*, 25, 467 (1956).
19. W. Moffit, *Proc. Nat. Acad. Sci. U.S.*, 42, 736 (1956).
20. P. Grabbé, *ORD and CD in Chemistry and Biochemistry*, Academic Press, New York, London (1972).
21. J. Frenkel, *Phys. Rev.*, 37, 17, 1276 (1931).
22. A. Cant, Honours Reports, University of Adelaide (1973).
23. D.L. Dexter and R.S. Knox, *Excitons*, John Wiley and Sons (1965).

24. J.B. Birks, *Photophysics of Aromatic Molecules*, John Wiley and Sons, chapter 11 (1970).

25. L.P. Gianneschi, Ph.D. thesis, University of Adelaide (1972).

26. R. Silbey, *Ann. Rev. Phys. Chem.*, 27, 203 (1976).

27. M. Kasha, *Radiation Res.*, 20, 55 (1963).

28. A. Szent-Györgi, *Science*, 93, 609 (1941).

29. A.S. Davydov, *J. Theor. Biol.*, 38, 559 (1973).

30. O.E. Weigang, Jr. and M. Nugent, *J. Am. Chem. Soc.*, 91, 4555 (1969).

31. D.J. Caldwell and H. Eyring, *The Theory of Optical Activity*, Wiley, New York, p. 103 (1971).

32. A.S. Davydov, *J. Expt. Theor. Phys.*, 18, 210 (1948).

33. M. Born and R. Oppenheimer, *Ann. Phys.*, 84, 457 (1927).

34. W.C. Johnson, Jr. and I. Tinoco, Jr., *Biopolymers*, 8, 701 (1969).

35. S.Y. Wooley and G. Holzwarth, *J. Am. Chem. Soc.*, 93, 4066 (1971).

36. J. Tanaka, K. Ozeki-Minakata, F. Ogura and M. Nakagawa, *Nature Phys. Sci.*, 241, 22 (1973).

37. B. Bonish, *Inorg. Chem.*, 7, 179 (1968).

38. G.S. Levinson, W.T. Simpson and W. Curtis, *J. Am. Chem. Soc.*, 79, 4314 (1957).

39. R. Grinter and S.F. Mason, *Trans. Faraday Soc.*, 60, 274 (1964).

40. K.E. Van Holde, J. Brahms and M.M. Michelson, *J. Mol. Biol.*, 12, 726 (1965).

41. M. Harada and K. Nakanishi, *Acc. Chem. Res.*, 5, 257 (1972).

42. M.J. Nugent and O.E. Weigang, Jr., *J. Am. Chem. Soc.*, 91, 4556 (1969).

43. E.G. McRae, *Aust. J. Chem.*, 14, 344 (1961).

44. T. Kurucsev and U.P. Strauss, *J. Phys. Chem.*, 74, 3081 (1970).

45. A.A. Ivanov, A.A. Puretskii, A.V. Lukaskin, V.I. Permagorov and M.D. Frank-Kamenetskii, *Opt. Spectrosc.*, 32, 252 (1972).

46. V.I. Permogorov, *Opt. Spectrosc.*, 34, 168 (1973).

47. W.T. Simpson and D.L. Peterson, *J. Chem. Phys.*, 26, 588 (1957).

48. D.S. McClure, *Can. J. Chem.*, 36, 59 (1958).

49. E.G. McRae, *Aust. J. Chem.*, 14, 329 (1961).

50. H.C. Longuet-Higgins, *Advan. Spectr.*, 2, 429 (1961).

51. A. Witkowski and W. Moffit, *J. Chem. Phys.*, 33, 872 (1960).

52. R.E. Merrifield, *Radiation Res.*, 20, 154 (1963).

53. R.L. Fulton and M. Gouterman, *J. Chem. Phys.*, 35, 1059 (1961).

54. R.L. Fulton and M. Gouterman, *J. Chem. Phys.*, 41, 2280 (1964).

55. M. Gouterman, *J. Chem. Phys.*, 42, 351 (1965).

56. A. Bierman, *J. Chem. Phys.*, 45, 647 (1966).

57. J.H. Young, *J. Chem. Phys.*, 49, 2566 (1968).

58. M. Zgierski, *Chem. Phys. Letters*, 21, 525 (1973).

59. M. Zgierski, *J. Chem. Phys.*, 59, 3319 (1973).

60. L.P. Gianneschi and T. Kurucsev, *J. Chem. Soc. Faraday II*, 72, 2095 (1976).

61. O.E. Wiegang, Jr., *J. Chem. Phys.*, 43, 71 (1965).

62. M.E. Gál, G.R. Kelly and T. Kurucsev, *J. Chem. Soc. Faraday II*, 69, 395 (1973).

CHAPTER II

Vibronic Exciton Coupling in Dinucleosides

3. INTRODUCTION

The aim of this research will be to extend the experimental application of the vibronic exciton theory to circular dichroism spectroscopy. Indeed, the validity and the importance of this theory have been already demonstrated in its application to absorption spectroscopy[1-7]. Although one recent research[8,9], devoted to exploring this particular problem did involve the use of circular dichroism spectroscopy, the results obtained did not permit any definitive conclusions regarding the validity of the vibronic exciton theory. This was due to the particular choice of molecule considered having far too complicated a spectrum, as well as the procedure followed in the calculations. We will follow the procedure which has been evolved for use in absorption spectroscopy. The strength of this procedure based on the vibronic character of the spectrum lies in the minimization of the number of parameters required (cf. appendix C).

The choice of example of application is limited because of the requirement of optical activity as well as the need of large spectral change on dimerization. The first requirement calls for the use of dissymmetric molecules and this is not the case with the dimeric dyes used previously in absorption spectroscopy. The second requirement can be partially met if one uses molecules in which transitions are strongly allowed. We can add that, as was the case with absorption, the optical properties of the molecule must be well known. This task is made easier if the molecules considered show a simple spectrum with no overlapping bands.

3.1 The Nucleic Acids and their Constituents

Nucleic Acids provide ideal subjects for study due to the number of molecules possessing optical activity and above all because the number of studies devoted to them provides us with a valuable source of comparison.

The importance of Nucleic Acids resides in the fact that they constitute the genetic material of the living cell and are responsible for the storage and the transmission of the genetic information. The determination of the structure of Deoxyribonucleic Acid (DNA) has been the subject of numerous investigations[10-15] which have supplied enough valuable information to enable Watson and Crick[16] to build a model of DNA. DNA (as does RNA) consists of two strands containing four bases: adenine, guanine, cytosine and thymine (uracyl in RNA). Each base is attached to a D-deoxyribose (D-ribose for RNA) and this constitutes then a so called nucleoside. These are linked together by a phosphate group, thus forming the strand of Nucleic Acids. The two strands run antiparallel in a right-handed sense, thus constituting a regular double helix, in which the bases on one strand form hydrogen bonds with those of the other strand so that the purine bases adenine and guanine are paired with the pyrimidine bases thymine and cytosine respectively.

Molecules as simple as dinucleosides can constitute a model for the understanding of more complex polymers. In fact, they are the smallest units which offer the base-base interactions characteristic of the polynucleotides. Of the homodimers, adenylyl-(3'-5')-adenosine (APA) and guanylyl-(3'-5')-guanosine (GPG) seem to respond best to the

previously formulated requirement necessary for the application of the vibronic exciton theory to CD. They possess optical activity, their transitions are strongly allowed and the changes occurring in the CD as well as in the absorption spectra on dimerization are by far the most marked of all the dinucleosides[17,18]. Their near U-V absorption spectra are well defined and this spectrum range has the advantage of presenting a limited amount of spectral noise in CD measurements. As we have previously emphasized, a study of dimeric molecules cannot be undertaken without a good understanding of the optical properties of their monomeric constituents. The purines, adenine and guanine, not only satisfy the above conditions but furthermore, from a theoretical point of view, they have been the most exhaustively studied biomolecules[19].

of page 21, 20 and 22 !

4. NUCLEOSIDES

The adenine and guanine bases are cyclic and planar molecules. The coordinates of all atoms have been well documented, in particular by Voet and Rich[20]. They are drawn to scale in figure 4.1.

4.1 Electronic Properties of Adenine

Correlation of the transitions of adenine with those of benzene were made by Mason[21] and Clark and Tinoco[22]. The 260 nm band is shown to be composite[21,22] and includes two transitions: the B_{2U} and B_{1U} bands[22]. Experimentally, the characteristic magnetic circular dichroism (MCD) spectrum confirms the presence of these two nearby transitions[23,24]. Numerous theoretical studies of the adenine molecule have been carried out using a variety of methods such as, the simple Hückel π electron model[25,26], the self-consistent field theory[27,34], the all valence electron calculation[35-37] and finally the all electron Ab-Initio calculations[38,39]. Although a lot of controversy exists about the position and the relative intensity of the $\pi \rightarrow \pi^*$ transitions, there is general agreement about the number of these transitions (table 4.1). The existence of $n \rightarrow \pi^*$ transitions has been the object of more recent calculations[37,40]. They have been postulated to explain some unresolved phenomena in the optical spectra[23,41-44,125]. The assumptions based on their presence are often questionable due to the low intensity of these transitions, the fact that their observations have been isolated and not reproduced in different laboratories[41,45], and that their methods of deduction can be subject to criticism: for example when the spectra are resolved into

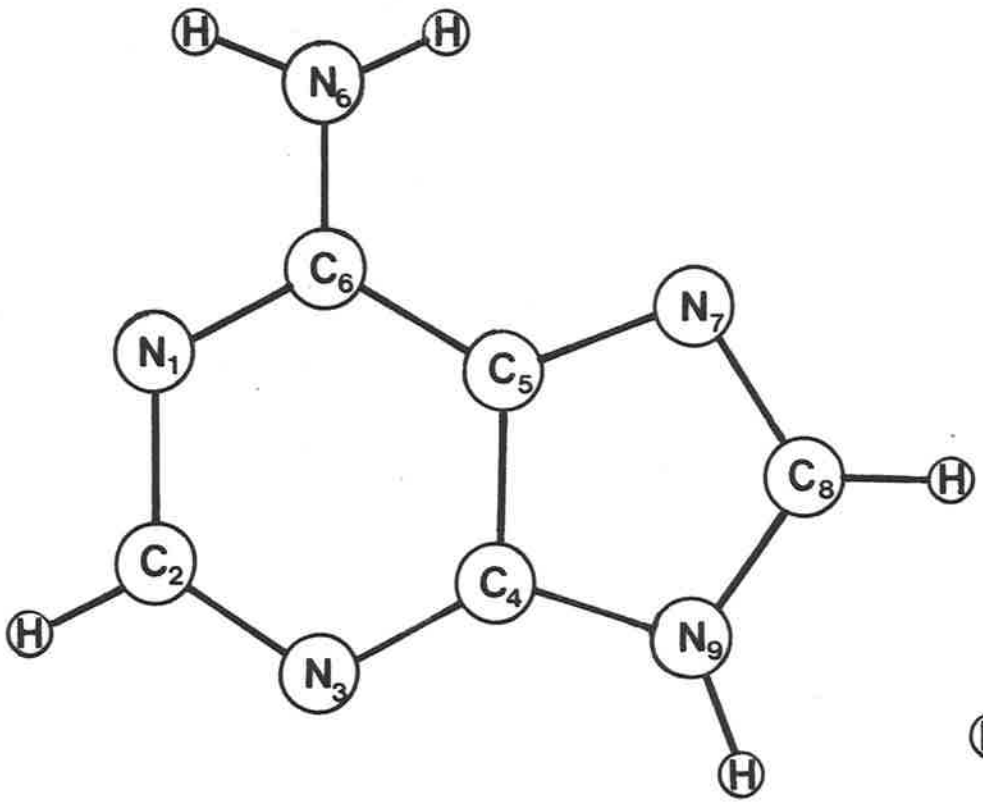

ADENINE

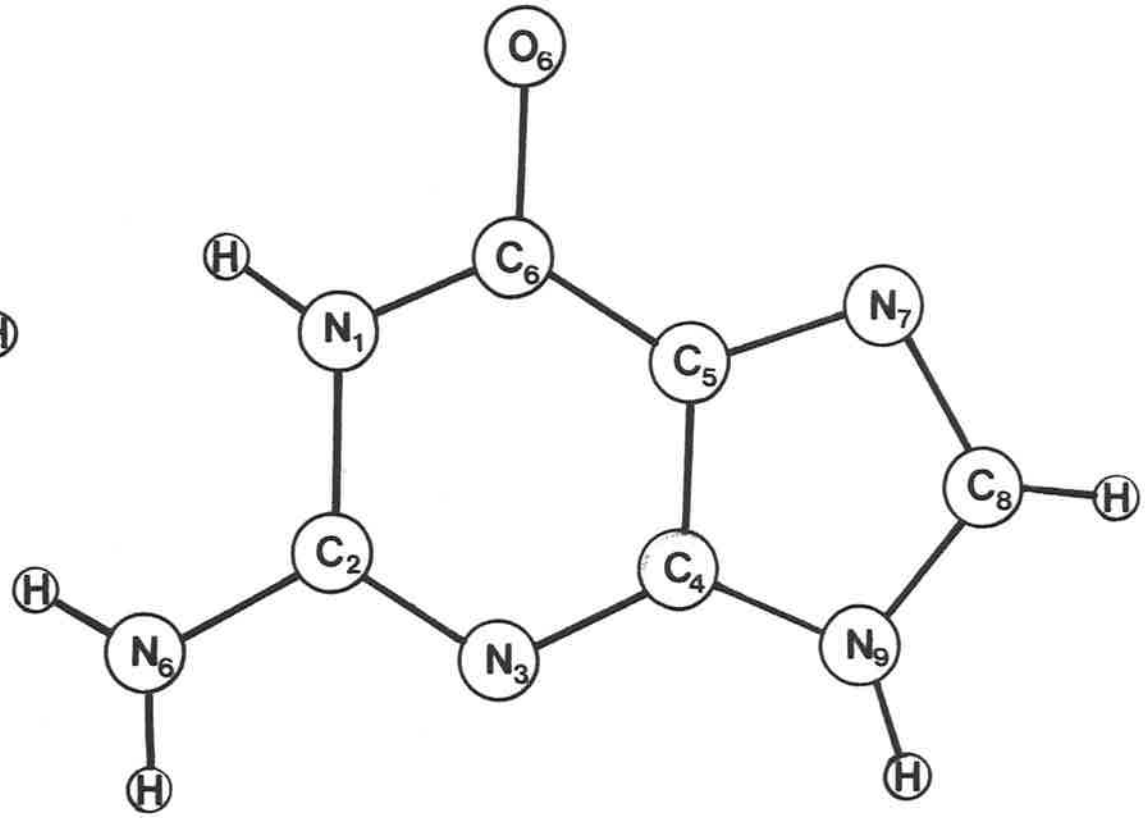

GUANINE

FIG.4.1 THE STRUCTURE OF THE PURINES.

Table 4.1 CALCULATED TRANSITION MOMENTS OF ADENINE

Methods of Calculation	Calculated Energy (eV)	Oscillator Strength	Transition Moment Direction[a]	References
SCF	5.2	0.4	-144°	30
	5.5	0.3	-58°	
	6.1	0.5	-78°	
SCF-CM	4.8	0.1	+37°	31
	5.0	0.1	-128°	
	5.8	0.2	-82°	
LCAO-SCF-CI	4.45	0.006	-30°	29
	4.81	0.21	-112°	
	5.61	0.39		
PPP-MO	4.69	0.02	-162°	22
	4.87	0.20	-144°	
	5.89	0.40	+110°	
	6.01	0.08		
SCF-LCAO-MO-CI	4.5	0.011	-28.4	17
	5.01	0.498	+60.6	
	5.83	0.777	-44.4	

a - The angle is measured relative to the C4-C5 axis. Positive angles are measured counterclockwise. The adenine base is oriented as shown in figure 4.1.

pure electronic transitions of gaussian shapes on a wavelength scale[44]. Finally the correlation between different molecules[46] must be made with care. In particular the shoulder around 265 nm in the absorption and the MCD spectrum of adenine has been attributed to a $n \rightarrow \pi^*$ transition; yet it has been clearly demonstrated that adenine exists in different tautomeric forms[47] which is not the case with adenosine or AMP. This casts doubt on all information arising from the interpretation of the adenine spectra. In conclusion, although we cannot ignore the presence of the $n \rightarrow \pi^*$ transitions because they can account for a large part of the CD spectrum, as in the case of the polypeptides, we must rely on observable facts and till now no clear and direct evidence has been given to prove their existence, especially in the near U-V region.

One important parameter for the interpretation of the optical spectra is the direction of polarization of the transition. It can be obtained either by theoretical calculations (table 4.1) or by experimental methods such as the polarised absorption and the polarised reflection of a single crystal[48]. In spite of the fact that they require us to make some assumptions[48], these two experimental methods are by far the most accurate compared to others which only give relative transition directions. These other methods include the polarised absorption measurement of stretched films[49] and the polarised fluorescence measurement[50,51], to which we can add the method used by Mason[21] which is based on the study of the effects of various substituents on the absorption spectrum.

4.2 Analysis of the Optical Spectra

4.2.1 Adenosine

Figure 4.2 shows the absorption, CD and linear dichroism spectra of adenosine. The diamond symbols correspond to the measured dichroic ratio in stretched film, defined as the ratio of absorbance with light polarised parallel and perpendicular with respect to the direction of stretch (cf. appendix B). All of these spectra are in concordance with previous experimental studies[24,46,49]. Molecular spectra will be interpreted through their vibronic character. Although molecules possess a number of vibrational modes, it has been shown that a single vibrational mode dominates the transition and it was assumed to be the totally symmetric vibrational mode for planar organic aromatic molecules[52,53]. The curve fitting method described in the appendix C has been successfully applied to fit the absorption spectra of many molecules[1-5,54] and will be applied to circular dichroism spectra. In fact as formulated by Moffit and Moscowitz[55] and later by Harnung *et al.*[56], the shape of both the absorption and circular dichroism bands have identical sources. Thus we will analyse the circular dichroism spectra into separate bands in the same way as we did for the absorption spectra. Furthermore, the parameters characterising the shape of the spectra that is to say, b_g the bandwidth at half maximum, V the separation between bands, X the ratio of the (1.0) to (0.0) band and $\tilde{\nu}_{oo}$ the position of the (0.0) band should be similar in the two spectroscopic methods. To restrain the number of indetermination of the fitting method, we fix the value of the separation between bands, V, at 1340 cm^{-1} which is the frequency of the most intense band of the Raman

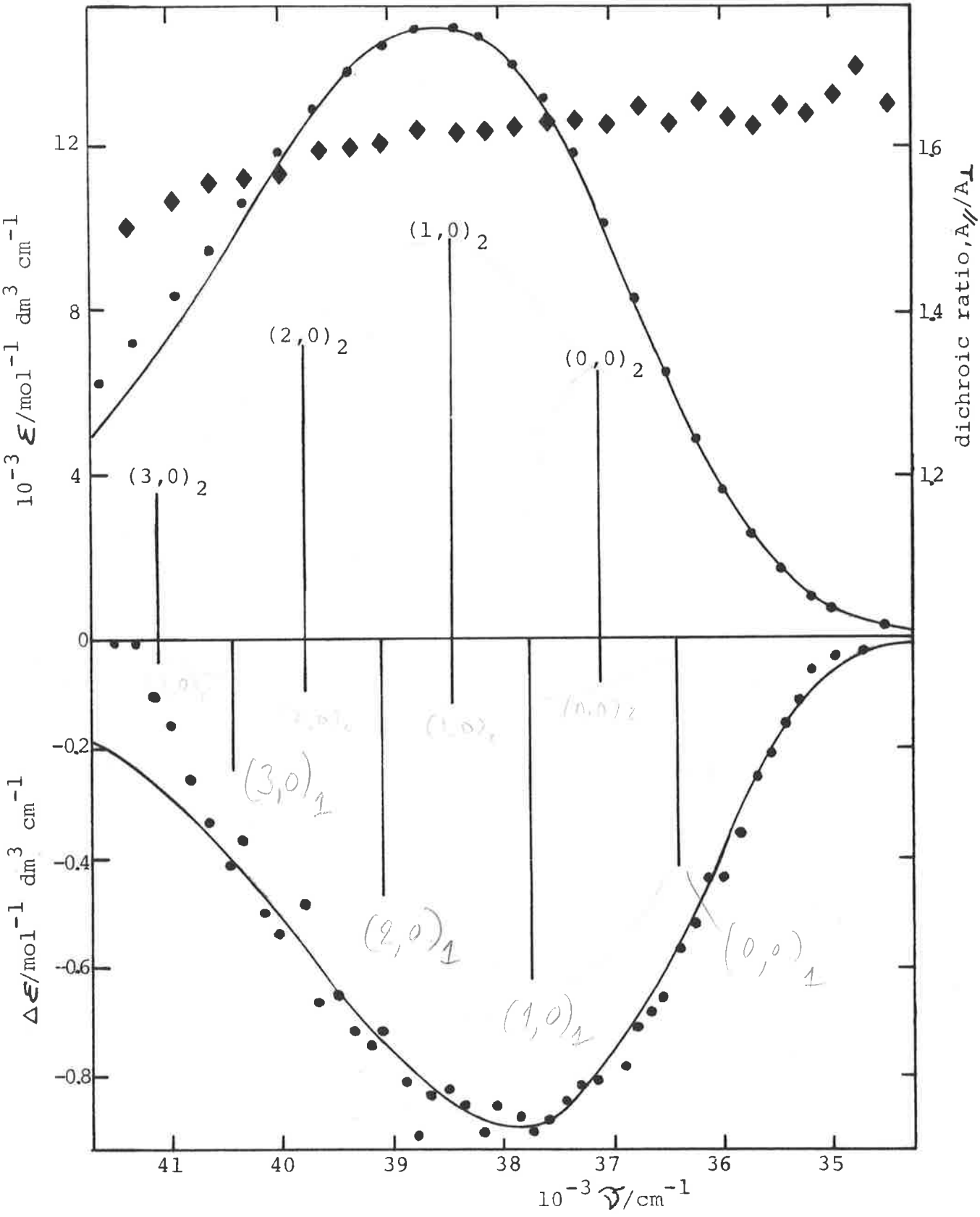

FIG.4.2 SPECTRA OF ADENOSINE. (●),experimental data; (◆), dichroic ratio in PVA films stretched 4.5 times; (—),fitted isotropic absorption and circular dichroism spectra of solution;the vertical lines are proportional to the intensities of the individual vibronic bands;the subscripts 1 and 2 correspond to the lower and higher energy bands, respectively.

spectrum of adenosine and AMP[57] and it represents the totally symmetric mode of vibration. Only the part of the spectrum whose wavenumbers are less than 40,000 cm^{-1} is retained because of the proximity of a higher energy transition which can add its contribution to the X band. Its presence is manifest if one looks at the drop of the dichroic ratio in this region of the spectrum (fig. 4.2). Comparison of the absorbance and CD spectra of adenosine reveals that one spectrum is shifted by about 700 cm^{-1} in relation to the other. In a first approximation we can assume that the two spectra are produced by two separate vibronic transitions and each spectrum is fitted to an harmonic progression of gaussian bands with the aid of the curve fitting procedure described in the appendix C. The next step is to include both progressions in each spectrum with the restriction of using the same value of the parameter b_g. For the absorption spectrum, the intensity of the low energy progression turns out to be negligeable; a result which is confirmed by the linearity of the dichroic ratio in this part of the spectrum. On the other hand, the CD spectrum is dominated by the low energy progression but the high energy one brings a small contribution to the overall envelope. The fitted isotropic absorption and circular dichroism spectra are represented in figure 4.2. The parameters pertaining to the absorption and CD spectra of adenosine are shown in table 4.2 and defined in appendix D.

4.2.2 Adenosine Derivatives

The interpretation of the presence of two transitions in the X band will be tested on some adenosine derivatives. The behaviour of AMP is different from the one of adenosine as can be seen in figure 4.3. In fact, the absorption and CD

Table 4.2 RESULTS OF FITTING SPECTRA TO TWO VIBRONIC PROGRESSIONS.

(Figures in brackets are linear estimates of the standard deviations of the best-fit parameters).

	Adenosine	AMP	*cis*-Pt adenosine	*trans*-Pt adenosine
$\tilde{\nu}_{oo}^{(1)}$ (cm^{-1})	36,400(100)	36,400(100)	35,300(100)	35,470(90)
$\tilde{\nu}_{oo}^{(2)}$ (cm^{-1})	37,100(60)	37,100(50)	36,900(80)	36,460(100)
$X^{(1)}$	1.50(.07)	1.50(.07)	1.76(.08)	1.78(.30)
$X^{(2)}$	1.48(.05)	1.48(.04)	1.67(.04)	1.90(.06)
$(b_g)_{abs}$ (cm^{-1})	2260(65)	2260(50)	2270(200)	2260(200)
$(b_g)_{CD}$ (cm^{-1})	1670(110)	1670(100)	1720(200)	1570(140)
$\mathcal{D}^{(1)} \times 10^{35}$ (cgs units)			0.29	0.42
$\mathcal{D}^{(2)} \times 10^{35}$ (cgs units)	1.59	1.66	0.76	0.69
$-\mathcal{R}^{(1)} \times 10^{40}$ (cgs units)	1.97-2.27	0.33	2.02-2.07	1.27
$-\mathcal{R}^{(2)} \times 10^{40}$ (cgs units)	0-0.30	3.18	0-0.05	1.31
$(g^{(1)} = 4\frac{\mathcal{R}^{(1)}}{\mathcal{D}^{(1)}})10^5$	>100[a]	>10[a]	28	12
$(g^{(2)} = 4\frac{\mathcal{R}^{(2)}}{\mathcal{D}^{(2)}})10^5$	0-0.75	7.6	0-0.3	7.6

a - Estimated value of g considering a minimum observable value for $\mathcal{D}$ of 0.01 - 0.02 x 10^{-35}.

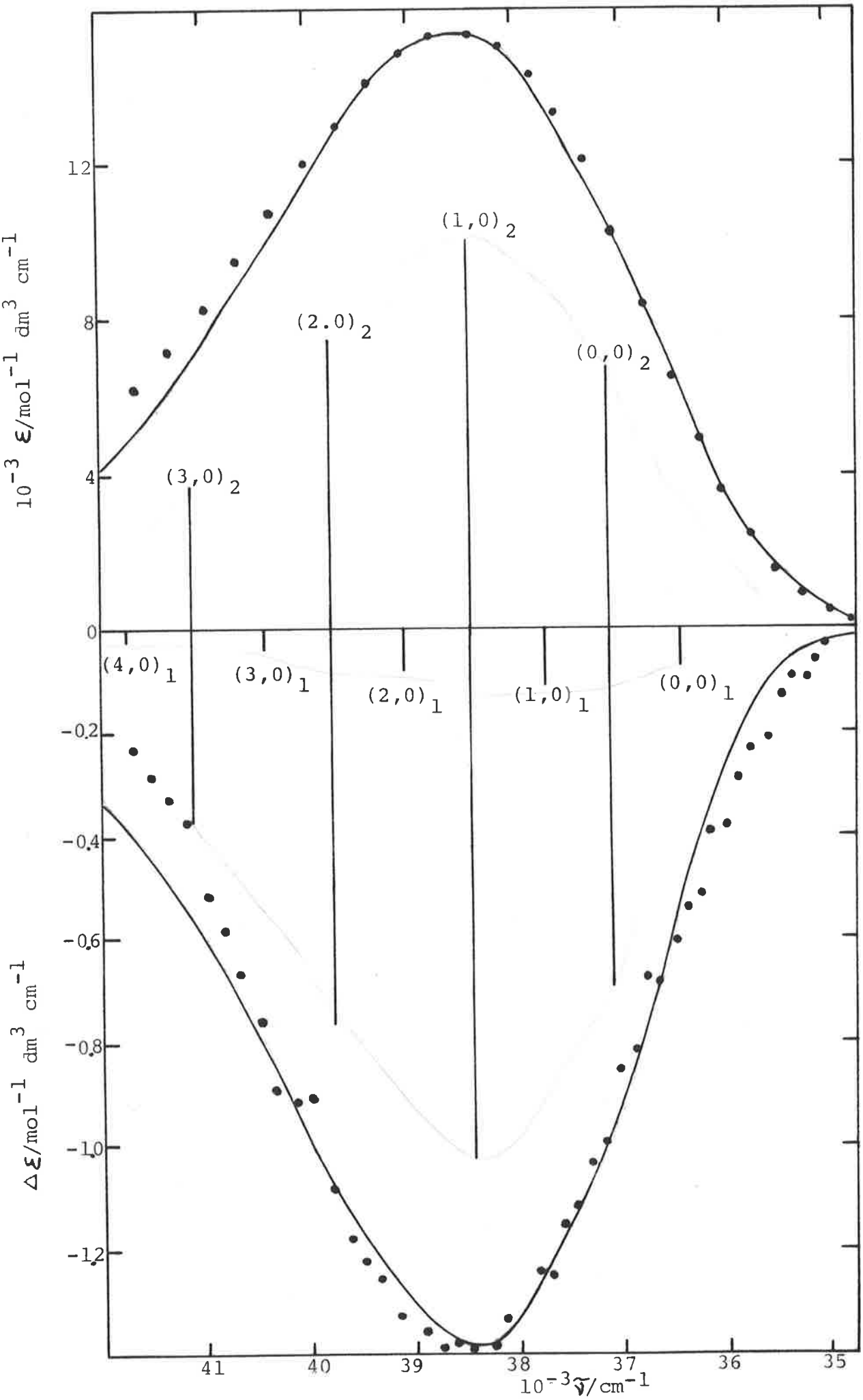

FIG.4.3 SPECTRA OF AMP. Symbols as in fig.4.2 .

envelopes are similar and originate from the same high energy vibronic transition as does the absorption spectrum of adenosine. As for the platinum-adenosine complexes, their linear dichroism spectra in figures 4.4 and 4.5 clearly reveal the presence of two transitions in the X band with the drop of the dichroic ratio at lower energy. This is also confirmed by the greater width of the envelope spectrum in both absorption and CD. The curve fitting procedure is performed using two vibronic progressions in which the parameter V is taken to be the one of adenosine, assuming that complexing to platinum would not change significantly the vibrational energy[58,59].

Looking at the parameters of Table 4.2, we can make some interesting observations. Firstly, for adenosine and AMP, the two transitions are separated by about 700 cm^{-1}; this is in total concordance with phosphorescence results for adenosine and AMP that show clearly a main vibrational progression of about 1300 - 1400 cm^{-1} with weaker peaks appearing at multiples of 700 cm^{-1}[51,60]. Secondly, the position and relative intensity of the two transitions are in perfect agreement with those of the $\pi \rightarrow \pi^*$ transitions predicted theoretically (see table 4.1) and found experimentally in single crystal studies[45]. Because of the reasonably good fit of these spectra and also the consistency for the adenosine derivatives of the various parameters generating the envelope spectra of these two progressions, the suggestion of the presence of $n \rightarrow \pi^*$ transitions is not supported just as it has been already refuted in linear dichroism[49], emission[51], CD[23,24] and MCD studies of adenosine.

It has been theoretically[23,61] shown that two transitions interacting in the presence of an external magnetic field will produce a MCD spectrum composed of two

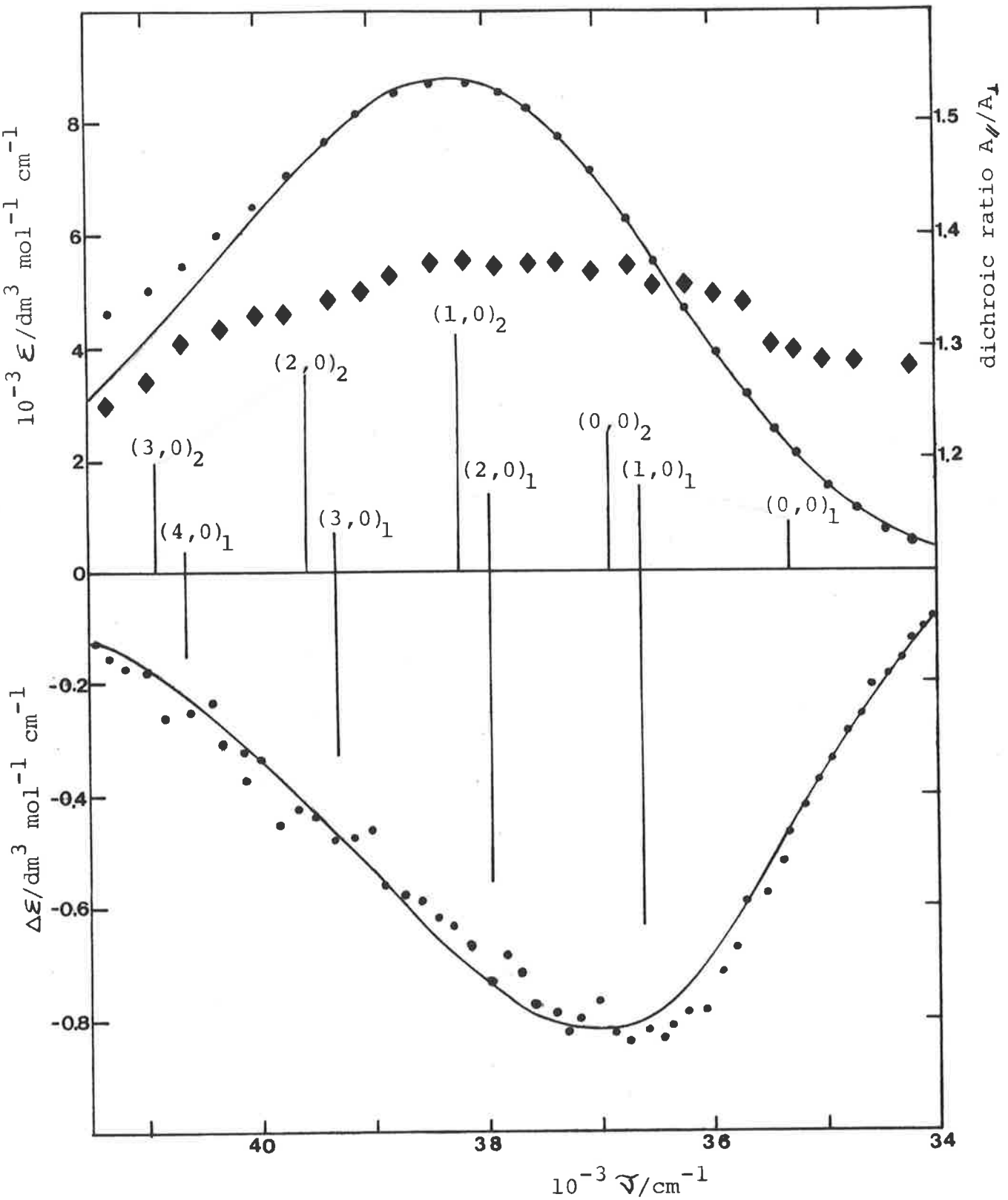

FIG.4.4 SPECTRA OF CIS-DIAMMINODICHLOROPLATINUM(II)-ADENOSINE COMPLEX. Symbols as in fig.4.2.

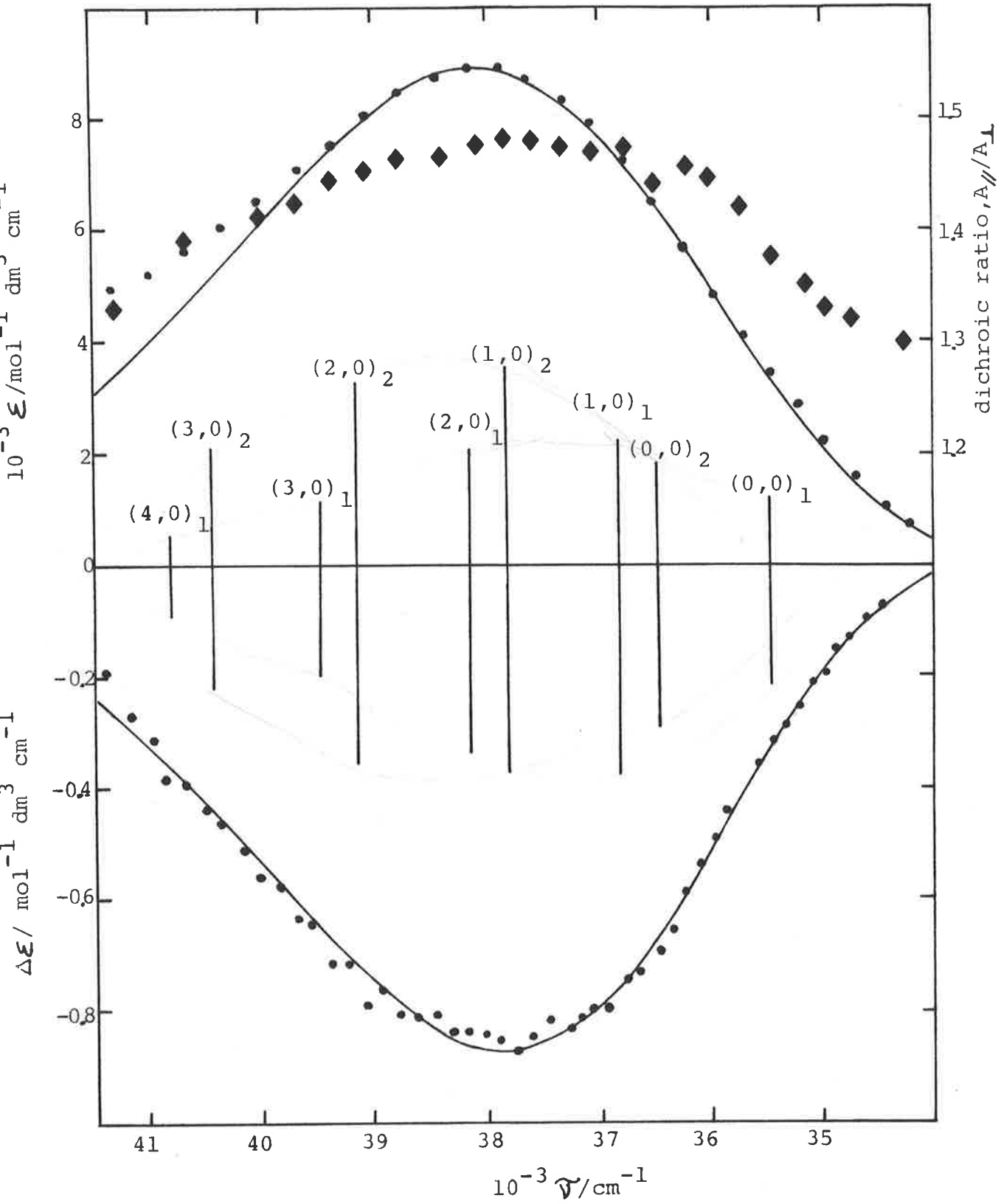

FIG.4.5 SPECTRA OF TRANS-DIAMMINODICHLOROPLATINUM (II)-ADENOSINE COMPLEX. Symbols as in fig.4.2 .

bands of equal intensity but different signs and located at the frequencies of the transitions considered. We have used the two progressions present in the adenosine spectrum, of equal intensity but of opposite sign, to generate a theoretical MCD spectrum. Figure 4.6 shows the computed MCD spectrum of adenosine as well as two experimental ones, taken from published results on adenosine[23,24] and normalised to the magnitude of the calculated negative trough. The rather close agreement between experimental and calculated MCD spectra provides more evidence in favour of our interpretation and shows clearly that the maxima in the "S-shaped" band may not correspond to those of the individual transitions.

4.2.3 Polarisation of the Different Transitions

As it was previously emphasized, the direction of polarization of the transitions is of key importance in determining the mechanisms behind the production of optical activity. The stretched film method used in this work has proved far more powerful than other linear dichroism techniques such as flow or electric dichroism, chiefly by the fact of the high degree of orientation obtained. This can be very significant for molecules of lower symmetry[62]. It is also a relatively simple method to use and a satisfactory level of reproduction can be obtained[63]. Although an exact description of the orientation of small molecules embedded in stretched polymer films is complex[64], their long axis tends to orient in the direction of stretch[65]. The positive value of the dichroic ratio for the 260 nm absorption band indicates, with regard to the definition of the dichroic ratio, that the corresponding transition is more or less long axis

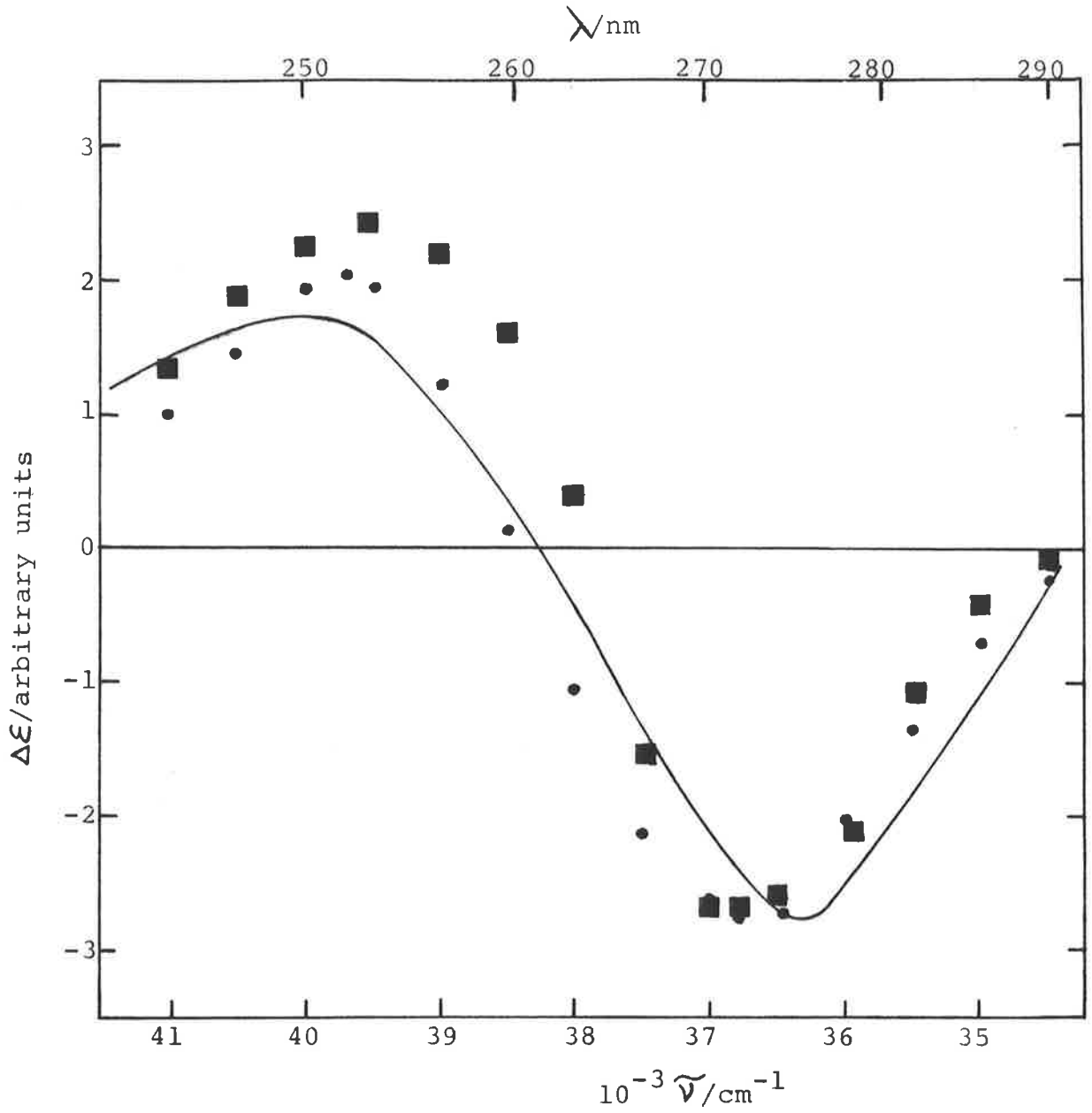

FIG.4.6 MCD SPECTRUM OF ADENOSINE.
Full line: calculated as explained in the text; circles:data extracted from figure 4 of reference 23 ; squares: data extracted from figure 2 of reference 24 .

polarised. The drop of the dichroic ratio on either side of this transition, a drop which is particularly obvious for the platinum adenosine complexes (fig. 4.4 and 4.5), suggests the presence of short axis polarised transitions. Although this is merely a rough determination, this interpretation of the polarization direction is fully consistent with previous determinations[41,45,49]. One can conclude that both transitions in the X band are perpendicular to one another, with the long axis polarised transition occuring at higher energy than the short axis polarised transition. Although our study is restricted to the near U-V region of the spectrum (for wavenumbers less than 40,000 cm^{-1}), the comparison between the fitted and experimental absorption and CD spectra reveals the presence at higher energies of a third transition which is polarised along the short axis of the base according to the value of the dichroic ratio. The low intensity of this transition prevents us from analysing its spectrum but by considering both the absorption and the CD spectra of adenosine, it is estimated that its (0,0) band would be near 41,500 cm^{-1}, a value that fits in with theoretical calculations[36] and experimental CD measurements[24,43,46].

4.3 Structure of the Nucleosides

4.3.1 Configuration at the Asymmetric Carbon

Now that we have studied the electronic properties of the base itself, we have to consider it in its close environment and investigate the possible perturbations that could affect them. The base is linked in the β or α configuration to the sugar (β stands for the attachment of the base on the same side of the sugar ring as the C5' carbon whereas α represents an attachment on the opposite side).

4.3.2 Conformation of the Sugar Ring

Two possible sources of perturbation coming from the sugar can be found. The first type of perturbation can be caused by the puckering of the sugar: Four atoms of the sugar ring form a plane while the fifth ring atom, C3' or C2', is significantly displaced out of this plane either on the same side of the C5' atom, as in the endo conformation, or on the opposite side, as in the exo conformation (figure 4.7a). This has been investigated using X-ray measurements[66,67]. Alhtough there are a few exceptions[67,68], the C3' and C2' endo conformations are the most commonly found. Nuclear magnetic resonance (NMR) studies which have the advantage of being carried out in aqueous solution, confirm X-ray results but clearly show the existence of a rapid C3' endo $\leftrightarrow$ C2' endo equilibrium[69].

4.3.3 Relative Orientation Between Adenine Base and Ribose Sugar

- definition:

The cause of the second perturbation arises from the rotation around the glycosyl bond, C1' to N9, joining the base to the sugar; this phenomenon received considerable attention. As its influence will be of major importance in our study, we give some definitions and examine the present state of research on this subject. The angle of rotation around the C1' to N9 bond will be expressed as ϕ_{CN}[70], defined as the angle between the plane of the base and the plane formed by the C1' to O1' bond of the sugar and the C1' to N9 bond. ϕ_{CN} will be equal to zero when the sugar bond C1' to O1' is *cis*-planar to bond N9 to C8 of the base and will be

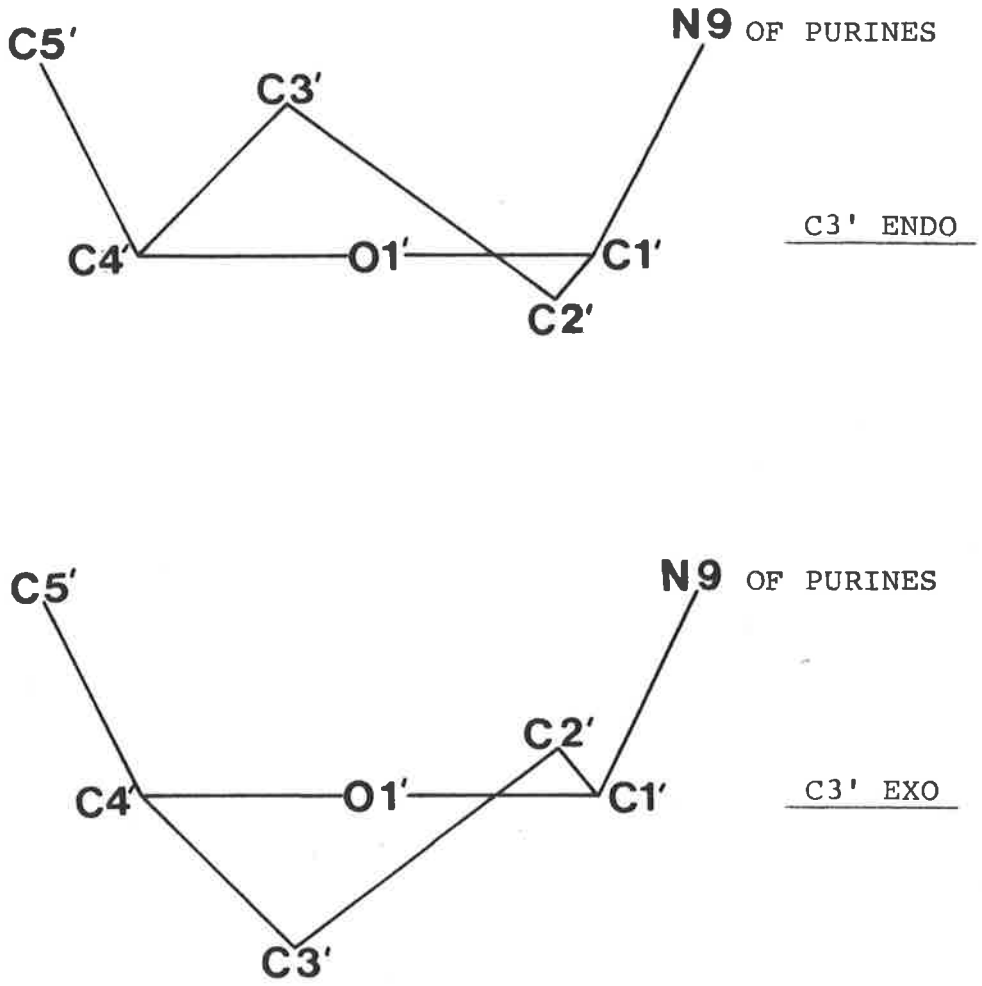

FIG.4.7.a CONFORMATION OF THE SUGAR RING.
The sugar rings are in the β configuration.

positive for a clockwise rotation of the C1' to O1' bond when viewing from C1' to N9 (figure 4.7b).

- NMR spectroscopy and X-ray diffraction as methods of investigation.

For this problem, NMR is the most reliable method of investigation. It indicates without any ambiguity that adenosine compounds are mainly in the anti conformation[71] ($+15° < \phi_{CN} < -75°$)[70]. AMP has been the principal target of investigation[71,72]. Its phosphate group was located in close proximity to the H8 proton of the base. Barry *et al.*[73,124], taking advantage of the induced shifts caused by the binding of lanthanide ions, were able to ascertain a mean rotation angle ϕ_{CN} of $-12° \pm 12°$ for AMP by a computational method.

Although the direct application of X-ray diffraction results to aqueous solution is limited, X-ray can provide accurate information about the coordinates of atoms and is a starting point for theoretical calculations. Measurements had been conducted on numerous crystals; the angles of rotation, ϕ_{CN}, obtained for these crystals as well as their sugar conformations are presented in table 4.3. The crystallographic survey shows the predominance of the anti conformation associated with a C3' endo puckering of the sugar. Some syn conformations ($105° < \phi_{CN} < 195°$)[70] have been found but they were all related to special structural reasons, as in 8-bromoadenosine[74], 5'-methylammonium-5-deoxyadenosine[75] or 3'-O-acetyladenosine[76].

Empirical calculations have been carried out in order to evaluate the rotational barrier existing between the anti and syn conformations. The first and simplest method is the "hard sphere" approximation developed by Haschemeyer and

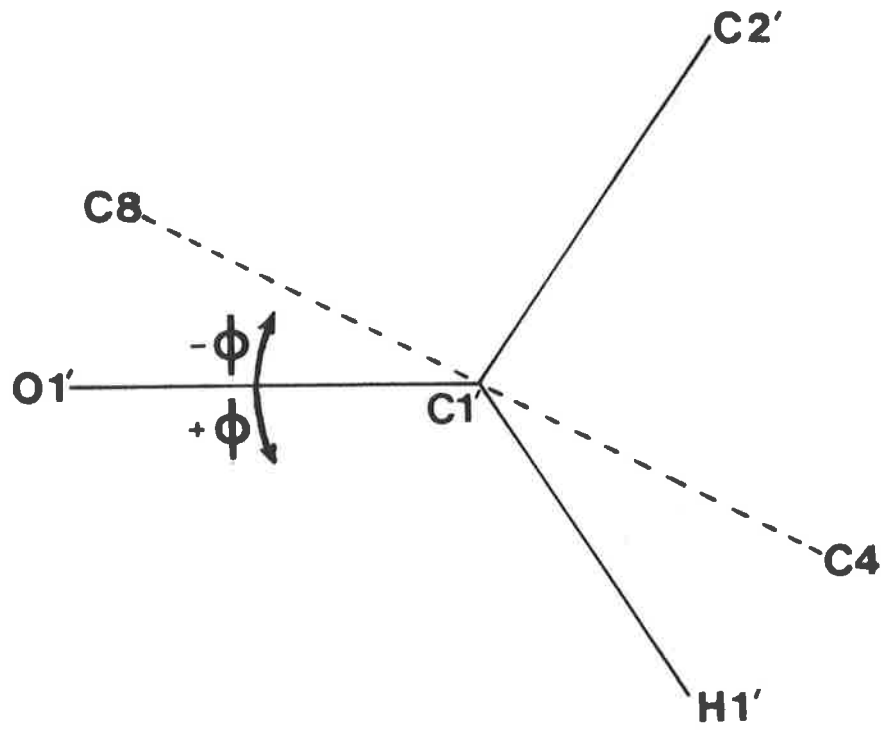

FIG.4.7.b CONFORMATION AROUND THE GLYCOSYL BOND C1'-N9.
One looks along the glycosyl bond from C1' to N9. For the definition of the torsion angle, ϕ_{CN}, see text.

Table 4.3 PUCKERING OF THE SUGAR AND THE GLYCOSYL TORSION ANGLE ϕ_{CN}.

Compound	Conformation of the sugar	ϕ^{d}_{CN} (degree)	References
Adenosine 3'-phosphate dihydrate (3'-AMP)	C3' endo	-3.8	a
Adenosine in complex with 5-Bromouridine	C3' endo	-12.4	a
Adenosine 5'-phosphate monohydrate (5'-AMP)	C3'endo	-25.7	a
Adenosine 3',5'-cyclic phosphate (3',5'-AMP)	C3' endo	-50.0	a
Deoxyadenosine (dA)	C3' exo	-10.9	a
Adenylyl 2'-phosphate 5'-uridine tetrahydrate (A2' p5'U-A)	C2' endo	-54.6	a
A-DNA	C3' endo	-14	b
10-RNA	C3' endo	-6	b
11-RNA	C3' endo	-11	b
A-RNA	C3' endo	-14	c

a - from table III of reference 67.

b - from figure 5 of reference 67.

c - from reference 90, p. 1024.

d - The published torsional angle χ was converted to ϕ_{CN} ($\phi_{CN} = -\chi$).

Rich[77]. Crystallographic data enabled them to evaluate the sterically "allowed" conformations using criteria for minimal contact distances, based on accepted Van der Waals radii, between various atoms of the sugar and the base. The map in figure 4.8 represents the interaction distances between various atoms of the sugar and the purine base function of the torsion angle ϕ_{CN}. This calculation as well as others based on the same model are consistent with experimental measurements[78]. More elaborate methods, such as the calculation of the potential energy of the system[79,80] or a more rigorous quantum mechanical calculation[81] were performed but no new information was obtained except perhaps further proof of the predominance of the anti conformation although the steric barrier to the syn conformation was rather small.

- circular dichroism (CD)

The third method used to determine the extent of perturbation caused by the sugar is circular dichroism (or ORD). This spectral method is not only dependent on the magnitude of the transition dipole moment of the base, as in the case of absorption spectroscopy, but by definition circular dichroism has the advantage of being sensitive to conformation through the geometrical relationship that exists between the transition dipole moments in the base and the perturbing sugar. Because of this dependence on the sugar-base geometry and in spite of the relatively large difference between their dipole strength, either or both the transitions in the X-band of adenine may contribute significantly to the CD spectrum. Although this method is more appealing than NMR from the experimental point of view, the interpretation of the CD spectrum is not yet fully understood. At an early stage of

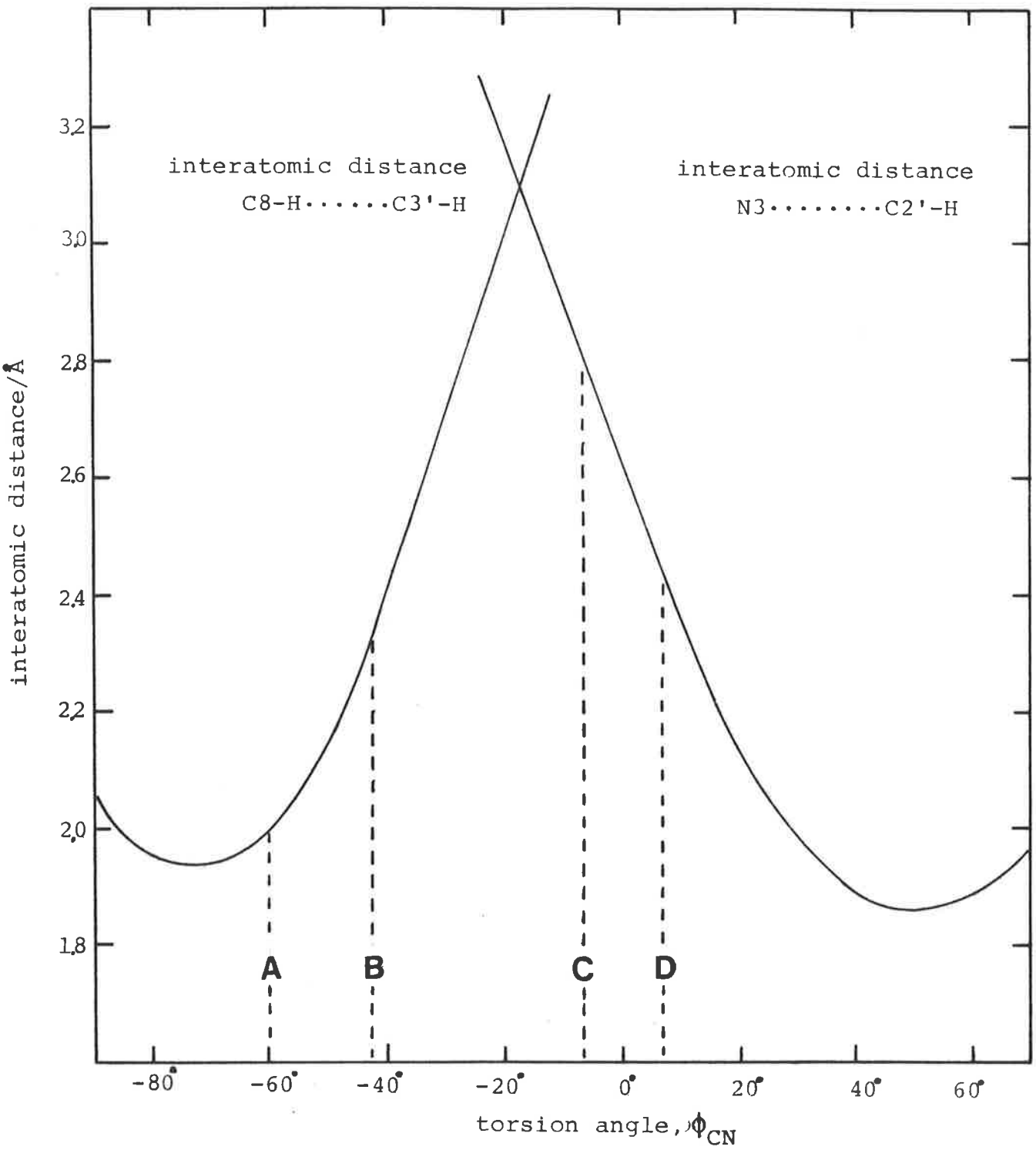

FIG.4.8 CONTACTS OF SUGAR ATOMS AS A FUNCTION OF ϕ_{CN} WITH N3 AND THE HYDROGEN ATOM ON C8 IN A PURINE NUCLEOSIDE HAVING A C3' ENDO PUCKERING. (From Haschemeyer and Rich, fig.5 of ref.77).
Broken lines are the limits of allowed torsion angle for C8-H····C3'-H (A), for C8-H····C3'-OH (B), for N3····C2'-OH (C) and for N3····C2'-H (D). The allowed torsion angles were calculated with the use of VAN DER WAALS radii of 1Å, 1.35Å and 1.45Å for the hydrogen, oxygen and nitrogen atoms, respectively.

development, detection of optical activity by the ORD technique was only used to assign the α and β configurations of nucleosides and no resolution of the spectra was possible because of the complexity of ORD curves as well as the low intensity of the signal. Ulbricht[82] proposed the rule that in purine, a β configuration is associated with a negative CD, whereas an α configuration gives a positive CD. This was confirmed by the ORD measurements of Nishimura *et al.*[83] and also by Miles *et al.*[84] with circular dichroism detection. Furthermore, relating the sign of the CD spectrum to the torsion angle has been the target of much research. To achieve this aim, one has to use nucleosides whose geometry is known or has been estimated. Extensive work[85,86] on cyclonucleosides[87], having a fixed torsion angle, enabled us to correlate the change in CD with different torsion angles. But the results obtained cannot be applied directly to ordinary nucleosides because of a possible perturbation to the electronic properties of the chromophores caused by the structural changes in these cyclonucleosides. The method of steric restriction to a syn conformation, which is achieved by introducing a bulky substituent on the C8 atom of the purine[24,84,86] (valid only if the substituent is not too polarizable) was more promising, as it enabled correlation with theoretical calculations.

Eyring's team performed calculations based on the coupled oscillator theory and using a bond-bond coupling approach[88]. The pyrimidine bases provided an ideal subject for the testing of this theory because of the quite simple nature of their electronic spectra[89]. Although some positive results were obtained for the theoretical study of the purines[84,87], the complexity of their spectra and the over

simplification of the problem (considering only one transition in the X band) prevented the elaboration of a definitive and satisfying interpretation. A more recent calculation based on the coupled oscillator theory and using this time a monopole-bond type coupling[34] brought an improvement over previous attempts by the fact that the two transitions B_{2U} and B_{1U} of the X band of the purines were included in the calculation. A general agreement between theory and experiment was found regarding the sign of the different transitions, with the exception of guanosine. However their study shows the weakness of theoretical calculations in the following respects: firstly the results depend on the choice of monopoles for the bases and of bond polarizabilities for the sugar, a choice which was neither obvious nor always justifiable and secondly the parameters used in the calculation need to be normalised to correspond to experimental values[37].

Steric hindrance which is caused by substituents attached to the C2' and C3' atoms of the sugar can constitute another means of restricting the possible range of the torsion angle ϕ_{CN}[24].

4.3.4 Correlation between Torsion Angles and CD Spectra

We have seen previously that changes in the intensity and the position of the maximum, as well as the overall shapes of the adenosine nucleosides' CD spectra are to be attributed to changes in the relative contribution to the optical activity of both the low and high energy transitions. A particular example of this modification in the CD spectrum was given by the series of α and β nucleosides published by Ingwall[44] and reproduced in figure 4.9. The change of the CD envelope (peak intensity and shift of the maximum position)

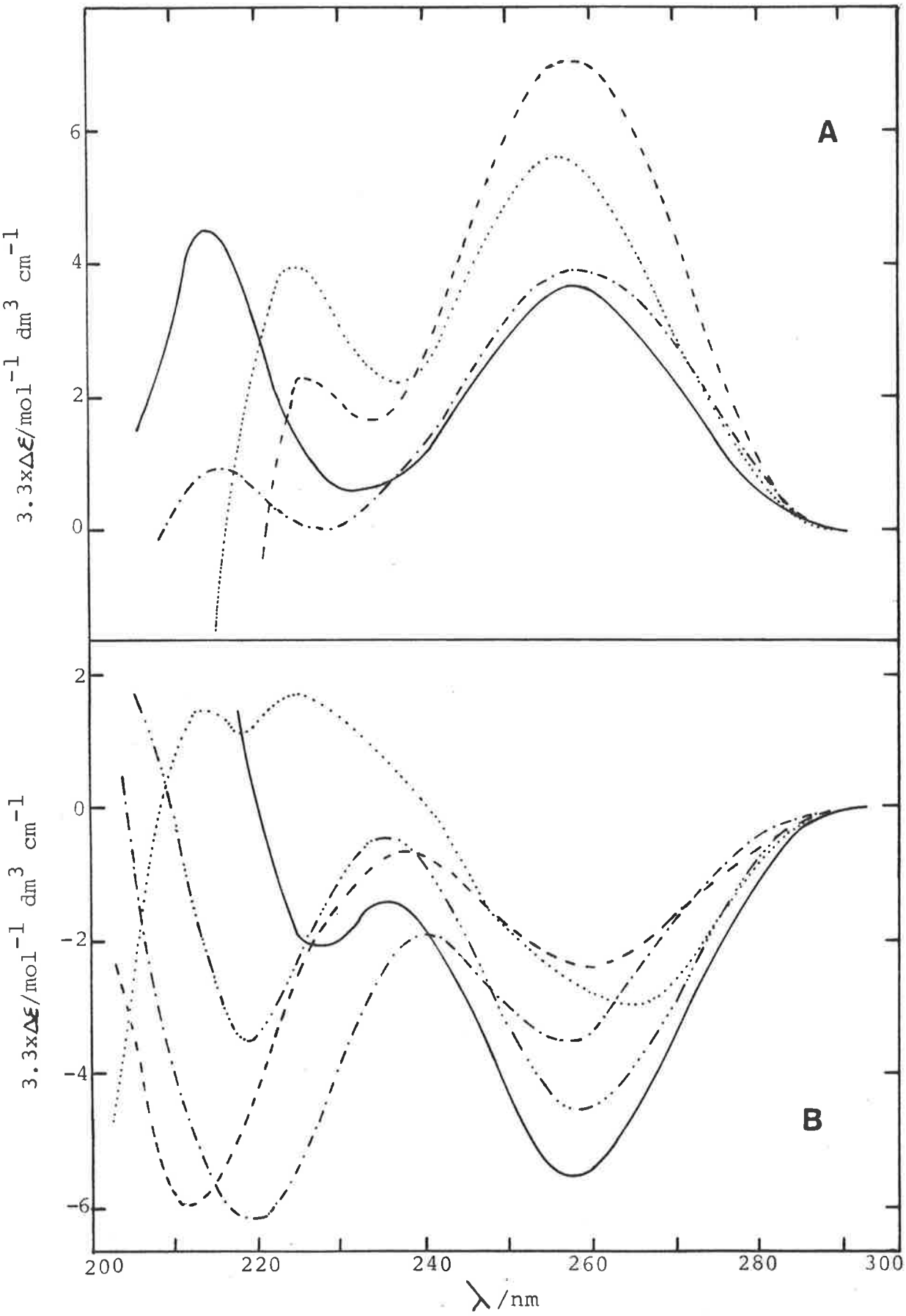

FIG.4.9 CIRCULAR DICHROISM SPECTRA OF α-D-PENTOFURANOSIDES (A) AND β-D-PENTOFURANOSIDES (B) OF ADENINE FROM INGWALD[44]. ara (—),lyxo (-·-),ribo (··),xylo (- -). The spectrum of AMP (-···-) has been included in figure (B) for comparison.

in the β series is linear with an increase in torsion angle, if we interpret this phenomenon as being due to steric hindrance between the hydroxyl groups of the sugar and the adenine atoms. A fact which reinforces this interpretation is shown by the CD of the α series which is the mirror-image of the β series, moving in the same direction in relation to steric hindrance. The fit of the CD spectra of these α and β conformers around 260 nm, using the two vibronic progressions which characterise the CD spectrum of adenosine and AMP, turned out to be adequate. (It was pointed out that the U-V spectra of these adenosine derivatives were essentially identical[44].) The results of this deconvolution are given in table 4.4. With the use of the conformation map in figure 4.8, based on the hard sphere model and developed by Haschemeyer and Rich[77], we are able to assign a mean torsion angle to each nucleoside considered. For these sterically restricted compounds, the anti conformation is considered to be the only one possible in relation with NMR and X-ray results of adenosine nucleosides on this problem. (See paragraph 4.3.3.) We used the C3' endo conformation for the β anomers which is consistent with the majority of crystal structures of adenosine derivatives[67] (table 4.3). The range of angle, ϕ_{CN}, for the two sets of anomers is taken to be enantiomeric. In figure 4.10 we plotted the rotational strength of the two transitions as a function of the mid-point of the estimated ϕ_{CN} range for each nucleoside. The broken line corresponds to the tentative correlation between these points. When this correlation was established, adenosine and its α enantiomer were not taken into consideration, firstly because adenosine can exist in both the anti and the syn conformations[90] and secondly because the progressive change of the entire CD

Table 4.4 CD SPECTRA OF ANOMERIC PAIRS OF ADENINE NUCLEOSIDES FITTED TO TWO VIBRONIC PROGRESSIONS.

β-D-Pentofuranoside of Adenine				
Compound	β-lyxo	β-ara	β-xylo	β-ribo
CD maximum (nm)	257	257.5	259.5	264
$\mathcal{R}^{(1)}$ x 10^{40} (cgs-esu)	0	0	-0.5	-1.7
$\mathcal{R}^{(2)}$ x 10^{40} (cgs-esu)	-2.5	-4.3	-1.4	-0.6

α-D-Pentofuranoside of Adenine				
Compound	α-lyxo	α-ara	α-xylo	α-ribo
CD maximum (nm)	260	258.5	258	257
$\mathcal{R}^{(1)}$ x 10^{40} (cgs-esu)	0.74	0.16	0	0
$\mathcal{R}^{(2)}$ x 10^{40} (cgs-esu)	2.27	2.54	5.31	3.97

a - From figures 1a and 1b, p. 5490 of reference 44.

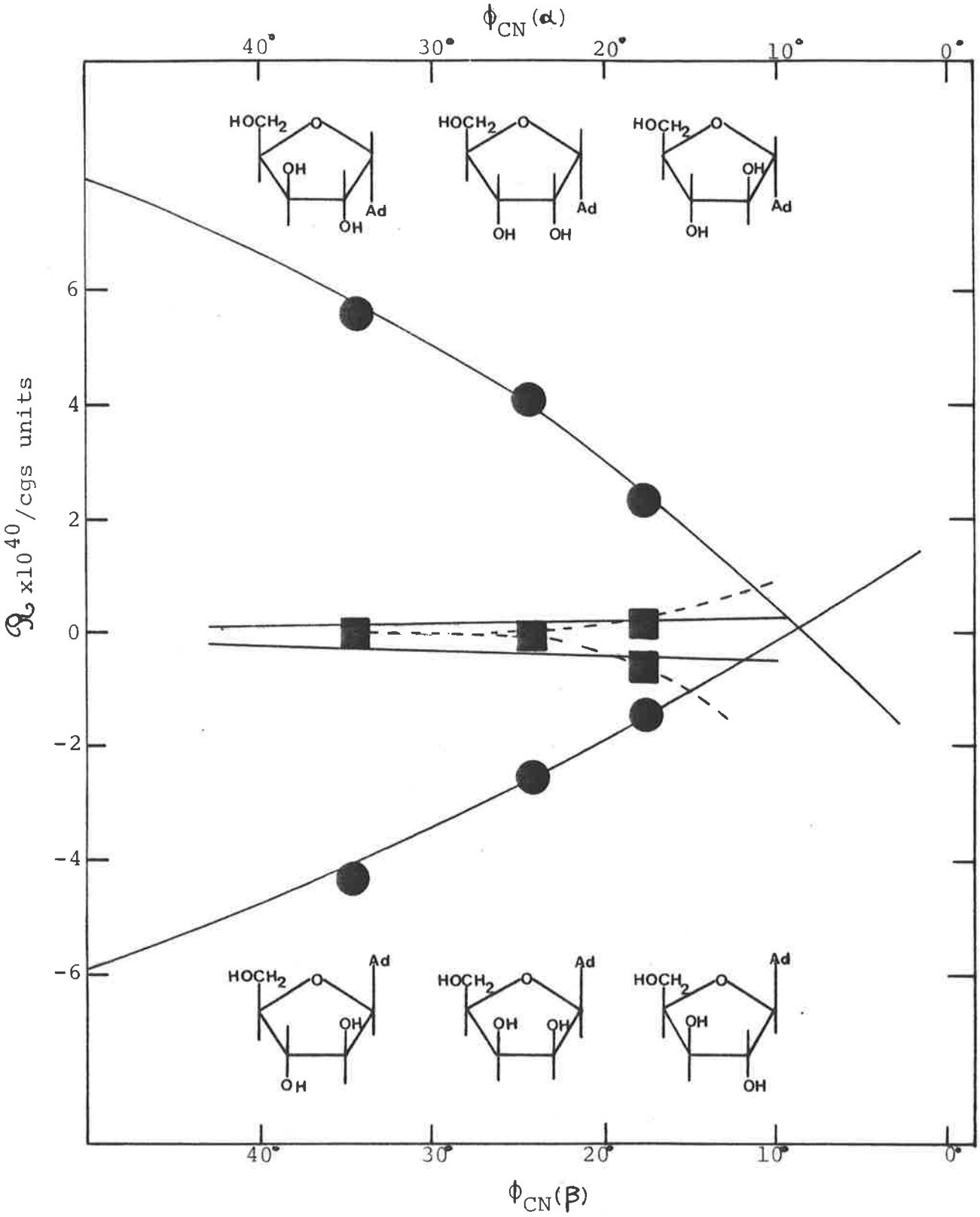

FIG.4.10 CORRELATION BETWEEN THE ROTATIONAL STRENGTH WITH THE GLYCOSYL TORSION ANGLE ϕ_{CN}.

Circles:high energy,long-axis polarised transition; squares:low energy,short-axis polarised transition; full lines are the calculated correlations; broken lines are the tentative correlations for the low energy transition.

envelope found when progressing from β-ara to β-xylo nucleosides does not occur with adenosine at high energy (fig. 4.9). We can test the precedent interpretation using other nucleosides. From figure 4.9, we can note that the CD envelope of AMP follows the trend observed with the other nucleosides. The magnitude of the rotational strength of the two transitions of AMP in table 4.2, enables us to predict from figure 4.10 a torsion angle, ϕ_{CN}, for AMP around -22°, value which is in perfect agreement with the X-ray data in table 4.3 and near the expected value for an anti conformation which places the H8 proton close to the 5'-phosphate (see paragraph 4.3.3). What about Adenosine? It has been established that it has a wide range of conformations with a preference for an anti conformation[90]. With our model, we find that the rotational strengths of the long and short axis polarised transitions enable us to estimate a torsion angle of approximately -10°, which may be considered to represent a reasonable weighted average angle for all adenosine conformers[90]. It is also close to the torsion angle ϕ_{CN} found in polynucleotides[67] (see table 4.3). If we look at published CD spectra of some other adenosine derivatives, we can see that for example 2'- and 3'-methyl adenosines[43] behave similarly, by showing a shift of the position of the CD maximum to lower energy and an absolute decrease in intensity in going from 2'- to 3'-methyl adenosine. This rules out possible interpretations concerning the hydroxyl groups of the sugar which could be thought to have formed some kind of interaction with the atoms of the adenine moiety and reinforces the importance of steric effects. The modification of the CD spectrum through steric effects can also be found in pyrimidine nucleosides such as cytidine and

β-D-ara-cytidine[91] or in uridine, β-D lyxo-, β-D ara-uracyl and α-D lyxo-, α-D ara-uracyl[89].

4.4 A Theoretical Approach

4.4.1 A Simple Model

Having established this empirical correlation, it seems to us of interest to test it against theoretical calculations. As we are in the presence of a large electric dipole moment, the optical activity is developed mainly by coupling the intense transition moments of the base with effective moments induced by them in the sugar through the coupled oscillator mechanism. Thus, the expression for the rotational strength[92] of the interacting transition moments is

$$\mathcal{R}_A = -\mathcal{R}_B = \frac{2\pi}{hc} V_{AB} \frac{\tilde{\nu}_A \tilde{\nu}_B}{\tilde{\nu}_A^2 - \tilde{\nu}_B^2} \vec{R}_{AB} (\vec{\mu}_A \times \vec{\mu}_B) \qquad (4.1)$$

where all symbols are as defined in appendix D. As we have already pointed out, the results of elaborate theoretical calculations depend on the choice of initial parameters used in the calculation such as the dipole strength and the transition moment direction. Furthermore the magnitudes of these parameters are adjusted to correspond to the experimental values[34,89,90]. This is why we are only concerned with justifying the trend observed in figure 4.10 and not about the magnitude of the rotational strength of the different compounds. The coupled oscillator theory in its simplest form seems to meet our needs and it has already been applied with success to conformational problems[93,94]. The equation for the geometrical interdependence of the two coupled transition moments or "geometric factor", using a dipole-dipole approximation, is[95]

$$V_{AB}\vec{R}_{AB}(\vec{e}_A \times \vec{e}_B) = \left[\vec{e}_A\vec{e}_B - \frac{3(\vec{R}_{AB}\vec{e}_A)(\vec{R}_{AB}\vec{e}_B)}{R_{AB}^2}\right]\frac{\vec{R}_{AB}(\vec{e}_A \times \vec{e}_B)}{R_{AB}^3} \quad (4.2)$$

where $\vec{e}_A$ and $\vec{e}_B$ are unit vectors oriented in the direction of the interacting transition moments and $\vec{R}_{AB}$ is the vector distance connecting the two coupled groups A and B. The transition moments of the base are treated as point dipoles and positioned at the center of the C4-C5 bond. Compounds having different substituents on the C2', C3' and even on the C5' carbon of the sugar have similar CD spectra, in particular intensity and overall shape: for example, 2'-3'-5'- o-triacetyl-adenosine, 2'-3'-o-diacetyl-adenosine, 2'-3'-o-isopropyl-5' acetyl-adenosine, 2'-3'-o-isopropyl adenosine[24] or 2'-3'-dideoxyadenosine[96]. These substituents are not likely to interfere with the range of sterically allowed torsion angles because of their location with regard to the sugar. This leads us to assume that the induced moment in the sugar is approximately the same for each anomeric set considered. Furthermore, it can be seen that this assumption is supported by theoretical calculations[40,89]. The details of the calculation of the geometric factor are described in the appendix E.

4.4.2 The Induced Moment in the Sugar

Our main preoccupation has been to find an effective moment (and in particular its direction) in the sugar moiety, which is positioned at C1' and whose interaction with the transitions of the base reproduces the trend observed in figure 4.10; that is to say, we were seeking to obtain, with increasing the value of the torsion angle ϕ_{CN}, a decrease of the calculated rotational strength for the long axis polarised transition of the adenosine base and an increase

for its short axis polarised transition. We must add that the choice of effective moment directions in the sugar is particularly limited if one wants to satisfy, at the same time, the trend for the two transitions of the base. The optimum result for each transition was normalised separately (due to their different dipole strength) in order to compare them with experimental rotational strengths. The fit in figure 4.10 for the long axis polarised transition is satisfactory both for the α and β configurations. For the short axis, although the trend is present, agreement is rather poor; this could be due to the simplicity of the model used in particular in taking the position of the induced moment origin at the C1' atom and not delocalized over all the bonds of the sugar[34,89]. The moment induced in the sugar has its origin in C1' and points towards the C2' atom. It forms an angle with the C1'-O1'-C4' plane of the sugar as shown in figure 4.11. This angle has approximately a mirror-image relationship with respect to the base in the α and β configurations. This is in perfect agreement with the exo conformation found both experimentally[68] and theoretically[97] in the α nucleosides. (endo conformation found for β nucleosides[68].) The finding that the magnitude of the experimental rotational strength is more important for the α than the β nucleosides can be explained by a decrease of the angle defined by the induced moment and the plane of the sugar in the case of the α nucleosides. We can note that this decrease in angle seems to be influenced by the position of the C5' atom in relation to the sugar plane as it can be seen in figure 4.11. It will be of vital interest to verify experimentally the validity of this last statement; if this is so, then the CD spectrum of the α-L and β-D

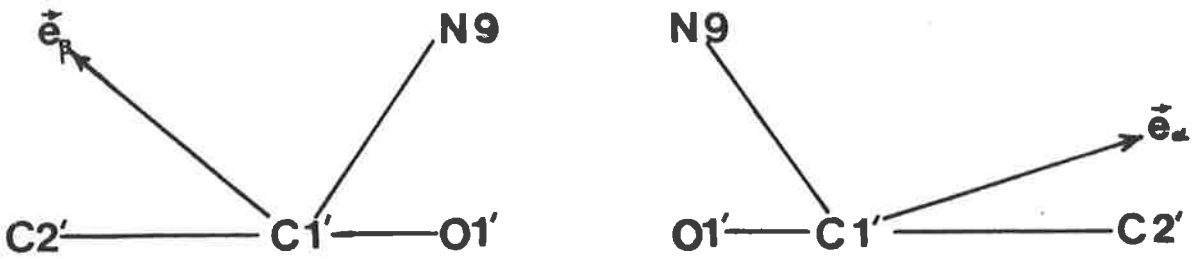

FIG.4.11 EFFECTIVE MOMENT DIRECTIONS IN THE FURANOSE MOIETY.
Both moments as well as the C1'-C2' bond are in the plane of the paper.
In the β-anomer, the C4'-C5' bond(not represented in the figure) is on the same side of the sugar plane as the C1'-N9 bond; in the α-anomer it is on the opposite side .

nucleosides should be the exact mirror image of the α-D and β-L nucleosides respectively and furthermore the intensity of the 260 nm CD band of the nucleosides in the α configuration should be more intense than that of the β configuration. Although the CD spectrum of all the compounds mentioned have not been studied so far in the case of the adenine base, the above statement can be verified in the case of the guanine base[84] whose electronic transitions[23,89,99] are similar to those of adenine (see paragraph 4.6).

The coupled oscillator model, although used in its simpler form, was able to reproduce the trend and signs of the CD spectrum of the adenosine derivatives as a function of the torsion angle, ϕ_{CN}, and the results obtained were as satisfactory as those obtained previously using a more elaborate model[100].

4.5 The Geometry of the Platinum-Adenosine Complex

Since 1969 when Rosember *et al.*[101] discovered that *cis*-diamminedichloroplatinum(II) showed antitumor activity whereas the *trans* isomer was inactive, a great amount of research was carried out using these products[102,103] or similar ones[104] in order to extend their range of promising anticancer activity. It was shown that the two isomers, the *cis* and the *trans* platinum, were able to bind to DNA[105] and to individual bases[106]. The site of reaction of the platinum on the base has retained the attention of numerous research laboratories and has been investigated using various methods[106-111]. In short, it can be said that the *cis*-platinum forms a bidentate chelate with either the $6NH_2$ group and the N7 atom or the $6NH_2$ group and the N1 atom of adenosine and that the *trans*-isomer binds monofunctionally to the N7 or the N1 atom of adenosine. Determining the exact

position of binding on the base is essential in order to find out the mechanism of interaction of the platinum with the dinucleoside[112] or DNA[113,114] where the existence of cross links between the $6NH_2$ group of adenine by the platinum was postulated.

Mason[21] was able to correlate the effect of various substituents attached to the purines with the changes in their absorption spectra. The use of this method will be most useful in determining the position of attachment of the platinum as we have just examined the electronic properties of adenosine and in particular the frequencies and polarization of the different transitions. From table 4.2, we can see that, on binding of the platinum to the base, the shift to the red (or bathochromic effect) of the low energy transition of adenine ($\Delta\tilde{\nu} \approx 1000\ cm^{-1}$) is more important than the shift of the high energy transition ($\Delta\tilde{\nu} \approx 600\ cm^{-1}$). In the same way, we observe a hyperchromic effect for the low energy transition on binding of the platinum. All of these correlations, in which the low energy transition polarised along the short axis of the adenine base is more affected on the platinum binding than the high energy transition polarised along the long axis of adenine, imply that the N7 atom, transversally disposed in relation to the long axis of the molecule, will be a more favourable binding position than the N1 atom, longitudinally disposed. Moreover, looking at table 4.2 we can see that for both transitions the anisotropy factor g, which we showed (append.D) as being dependent only on geometrical factors, is similar for adenosine and *cis*-platinum adenosine complex on the one hand and similar for AMP and *trans*-platinum adenosine complex on the other. As it was

emphasized that the magnitude of CD spectrum is a good estimation of the torsion angle, ϕ_{CN}, between the base and the sugar, it can be inferred that the similarity in g values also reflects a similarity in ϕ_{CN} values. The bidentate *cis*-platinum binds to the $6NH_2$ group as well as to the N7 atom of the adenosine. It follows that the square planar *cis*-platinum(II) isomer will be fixed in the same plane as the one of the adenine base. Thus it will not cause any more restrictions in the relative free rotation of the sugar than in adenosine. As for the monodentate *trans*-platinum(II), it binds to the N7 atom of adenosine and may have one of its amino groups in close contact with the C5'-OH group of the sugar causing some restriction of rotation around the glycosyl bond as in the case of AMP. On the other hand, the *trans*-platinum binding to the N1 position of the adenine base, due to its distance from the sugar, could not have affected the rotation of the sugar around the glycosyl bond.

4.6 Guanosine

Among all the bases in Nucleic Acids, guanine occupies a special place. Indeed it has been shown that the biological effects of a wide variety of drugs such as antibiotic, anticancer and antimalarial as well as carcinogen have their primary origin in an interaction with the guanine base[115-118]. The two electronic transitions of guanosine, called the B_{2U} and B_{1U} transitions[46,84,119] are more explicit than in the case of adenosine. We have carried out the same procedure used previously to extract the different parameters characteristic of the absorption and CD envelopes of the near U-V spectrum. The value of the separation between consecutive bands, V, was taken to be the frequency

of the most intense Raman peak (1490 cm^{-1})[120]. The similarity between the CD and the absorption spectra in figure 4.12 is also reflected in table 4.5 by the parameters characterising their envelopes. At the opposite of adenosine, the two progressions contribute to the overall envelope and are both negative in CD. In figure 4.13 we have used these two progressions, of equal intensities but opposite signs, to produce a theoretical MCD spectrum. It looks similar to the experimental ones[23,119] with maxima at 277 nm and 247 nm and a crossover at 261.5 nm. This agreement, already found for the MCD spectrum of adenosine, shows clearly that the mechanism responsible for MCD[23] is the mixing of the excited states of the B_{2U} and B_{1U} transitions of the purine by an external magnetic field. The high intensity of the MCD bands suggests that the two transitions considered are rather perpendicular to each other in agreement with stretched films studies[49] and polarization of fluorescence measurements[50,121]. Furthermore, it has been found that the low energy transition is rather short axis polarised while the high energy transition is long axis polarised[98,99]. Theoretical calculations give inverted polarization directions for the B_{2U} and B_{1U} transitions although the calculated energies of transition are in agreement with experimental ones[122].

Although the electronic properties of guanosine look similar to the one of adenosine, no conclusion on the possible relations existing between the CD spectrum and the glycosyl angle can be made because of the wider range of conformation allowed in the case of guanosine[123] and also because of the lack of comparison with guanosine derivatives.

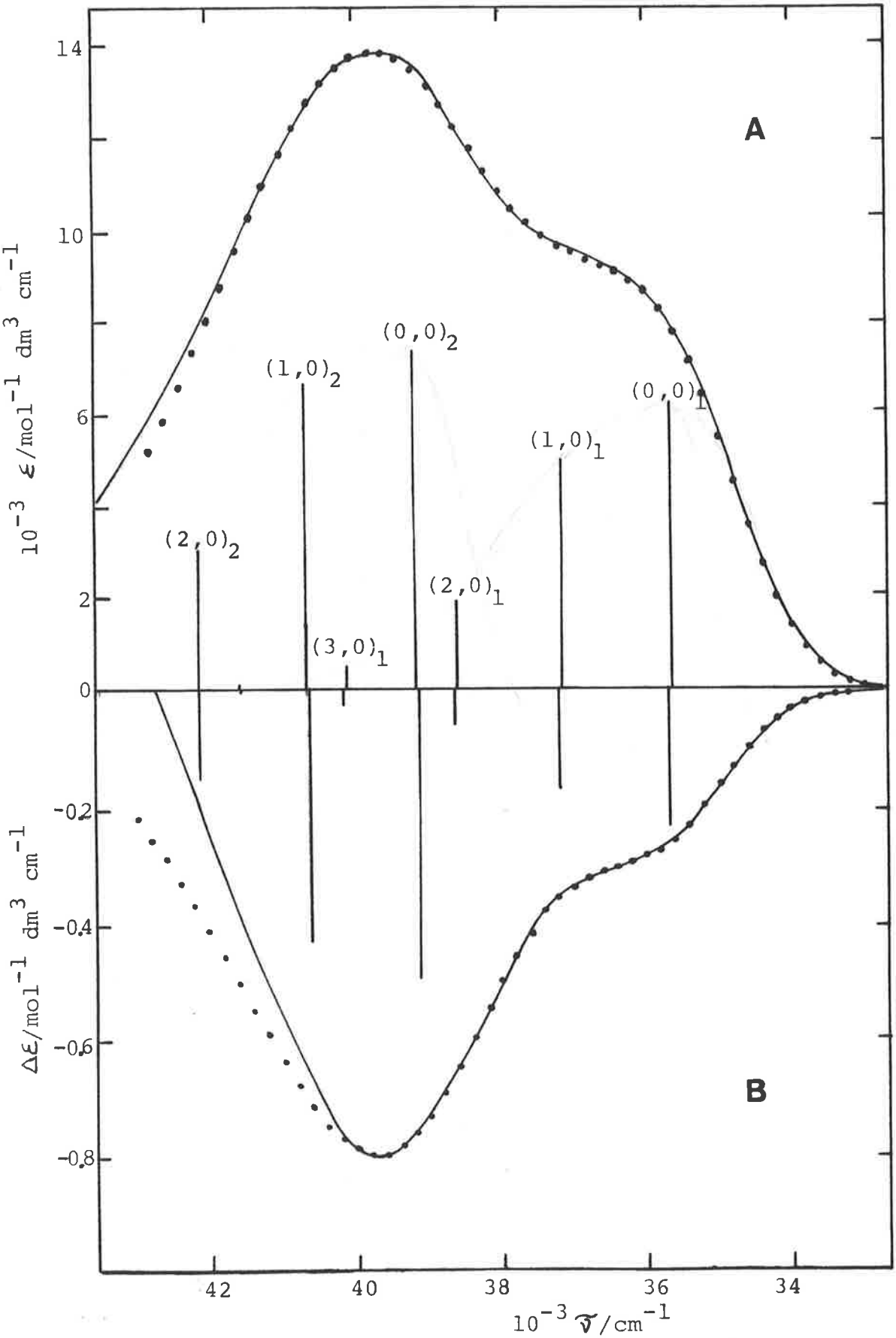

FIG.4.12 SPECTRA OF GUANOSINE.
Full lines: experimental absorption (A) and CD (B) spectra; dots, spectra fitted to an harmonic progression with band positions and intensities indicated by the vertical lines.

Table 4.5 FITTING PARAMETERS FOR THE GUANOSINE SPECTRA.

parameters \ methods	absorption	circular dichroism
$\tilde{\nu}_{oo}^{(1)}$ (cm^{-1})	35,600 (20)	35,700 (76)
$\tilde{\nu}_{oo}^{(2)}$ (cm^{-1})	39,150 (100)	39,100 (140)
$X^{(1)}$	0.80 (0.05)	0.75 (0.20)
$X^{(2)}$	0.92 (0.10)	0.87 (0.20)
$b_g^{(1)}$ (cm^{-1})	2220 (35)	2010 (90)
$b_g^{(2)}$ (cm^{-1})	3020 (160)	2600 (360)
	$\varepsilon_{oo}^{(1)}$ = 6160 (80)	$\Delta\varepsilon_{oo}^{(1)}$ = 0.23 (0.01)
	$\varepsilon_{oo}^{(2)}$ = 7160 (400)	$\Delta\varepsilon_{oo}^{(2)}$ = 0.49 (0.05)

The molar absorptivity (ε) and molar circular dichroism ($\Delta\varepsilon$) are given in dm^3 per mol cm^{-1}.

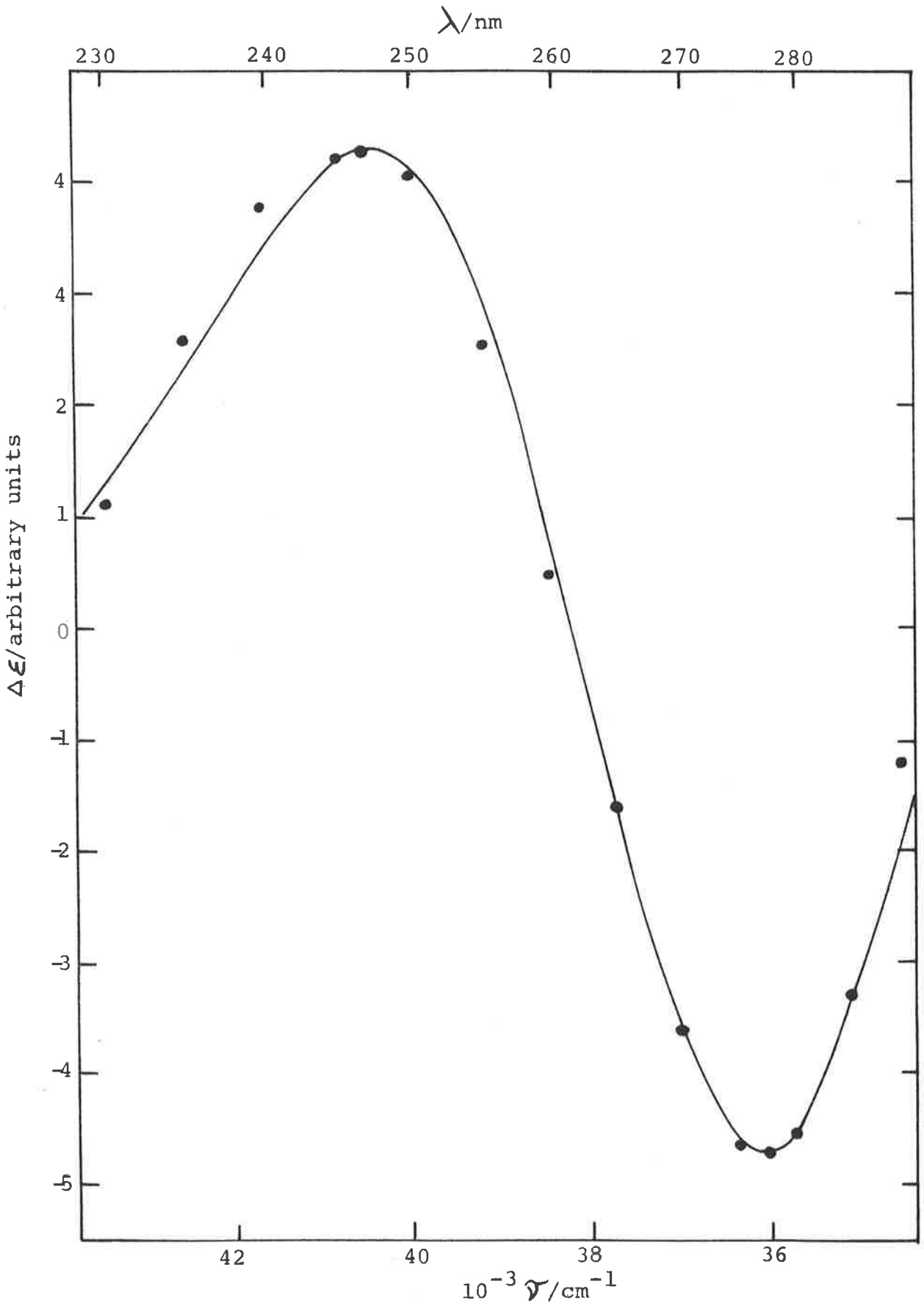

FIG.4.13 MCD SPECTRUM OF GUANOSINE.
Full curve:calculated as explained in the text;
circle:data extracted from figure 2 of reference 23.

4.7 Conclusion

The various parameters that we have extracted using different approaches are characteristic of the electronic properties of the nucleosides studied and permit us to give a consistent interpretation of the spectra involved in our study. They also constitute a definite starting point for further theoretical calculations and above all for the interpretation of the electronic spectra of Nucleic Acids.

5. DINUCLEOSIDES

5.1 Introduction

The study of dinucleosides is a starting point in order to understand the structure of more complicated Nucleic Acids such as polynucleotides. In a dinucleoside as it would occur in natural Nucleic Acids, the two monomeric nucleosides are joined together by a 3'→5'-phosphodiester linkage as in figure 5.1.

This linkage is of importance because the distances and torsion angles of the bonds composing it will define the conformation of the Nucleic Acids, that is to say: the screw axis of the dimer, the amount of overlap of the two bases and finally the conformation of the nucleoside unit.

The dinucleoside has some properties similar to those of the monomeric moiety but some new ones emerge that are characteristic of the association or stacking between the bases. It has been shown that perturbations applied to the system, such as adding alcohol, decreasing the pH to an acid value or raising the temperature, reduce the stacking of the bases.

We will be mainly concerned in this study with the spectroscopic properties of adenylyl-(3'→5')adenosine (APA) and deoxyadenylyl-(3'→5')deoxyadenosine (dApdA) as we have just studied their monomeric constituents.

5.2 Spectroscopic Methods and their Relation to Molecular Structure.

Interest for the study of dinucleosides comes from the important repercussions they can bring in the understanding of Nucleic Acids but also from the fact that no consistent conclusions about their conformations have as yet been made

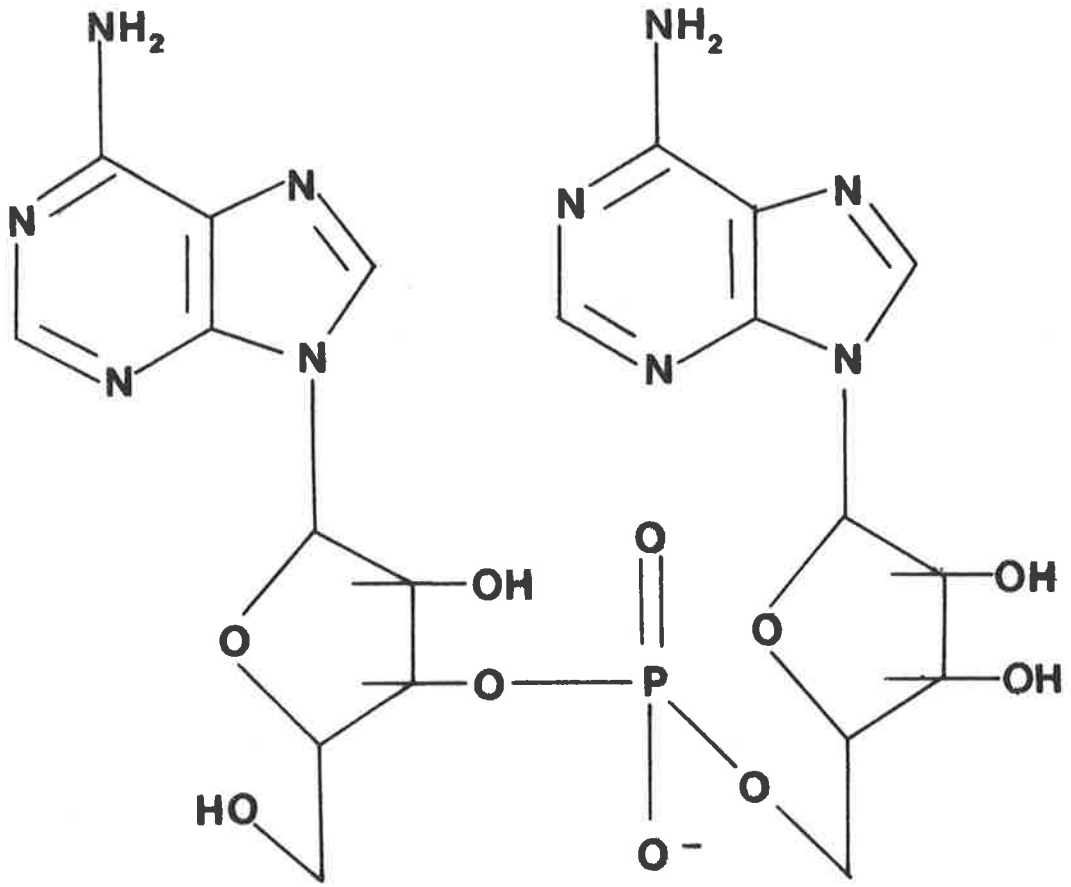

FIG.5.1 STRUCTURE OF ADENYLYL-(3'-5')-ADENINE (APA).

through the use of different methods of investigation.

We will first make a survey of what is known of this particular problem. Most of the methods of investigation have been based on spectroscopy, that is to say: absorption, circular dichroism (and ORD) and nuclear magnetic resonance (NMR). Attempts to establish a common basis for the interpretation of the spectral data has been the major preoccupation of a lot of research[126-128].

5.2.1 Absorption Spectroscopy

From absorption measurements, one can calculate the percentage hypochromism[129] which is defined as

$$H\% = (1 - \frac{f_D}{f_M}) \times 100 \qquad (5.1)$$

where f_D and f_M are the oscillator strength of the dinucleoside and the monomer respectively. This method has the advantage of being very accurate but the change in the spectrum on stacking is rather small (H% is less than 10% generally). Assuming a model of dinucleoside where the plane of the bases, labelled 1 and 2, are parallel, the vector $\vec{R}_{AB}$ connecting the centre of the two bases being perpendicular to the plane of the bases, Glaubiger *et al.*[130] were able to express the hypochromism of a dinucleoside as

$$H(\theta) = \frac{2}{|R_{AB}|^3}[\alpha_A \cos^2(\theta + \phi) + \alpha_B \sin^2(\theta + \phi)] \qquad (5.2)$$

where θ is the angle between the transition moments, α_A and α_B are the polarizabilities at the frequency considered along two principal axes e_A and e_B which lie in the plane of the base and ϕ is the angle between the transition moment of base B and e_A. For a homodimer like APA, it is a good approximation to consider the adenine bases to be isotropic with respect to

the polarizabilities ($\alpha_A \approx \alpha_B \approx \alpha$)[128,130]. With this assumption the θ-dependence of hypochromism disappears and its expression is reduced to

$$H(\theta) = \frac{2}{|R_{AB}|^3}.\alpha \qquad (5.3)$$

5.2.2 Circular Dichroism

Circular dichroism has been extensively exploited experimentally[18,126,127,130-136], and one has tried to interpret the results on a theoretical basis[130,137-141].

The rotational strength[130] associated with the coupling of two electric transition moments may be written as

$$\mathcal{R}^{\pm} = \pm\frac{\pi\tilde{\nu}_o}{2}\,\vec{R}_{AB}(\vec{\mu}_A \times \vec{\mu}_B) \qquad (5.4)$$

where $\vec{\mu}_A$ and $\vec{\mu}_B$ are the transition moments of the bases A and B respectively, $\tilde{\nu}_o$ is the frequency of the transition considered and $\vec{R}_{AB}$ is defined as in equation (5.2). If the planes of the bases are parallel and furthermore if $\vec{R}_{AB}$ is perpendicular to both base planes, the expression for the rotational strength is simplified and becomes proportional to

$$\mathcal{R}^{\pm} = \pm\frac{\pi\tilde{\nu}_o}{2}\,R_{AB}\mu_A\mu_B \sin\theta \qquad (5.5)$$

where θ is the angle between the transition moments. We can note in this expression the dependence of the Rotational strength on the angle θ unlike in the case of hypochromism (5.2).

The use of all these formulae should be subject to some precautions and the assumptions made should be kept in mind. In particular, comparison of the hypochromism of different compounds at room temperature could lead to erroneous interpretations due to the possible monomeric

contribution to the absorption spectrum at this temperature. Understanding of dimeric and monomeric properties is essential before any attempt at interpreting a spectrum is made and then a critical choice of the parameters used should be made.

5.2.3 Nuclear Magnetic Resonance Spectroscopy

The nuclear magnetic resonance spectrum contains a considerable amount of information about the conformation of dimers. The protons of the base and the sugar give characteristic NMR peaks. It is possible using various techniques such as specific deuteration and spin decoupling experiments[142], to distinguish between each proton in the base and also between protons of the two bases[143]. One important indication of the stacking is revealed by the dimerization shift representing the change in the chemical shift of each proton, a change which is caused by the interaction of the two bases in the dinucleoside compared to that in the monomer. The only problem encountered using NMR comes from the need to use high concentrations of compounds; this can lead to erroneous interpretations of results because of the possibility of aggregation.

5.3 Conformational Model for Dinucleosides

The decrease in absorbance or hypochromicity in going from the monomer to the dinucleoside spectrum is consistent with the bases being stacked together[126,128,129,144-146] (overlapping of their π orbitals). Circular dichroism as well, with its characteristic "S-shaped" spectrum, shows that the transition moments of the two bases in the dinucleoside interact. From the sign of the CD, we can conclude that the bases are in a right handed conformation. The good

agreement between experimental CD spectra and those calculated using the geometry of B-DNA[137-140,147] and that of RNA[140,147] where the bases are in anti-conformation, spaced 3.4Å apart and having a right handed conformation with an angle of 36° between them, confirm the conformational model of dimer as being similar to the one found in helical Nucleic Acids.

NMR studies indicate the anti-conformation of the nucleoside[143,148-151]. A simultaneous use of model building, dimerization shift data (due to the diamagnetic anisotropy of the neighbouring base) and calculated isoshielding curves can give a good representation of the structure of the dinucleoside: bases parallel to each other separated by a distance of 3.4Å, having an anti-conformation and a right handed screw axis[136,152].

Although NMR brings a more refined picture of the conformation of dinucleoside in comparison with UV and CD measurements, we must not forget that the structure derived is only the representation of the time-average results of a dynamic phenomenon. In reality a wide range of conformations is present and there is a rapid interconversion of the species[126,153,154].

To overcome this problem, some theoretical methods have been developed recently; these are based on potential-energy calculations coupled with the minimization of the total energy. These works led to the proposal of there being several possible stacked conformations having an A-RNA, Watson-Crick and A-DNA type and some conformations being unstacked[155-158]. Although these methods show good promises, they are as yet not sufficiently refined to be of use in our studies. For example nearly no difference in APA

and dApdA conformation is found, unlike with spectroscopic measurements. In particular Ts'o research group has carried out extensive investigations on APA and dApdA using combinations of spectroscopic methods with the aim of resolving their conformational differences. From hypochromism and PMR data, they have suggested that the steric hindrance of the 2'-OH group in the 3'-ribosyl moiety of APA forces the screw axis of the bases to become more twisted (45° - 50°) and thus prevent an extensive overlap of the bases unlike with dApdA where the bases are nearly parallel (15°) and have a high amount of overlap[136].

5.4 Conformational Dynamics

5.4.1 Choice of a Model

Temperature studies have been carried out to try to understand the conformational problem of the dinucleosides. Although optical methods such as absorption or CD fit a two-state process[126,127,131,133,159-161] (equilibrium between a stacked and an unstacked form), the NMR data show clearly the existence of several conformations[152-154] whose number increases with temperature. A stacked form exists at very low temperatures but as the temperature increases so do the oscillations of the bases with respect to one another and the nucleoside moieties are more often found in an unstacked conformation. Nevertheless, we shall show that the two-state model not only fits the spectral data quite well but it is also capable of physical interpretation.

5.4.2 The Two-State Model

Our work will not be confined to repeat some previous works[126,127,131,133,159-161] on the same subject, but our

task will be principally to obtain the spectrum of the stacked form by using separately two techniques, CD and absorption spectroscopy, and then to extract from it some geometrical information that was previously only obtained using high resolution NMR measurements associated with sophisticated methods of interpretation.

Although the two-state model is an oversimplified model, it has proved to be adequate in the interpretation of the evolution of the optical spectra of absorption, CD or ORD with temperature and above all it is the only simple model available that enables us to reach the lower temperature spectrum of the stacked form using standard conditions.

5.4.3 Its Theory

As the temperature is raised, all the optical spectra are modified. We can see in figure 5.2 an increase in intensity of the absorption spectrum as well as a progressive shift in the maximum toward that of the monomeric constituents and in figure 5.3 we can see a decrease in intensity of the CD spectrum which envelope is characteristic of a dimer spectrum. We can also see a decrease in the value of the dimerization shift of various protons in NMR spectroscopy as well as the increase in the coupling constants of the protons toward those of the corresponding monomers[136]. All of this behaviour can be interpreted as an equilibrium between a stacked form or dimer predominant at low temperature and an unstacked form at high temperature.

$$\text{stacked} \underset{\longleftarrow}{\overset{K(T)}{\rightleftharpoons}} \text{unstacked}$$

The equilibrium constant K(T) can be related to thermodynamic parameters with the use of the Van't Hoff equation

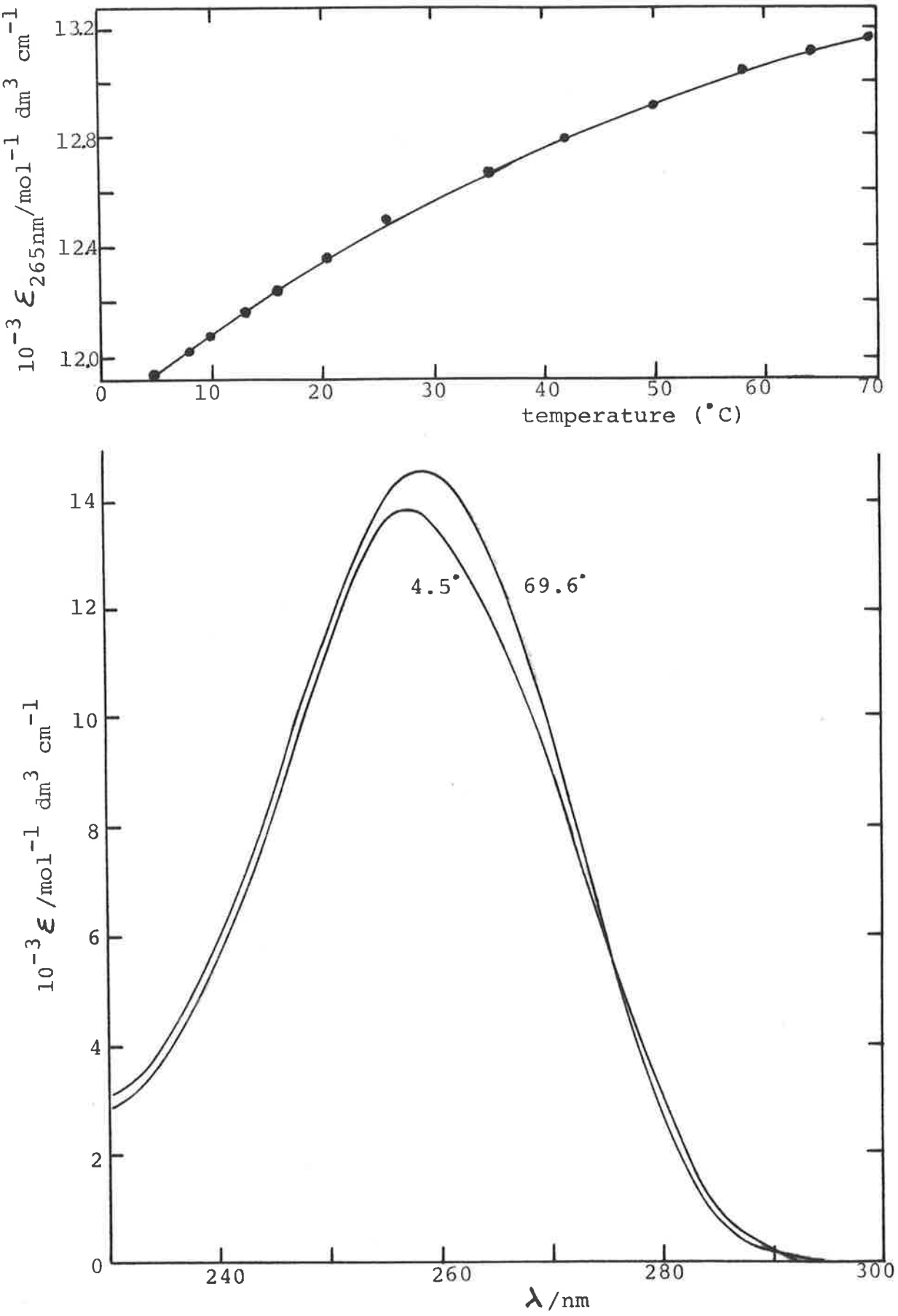

FIG.5.2 TOP: MOLAR ABSORPTIVITY VERSUS TEMPERATURE PROFILE FOR APA.
BOTTOM: ABSORPTION SPECTRA OF APA AT THE TWO EXTREME TEMPERATURES STUDIED.

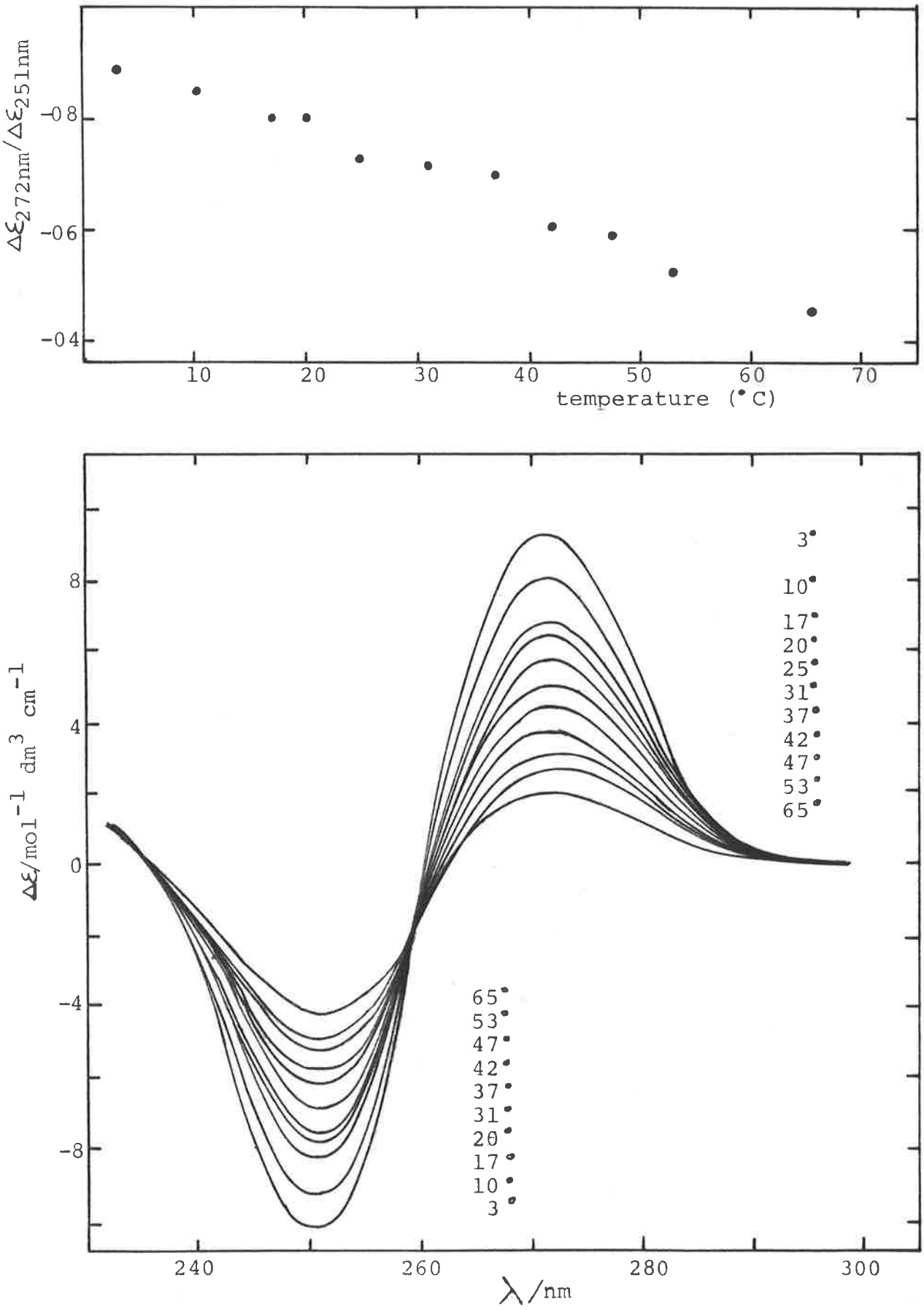

FIG.5.3 CIRCULAR DICHROISM OF APA AS A FUNCTION OF TEMPERATURE. The spectra show the presence of two isosbestic points at 259.2nm ($\Delta\varepsilon$=-2.0±0.1 mol^{-1} dm^3 cm^{-1}) and at 235nm.

$$\ln K(T) = \ln \frac{\alpha_u - \alpha_{(T)}}{\alpha_{(T)} - \alpha_s} = \frac{\Delta S^\circ}{R} - \frac{\Delta H^\circ}{RT} \qquad (5.6)$$

where $\alpha_{(T)}$ represents a measured property of the equilibrium system (for our study, the absorbance A^λ or the sum of the intensity of the positive and the negative CD bands $|\Delta\varepsilon^+|^\lambda + |\Delta\varepsilon^-|^\lambda$), the subscript u and s refer to the unstacked and stacked state respectively, ΔH° and ΔS° are the standard enthalpy and standard entropy of the stacking equilibrium. We will assume that the properties α_u and α_s as well as ΔH° and ΔS° are independent of the temperature[159].

A method of computing ΔH° and ΔS° as well as the optical parameters was developed (appendix C). Iterative least square methods have been used quite successfully to work out the four parameters of equation (5.6), ΔH°, ΔS°, α_u and α_s[127,133,161]. However the uncertainties in the determination of the parameters depend on their numbers, on the number of spectra recorded at different temperatures and on the accuracy of their measurements. Unlike these previous studies, as we are mainly concerned in the determination of the shape of the stacked form spectrum, with enough accuracy to be able to analyse it, we decided to remove the last degree of freedom in equation (5.6) by reducing the number of parameters to three ΔH°, ΔS° and α_s[159]. We used the good linearity of the high temperature absorbance data to extrapolate the unstacked form spectrum to infinite temperature. This procedure is more justifiable than an arbitrary choice of the unstacked form spectrum as being that of the monomeric constituents.

5.5 Analysis of the Temperature Dependent Spectra of APA.

5.5.1 Effect of Temperature on the CD Spectra of APA.

Figure 5.3 shows the CD spectra of APA. The trend with temperature is similar to the ones previously investigated (figure 5.4). CD spectra are generally a composite of different CD contributions emanating from the various interactions within the molecule[95]. As we are in the presence of a strongly allowed transition (the high energy transition of the X band of the Adenine molecule), we will only consider the contribution of the CD coming from the base-base interaction through the coupling of their transition moments as well as the one from the base-sugar interaction investigated in paragraph 4.

From the CD spectra in figure 5.3 two well enough defined isosbestic points[127,133] emerge; one at 259.2 nm with a $\Delta\varepsilon$ of -2.0 and the other one at 235 nm. They are a good indication of the presence of an equilibrium between two predominant spectroscopically distinct species: a stacked form at low temperature and an unstacked form at high temperature. Due to the distance between the two bases, the unstacked form will not contribute to the CD spectrum except by the base-sugar interaction. At this stage, it will be appropriate to check the validity of our assumption. Thus, we will separate the two different kinds of interactions, that is to say we subtract from the overall CD spectrum a monomeric CD spectrum, determined previously, having a $\Delta\varepsilon$ of -2.0 at 259.2 nm and corresponding to the high energy transition of the X band of Adenosine. In fact, as the bases in APA are in anti-conformation[143,148-151], a look at figure 4.10 (paragraph 4.3.4) reveals that a high

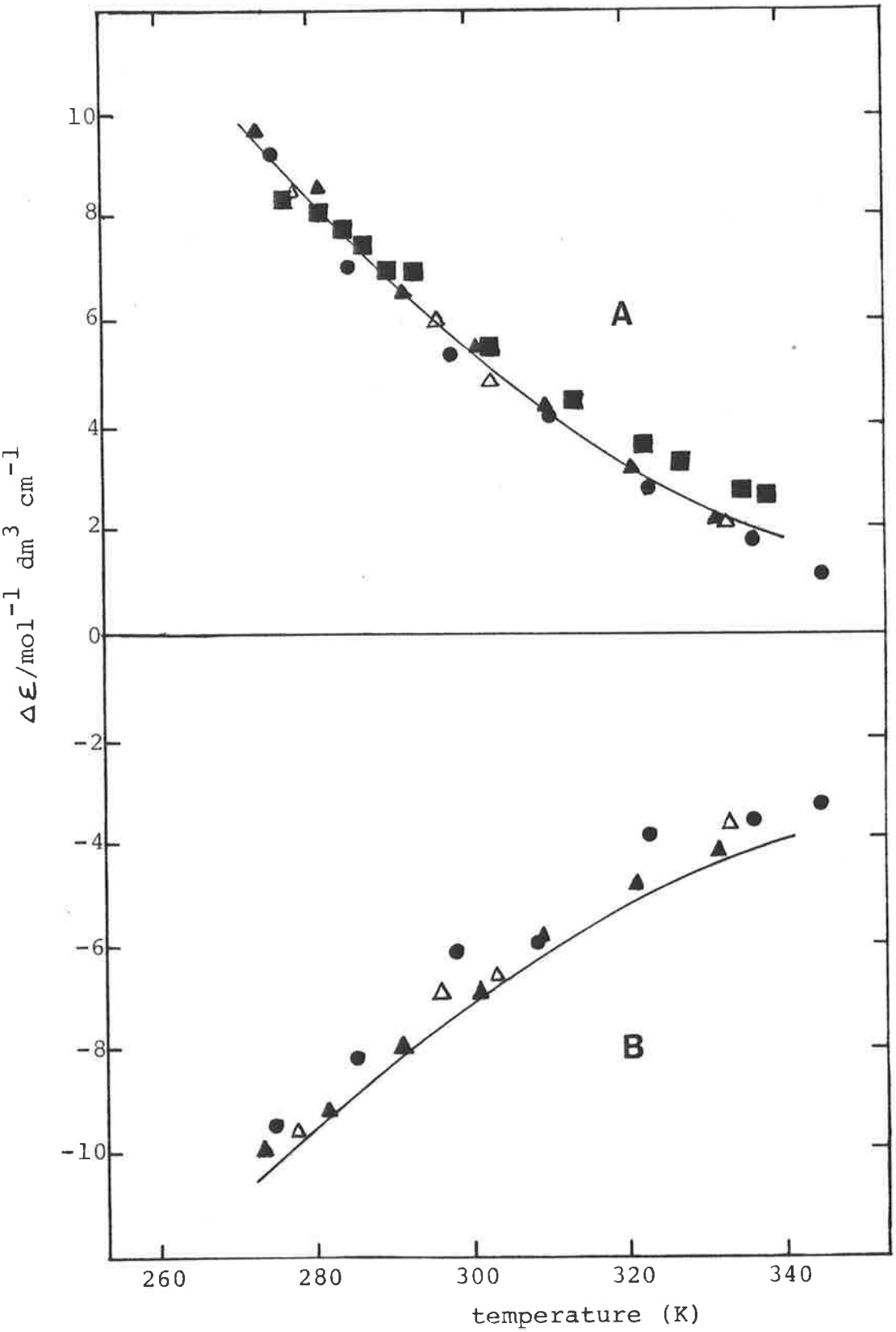

FIG.5.4 MOLAR CIRCULAR DICHROISM OF THE POSITIVE (A) AND NEGATIVE (B) EXTREMA OF THE CD SPECTRUM OF APA AS A FUNCTION OF TEMPERATURE.
(Δ), data from Kondo et al[128]; (▲), data from Olsthoorn et al[133]; (■), data from Powell et al[127]; (●), data from Baker et al[173]; (—), this study.

value of $\Delta\varepsilon^{259.2\ nm} = -2.0$[$\mathcal{R} = -4.6 \times 10^{-40}$ cgs units, corresponding to a torsion angle around the glycosyl bond $\phi_{CN} \approx -37°$] can be only achieved with the high energy transition of the X band. We note that Olsthoorn *et al.*[133], using four unknowns in equation (5.6), derived an unstacked CD spectrum of monomeric appearance with a maximum located between 250 and 260 nm (as is the case with the high energy transition of Adenosine in the X band) and having a value of $\Delta\varepsilon$ around -2. As we can see in figure 5.5, the resultant CD spectra, characteristic of the pure dimer, are identical in shape and have a ratio of the $\Delta\varepsilon$ maximum of the positive peak to that of the negative peak which is constant as the temperature increases and equal to 1.24 ± 0.02.

Using the vibronic exciton theory discussed in paragraph 2.2 as well as the program developed in the appendix C, we are able to compute a dimer CD spectrum with the use of the monomeric parameters derived from the absorption spectrum of adenosine (table 4.2 in paragraph 4.22). In changing the magnitude of the exciton coupling parameter, it is possible to alter the shape of the compute CD envelope and in particular the ratio $\frac{\Delta\varepsilon^{+}_{max}}{\Delta\varepsilon^{-}_{max}}$. We found that an exciton coupling parameter of 0.45 (600 cm^{-1}) to be the most suitable value for the fitting of the experimental dimeric spectra (figure 5.6). The poor fit for wavenumbers less than 41,000 cm^{-1} can be explained by the contribution to the CD spectrum of transitions of higher energies, in particular the one whose (0,0) band is situated near 41,500 cm^{-1} (paragraph 4.2.3). The computed spectrum has to be shifted 300 cm^{-1} to the red to coincide with the experimental spectrum. This shift occurs because of the Coulombic

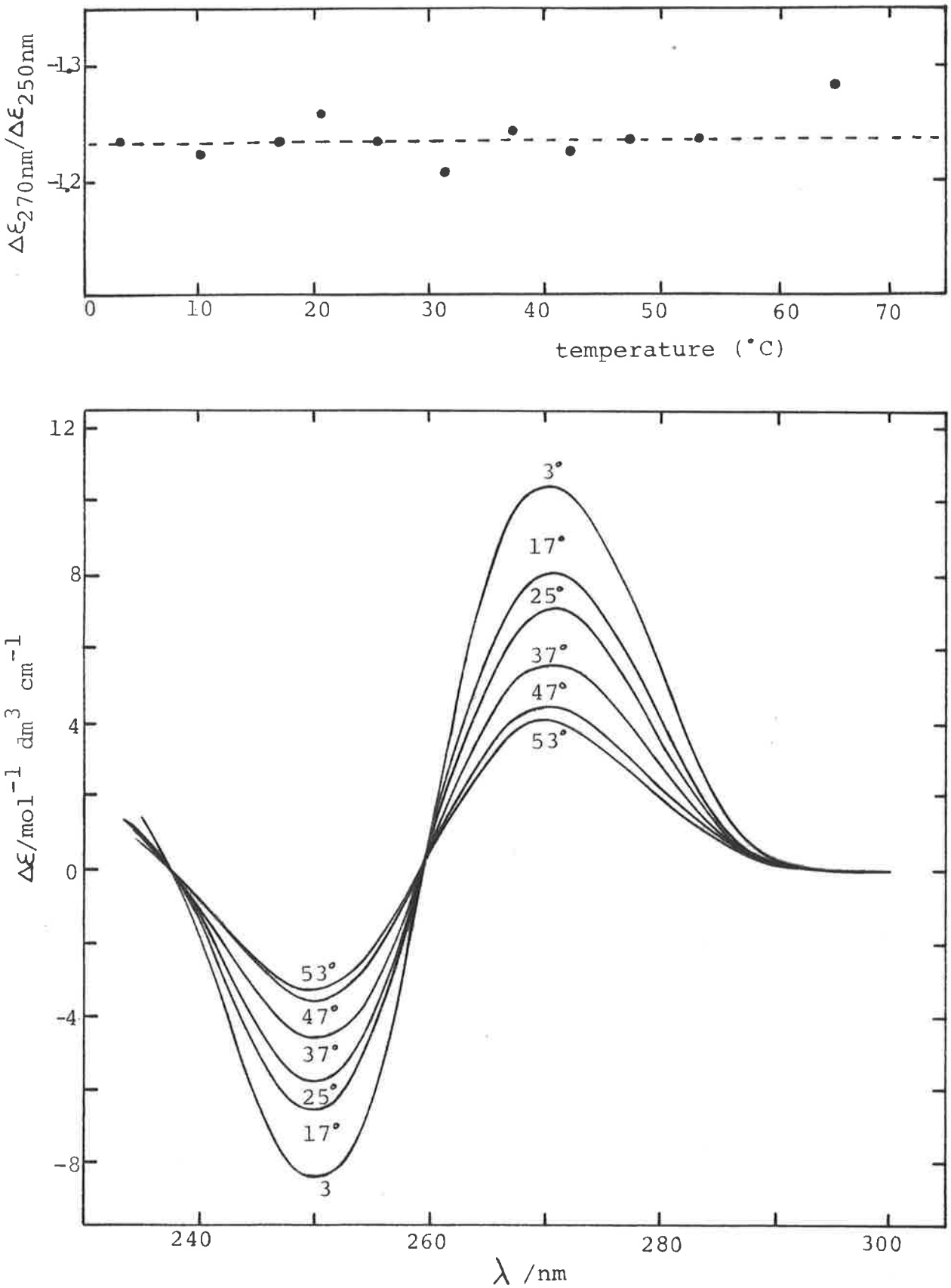

FIG.5.5 CIRCULAR DICHROISM SPECTRA OF APA IN A STACKED FORM AS A FUNCTION OF TEMPERATURE. Each curve is computed as the molar CD per mole of base residue minus the molar CD of the monomer, $\Delta\varepsilon$(ApA)-$\Delta\varepsilon$(A), with $\Delta\varepsilon$(A) at 259.2nm equal to -2.0 mol^{-1} dm^3 cm^{-1}.

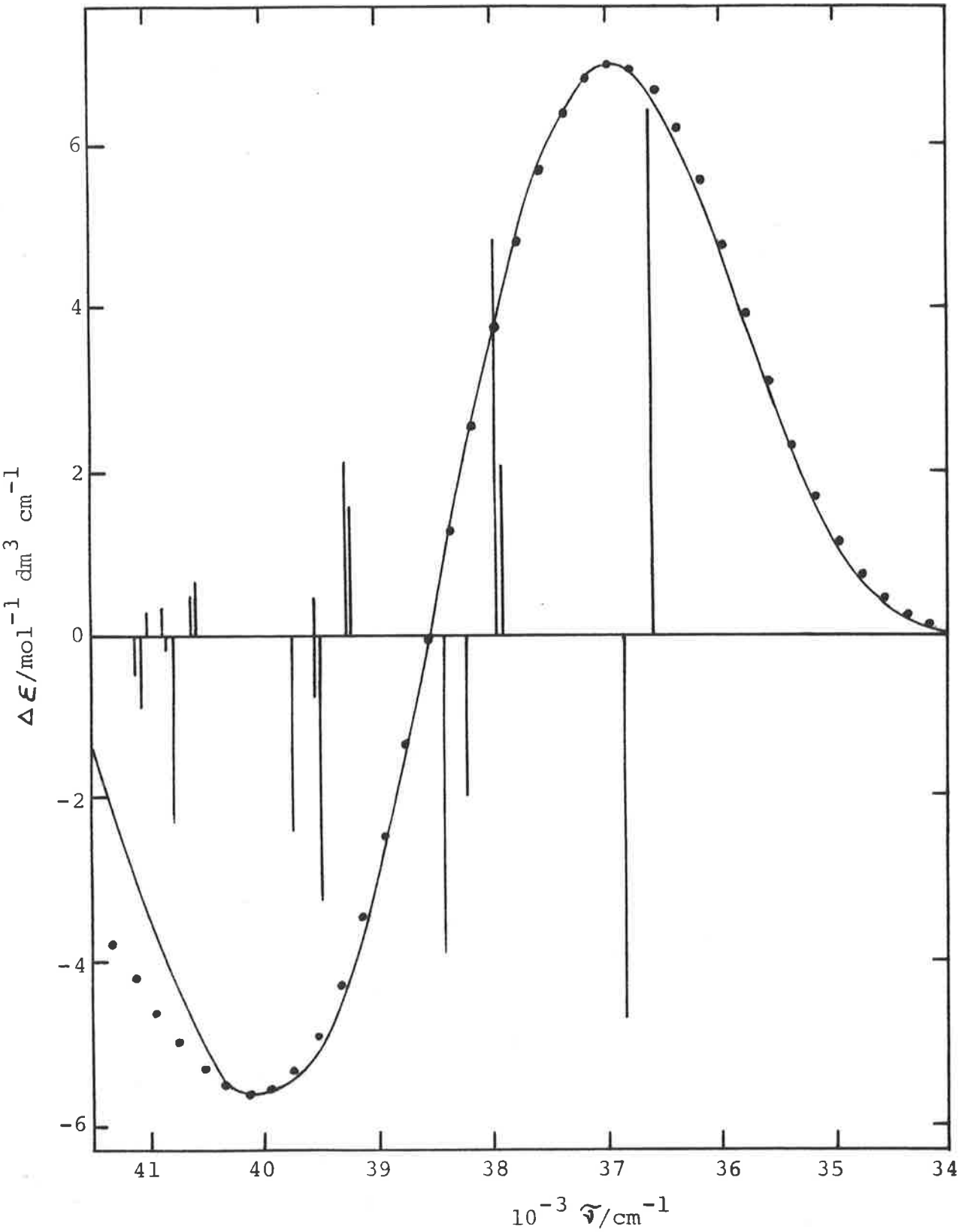

FIG.5.6 DIMERIC CIRCULAR DICHROISM SPECTRA OF APA AT 25°C. Full curve, experimental spectrum (fig.5.5); dots, computed spectrum shifted 300 cm^{-1} to the red with vertical lines referring to the exciton bands (the value of the exciton coupling parameter is 600 cm^{-1}).

interactions between the two moieties as the result of their dimerization. We note that although the conservative rule of the CD spectrum is verified with the rotational strength of the positive component being equal to that of the negative component (equation 2.18), the resultant positive and negative peaks of the CD spectrum have different magnitudes.

5.5.2 Effect of Temperature on the Absorption Spectra of APA.

The change in absorbance versus temperature is shown in figure 5.2. As was the case with CD, we observe two isosbestic points; the first one centred at 275 nm and the second one at 287 nm[127,161]. The good linearity of the data at high temperature enables us to obtain the unstacked spectrum. It is interesting to note in figure 5.7 the perfect coincidence, both in shape and intensity, of its spectrum with that of adenosine recorded at 20°C, (paragraph 4.2.1) apart from a small red shift of 60 cm^{-1} of the unstacked form extrapolated spectrum. This shift is fully justified if we take into account the Coulombic interaction between the two adenine moieties.

Comparisons of our extrapolated unstacked spectrum with the ones previously derived using four unknowns in equation (5.6)[127,161] are very satisfactory as we can see in Table 5.2.

The optical and thermodynamic parameters for the stacking of APA, derived as indicated above in terms of the Van't Hoff equation (5.6), are shown in figure 5.8. The vibronic exciton theory applied to absorption enables us to fit the derived spectrum representing the stacked form to a computed dimeric spectrum having only two variable parameters: the exciton coupling parameter and the angle θ between the

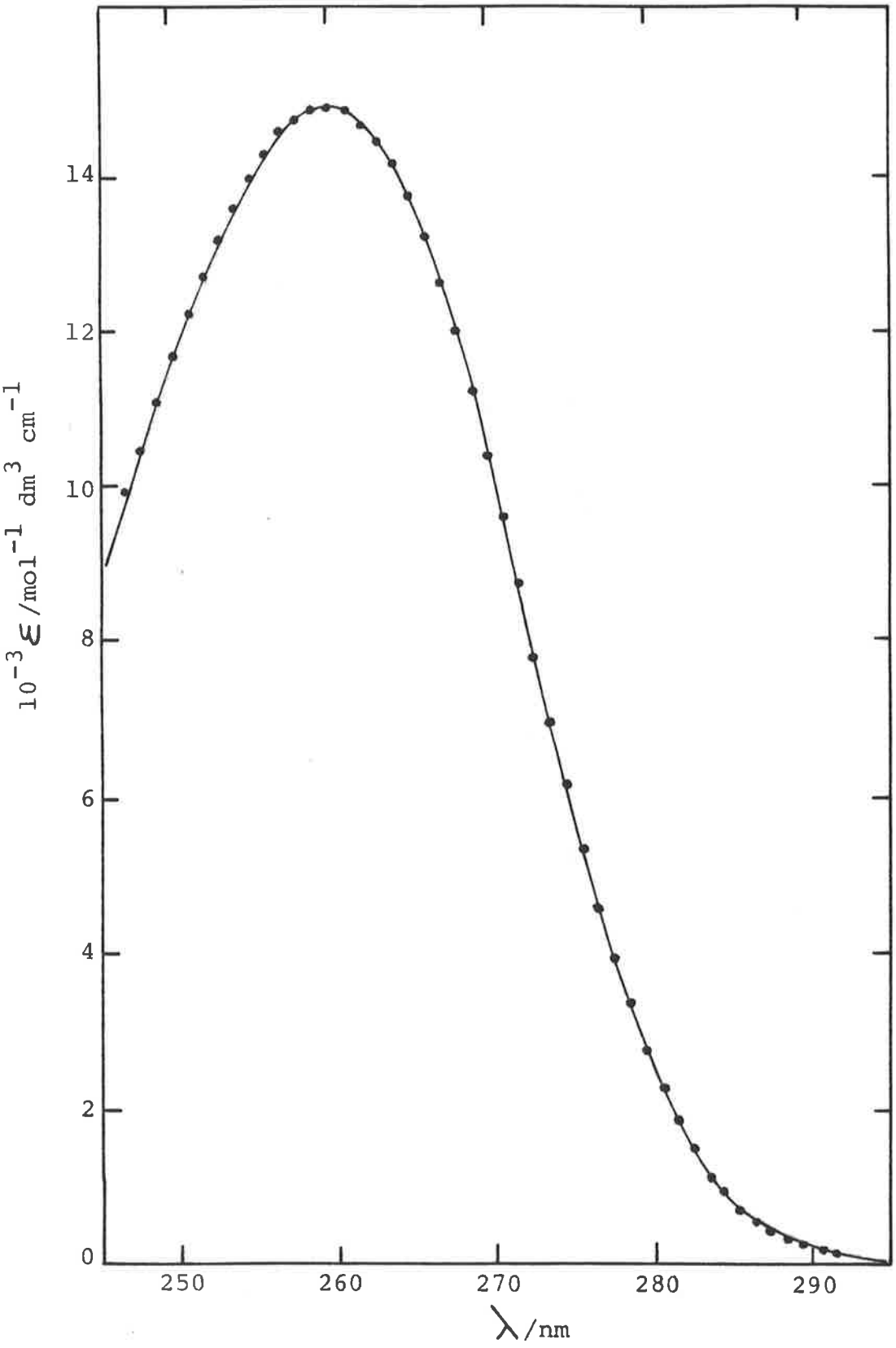

FIG.5.7 COMPARISON BETWEEN THE ABSORPTION SPECTRA OF ADENOSINE AT 20°C (—) AND APA EXTRAPOLATED TO INFINITE TEMPERATURE (···).
The extrapolated spectrum has been shifted 60 cm^{-1} to the blue.

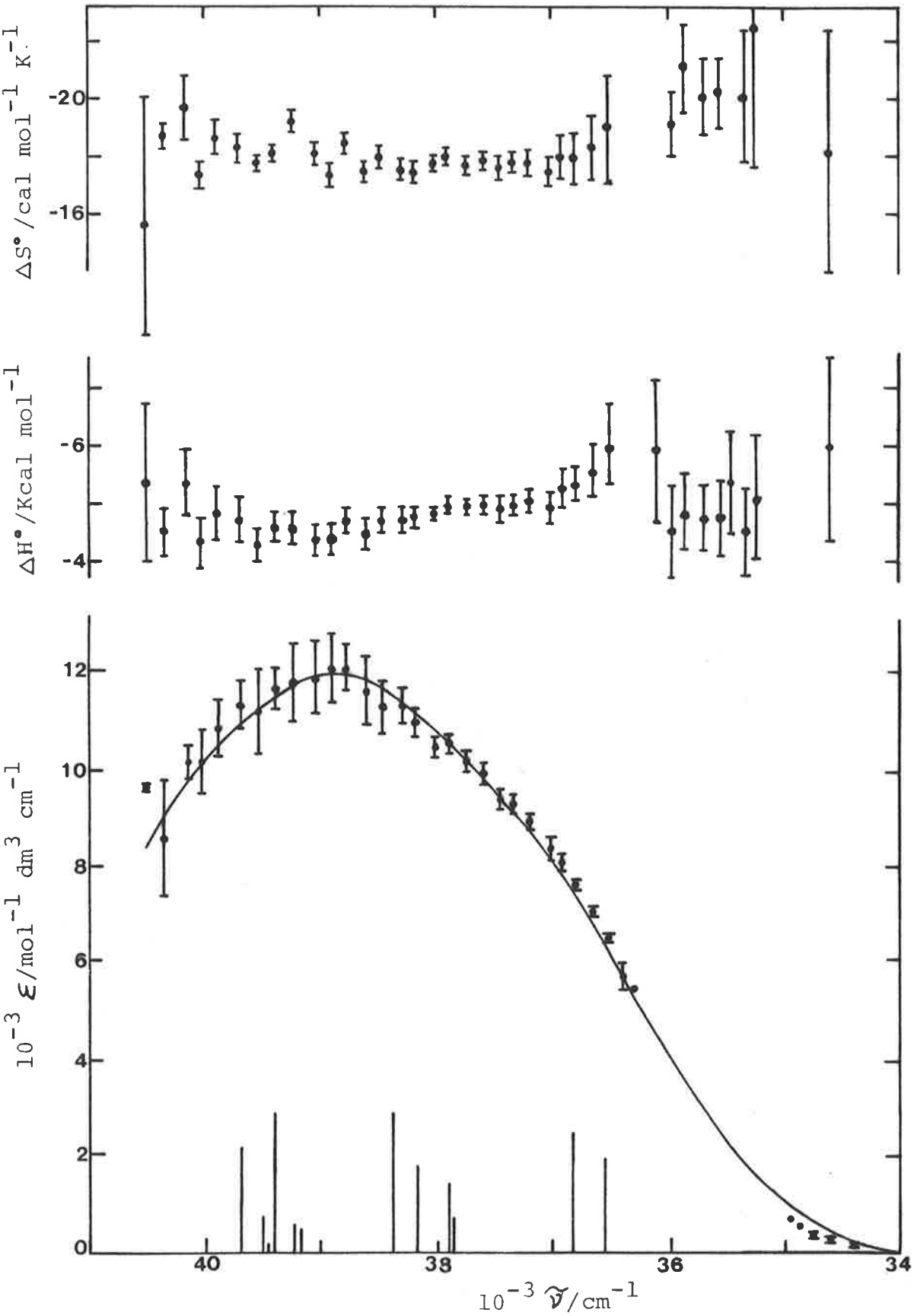

FIG.5.8 ABSORPTION SPECTRUM OF APA IN A STACKED FORM AND THERMODYNAMIC PARAMETERS OF STACKING.
(—),computed dimeric spectrum shifted 300 cm^{-1} to the red with vertical lines referring to the exciton bands(the value of the exciton coupling parameter is 600 cm^{-1},the angle between the two moieties of the dimer is 60°);(••),absorption spectrum of APA in a stacked form derived with use of the two-state model.

transition moments in the two moieties: (appendix C).

The overall results for APA obtained in this study are gathered in table 5.1. They can be compared to literature values in tables 5.2 and 5.3.

5.5.3 Comparison with Previous Studies on APA

The use of the two-state model is again vindicated by the agreement between the thermodynamic parameters derived from the two spectroscopic methods, absorption and circular dichroism. In addition, we have also shown that as expected, the value of the parameters is independent of the wavelength. The accuracy is not constant but it is directly proportional to the magnitude of the absorbance change between the two extreme temperatures.

Our derived thermodynamic parameters, although their absolute values are lower than the average, are in agreement with previous determinations using different approaches (tables 5.1 and 5.3). Table 5.2 shows that this agreement is also found for the derived optical parameters obtained from absorbance measurements. The wide variation in the thermodynamic parameters recorded to date cannot only be explained by experimental errors, but is due, more likely, to the assumptions concerning the spectra of the stacked and unstacked states. These spectra were rarely justified and too few attempts have been made to correlate them to a theoretical model.

Unlike absorption, the CD magnitude of the stacked form differs in all the previous investigations[127,131,133]. Our results and all the values given below are given in terms of pure dimeric CD spectrum with monomeric contributions subtracted. In this way a straightforward comparison can be

Table 5.1 THERMODYNAMIC AND OPTICAL PROPERTIES OF APA (results obtained in this study).

parameters / methods	ΔH° (Kcal $mole^{-1}$)	ΔS° (cal $mole^{-1}K^{-1}$)	unstacked	stacked
Absorption[c]	-5.0[a]	-18.0[a]	$\varepsilon_{max}^{259\ nm} = (14.87\pm0.01)10^3$	$\varepsilon_{max}^{257\ nm} = (11.92\pm0.05)10^3$ exciton coupling of 0.45 ± 0.05 (600 cm^{-1}) $\theta = 60° \pm 5°$, shift of 300 cm^{-1} to the red
CD[c]	-5.5 ± 0.2	-19.4 ± 0.6	$\Delta\varepsilon^{259.2\ nm} = -2.0$	$\lvert\Delta\varepsilon^{270nm}\rvert + \lvert\Delta\varepsilon^{250nm}\rvert = 33\pm2$[b] $\Delta\varepsilon^{270\ nm} = 18.2 \pm 1$[b] $\frac{\Delta\varepsilon^{270}}{\Delta\varepsilon^{250}} = -1.24 \pm 0.2$[b] exciton coupling of 0.45 (600 cm^{-1}), shift of 300 cm^{-1} to the red

a - The standard deviations are represented in figure 5.6.

b - The monomeric contribution has been subtracted.

c - The molar absorptivity (ε) and circular dichroism ($\Delta\varepsilon$) are given in $mol^{-1}\ dm^3\ cm^{-1}$.

Table 5.2 A COMPARISON BETWEEN THE EXTRAPOLATED ABSORBANCE DATA OF APA.

wavelength / molar absorptivity[a] (ε)	260 nm	268 nm	268 nm	references and comment
unstacked APA	$(14.86 \pm 0.05)10^3$		$(11.70 \pm 0.05)10^3$	ref. 127 with $\varepsilon_{APA}^{260\ nm} = 13.9 \times 10^3$ at 20°C.
		14.81×10^3		ref. 161 ($\varepsilon_{APA}^{260\ nm}$ at 20°C was not quoted)
	$(14.87 \pm 0.01)10^3$	$(14.59 \pm 0.02)10^3$	$(11.97 \pm 0.02)10^3$	this study with $\varepsilon_{APA}^{260\ nm} = 13.9 \times 10^3$ at 20°C.
stacked APA	$(13.06 \pm 0.05)10^3$		$(9.90 \pm 0.05)10^3$	ref. 127
		10.89×10^3		ref. 161
	11.47×10^3	10.87×10^3	9.05×10^3	this study[b]

a - The molar absorptivity (ε) and circular dichroism (Δε) are given in $mol^{-1}\ dm^3\ cm^{-1}$.

b - The standard deviations are represented in figure 5.6.

Table 5.3 THERMODYNAMIC PARAMETERS FOR THE STACKING OF APA

Methods	$\Delta H°$ (Kcal $mole^{-1}$)	$\Delta S°$ ($cal^{-1}mole^{-1}K^{-1}$)	ref.	comment
ORD	-5.3	-20	126	ionic strength of 0.1
ORD	-5.3	-19	126	$\Delta\varepsilon^{270\ nm}$ = +18.3 at -64°C in 25.2% LiCl with $\frac{\Delta\varepsilon^{270}}{\Delta\varepsilon^{250}} \approx -1.35$; the monomeric contribution has been subtracted; ORD transformed to CD[137].
ORD	-6.5	-21.4	162	
ORD	-6.6	-23	159	
CD	-8	-25 → -30	131	We extrapolated a value of $\Delta\varepsilon^{270\ nm}$ around +15 for the stacked CD spectrum.
CD	-6		160	
CD	-6.8 ± 0.3	-23 ± 1.1	133	$\Delta\varepsilon^{270\ nm}_{stacked} \approx +13.5$, $\Delta\varepsilon^{250\ nm}_{stacked} \approx -13.1$; $\Delta\varepsilon^{260\ nm}_{unstacked} \approx -2.0$.
Absorption	-5.5 ± 0.3	-18 ± 0.95	161	
ORD	-9.8 ± 0.8	-33 ± 2.4	127	
CD	-9 ± 0.7	-30 ± 2	127	
Absorption	-8.3 ± 0.5	-28 ± 1.5	127	
NMR	-3 → -4	-10 → -15	154	

made between experimental and theoretical values. If we applied the correction to the results of Olsthoorn *et al.*[133], we found for the stacked form: $\Delta\varepsilon^{270\ nm}_{stacked} \approx +14.3$, $\Delta\varepsilon^{250\ nm}_{stacked} \approx -11.5$ and a ratio $\frac{\Delta\varepsilon^{270}}{\Delta\varepsilon^{250}} = -1.24$. This last value is the same as the one we found. However the magnitude of their CD spectrum and mostly the one derived by Powell *et al.*[127] are much lower than ours ($\Delta\varepsilon^{270\ nm} = +18.2$), that of Davis and Tinoco[126] with a $\Delta\varepsilon^{270} = +18.3$ obtained at -64°C in a high salt concentration of 25.2% LiCl. (Transformation from ORD to CD made by Johnson *et al.*[137]) or that obtained by Pettegrew *et al.*[134] ($\Delta\varepsilon^{270} \approx +18.2$ at -60° and in 25% LiCl). The last two measurements are the only experimental ones for the CD of the stacked form, or rather the nearest ones (in fact, around -60°C, the temperature dependence curve for the optical properties begins to level off). However, the use of high salt concentrations to enable approaching the low temperature state has been questioned[127] and it has been shown that high salt concentrations destabilize the base-base interaction[163]. The magnitude of the CD spectra reflects this destabilization. In fact, Davis and Tinoco[126] have mentioned the smaller optical rotation in 25.2% LiCl compared to that in dilute buffers. Recently, too, the same proposal was considered to account for the lower CD magnitude encountered in high salt concentrations in the temperature range 0-70°[134]. Thus, the magnitude of the CD spectrum of APA in the stacked conformation is expected to be somewhat higher in dilute buffers than in high salt concentrations.

Furthermore, we note that the theoretical calculations have produced a CD spectrum of APA[137,140] similar in magnitude to the one measured experimentally by Davis and Tinoco[126] at -64°C. As it was already pointed out some

caution should be exercised in the derivation of the optical properties of the stacked form. Its value depends on the conditions imposed for the best fit of the Van't Hoff equation (5.6).

We consider our value for the stacked form ($\Delta\varepsilon^{270\ nm}_{stacked} = +18.2$) to be fully justified in relation to theoretical calculations[137,140] and experimental measurements at low temperatures[126,134].

5.6 Analysis of the Temperature-Dependent Spectra of dApdA.

Although the difference between APA and dApdA is of fundamental importance to the understanding of the structure of Nucleic Acids, very few experiments involving dApdA have been carried out.

We have investigated the stacking of dApdA through its thermodynamic parameters and its optical properties using the same methods as for ApA.

5.6.1 Effect of Temperature on the CD Spectra of dApdA.

Figure 5.9 shows some CD spectra of dApdA at different temperatures. The magnitude of the CD spectra is not greatly modified as the temperature is changed. The isosbestic point at 258.1 nm with a $\Delta\varepsilon^{258.1\ nm} = -1.36$ enables us to subtract from the overall spectra the monomeric contribution of the base-sugar interaction and thus leaves the CD spectra of the pure stacked dApdA arising only from the base-base interaction. They have a similar shape (figure 5.10) with a ratio $\frac{\Delta\varepsilon^{269\ nm}}{\Delta\varepsilon^{250\ nm}} = -1.30 \pm 0.02$. Their fit to the theoretical CD spectra derived from the vibronic exciton theory is less successful than for APA. We can see that the two peak maxima are closer than the ones in the CD spectra of APA which

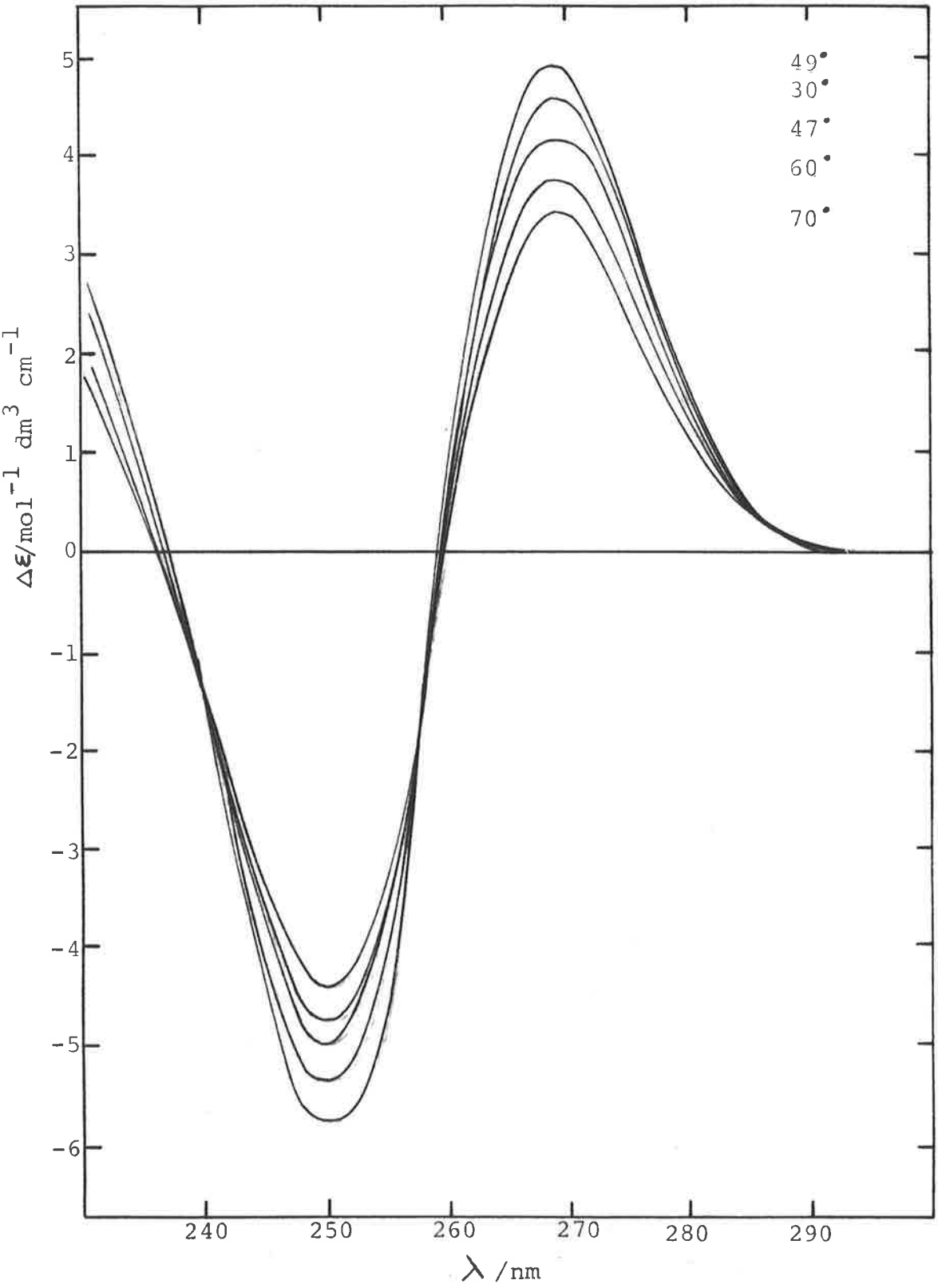

FIG.5.9.a CIRCULAR DICHROISM SPECTRA OF DAPDA AS A FUNCTION OF TEMPERATURE. The spectra show the presence of an isosbestic point at 258 nm ($\Delta\varepsilon$=-1.36 $mol^{-1}\ dm^3\ cm^{-1}$).

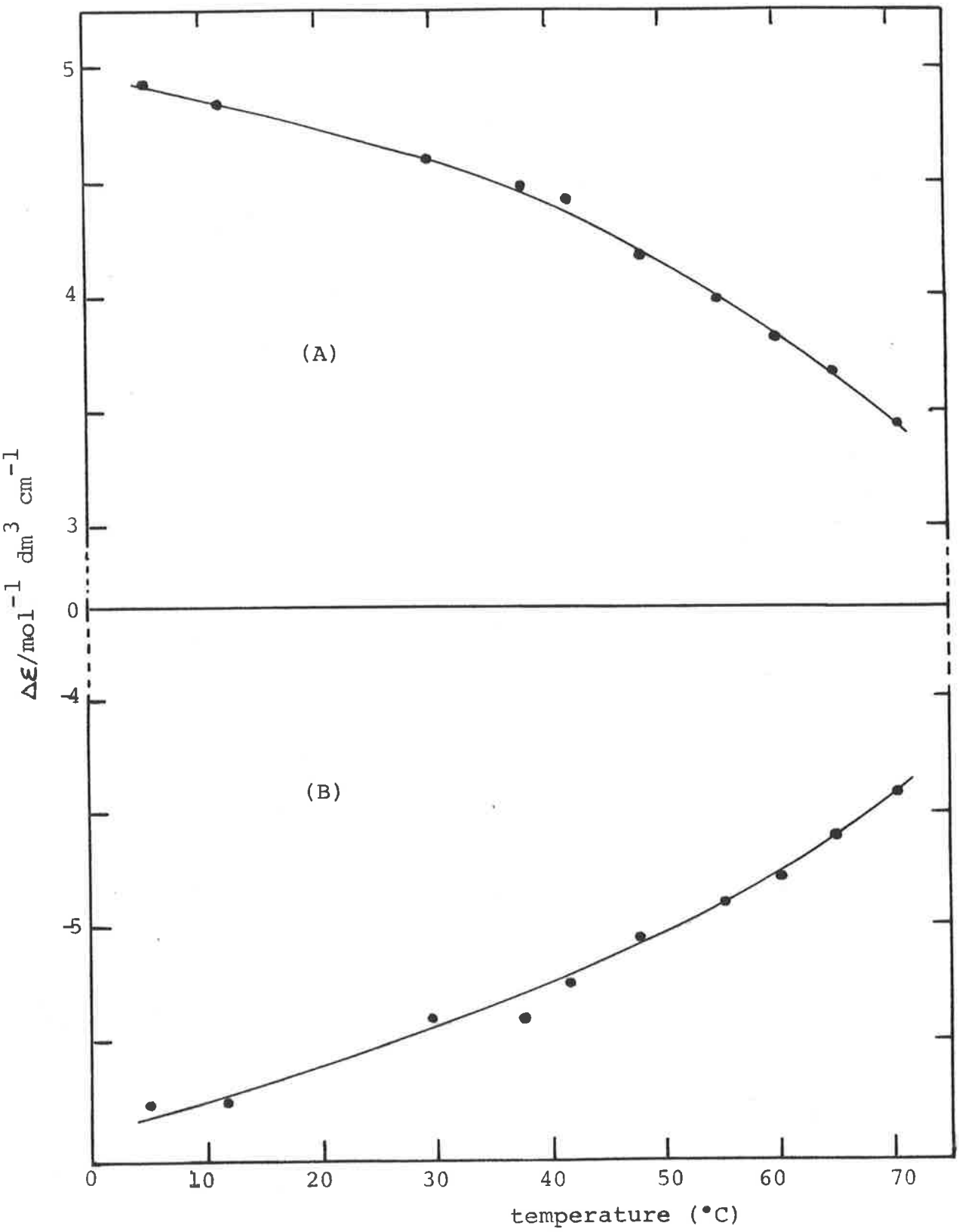

FIG.5.9.b CHANGE OF THE MOLAR CIRCULAR DICHROISM OF DAPDA WITH TEMPERATURE AT 269 NM (A) AND AT 250 NM (B).

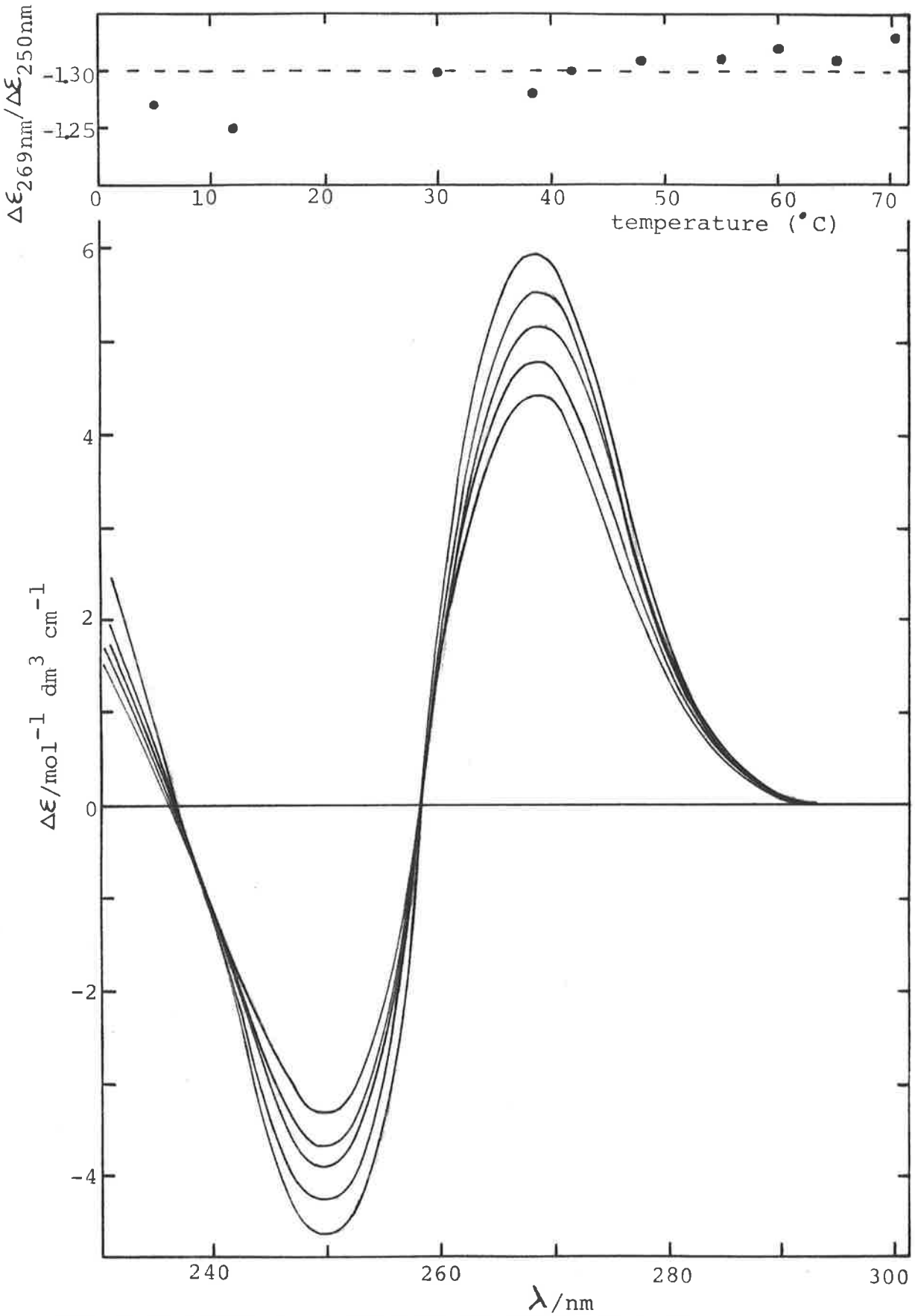

FIG.5.10 CIRCULAR DICHROISM OF DAPDA IN A STACKED FORM AS A FUNCTION TEMPERATURE. $\Delta\varepsilon$(dApdA)-$\Delta\varepsilon$(dA) with $\Delta\varepsilon$(dA) at 258 nm equal to -1.36 mol^{-1} dm^3 cm^{-1}. (see fig.5.5).

indicates less exciton coupling interactions between the two bases. Indeed, the best fit (mainly based on the ratio $\frac{\Delta\varepsilon^{269\ nm}}{\Delta\varepsilon^{259\ nm}}$) gives a value of the exciton coupling parameter of 0.2 or 270 cm^{-1} (figure 5.11).

The fit of the change of the magnitude of the CD spectra, $|\Delta\varepsilon^{269\ nm}|+|\Delta\varepsilon^{250\ nm}|$, with increasing temperature to a two-state model enables us to obtain the value of the thermodynamic parameters for the stacking as well as the CD magnitude of the stacked form (table 5.4).

5.6.2 Effect of Temperature on the Absorption Spectra of dApdA.

Figure 5.12 shows some absorption spectra of dApdA at different temperatures, together with the extrapolated spectrum to infinite temperature. As was the case with the CD data, there is a smaller variation in the absorbance of dApdA with increasing temperature in comparison to APA. Two isosbestic points are found, one around 278.5 nm and the other around 256 nm. From the use of the Van't Hoff equation (5.6) we obtain the absorption spectrum characteristic of the stacked form together with the thermodynamic parameters $\Delta H°$ and $\Delta S°$ (figure 5.13).

The vibronic exciton theory enables us to calculate the dimeric absorption spectrum of the dApdA in stacked form. We found that a theoretical spectrum with a value of the exciton coupling parameter of 0.30± 0.05 (400 cm^{-1}), a value of θ (angle between the transition moments of the bases) of 20° ± 5° and an overall shift of the spectrum of 300 cm^{-1} to the red, give the best fit for the derived experimental spectrum (figure 5.13).

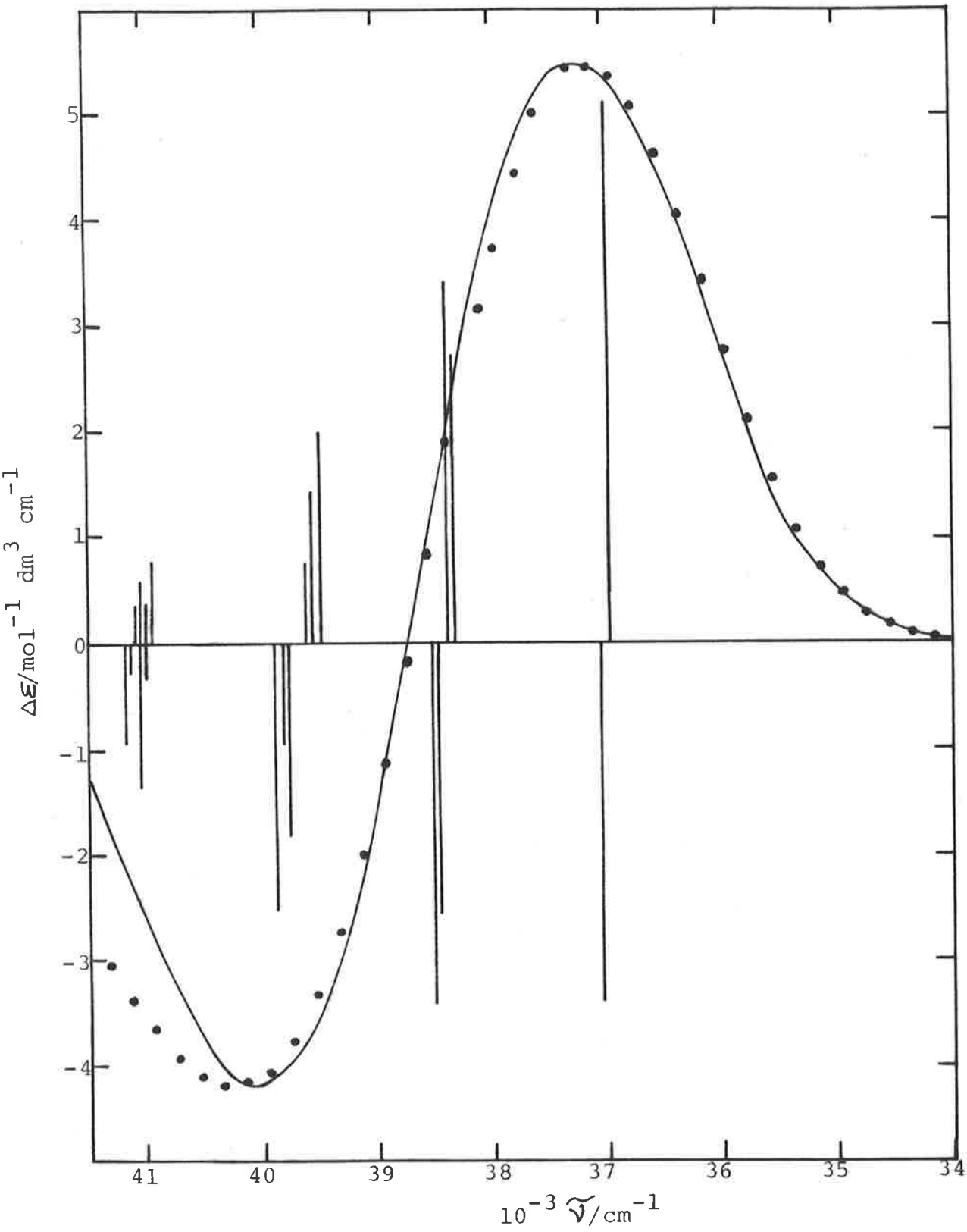

FIG.5.11 DIMERIC CIRCULAR DICHROISM SPECTRA OF DAPDA AT 41.7°C. Full curve, experimental spectrum (fig.5.10); dots, computed spectrum with vertical lines referring to the exciton bands (the value of the exciton coupling parameter is 300 cm^{-1}).

Table 5.4 THERMODYNAMIC AND OPTICAL PROPERTIES OF DAPDA.

parameters / methods	ΔH° (Kcal $mole^{-1}$)	ΔS° (cal $mole^{-1}$ K^{-1})	optical properties of dApdA
CD	-7.4 ± 0.2	-19.6 ± 0.2	$\Delta\varepsilon^{269\ nm}_{stacked} = +6.21$ $\Delta\varepsilon^{250\ nm}_{stacked} = -4.79$ $\Delta\varepsilon^{260\ nm}_{unstacked} = -1.36$
Absorption[a]	-6.5	-19	$\varepsilon^{258\ nm}_{stacked} = 12.69 \times 10^{3}$ $\varepsilon^{259.5\ nm}_{unstacked} = 13.47 \times 10^{3}$

a - The standard deviations are represented in figure 5.13.

b.- The molar absorptivity (ε) and circular dichroism ($\Delta\varepsilon$) are given in mol^{-1} dm^{3} cm^{-1}.

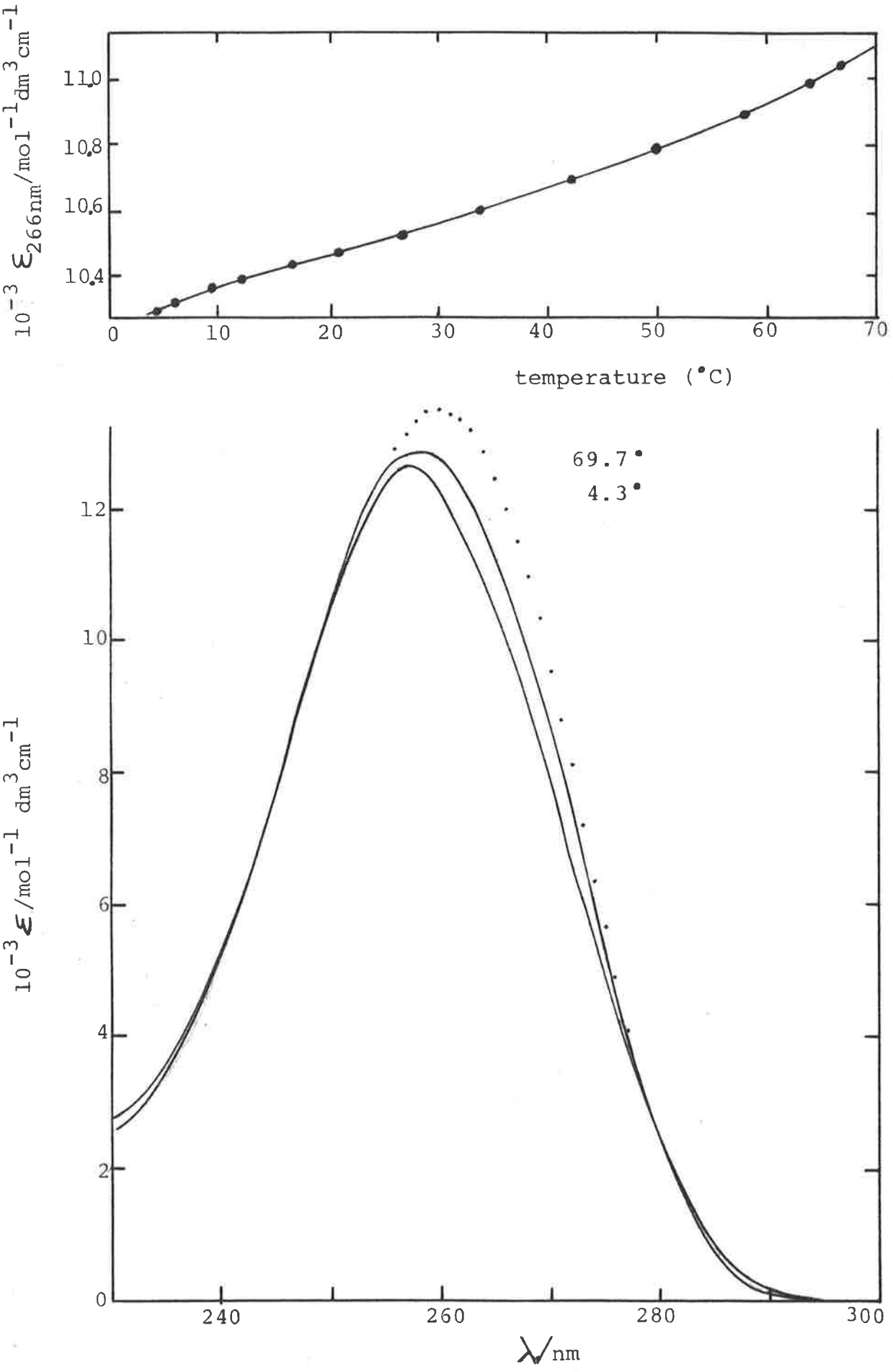

FIG.5.12 TOP: MOLAR ABSORPTIVITY VERSUS TEMPERATURE PROFILE FOR DAPDA.
BOTTOM: ABSORPTION SPECTRA OF DAPDA AT THE TWO EXTREME TEMPERATURES STUDIED AND EXTRAPOLATED SPECTRUM AT INFINITE TEMPERATURE (··).

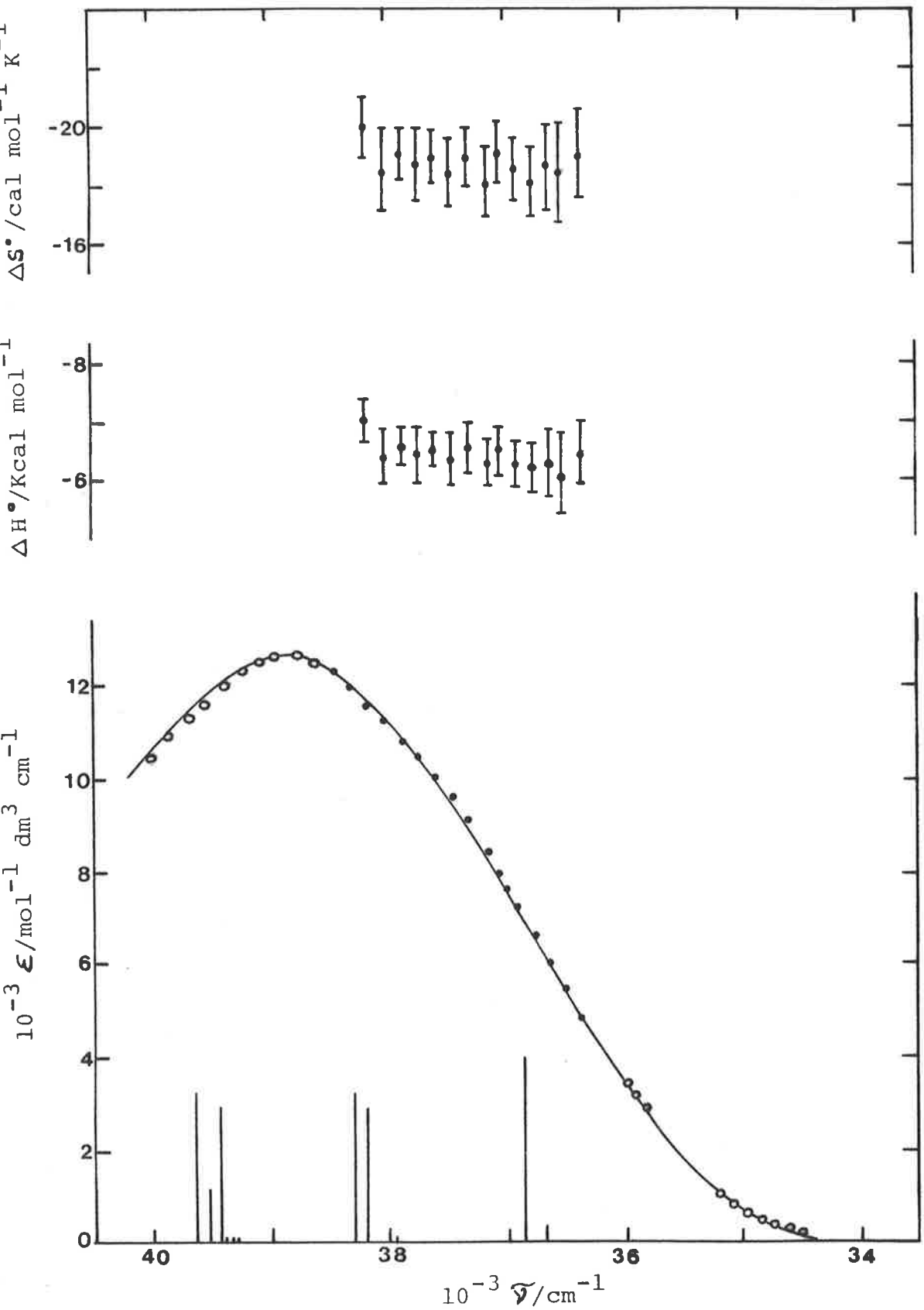

FIG.5.13 ABSORPTION SPECTRUM OF DAPDA IN A STACKED FORM AND THERMODYNAMIC PARAMETERS OF STACKING.
(—),computed dimeric spectrum shifted 300 cm^{-1} to the red with vertical lines referring to the exciton bands(the value of the exciton coupling parameter is 400 cm^{-1},the angle between the two moieties of the dimer is 20°); (··),absorption spectrum of dApdA in a stacked form derived with the use of the two-state model; (oo),absorptivity of dApdA at 4.3°C (no or little change was observed with increasing the temperature).

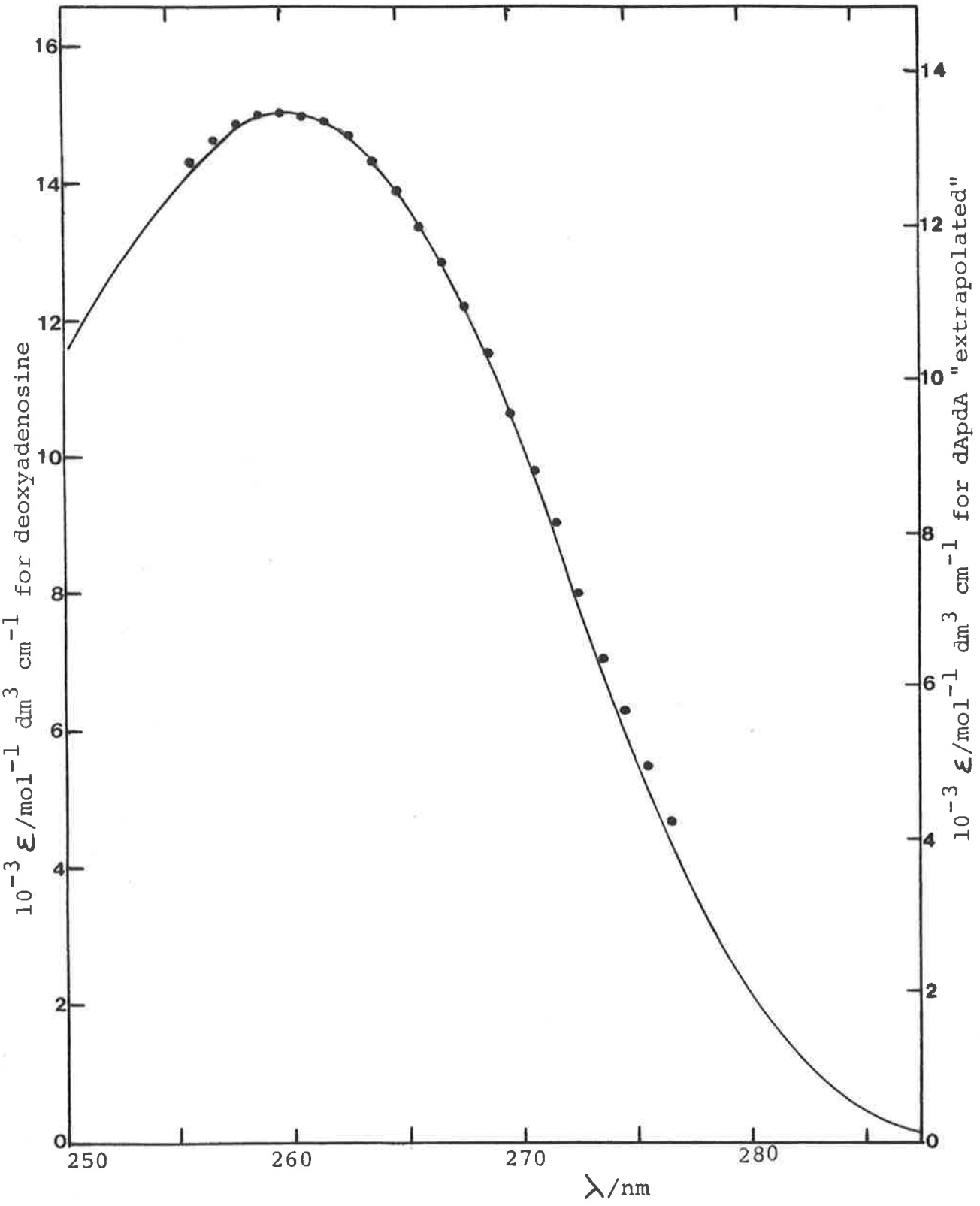

FIG.5.14 COMPARISON BETWEEN THE ABSORPTION SPECTRA OF DEOXYADENOSINE AT 21°C,(—) AND DAPDA EXTRAPOLATED TO INFINITE TEMPERATURE, (••).
The extrapolated spectrum of DAPDA has been shifted 60 cm^{-1} to the blue.

The uncertainties in the derived spectrum are in general more important than for APA but this is related to the smaller change of the optical data over the range of temperature studied. In particular our CD spectra were more noisy due to the smaller magnitude of the signal (half value compared to APA) and especially in the low temperature range, more spectra have to be recorded at each temperature considered and then averaged because of the poor reproducibility.

The presence of isosbestic points both in CD and in absorption spectra, the similar envelope of the derived dimeric CD spectra at different temperatures, the good linearity of the thermodynamic parameters over the range of wavelengths considered, the satisfactory correspondence between CD and absorption derived parameters, demonstrate the validity of the two-state model.

A word about the extrapolated absorption spectrum of dApdA to infinite temperature must be said at this point. Its maximum intensity is lower than that of dA but their shapes are rather similar as we can see in figure 5.14. As was the case for APA, the extrapolated spectrum is shifted towards the red by 60 cm^{-1} in relation to that of dA due to Coulombic interactions between the two moieties. The lower intensity can be the result of the incomplete unstacking of the bases. (In fact, as it will be pointed out later, the thermodynamic parameters indicate the greater stability of dApdA compared to APA.) Although shapes and positions of maxima will not change by relatively small perturbations of the chromophore, transition probabilities will, due to the mixing between the excited states and the resultant intensity borrowing. We cannot give a better explanation to this

problem neither of the fact of the lower molar absorptivity of dA compared with that of dAMP (or adenosine compared to AMP). What is in favour of this extrapolated dApdA spectrum is the good constancy of the derived thermodynamic parameters over the range of wavelengths considered. This cannot be achieved if one uses the absorption spectrum of dA as representative of the unstacked form. For example, this produces an enthalpy minimum at 265 nm of -4.5 Kcal $mole^{-1}$, which value increases on each side of this minimum to a value of -6.3 Kcal $mole^{-1}$ at 273 nm and of -6.4 Kcal mol^{-1} at 260 nm.

5.6.3 Comparison with Previous Studies on dApdA

The previous lack of accurate measurements for dApdA prevents a direct comparison of our results with others. However, we can say that the sum of the intensity of our positive and negative CD bands at 26°C is similar to that measured by Cantor *et al.*[132] or by Maurizot *et al.*[160] but differs from the one measured by Miller *et al.*[146]. There is not much agreement about the change of the CD with temperature. However a positive point of comparison lies in the similarity between the CD intensity measured at -20°C by Maurizot *et al.*[160] and our derived value of the CD intensity of the stacked form. The only determination of the enthalpy of stacking has been rather uncertain. Maurizot *et al.*[160] with the use of CD data indicate that the enthalpy of unstacking is "below 3 Kcalories". In order to arrive at this conclusion, they assume that the low temperature limit of the CD is the same for APA and dApdA!

5.7 Differences between Deoxy and Ribodinucleoside Phosphates

5.7.1 Thermodynamic Differences

From the value of the thermodynamic parameters, we observe that the entropies of stacking of APA and dApdA are similar but that the enthalpy of stacking of dApdA is larger than that of APA. Thus the stabilization of the stacked conformer of dApdA in relation to that of APA (figure 5.15) is brought about by a more favourable enthalpy of stacking. This is in perfect agreement with the finding of the higher stability toward dioxane of poly dA compared to poly A[164]. The origin of the stabilizing forces is not yet fully understood[159,163]. Although the stacking interaction appears to be the dominant stabilizing force, the importance of the steric requirement of the molecule has been demonstrated[128]. In particular the 2'-OH group of the ribose exercises some steric hindrance which influences the conformation of the dinucleoside[18,136].

5.7.2 Conformational Differences

Our objective has been achieved. We have extracted the optical properties of the stacked dinucleosides. Furthermore the interpretation of these properties using the vibronic exciton theory has given some information about the geometry of the dinucleosides. Their conformations are in perfect concordance with those of Kondo *et al.*[128,136] and they confirm the early observations about the optical differences between APA and dApdA[18,160].

At low temperature, the bases are stacked with a right handed conformation (sign of the doublet of the CD spectrum). The angle θ formed between the transition moments

in the two moieties is 60° for APA and 20° for dApdA. If we assume the simple model of Glaubiger *et al.*[130], with the use of equation (5.5), the ratio of the theoretical rotational strength of APA to that of dApdA can thus be written:

$$\frac{\mathcal{R}_{APA}}{\mathcal{R}_{dApdA}} = \frac{\sin \theta_{APA}}{\sin \theta_{dApdA}} = \frac{\sin 60}{\sin 20} = 2.5$$

The rotational strength can also be measured from the area under the envelope of the positive or the negative component of the stacked CD spectrum. This gives for APA

$$\mathcal{R}^{-}_{APA} = -\mathcal{R}^{+}_{APA} = 2.295 \times 10^{-39} \int \frac{\Delta\epsilon d\nu}{\nu} = 8.28 \times 10^{-39} \text{ (cgs-units)}$$

for a value of the exciton coupling parameter of 0.45 (600 cm^{-1}). Similarly for dApdA

$$\mathcal{R}^{-}_{dApdA} = -\mathcal{R}^{+}_{dApdA} = 5.68 \times 10^{-39} \text{ (cgs-units)}$$

for a value of the exciton coupling parameter of 0.3 (400 cm^{-1}). Their ratio give

$$\frac{\mathcal{R}^{-}_{APA}}{\mathcal{R}^{-}_{dApdA}} = \frac{8.28 \times 10^{-39}}{3.94 \times 10^{-39}} = 2.1$$

This value is rather similar to the theoretical one if we consider that the angles were determined with an uncertainty of ±5°.

In the same way, using a similar model, it has been demonstrated theoretically that hypochromism was not sensitive to θ (equation (5.3)). The percentage hypochromism can be also determined experimentally (equation (5.1)). The oscillator strength, f, can be obtained by the measurement of the entire area under the envelope of the fitted absorption spectrum. We found:

f(APA stacked) = 0.261; f(dApdA stacked) = 0.263

f(Adenosine) = 0.292; f(dA) = 0.294

so that H%(APA) = 10.6 and H%(dApdA) = 10.5

(Similar results could be obtained by taking AMP and dAMP instead of Adenosine and dA for the monomers.) Our experimental CD and absorption measurements confirm the theoretical relationships established by Glaubiger *et al.*[130] and thus give a good indication of the validity of our model.

5.8 The Two-State Model Opposed to a Multi-State Model.

As was found previously[127,133,159,161], the optical data (ORD, CD and absorption) can be analysed in terms of a two-state model but NMR measurements do not support this simple model[128,136,152-154] and show that the stacked and unstacked states are a collection of many conformers. How can we explain these two different conclusions about the same phenomenon? First we have to say a word about the various methods of investigation. Absorption, as we have seen in paragraph 4, is not sensitive to conformation and depends mainly on the magnitude of the transition dipole. CD and ORD show similar dependence to absorption but in addition, they are sensitive to the geometrical relation existing between the transition moment considered and the perturber. (In the case of the dinucleoside, the perturber stands for the transition moment of the other base.) NMR spectroscopy, due to its power of discrimination between different protons, can give multiple geometrical relationships between the different atoms composing a molecule, unlike CD which can only provide one relationship. So the differences encountered are simply due to the fact that NMR spectroscopy is a more sensitive and

detailed analytical method because of the larger amount of information gathered.

What, then, are the relationships between our derived stacked and unstacked dinucleosides and the conformers present described by NMR spectroscopy?

Firstly, at high temperature, NMR data converge to the values characteristic of the monomers indicating that the bases are away from each other. If we adopt an oscillating model[126,153] where the bases oscillate relative to each other, the amplitude of the oscillations is increased at high temperature until a continuous rapid rotation occurs. Thus the bases spend much of their time in an unstacked conformation (the bases do not overlap and are far from each other). Therefore, the coupling interaction between the transition moment of each base is nil or very weak which results in a monomer type CD or absorption spectrum. In NMR, the rapid rotation of the bases makes the protons of one base magnetically indistinguishable from the same proton of the other base[153]. The same explanation applies if we adopt a multistate model[152,154,165].

At lower temperatures, two[142,152] to three[154,158] stacked APA conformers have been proposed from NMR measurements in equilibrium with unstacked forms. The three stacked forms derived by Lee and Tinoco[154] have their base-planes nearly parallel and have approximately an angle θ (angle between the transition moments) between 40° and 60° corresponding perfectly with our stacked APA dinucleoside. Of the two stacked forms of Kondo and Danyluk[152], one has the bases forming an angle of 35° while the other one with an angle of 90° should have an exciton coupling value of zero (with the use of the dipole approximation[130]). An average

stacked form can give a good representation of these different stacked conformers because of their similar angle θ. This last point is important for the validity of the two-state model in absorption and CD spectroscopy.

We have established some relations between the behaviours of CD and absorption and that of NMR as the temperature changes and thus shown the validity of the application of the two-state model. This agreement between the three methods of measurement can also be found if one compares the amount of APA in stacked form determined from NMR and that obtained by CD or absorption spectroscopy. Altona[165], using NMR spectroscopy, has related the occurrence of N conformation (3'-endo) with the stacked conformation. The percentage of N-conformers can be easily measured and can be used to estimate the amount of stacking[166]. For example Lee *et al.*[142], with this method, found 38% of stacked forms for APA at 20°C and 19% at 72°. Chachaty *et al.*[151] proposed a percentage of N-conformers of 30% at 25°C. All these values derived from NMR measurements[142,151,154] can be compared with the ones we obtained using our thermodynamic parameters and the Van't Hoff equation (5.6) in figure (5.15). A better agreement is obtained with our parameters than with some previously determined[127,133,161].

5.9 GPG Dinucleoside

In comparison with APA dinucleoside, only a few studies of guanosyl-(3'-5')guanosine (GPG) have been carried out. This can be explained by the ease with which guanosine can form aggregates[167,169]. In this study, this is unlikely to happen due to the range of concentrations used (less than 6×10^{-5} M) where the Lambert-Beer law is followed[168]. The

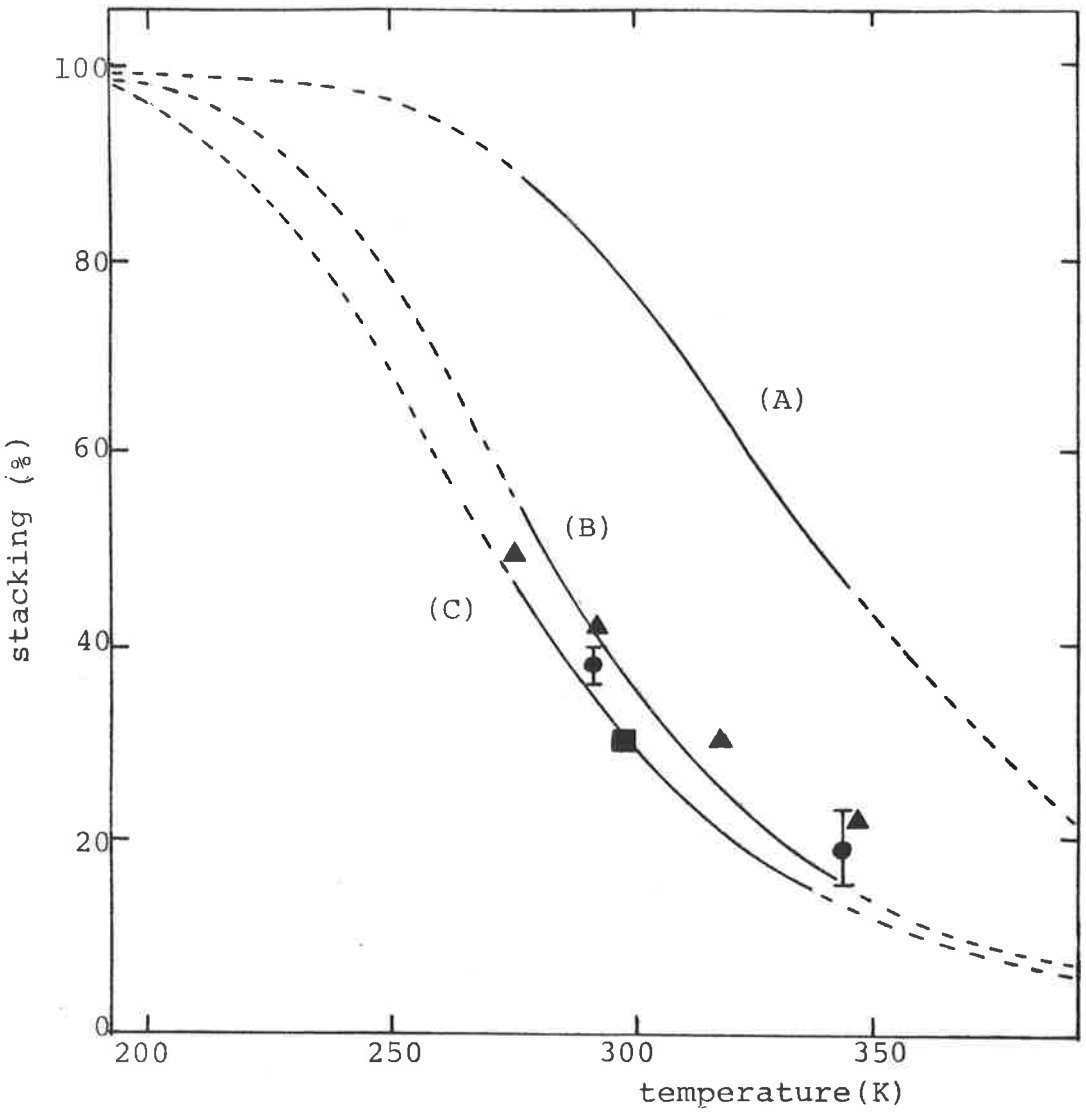

FIG.5.15 THE PERCENTAGE OF STACKING AS A FUNCTION OF TEMPERATURE.
Curve (A),dApdA from absorption data;curve (B), ApA from circular dichroism data;curve (C), ApA from absorption data.
The solid part of each curve is the percentage of stacking in the experimental temperature range. (▲), NMR measurements of Lee and Tinoco[154]; (●), NMR measurements of Lee et al[142]; (■), NMR measurements of Chachaty et al[151].

absorption spectrum envelope of GPG (figure 5.16) shows a shift to high energy and a hypochromicity effect in relation to the envelope of its constituent monomers which is characteristic of dimerization. The shape of the CD spectrum (figure 5.17) is very similar to those previously recorded[18,172] at low concentrations of GPG, but differs from those measured[170,172] at much higher concentrations where aggregation has been shown to be present[170,172]. In particular the negative CD lobe at low energy, which is present at low concentrations of GPG, vanishes at higher concentrations. To analyse the interactions existing between the two moieties of the dinucleoside, we subtract from the CD spectrum of GPG the contribution of its constituent monomers as shown in figure 5.17.

Although the presence of two transitions of similar intensity can be an advantage in characterizing the geometry of the dinucleoside, through the geometric relation existing between the different transitions in each moiety, this proves for our particular example to be a disadvantage. In fact the proximity of the two transitions makes the separation between the different contributions to the overall CD envelope rather difficult. That is why our task has merely been to attempt an analysis of the CD spectrum which shows a greater alteration of its envelope on dimerization than does the absorption spectrum.

Since the two near-UV transitions of guanosine are of similar intensity, not only do degenerate interactions exist between alike transitions of each moiety in the dinucleoside but non-degenerate interactions between different transitions also take place. The latter produces a CD spectrum of monomeric character. The procedure for calculating the

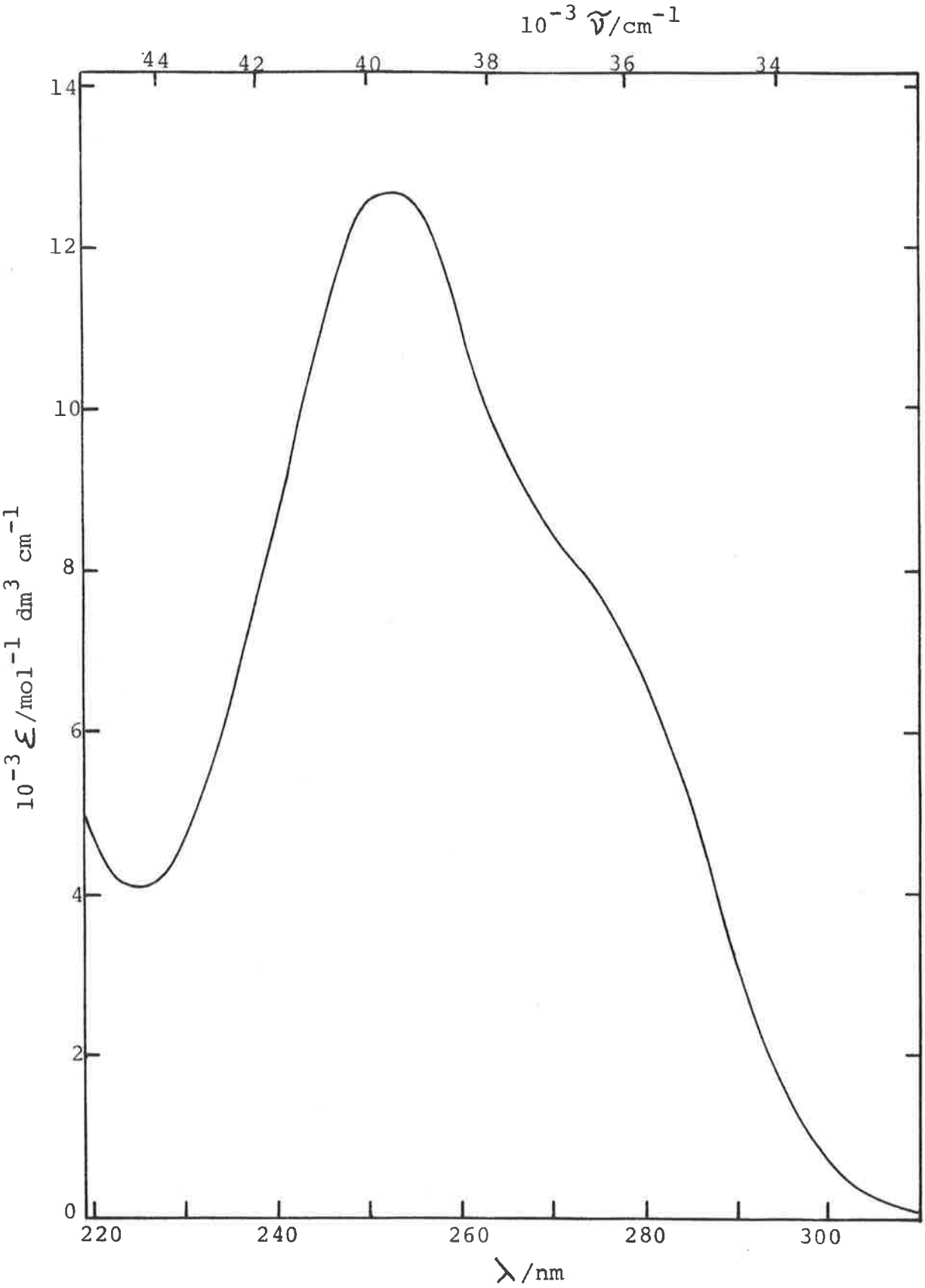

FIG.5.16 ABSORPTION SPECTRUM OF GPG IN A CACODYLIC ACID-SODIUM CACODYLATE BUFFER, I=0.05, AT PH=6.9 .

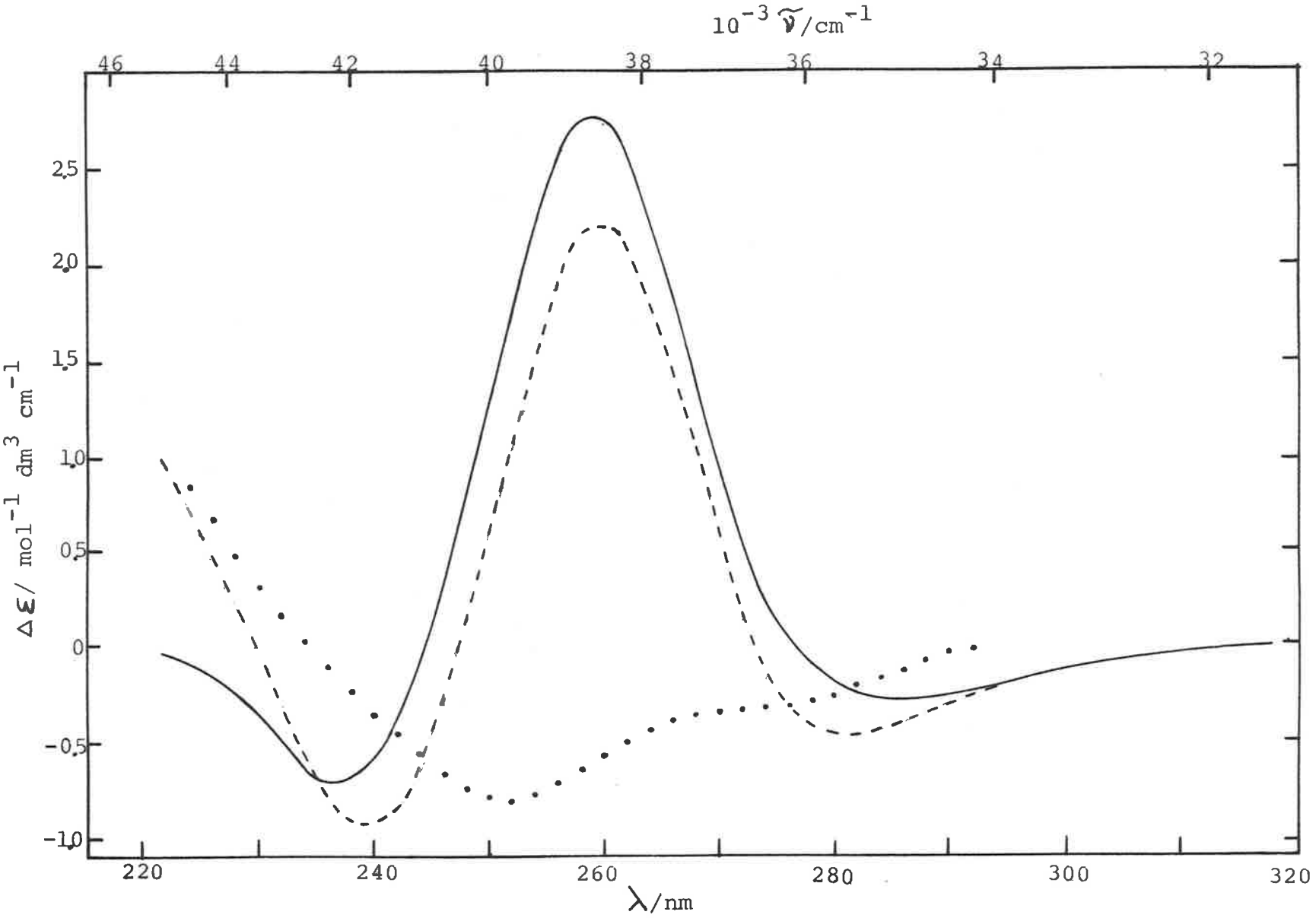

FIG.5.17 CIRCULAR DICHROISM SPECTRA OF GUANOSINE (··), GPG (--), AND DIFFERENCE BETWEEN THE CIRCULAR DICHROISM SPECTRA OF GPG AND GUANOSINE (—).

theoretical CD spectrum of GPG will be similar to the one used in the case of APA with the restriction that we fix an arbitrary value of 0.1 for the exciton coupling parameter. We should point out that the shape of the theoretical CD spectrum is not particularly sensitive as regards to the value of the exciton coupling parameter. Due to the great dissymmetry existing between the positive and the negative CD bands of the high energy transition, it is necessary to add a positive monomeric contribution to the theoretical CD spectrum in order to reproduce the experimental CD spectrum. Figure 5.18 shows a tentative resolution of the CD spectrum of GPG. The development of the vibronic exciton theory does not allow us to characterize the non-degenerate interactions nor to separate the contributions of the base-base interactions from the base-sugar interactions. Nevertheless, using the simple coupled oscillator theory we can predict the sign of the CD bands of GPG which result from the exciton splitting. For example, in figure 5.19, the signs of the long wavelength CD bands corresponding to the short and the long axis polarised transitions of guanosine are represented in relation to the angle of rotation between the two moieties in the dinucleoside. From figure 5.19, we can postulate two models for the dinucleoside GPG; the corresponding schematic diagrams are shown in figure 5.20. The angle between the two near-UV transition moments of guanosine was taken to be $70°$[171]. The low energy transition is more or less short axis polarised, while the high energy transition is long axis polarised (paragraph 4.6).

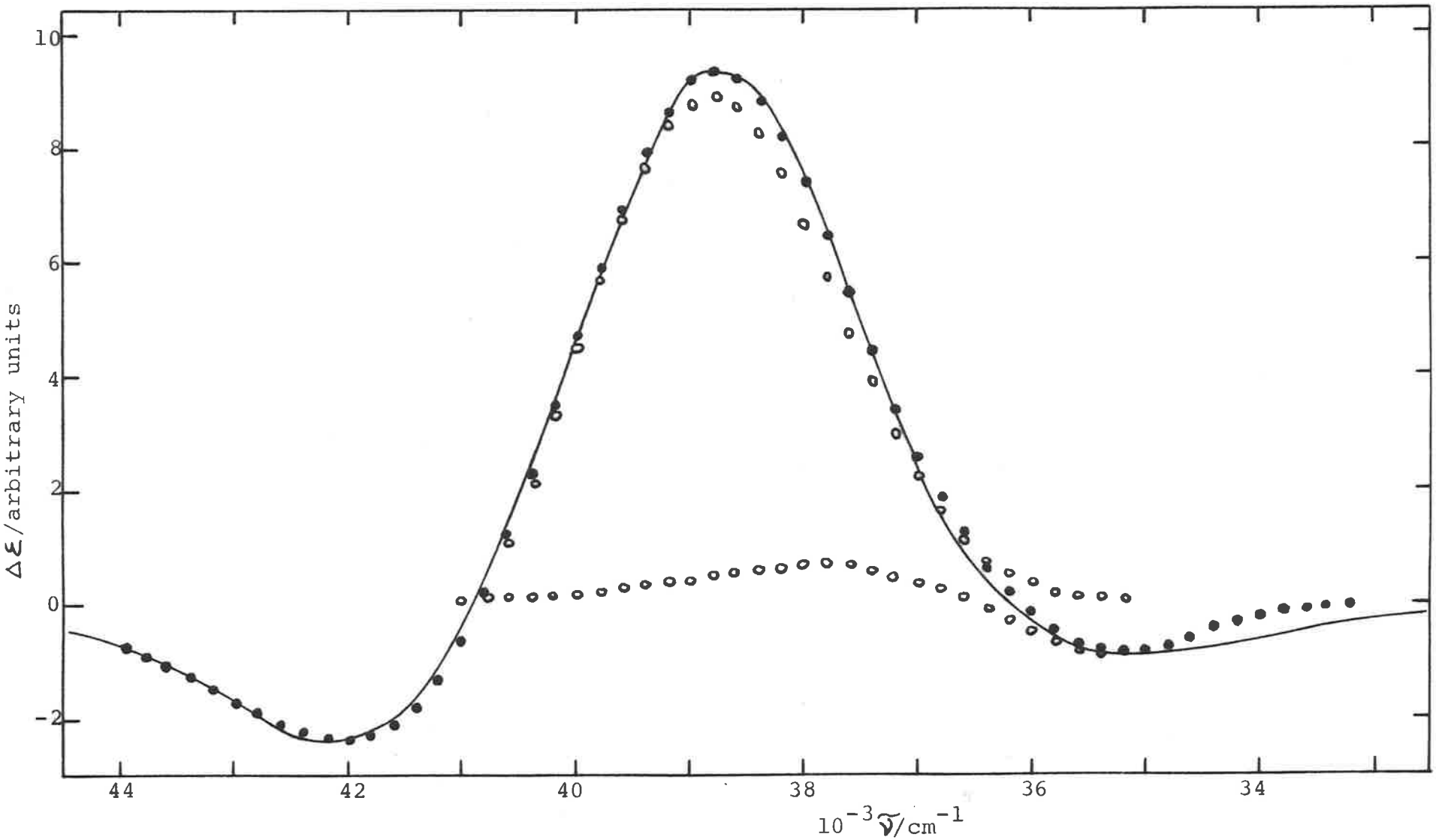

FIG.5.18 CIRCULAR DICHROISM SPECTRA OF GPG. (—),CD of GPG minus CD of guanosine(fig.5.17); (oo),computed dimeric CD spectra corresponding to the low and high energy transitions of guanosine; (●),sum of these two computed dimeric spectra.

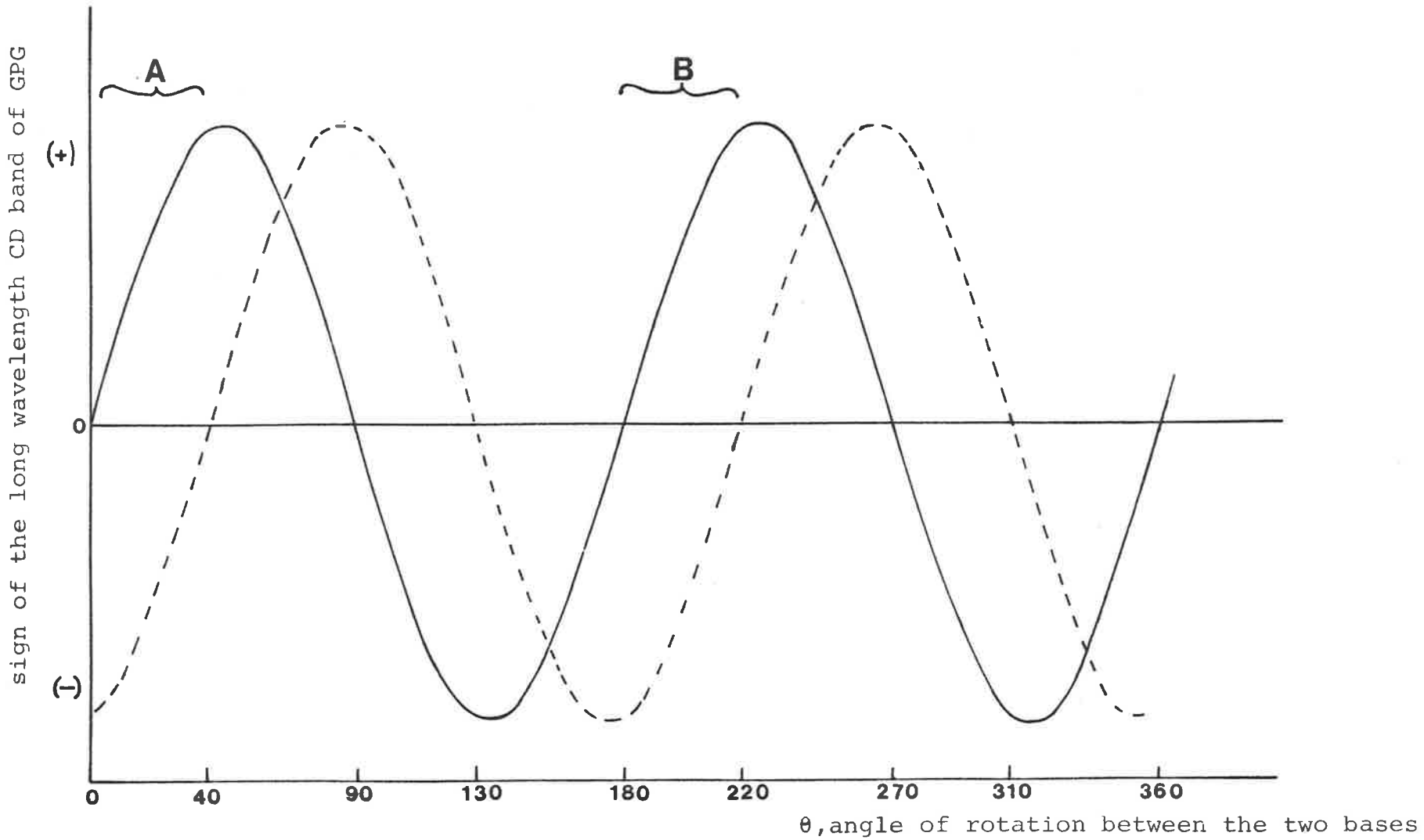

FIG.5.19 CALCULATION OF THE SIGN OF THE LONG WAVELENGTH CD BAND OF GPG ACCORDING TO EQU.5.5
The full line and the broken line correspond to the long and the short axis polarised transitions,respectively.A and B are the ranges of θ angles where the theoretical CD sign coincides with the experimental one.

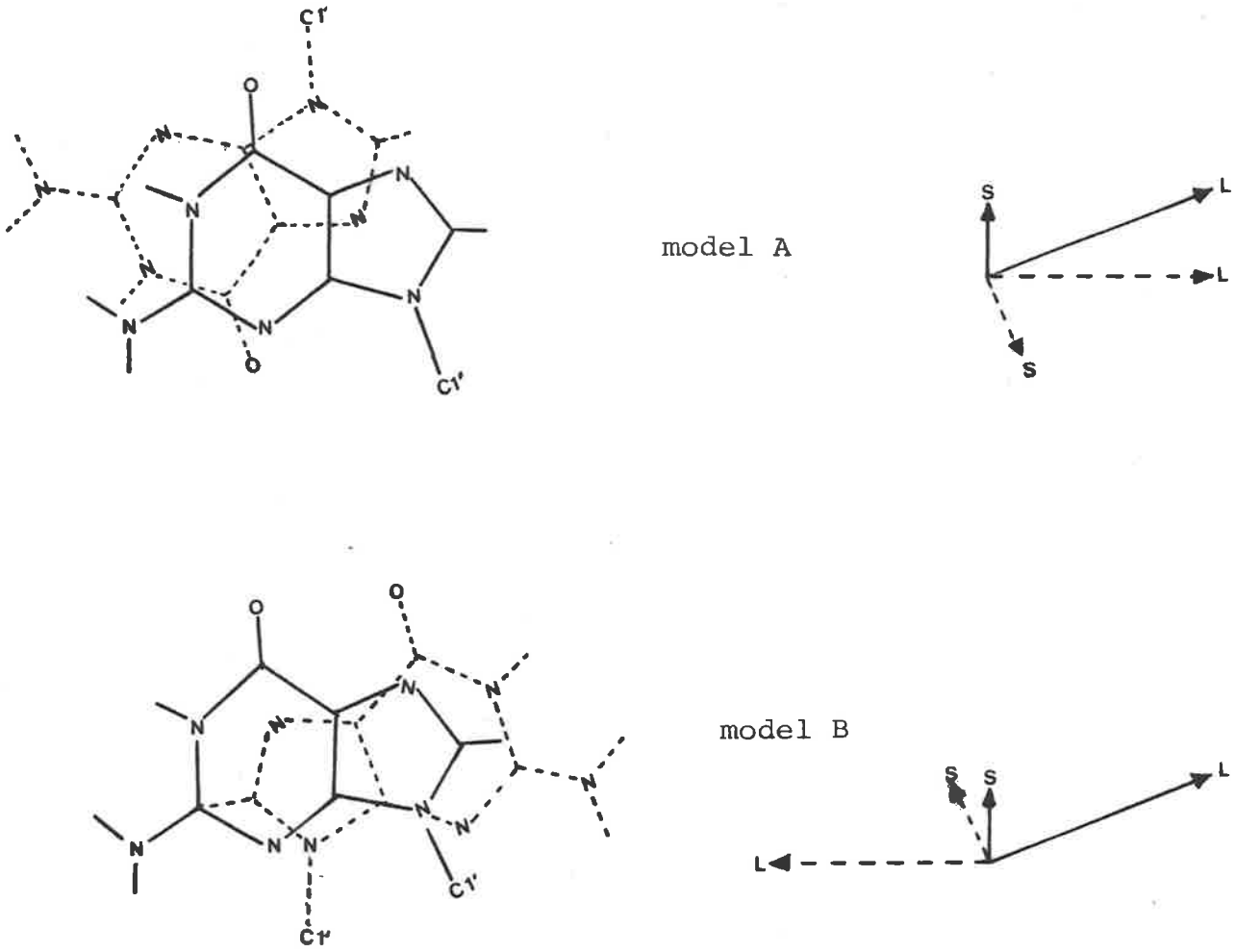

FIG.5.20 SCHEMATIC REPRESENTATION OF THE FRONT VIEW OF THE BASES OF GPG. (see text for additional information).The base with the broken line is in back and the base with the heavy line is in front. On the right,the transition moments of the corresponding bases are represented.S and L stand for the short and long axis polarised transitions of the bases, respectively.

5.10 Conclusion

As a result of the successful resolution of the monomeric spectra into vibronic bands, it was possible to show the adequacy of the vibronic exciton coupling theory in the interpretation of dimeric spectra both in CD and in absorption spectroscopy.

Temperature-dependent absorption and CD measurements of APA and dApdA enable us to obtain some information about the thermodynamics of stacking as well as some geometrical features of the dinucleosides. The agreement between the two methods of investigation as well as the coherence of the parameters extracted are a good indication of the validity of the simple model of stacking chosen for this study. More sophisticated models proposed through NMR spectroscopy can be explained in terms of this simple model and lead to the same conclusion which we obtained.

REFERENCES

1. J.N. Kikert, G.R. Kelly and T. Kurucsev, *Biopolymers*, 12, 1459 (1973).
2. M. Gal, G.R. Kelly and T. Kurucsev, *J. Chem. Soc. Faraday II*, 69, 395 (1973).
3. G.R. Kelly and T. Kurucsev, *Biopolymers*, 13, 769 (1974).
4. D.E. Joyce and T. Kurucsev, *Biophys. Chem.*, 2, 273 (1974).
5. L.P. Gianneschi, A. Cant and T. Kurucsev, *J. Chem. Soc. Faraday II*, 73, 664 (1977).
6. T. Kurucsev and U.P. Strauss, *J. Phys. Chem.*, 74, 3081 (1970).
7. L.P. Gianneschi, Ph.D. Thesis, University of Adelaide (1977).
8. S. Czarniescki, A. Witkowski and M.Z. Zgierski, *Acta Phys. Polonica*, 51, 451 (1977).
9. S. Czarniescki and A. Witkowski, *Acta Phys. Polonica*, 53, 235 (1978).
10. R. Signer, T. Capersson and E. Hammersten, *Nature*, 141, 122 (1938).
11. W.T. Astbury, *Symp. Soc. Exp. Biol. I. Nucleic Acids*, Cambridge University Press (1947).
12. J.M. Gulland and D.O. Jordan, *Symp. Soc. Exp. Biol. I. Nucleic Acids*, Cambridge University Press (1947).
13. E. Chargaff, *Experimentia*, 6, 201 (1950).
14. M.H. Wilkins, R.H. Gosling and W.E. Seeds, *Nature*, 167, 759 (1951).
15. G.R. Wyatt and S.S. Cohen, *Biochem. J.*, 55, 774 (1953).
16. J.D. Watson and F.H.C. Crick, *Nature*, 171, 964 (1953).
17. C.R. Cantor and M.M. Warshaw, *Biopolymers*, 9, 1059 (1970).
18. M.M. Warshaw and C.R. Cantor, *Biopolymers*, 9, 1079 (1970).

19. A. Pullman and B. Pullman, *Jerusalem Symp. Quant. Chem. Biochem.*, 4, 1 (1972).

20. D. Voet and A. Rich, *Progr. Nucl. Acids Res. Mol. Biol.*, 10, 183 (1970).

21. S.F. Mason, *J. Chem. Soc.*, 2071 (1954).

22. L.B. Clark and I. Tinoco, Jr., *J. Am. Chem. Soc.*, 87, 11 (1965).

23. W. Voelter, R. Records, E. Bunnemberg and C. Djerassi, *J. Am. Chem. Soc.*, 90, 6163 (1968).

24. J.M. Delabae, W. Guschlbauer, C. Schneider and J. Thiery, *Biochimie*, 54, 1041 (1972).

25. A. Pullman, B. Pullman and G. Berthier, *C. R. Acad. Sci. (Paris)*, 243, 380 (1956).

26. H. De Voe and I. Tinoco, Jr., *J. Mol. Biol.*, 4, 518 (1962).

27. H. Berthot and A. Pullman, *J. Chim. Phys.*, 55, 942 (1965).

28. J. Ladik and K. Appell, *Theoret. Chim. Acta*, 4, 132 (1966).

29. M. Tanaka and S. Nagakura, *Theoret. Chim. Acta*, 6, 320 (1966).

30. H. Berthot, C. Giessner-Prettre and A. Pullman, *Theoret. Chim. Acta*, 5, 53 (1966).

31. H. Berthot, C. Giessner-Prettre and A. Pullman, *Int. J. Quant. Chem.*, 1, 123 (1967).

32. V.A. Kuprievich, *Int. J. Quant. Chem.*, 1, 561 (1967).

33. M.L. Bailey, *Theoret. Chim. Acta*, 16, 309 (1970).

34. N.N.H. Teng, M.S. Itzkowitz and I. Tinoco, Jr., *J. Am. Chem. Soc.*, 92, 6257 (1971).

35. C.A. Bush, *J. Chem. Phys.*, 53, 3522 (1970).

36. W. Hug and I. Tinoco, Jr., *J. Am. Chem. Soc.*, 95, 2803 (1973).

37. N.V. Zheltovkii and V.I. Danilov, *Biophysics*, 19, 802 (1974).

38. B. Mely and A. Pullman, *Theor. Chim. Acta*, 13, 278 (1969).

39. E. Clementi, J.M. Andre, M.C. Andre, D.K. Lint and D. Hahn, *Acta Phys.*, 27, 493 (1969).

40. C.A. Bush, *J. Am. Chem. Soc.*, 95, 214 (1973).

41. R.F. Stewart and N. Davidson, *J. Chem. Phys.*, 39, 255 (1963).

42. J. Brahms, H. Sellini and S. Brahms, *Third Intern. Biophys. Congr. Abstracts*, p. 171 (1969).

43. D.W. Miles, M.J. Robins, R.K. Robins and H. Eyring, *Proc. Natl. Acad. Sci. U.S.*, 62, 22 (1969).

44. J.S. Ingwall, *J. Am. Chem. Soc.*, 94, 5487 (1972).

45. H.H. Chen and L.B. Clark, *J. Chem. Phys.*, 58, 2593 (1973).

46. C.A. Sprecher and W.C. Johnson, Jr., *Biopolymers*, 16, 2243 (1977).

47. R.W. Wilson and P.R. Callis, *Photochem. Photobiol.*, 31, 323 (1980).

48. H.H. Chen and L.B. Clark, *J. Chem. Phys.*, 51, 1862 (1969).

49. A.F. Fucarolo and L.S. Foster, *J. Am. Chem. Soc.*, 93, 6443 (1971).

50. P.R. Callis, F.J. Rosa and W.T. Simpson, *J. Am. Chem. Soc.*, 86, 2242 (1964).

51. V. Kleinwachter, J. Drobnik and L. Augenstein, *Photochem. Photobiol.*, 6, 147 (1967).

52. M. Roche and H.H. Jaffe, *Chem. Soc. Rev.*, 5, 165 (1976).

53. R.M. Hochstrasser, *Molecular Aspects of Symmetry*, p. 229, W.A. Benjamin Inc., New York (1966).

54. T. Kurucsev, *J. Chem. Educ.*, 55, 128 (1978).

55. W. Moffit and A. Moscowitz, *J. Chem. Phys.*, 30, 648 (1959).

56. S.E. Harnung, E.C. Ong and O.E. Wiegang, Jr., *J. Chem. Phys.*, 55, 5711 (1971).

57. R.C. Lord and G.J. Thomas, *Spectrochim. Acta*, 23A, 2551 (1967).

58. T. Theophanides, N. Hadjiliadis, M. Berjot, M. Maufait and L. Bernard, *J. Raman Spectr.*, 5, 315 (1976).

59. T. Theophanides, M. Berjot and L. Bernard, *J. Raman. Spectr.*, 6, 109 (1977).

60. J. Einsinger, *Photochem. Photobiol.*, 7, 597 (1968).

61. P.N. Schatz and A.J. McCaffery, *Quart. Rev.*, 23, 552 (1969).

62. C.C. Bott and T. Kurucsev, *J. Chem. Soc. Faraday II*, 71, 749 (1975).

63. G.R. Kelly and T. Kurucsev, *Biopolymers*, 15, 1481 (1976).

64. E.W. Thulstrup and J. Michl, *J. Am. Chem. Soc.*, 98, 4533 (1976).

65. C.C. Bott and T. Kurucsev, *Chem. Phys. Lett.*, 55, 585 (1978).

66. S. Arnott and D.W.L. Huckins, *Nature*, 224, 886 (1969).

67. M. Sundaralingam, *Biopolymers*, 7, 821 (1969).

68. M. Sundaralingam, *J. Am. Chem. Soc.*, 93, 6644 (1971).

69. P.O.P. Ts'o, *Basic Principles in Nucleic Acids Chemistry*, Vol. I, p. 478, P.O.P. Ts'o, ed., Academic Press, New York (1974).

70. J. Donohue and K.N. Trueblood, *J. Mol. Biol.*, 2, 363 (1960).

71. S.S. Danyluk and F.F. Hruska, *Biochemistry*, 7, 1038 (1968).

72. M.P. Schweizer, A.D. Broom, P.O.P. Ts'o and D.P. Hollis, *J. Am. Chem. Soc.*, 90, 1042 (1968).

73. C.D. Barry, A.C.T. North, J.A. Glasel, R.J.P. Williams and A.V. Xavier, *Nature*, 232, 236 (1971).

74. S.S. Tavale and H.M. Sobell, *J. Mol. Biol.*, 48, 109 (1970).

75. W. Saenger, *J. Amer. Chem. Soc.*, 93, 3035 (1971).

76. S.T. Rao, M. Sundaralingam, S.K. Arora and S.R. Hall, *Biochem. Biophys. Res. Commun.*, 38, 496 (1970).

77. A.E.V. Haschemeyer and A. Rich, *J. Mol. Biol.*, 27, 369 (1967).

78. H.R. Wilson, A. Rachman and P. Tollin, *J. Mol. Biol.*, 46, 585 (1969).

79. I. Tinoco, Jr., R.C. Davis and S.R. Jaskunas, *Molecular Associations in Biology*, p. 77, B. Pullman, ed., Academic Press, New York (1968).

80. A.V. Lakshminarayanam and V. Sasisekharam, *Biochim. Biophys. Acta*, 204, 49 (1970).

81. F. Jordan and B. Pullman, *Theoret. Chim. Acta*, 9, 242 (1968).

82. T.R. Emerson, R.J. Swan and T.L.V. Ulbricht, *Biochem. Biophys. Res. Commun.*, 22, 505 (1966).

83. T. Nishimura, B. Shimizu and I. Iwai, *Biochim. Biophys. Acta*, 157, 221 (1968).

84. D.W. Miles, L.B. Townsend, M.J. Robins, R.K. Robins, V.H. Inskeep and H. Eyring, *J. Am. Chem. Soc.*, 93, 1600 (1971).

85. G.T. Rogers and T.L.V. Ulbricht, *Biochem. Biophys. Res. Commun.*, 39, 419 (1970).

86. M. Ikehara, S. Uesugi and K. Yoshida, *Biochemistry*, 11, 830 (1972).

87. D.W. Miles, R.K. Robins and H. Eyring, *J. Phys. Chem.*, 71, 393 (1967).

88. W.H. Inskeep, D.W. Miles and H. Eyring, *J. Am. Chem. Soc.*, 92, 3866 (1970).

89. D.W. Miles, W.H. Inskeep, M.J. Robins, M.W. Winkley, R.K. Robins and H. Eyring, *J. Am. Chem. Soc.*, 92, 3872 (1970).

90. D.S. Moore, *Biopolymers*, 19, 1017 (1980).

91. D.W. Miles, M.J. Robins, R.K. Robins, M.W. Winkley and H. Eyring, *J. Am. Chem. Soc.*, 91, 831 (1969).

92. J.A. Schellman, *Accounts Chem. Res.*, 1, 144 (1968).

93. M.J. Nugent and O.E. Weigang, Jr., *J. Am. Chem. Soc.*, 91, 4555, 4556 (1969).

94. N. Harada and K. Nakanishi, *Accounts Chem. Res.*, 5, 257 (1972).

95. I. Tinoco, Jr., *Adv. Chem. Phys.*, 4, 113 (1962).

96. D.W. Miles, S.H. Hahn, R.K. Robins, M.J. Robins and H. Eyring, *J. Phys. Chem.*, 72, 1483 (1968).

97. H. Berthot and B. Pullman, *Jerusalem Symp. Quant. Chem. Biochem.*, 4, 30 (1972).

98. W.A. Eaton and T.P. Lewis, *J. Chem. Phys.*, 53, 2164 (1970).

99. P.R. Callis, B. Fanconi and W.T. Simpson, *J. Am. Chem. Soc.*, 93, 6679 (1971).

100. D.W. Miles, W.H. Inskeep, L.R. Townsend and H. Eyring, *Jerusalem Symp. Quant. Chem. Biochem.*, 4, 325 (1972).

101. B. Rosember, L. Van Camp, J.E. Trosko and V.E. Mansour, *Nature*, 222, 385 (1969).

102. P.D. Braddock, T.A. Connors, M. Jones, A.R. Khokhar, D.H. Melzack and M.E. Tobe, *Chem. Biol. Interact.*, 11, 145 (1975).

103. M. Rozencwerg, D.D. Von Hoff, J.S. Penta and M.S. Muggia, *J. Clin. Hematol. Oncol.*, 7, 672 (1977).

104. M.J. Cleare and J.D. Hoeschele, *Platinum Med. Rev.*, 17, 1 (1973).

105. J.P. Macquet and J.L. Butour, *Eur. J. Biochem.*, 83, 375 (1978).

106. S. Mansy, R. Rosenberg and A.J. Thomson, *J. Am. Chem. Soc.*, 95, 1633 (1973).

107. A.B. Robins, *Chem. Biol. Interactions*, 7, 11 (1973).

108. I.A.G. Roos, A.J. Thomson and J. Eagles, *Chem. Biol. Interactions*, 8, 421 (1974).

109. V. Kleinwachter, *Studia Biophysica*, 51, 35 (1975).

110. J.P. Macquet and T. Theophanides, *Biopolymers*, 14, 781 (1975).

111. V. Kleinwachter and R. Zaludowa, *Chem. Biol. Interactions*, 16, 207 (1977).

112. I.A.G. Roos, A.J. Thomson and S. Mansy, *J. Am. Chem. Soc.*, 96, 6484 (1974).

113. I.A.G. Roos and M.C. Arnold, *J. Clin. Hematol. Oncol.*, 7, 374 (1977).

114. I.A.G. Roos, *Chem. Biol. Interactions*, 16, 39 (1977).

115. M.J. Waring, *Nature*, 219, 1320 (1968).

116. G. Hartmann, W. Behz, K.A. Beissner, K. Honikel and A. Sippel, *Angew. Chem. Int. Edit.*, 7, 693 (1968).

117. J.P. Schreiber and M.P. Daune, *J. Mol. Biol.*, 83, 487 (1974).

118. R. Lavery and B. Pullman, *Int. J. Quant. Chem.*, 16, 175 (1979).

119. J.M. Delabar and W. Guschlbauer, *J. Am. Chem. Soc.*, 95, 5729 (1973).

120. K.A. Hartman, R.C. Lord and G.J. Thomas, *Physico-Chemical Properties of Nucleic Acids*, p. 52, J. Duchesne, ed., Academic Press, London (1973).

121. R.W. Wilson and P.R. Callis, *J. Phys. Chem.*, 80, 2280 (1976).

122. V.A. Bloomfield, D.M. Crothers and I. Tinoco, Jr., *Physical Chemistry of Nucleic Acids*, p. 50, Harper-Row Publ. New York (1974).

123. T.D. Son, W. Guschlbauer and M. Gueron, *J. Am. Chem. Soc.*, 94, 7903 (1972).

124. C.D. Barry, J.A. Glasel, A.C.T. North, R.J.P. Williams and A.V. Xavier, *Biochem. Biophys. Res. Commun.*, 47, 166 (1972).

125. W. Hug and I. Tinoco, Jr., *J. Am. Chem. Soc.*, 96, 665 (1974).

126. R.C. Davis and I. Tinoco, Jr., *Biopolymers*, 6, 223 (1968).

127. J.T. Powell, E.C. Richards and W.B. Gratzer, *Biopolymers*, 11, 235 (1972).

128. N.S. Kondo and H.M. Holmes, L.M. Stempel and P.O.P. Ts'o, *Biochemistry*, 9, 3479 (1970).

129. M.M. Warshaw and I. Tinoco, Jr., *J. Mol. Biol.*, 20, 29 (1966).

130. D. Glaubiger, D.A. Lloyd and I. Tinoco, Jr., *Biopolymers*, 6, 409 (1968).

131. K.E. Van Holde, J. Brahms and A.M. Michelson, *J. Mol. Biol.*, 12, 726 (1965).

132. C.R. Cantor, M.M. Warshaw and H. Shapiro, *Biopolymers*, 9, 1059 (1970).

133. C.S.M. Olsthoorn, C.A.G. Haasnoot and C. Altona, *Eur. J. Biochem.*, 106, 85 (1980).

134. J.W. Pettegrew, D.W. Miles and H. Eyring, *Proc. Natl. Acad. Sci. USA*, 74, 1785 (1977).

135. M.M. Warshaw and I. Tinoco, Jr., *J. Mol. Biol.*, 13, 54 (1965).

136. N.S. Kondo, F.N. Fang, P.S. Miller and P.O.P. Ts'o, *Biochemistry*, 11, 1991 (1972).

137. W.C. Johnson, Jr., M.S. Itzkowitz and I. Tinoco, Jr., *Biopolymers*, 11, 225 (1972).

138. C.A. Bush and I. Tinoco, Jr., *J. Mol. Biol.*, 23, 601 (1967).

139. M.L. Bailey, *Biopolymers*, 11, 1091 (1972).

140. N.P. Johnson and E. Switkes, *Biopolymers*, 17, 857 (1978).

141. C.L. Check, W. Hug and I. Tinoco, Jr., *Biopolymers*, 15, 131 (1976).

142. C.H. Lee, F.S. Ezra, N.S. Kondo, R.H. Sarma and S.S. Danyluk, *Biochemistry*, 15, 3627 (1976).

143. S.I. Chan and J.H. Nelson, *J. Am. Chem. Soc.*, 91, 168 (1969).

144. H. De Voe, *J. Chem. Phys.*, 43, 3199 (1965).

145. M. Leng and G. Felsenfeld, *J. Mol. Biol.*, 15, 455 (1966).

146. P.S. Miller, K.N. Fang, N.S. Kondo and P.O.P. Ts'o, *J. Am. Chem. Soc.*, 93, 6657 (1971).

147. W.C. Johnson, Jr. and I. Tinoco, Jr., *Biopolymers*, 8, 715 (1969).

148. K.N. Fang, N.S. Kondo, P.S. Miller and P.O.P. Ts'o, *J. Am. Chem. Soc.*, 93, 6647 (1971).

149. P.O.P. Ts'o, N.S. Kondo, M.P. Schweizer and D.P. Hollis, *Biochemistry*, 8, 997 (1969).

150. S.S. Danyluk and F.E. Hruska, *Biochemistry*, 7, 1038 (1968).

151. C. Chachaty, B. Perly, A. Forchioni and G. Langlet, *Biopolymers*, 19, 1211 (1980).

152. N.S. Kondo and S.S. Danyluk, *Biochemistry*, 15, 756 (1976).

153. L.S. Kan, J.C. Barrett, P.S. Miller and P.O.P. Ts'o, *Biopolymers*, 12, 225 (1973).

154. C.H. Lee and I. Tinoco, Jr., *Biochemistry*, 16, 5403 (1977).

155. P. Thiyagarajan and P.K. Ponnuswamy, *Biopolymers*, 17, 533, 2143 (1978).

156. S.B. Broyde, R.M. Wartell, S.D. Stellman, B. Hingerty and R. Langridge, *Biopolymers*, 14, 1597 (1975).

157. S.B. Broyde, R.M. Wartell, S.D. Stellman and B. Hingerty, *Biopolymers*, 17, 1485 (1978).

158. C.H. Lee, E. Charney and I. Tinoco, Jr., *Biochemistry*, 18, 5636 (1979).

159. M.J. Lowe and J.A. Schellman, *J. Mol. Biol.*, 65, 91 (1972).

160. J.C. Maurizot, J. Brahms and F. Eckstein, *Nature*, 222, 559 (1969).

161. N. Ogasawara and Y. Inoue, *J. Am. Chem. Soc.*, 98, 7054 (1976).

162. J.P. Poland, J.N. Vournakis and H.A. Sheraga, *Biopolymers*, 4, 223 (1966).

163. N.P. Johnson and T. Schleich, *Biochemistry*, 13, 981 (1974).

164. A.J. Alder, L. Grossman and G.D. Fasman, *Biochemistry*, 8, 3848 (1969).

165. C. Altona, *Structure and Conformation of Nucleic Acids and Protein-Nucleic Acids interactions*, p. 613, Eds. M. Sundaralingam and S.T. Rao, University Park Press, Baltimore (1975).

166. D.B. Davies, *Prog. NMR Spectrosc.*, 12, 135 (1978).

167. J.F. Chantot, M. Th. Sarochi and W. Guschlbauer, *Biochimie*, 53, 347 (1971).

168. D.E. Joyce, Honours Report, University of Adelaide (1973).

169. J.F. Chantot and W. Guschlbauer, *Jerusalem. Symp. Quant. Chem. Biochem.*, 4, 205 (1972).

170. R. Savoie, H. Klump and W.L. Peticolas, *Biopolymers*, 17, 1335 (1978).

171. R.W. Wilson and P.R. Callis, *J. Phys. Chem.*, 80, 2280 (1976).

172. J.F. Chantot, T. Haertle and W. Guschlbauer, *Biochimie*, 56, 501 (1974).

173. B.M. Baker, J. Vanderkooi and N.R. Kallenbach, *Biopolymers*, 17, 1361 (1978).

CHAPTER III

Interaction between Dyes and DNA

6. INTRODUCTION

After our study of the components which make up the Nucleic Acids and in particular of the forces which bind them together to form the structure of the DNA double helix, we would like to investigate how some substances such as dyes are capable of altering not only these forces but also the biological functioning of the Nucleic Acids[1]. Indeed, dyes are known to cause frameshift mutations[2-5], to inhibit the DNA and RNA synthesis[6,7], and also to possess antibacterial and antiviral properties[8]. The effects of these dyes have their origin in a particular interaction with the Nucleic Acids. The chemical structures of some dyes are shown in figure 6.1.

6.1 Modes of Binding of Dyes to DNA

Their binding abilities have been exploited for many years in the staining of Nucleic Acids in cells[8-10]. In 1947, Michaelis[11] envisaged the possibility for the dye to insert into the DNA helix. This hypothesis was confirmed later by fluorescence[12,13] studies which indicated a close interaction between the DNA bases and the dye molecules. Upon absorption and equilibrium dialysis measurements, Peacocke and Skerrett[14], in 1956, were able to distinguish two types of binding. The first type, referred to as strong binding, predominates at low values of r (r is the ratio of the bound dye to the DNA phosphate concentration) but as r increases, it is progressively replaced by a weak binding up to the electroneutrality limit of one dye bound per nucleotide. The terms strong and weak binding refer to the values of the association constants derived from the Scatchard plots for the two types of binding. An association constant of the

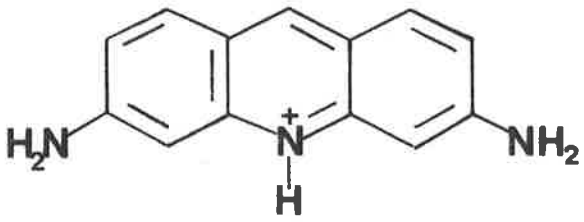

PROFLAVINE

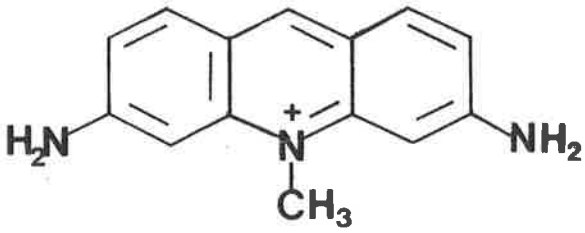

ACRIFLAVINE

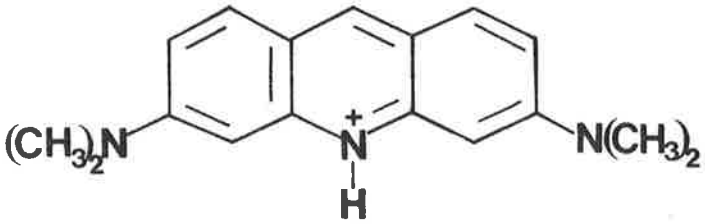

ACRIDINE ORANGE

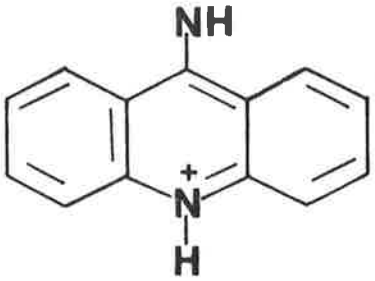

9-AMINOACRIDINE

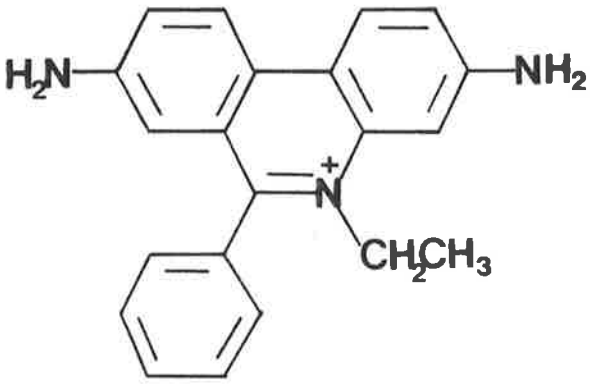

ETHIDIUM BROMIDE

FIG.6.1 CHEMICAL STRUCTURE OF SOME ACRIDINE DYES AND OF THE PHENANTHRIDINE ETHIDIUM BROMIDE.

order of 10^6 mol^{-1} dm^3 was found for the strong binding process, while a much lower value was attributed to the weak binding. Whereas the weak binding was associated with the binding of dye aggregates to the phosphates on the surface of the DNA helix, the strong binding was found to involve a close interaction between the aromatic rings of the dyes and the DNA bases (an overlapping of their π-orbitals was suggested). It was not until 1961 that an elaborate study of the interaction of a dye with DNA was carried out. In this case, Lerman, by using different methods of observation, was able to give a more detailed picture of the binding process[4]. The combination of different methods such as viscosity[15] and sedimentation measurements[16], flow dichroism and flow polarised fluorescence[17], chemical reactivity[18] and X-ray diffraction enabled Lerman to arrive at the conclusion that the dyes, in particular proflavine, were intercalated between the DNA base pairs[4]. The intercalation proposed by Lerman has since been confirmed on many occasions[19,20] and can be represented as follows:

- the intercalation of a dye molecule between two base-pairs causes the flexible DNA helix to unwind so that the distance of 3.4Å separating two consecutive base-pairs is approximately doubled in order to allow for the flat ring of the dye[15,21-27]. The unwinding of the double helix has been the subject of a lot of controversy[28,29]. An intercalation unwinding angle of 45° was proposed by Lerman[15], but in more recent studies[25,30,31], it has been determined that most aminoacridines caused the DNA helix to unwind at an angle of only 17° on intercalation. An increase in this unwinding angle can be found for molecules such as ethidium bromide[31]

whereas a decrease has been noted for the anthracyclines[32]. The presence of an outside binding which does not affect the unwinding of the DNA helix[26,33] could partially explain these differences, as Waring[32] has proposed, but it has also been shown[31] that other factors, which can include steric factors or the formation of hydrogen bonds, may account for these differences in unwinding angles.

- the plane of the intercalated dye lies approximately perpendicular to the helix axis and parallel to the base-pairs[17,35]. Although the structure of the aminoacridine dyes is rather similar, it has been found in this laboratory that their intercalation geometry in relation to the DNA helix axis is different[36].

- in order to account for the quite pronounced insensitivity of the bound dye amino-groups to chemical attack[18], Lerman placed the dye with its ring nitrogen centrally positioned above and below the hydrogen bonds of the base-pairs in order to allow for maximum overlapping of the aromatic rings of the dyes and the base-pairs. In this position the 3 and 6-amino-groups of proflavine (PF), for example, are in close proximity to the phosphate groups of DNA[4] (figure 6.2). The intercalation of dyes between base-pairs increases the thermal stability of the DNA[38,39]. Hydrophobic forces were also found to be an important factor in the stabilization of the dye-DNA complex[18,40].

The application of the Lerman model is limited, however, because it can not account for the intercalation of dyes into single stranded polynucleotides or into denatured disordered DNA[41,42]. Indeed, the fact that the amount of binding is similar in native and in denatured DNA has led Pritchard *et al.*[43] to propose a modified intercalation model in which

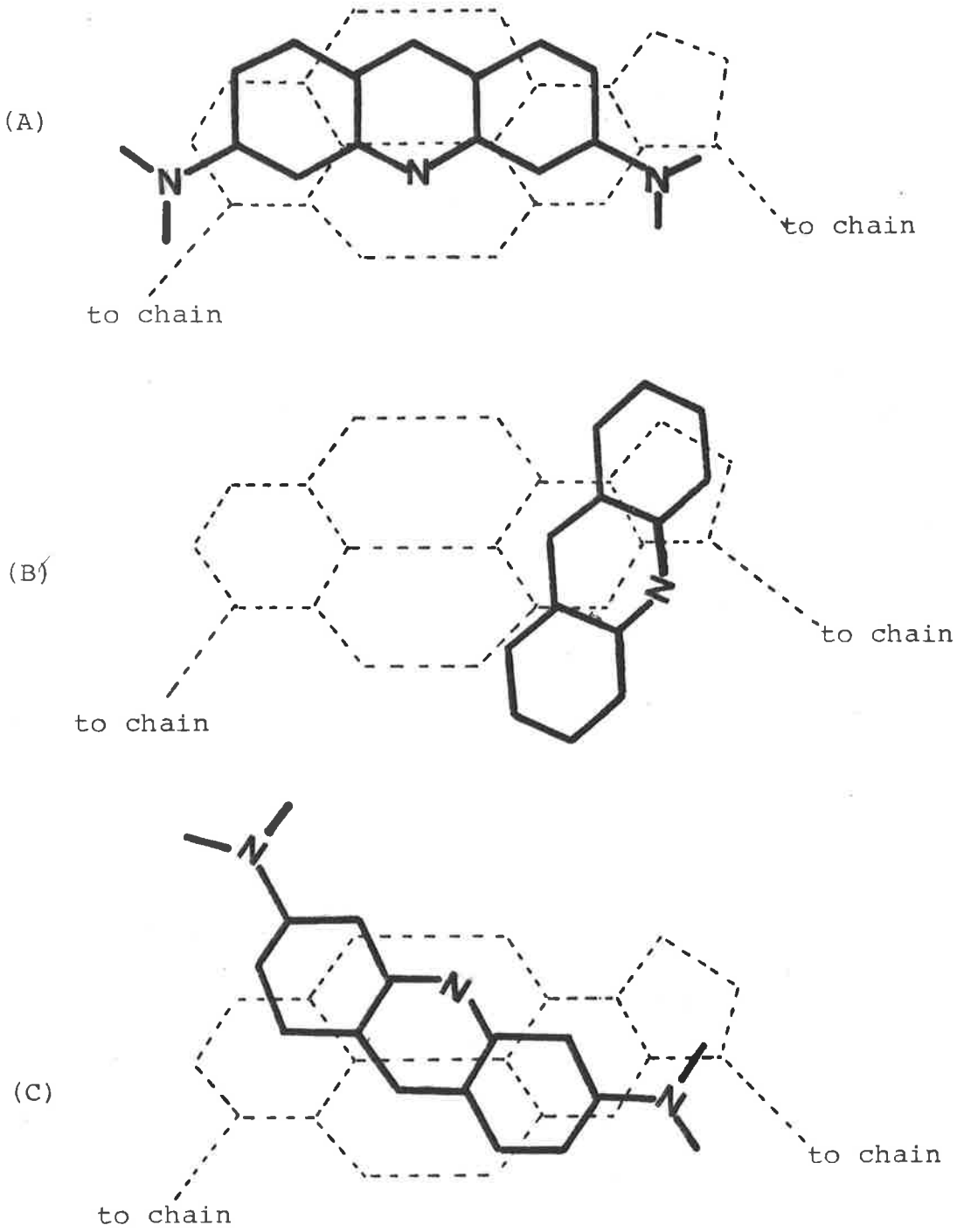

FIG.6.2 INTERCALATION MODELS PROPOSED BY LERMAN[4] (A), PRITCHARD ET AL[4] (B) AND DALGLEISH ET AL[46] (C). The models are viewed along the DNA helix axis. The broken and full lines represent the base pair and the intercalated dye, respectively.

the dye intercalates between two consecutive bases on the same DNA strand and, as a result, its charged ring nitrogen is in close proximity to the phosphate group (figure 6.2). This position could explain the decrease in binding abilities found in dyes carrying substituent groups on the heterocyclic nitrogen atom[44].

It has also been found that the positions of the intercalated ethidium bromide molecule in the DNA are rather limited because of its bulky phenyl and ethyl groups[45]. Dalgleish *et al.*[46], taking as a reference the "allowed" positions of the intercalated ethidium bromide[45], were able to define an intercalation position which is intermediate to the ones proposed by Lerman and by Pritchard. This model is based on the presence of a common 7-aminoquinoline sub-structure in dyes such as PF, ethidium bromide and 3-aminoacridine which can all make a hydrogen bond between one of their amino-groups and the DNA phosphate (figure 6.2). In addition to these intercalated dyes, the existence of non-intercalated dyes in the strong binding region, postulated by Armstrong, Kurucsev and Strauss[26] to explain their viscometry data behaviour, has been confirmed by temperature jump studies[33,47-49] as being part of an initial binding stage of the dye to the DNA (as much as 70% at $r = 0.05$ for an ionic strength of 0.001[47]) and also by fluorescence decay measurements[76,115].

Nevertheless, even though these models give us a satisfactory understanding of most of the binding processes, they are all lacking in structural details which would enable us to comprehend all the various biological activities associated with intercalation[50]. It is in order to satisfy these requirements that X-ray diffraction studies[15,45] on

fibre associated with computerised model-building[51] have been extensively used. However, because of the high molecular weight of Nucleic Acids, an atomic resolution is only reached with X-ray diffraction of single-crystals of dinucleoside-dye complexes[53]. Important information has, in fact, been gathered from these studies - the confirmation of a symmetrical intercalation position[54,55] similar to the one proposed by Lerman, as well as a more asymmetrical intercalation position[50,56,57], the presence of non-intercalated bound dyes[58,59] and the importance of hydrogen bonds[54,57,59] and water molecules in the stabilization of the complex[60] - but their application to dideoxynucleosides or indeed DNA is not straightforward[20,61].

6.2 Heterogeneity of the Binding Sites

The existence of a binding specificity for adenine-thymine (A-T) or guanine-cytosine (G-C) base-pairs has been the subject of much controversy[62,63]. In most studies involving the aminoacridines proflavine (PF), acriflavine (AC), 9-aminoacridine (9-AA) as well as ethidium bromide, it has been shown that the strong binding is not base-specific and the dye is randomly distributed among the available binding sites[63-67]. On the other hand, the heterogeneity of binding sites has been demonstrated by different methods. Temperature studies[38] and free energy calculations[68,69] have shown the higher stabilization caused by a dye intercalated between the A-T base-pairs. Kinetic[49] and viscosity[33] studies have linked the binding site of non-intercalated dyes to G-C rich regions. Fluorescence spectroscopy has proved the most sensitive method for studying this heterogeneity[70]. Indeed, it has been possible to

distinguish two types of strong binding sites according to the fluorescence behaviour of the dye-DNA complexes: one site, associated with a G-C base-pair, quenches the fluorescence of the bound dye while the other site, associated with an A-T base-pair, enhances the fluorescence of the bound dye[62,64,66,71,72]. Guanine has been shown to be responsible for the quenching phenomenon[74].

Of the two more recent and sensitive techniques used so far for the study of the dye-DNA complexes, that is to say nanosecond fluorescence decay studies[65,67,75] and temperature-jump relaxation studies using fluorescence detection[77], no new major and definitive information has been provided but they have shown the complexity of the intercalation process and revealed the importance of the heterogeneity of the binding sites for the understanding of the biological effects produced by the dye molecules.

6.3 Spectroscopic Methods for the Study of the Dye-DNA Interaction

In the second part of this thesis, we will look at the interaction between dyes and DNA from a spectroscopic point of view, using absorption and circular dichroism techniques with the intention of correlating the data obtained with observations previously made and in order to determine whether we can apply the different theoretical approaches outlined in the first part of this thesis to this new problem.

6.3.1 Absorption Spectroscopy

Absorption spectroscopy has been intensively used in this domain and has already given important information on the binding process. The binding of a dye to DNA (or any other polymer) is characterised by a shift to the red of its

absorption spectrum with respect to that of the free dye; this shift is accompanied by a hypochromic effect[11,14,41,78] if the dye intercalates into the DNA helix, whereas hyperchromic effects[30,79,80] have been found for dyes which bind only to the outside of the DNA helix. Even though the number of examples is insufficient to allow us to generalise upon this finding, we can say that the hypochromic effect is totally compatible with a model in which close contact or stacking occurs between the dye and the base-pair rings on intercalation. In table 6.1 we have calculated, with the use of equation 5.1, the percentage hypochromism, H%, of the dye electronic transition which results from the binding of the dye to the DNA. Theoretical calculations enable us to correlate the hypochromism to its geometrical contribution as in equation 5.2 or in a more detailed form[34]

$$H = \frac{4\mu^2_{DNA}}{h} \cdot \frac{\tilde{\nu}_{DNA}}{\tilde{\nu}^2_{DNA} - \tilde{\nu}^2_{DYE}} \cdot \frac{1}{R^3}(\cos\theta_{ij} - 3\cos^2\theta_i)\cos\theta_{ij} \qquad (6.1)$$

where R is the distance separating the two coupled transition moments μ_{DNA} and μ_{DYE}, $\tilde{\nu}_{DNA}$ and $\tilde{\nu}_{DYE}$ are the transition frequencies. The angles θ_i, θ_{ij} are defined in figure 6.3. We can note, in equation 6.1, that the hypochromism will be mainly dependent on the distance R. Using the simplified model in figure 6.3 we can write equation 6.1 as

$$H \propto \frac{\tilde{\nu}_{DNA}}{\tilde{\nu}^2_{DNA} - \tilde{\nu}^2_{DYE}} \cdot f(\theta_{ij},\theta_i) \qquad (6.2)$$

with

$$f(\theta_{ij},\theta_i) = (\cos\theta_{ij} - 3\cos^2\theta_i)\cos\theta_{ij}\sin^3\theta_i \qquad (6.3)$$

The geometrical factor $f(\theta_{ij},\theta_i)$ depends only on the geometrical relation existing between the dye and the DNA base-pair transition moments. In figure 6.4 we have plotted

Table 6.1 CALCULATION OF THE GEOMETRICAL FACTOR IN EQUATION 6.2 FOR DYE-DNA COMPLEXES.

	Dye complexed to DNA	Polarisation of the transition	H%	$10^5 \times \frac{\tilde{\nu}_{DNA}}{\tilde{\nu}^2_{DNA}-\tilde{\nu}^2_{DYE}}$ (cm)	$10^{-5} \times H\% / \frac{\tilde{\nu}_{DNA}}{\tilde{\nu}^2_{DNA}-\tilde{\nu}^2_{DYE}}$ (cm^{-1})
intercalated dye	Acridine Orange (AO)	long axis	22.9	3.55	6.4
	Proflavine (PF)	long axis	24.6	3.81	6.5
	Acriflavine (AC)	long axis	30.2	3.76	8.0
	9-aminoacridine (9AA)	long axis	42.1	6.85	6.2
		short axis	52.6	4.10	12.8
	Ethidium bromide	long axis	57.8	10.44	5.6
		short axis	35.4	3.43	10.3
non-intercalated dye	di-tert-butyl PF[a]	long axis	4.0	3.73	1.0
	Methyl green (MG)[b]		-5.6	3.11	-1.8

a - from figure 2a of reference 52.

b - from figure 2 of reference 30.

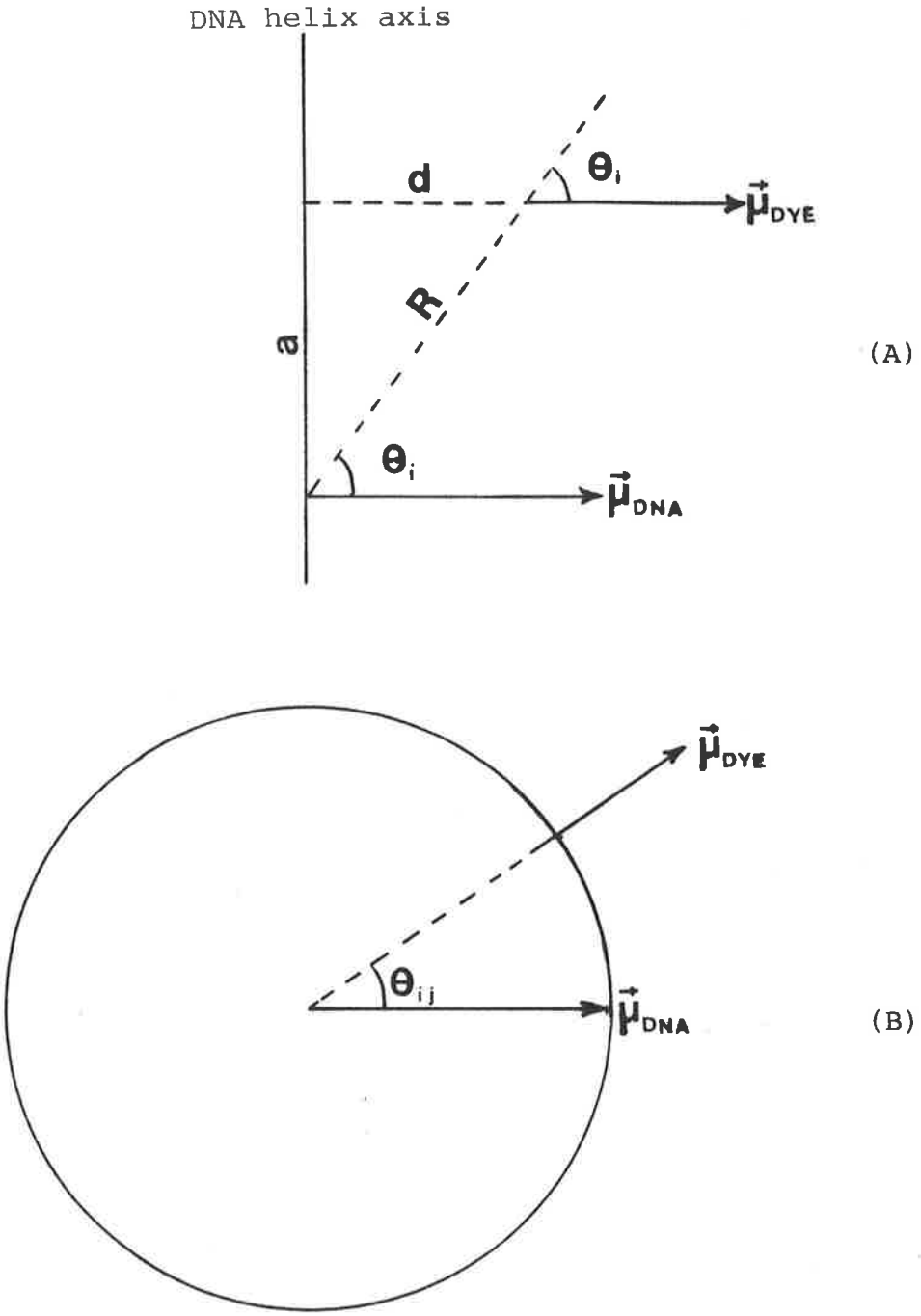

FIG.6.3 SCHEMATIC DIAGRAM SHOWING THE GEOMETRY USED IN CALCULATING THE GEOMETRICAL FACTOR IN EQUATION 6.3.
(A),view perpendicularly to the DNA helix axis;
(B),view along the DNA helix axis.

$f(\theta_{ij},\theta_i)$ versus the distance, d, separating the dye from the DNA helix axis ($d = a/\tan\theta_i$). The distance, a, which separates the base-pair to the dye was fixed to 3.4Å[15]. It was assumed in figure 6.4 that the non-intercalated dye binds in one of the grooves of the DNA[73] and that the limit of intercalation domain coincides with the non-overlapping of the dye and the base-pair rings. A satisfactory correlation is found between the experimental geometrical factor in table 6.1 and the theoretical geometrical factor, $f(\theta_{ij},\theta_i)$, in figure 6.4 as regards their dependence on the distance d, which separates the DNA helix axis to the dye molecule. The negative value of the geometrical factor, obtained in table 6.1 for the methyl green-DNA complex, can be explained by the fact that the bound methyl green molecule is situated in the wide groove of the DNA at a distance of 5 to 6Å from the helix axis[73]. The geometrical factor for the long axis polarised transition of the intercalated dye ranges from $5.6\ 10^5$ to $8\ 10^5\ cm^{-1}$, which indicates that the position of intercalation, in relation to the DNA helix axis, is rather similar for these dyes. The differences in these values can be attributed to differences in the angle θ_{ij} (the geometrical factor associated with the short axis polarised transition of the intercalated dye is nearly two times more important than the one associated with the long axis polarised transition) or to differences in the twist and tilt angles[36] between the base pair and the dye. In fact, the relatively high value of the geometrical factor obtained for acriflavine can be explained (equation 4.8 of reference 34) by the fact that its orientation inside the DNA, is more perpendicular to the helix axis than any other bound dyes[36].

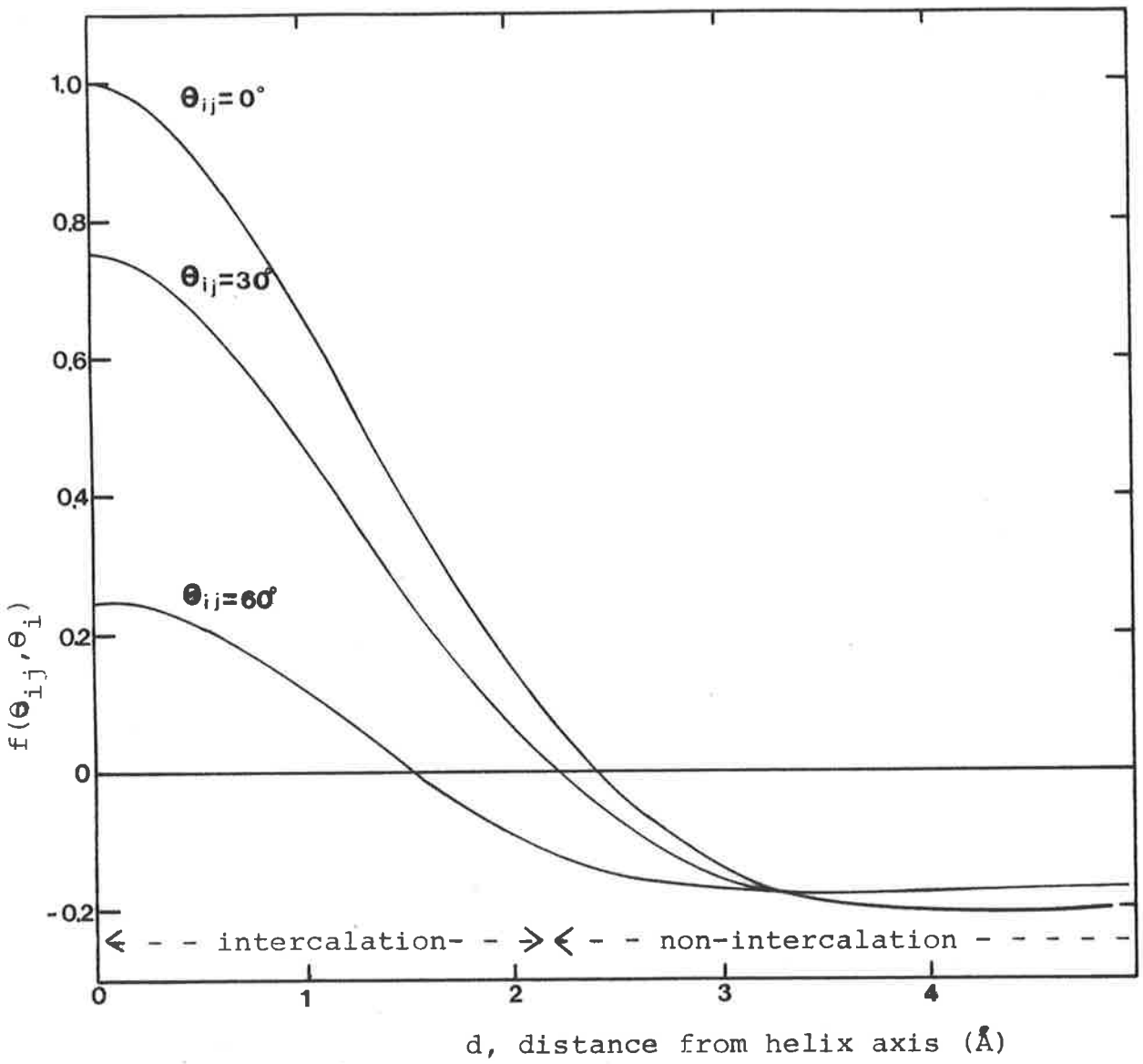

FIG.6.4 CALCULATION OF THE GEOMETRICAL CONTRIBUTION TO THE HYPOCHROMICITY OR GEOMETRICAL FACTOR IN EQUATION 6.2 VERSUS THE DISTANCE BETWEEN THE DYE AND THE DNA HELIX AXIS.

Until now we have only considered the binding of a monomeric dye to the DNA in the strong binding region, as has most of the research done so far, but absorption and above all circular dichroism, as we will see later, have revealed beyond all doubt the presence of a dimeric dye species which is to be found well before the apparition of the aggregate bound dye in the weak binding region[26]. The dimeric absorption spectrum is characterized by a shift to the blue of its maximum position with respect to that of the monomeric dye as well as by a hypochromic effect due to the stacking of the two moieties of the dimer[26]; these changes are similar to the ones observed for the dimeric dye in free solution[81,82], although less perceptible[26]. Among the theories which have been invoked for explaining the spectral changes that take place upon dimerization[83], the exciton theory[84] has received considerable attention and strong support. It is important to note that, the outside bound dye observed in temperature-jump studies[33,47-49], is in fact a bound dimeric dye[76] (conclusion based on the shape of the absorption spectrum attributed to the "outside bound dye"), which casts some doubt on the results obtained from the use of this technique.

6.3.2 Circular Dichroism (CD)

In 1961, Neville and Bradley[85] found that the optically inactive dyes acquired optical activity on binding to DNA as it was observed earlier when they bind to asymmetric helical polymers[86,87]. A lot of research has been devoted to this particular phenomenon in order to find a mechanism capable of inducing optical activity in a dye on binding to DNA. Several mechanisms[88] emerge if we consider the optical

properties of both the dye and of the DNA and they are all described in paragraph 1.1.

The use of CD as a new method of investigation has become very popular in the last two decades and various attempts at interpreting the CD spectrum have been made. In the statistical analysis method, it was assumed that the optical activity depends on the succession of binding sites occupied by a dye molecule separated by empty sites[85,89-94]. The good fit of the evolution of the CD spectrum with the square of the bound dye to phosphate ratio (r^2) led to the interpretation that the dye-dye interaction was mainly responsible for the induced optical activity through the formation of a dimeric species[89,92-94] or of a helical array of bound dye molecules[35,85,95,96]. Although statistical methods gave satisfactory results, their meanings can be questioned because of the use of only one wavelength of observation. They are also questionable because of the use of a single equation representing only one type of binding, in spite of the fact that different types of binding occur over such a larger range of binding as shown by other experimental techniques[92] and by the variations in the shape of the CD spectrum envelope as the binding proceeds[92]. The changes which occur in the CD spectrum with an increase in the amount of binding or with an increase in temperature led some studies into consideration of the deconvolution of the spectrum in different bands[91,92,97-99]. This method, which originally seemed quite promising, gave rise to all sorts of interpretations about the number of bands, the number of transitions or the number of exciton interactions present in the CD spectrum. Furthermore, most of these interpretations proved inadequate in that they were not backed up by current

theories. The very few theoretical calculations done on the CD spectrum of the dye-DNA complex were unable to reproduce the experimental CD spectrum[96,100].

In conclusion, we can say that, although CD measurements have been widely used for the study of dye-DNA interactions, there has not emerged, as yet, a satisfactory unified model for the interpretation of the induced optical activity.

Recently, Dalgleish *et al.*[46,90] were able to distinguish through CD measurements, two groups of dyes binding to DNA. The first group, which includes proflavine, ethidium bromide and 3-aminoacridine dyes, shows, when complexed to DNA, a great change in the magnitude of the CD spectrum with an increase in the amount of binding. Each one of these dyes possesses a common sub-structure, the 7-aminoquinoline. These dyes could bind to DNA in a similar manner by making hydrogen bonds between their 3-amino groups and the phosphate groups of DNA. 1,2 and 9-aminoacridine, which show little variation in their CD spectra when the binding to DNA proceeds, are characteristic of the second group and are supposed to have a different geometry of binding from the first group. To test the validity of this differentiation between dyes, we will study the CD spectra of several dye-DNA complexes, choosing dyes that are characteristic of both groups.

7. THE ACRIDINE ORANGE AND PROFLAVINE-DNA COMPLEXES

7.1 Electronic Properties of the AO and PF Dyes

The electronic properties of dye molecules have been extensively studied by Zanker[101-104]. Through the use of fluorescence polarization and low temperature measurements, he was able to assign each band present in the absorption spectrum to an electronic transition, according to the Platt classification[105]. In particular, by correlating the absorption spectrum of proflavine with other similar dyes, Wittwer and Zanker[103] predicted that its visible absorption spectrum was composite, with a strong long axis polarised transition and, on its low energy side, a short axis polarised transition of lower intensity. Figure 7.1 shows the absorption spectrum and its tentative resolution into vibronic bands, as well as the dichroic spectrum for the two dyes studied, acridine orange (AO) and proflavine (PF). Their envelopes are rather similar in shape but the position of the intensity maximum occurs at different wavelengths. The constancy of the dichroic ratio over the entire visible band as well as the agreement between experimental and calculated envelopes of the absorption band for the two dyes indicate beyond all doubt the presence of only one transition which is long axis polarised according to the value of the dichroic ratio. Thus a second transition at a longer wavelength as predicted by Wittwer and Zanker[103] if it existed, would have a very low intensity[106]. The concentration of the dyes used in Zanker's work[103] (10^{-4} mol dm^{-3}) was too high, especially when using these dyes which have a high tendency to dimerize[81,107]. Their weak shoulder observed on the low energy side of the absorption envelope

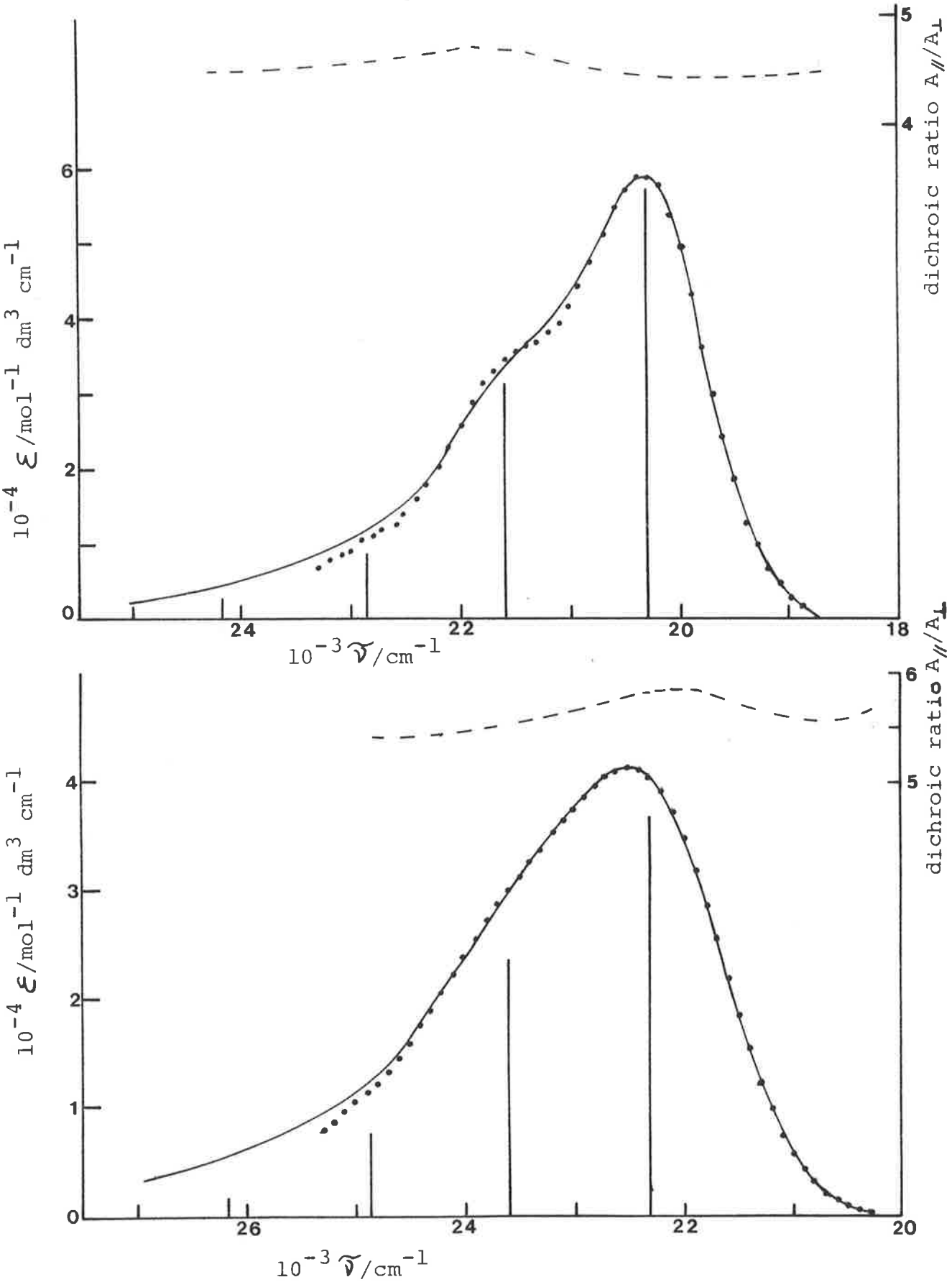

FIG 7.1 ABSORPTION SPECTRA OF ACRIDINE ORANGE (TOP) AND PROFLAVINE (BOTTOM) DYES IN 0.001 M NACL SOLUTION. The total dye concentration is 1.0×10^{-6} mol dm^{-3}. (—),experimental spectrum;(..),spectrum fitted to an harmonic progression with bands positions and intensities indicated by vertical lines(see table 7.1); (---),dichroic ratio in PVA film stretched 4 times.

Table 7.1 PARAMETERS OBTAINED FROM THE FIT OF THE ABSORPTION SPECTRA OF DYES.

(Figures in brackets are linear estimates of the standard deviations of the best-fit parameters.)

Parameters[a]	Acridine Orange	Proflavine
$\tilde{\nu}_{oo}$ (cm^{-1})	20300 (10)	22290 (10)
X	0.55 (0.01)	0.64 (0.02)
V (cm^{-1})	1290 (20)	1290 (20)
b_g (cm^{-1})	1260 (20)	1590 (20)
ε_{oo} (mol^{-1} dm^3 cm^{-1})	57300 (600)	36600 (400)
f	0.57_5	0.50_7

a - The parameters are defined in appendix C.

and attributed to a short axis polarised transition could well be the result of exciton splittings[82]. Furthermore, previous theoretical calculations of the electronic transitions of these dyes[108,109] including those made in this laboratory (table 7.2) do not show any sign of transition on the lower energy side of the intense long axis polarised transition but, on the contrary, have indicated the presence of a weak short axis polarised transition at higher energies. The synthesis of the acridine orange reporter N,N,N-Trimethyl-N',N'-dimethyl-N'-2[(3,6-di(dimethylamino)acridin-9-yl)amino]ethyl-1,3-diammoniumpropane dichloride[110] has allowed us to resolve the problem of the electronic transitions of these dyes. The dichroic ratio behaviour over the visible region of the spectrum (figure 7.2) confirms the results obtained from theoretical calculations.

7.2 The Armstrong, Kurucsev and Strauss Binding Model

In order to interpret the evolution of the optical data according to the amount of binding, it is essential to establish a binding model. Although the distinction between a strong binding, with intercalation of the dye into the DNA, and a weak binding, with fixation of the dye on the surface of the DNA, seems at first a satisfactory explanation of the general features of the binding process[14], it proves to be oversimplified especially with the recent development of more and more sensitive methods of detection that show clearly the complexity of the phenomenon. For example, the presence of an isosbestic point in the absorption spectra of AO, PF and 9AA-DNA complexes at different values of r (ratio of the bound dye to DNA phosphate concentration), which is a good indication of the existence of two spectroscopically distinct

Table 7.2 CALCULATED ENERGIES, INTENSITIES AND POLARISATIONS OF PROFLAVINE CATION.

Energy[a] of the (0.0) band in cm^{-1}	Oscillator strength f	Polarisation direction[b]	reference
23,700	1.052	X	
26,950	0.045	Y	108
31,250	0.002		
24,490	1.062	X	
25,630	0.077	Y	this study[c]
30,010	0.000	X	

a - Only the transitions in the visible part of the spectrum were considered.

b - The polarisation directions X and Y correspond to the long and short molecular symmetry axis of the proflavine, respectively.

c - The theoretical calculations were carried out using the SCF-CI-PPP method described by Bailey[37].

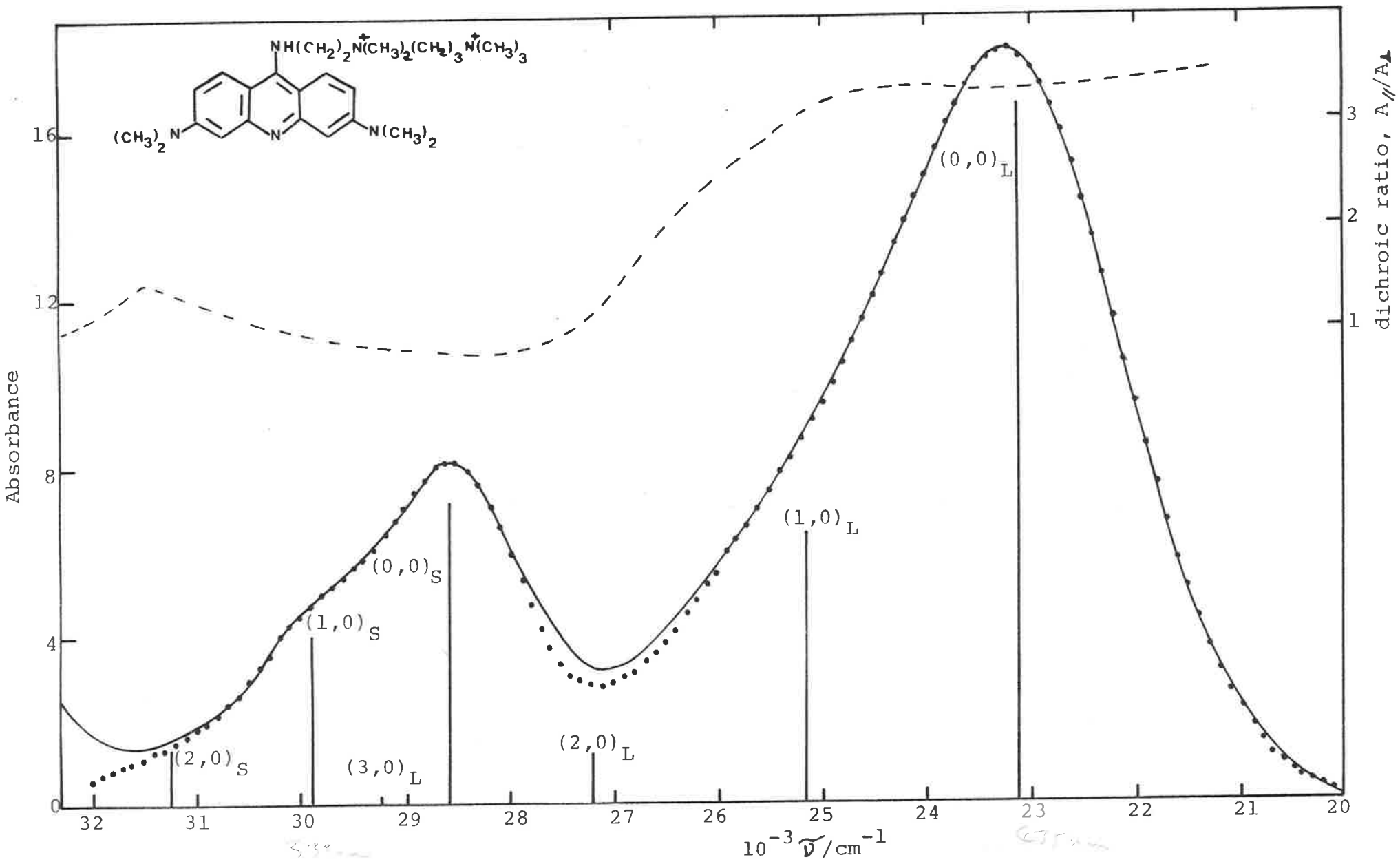

FIG.7.2 ABSORPTION SPECTRUM OF ACRIDINE ORANGE REPORTER (SEE TEXT). Symbols as in fig.7.1 . The subscripts L and S stand for the long and short axis polarised transitions.

species, has been refuted by more recent investigations[26,92]. Furthermore, numerous binding studies have shown that the amount of binding is restricted. The nearest neighbour exclusion model, where all base-pairs are potential intercalation sites, with the restriction that intercalation occurs at adjacent sites, has provided a satisfactory representation for the binding of several dyes[26,28,35,92,111,112]. Although the binding process seems to be relatively complex[113,114], the simple model postulated by Armstrong, Kurucsev and Strauss[26] has proved satisfactory for a quantitative interpretation of the data from various experimental techniques[26,92] such as equilibrium dialysis and viscosimetry as well as absorption and fluorescence spectroscopy. This model incorporates all the characteristics of the nearest neighbour exclusion model but, in addition, it allows for the binding of a non-intercalated dye next to an already intercalated dye, the two dyes therefore constituting a dimer. The model thus formulated can be represented by the following equilibria

$$A_F + DNA \overset{K_1}{\rightleftharpoons} A_1 + A_F \overset{K_2}{\rightleftharpoons} A_1A_2$$

where A_F, A_1 and A_1A_2 represent respectively the free dye of concentration C_F, the intercalated dye of concentration C_1 and the bound dye in dimeric form of concentration C_{12}. The dimer A_1A_2 is made up of a non-intercalated dye, A_2, bound to an already intercalated dye A_1. The dimerization constant, K_2, is given by the expression

$$K_2 = \frac{C_{12}}{C_F(C_1 - C_{12})} \qquad (7.1)$$

The expression for the binding constant K_1 is, in general, more complex. In this thesis, we will not limit ourselves to the original description of the model, but will use it in a

more general way with no restrictions on the number of sites excluded. Crothers[111], Schellman[116] as well as McGhee and Von Hippel[117], using different approaches, were able to derive a binding isotherm for the general site exclusion model. If we include the dimeric contribution, their expression takes the following form

$$\frac{r}{C_F} = \frac{K_1}{2} \frac{\{[1 - 2nr] + 2K_2C_F[1 - nr]\}^n}{\{[1 - 2(n-1)r] + 2K_2C_F[1 - (n-1)r]\}^{(n-1)}} \qquad (7.2)$$

where n represents the number of base-pairs per binding site and r represents the ratio of bound dye to the total DNA phosphate concentration ($r = C_B/C_{DNA}$).

As the dyes studied present no optical activity when free in solution[95], it is of interest, in order to give a more accurate picture of the phenomena, to correct the data for the free dye contribution and thus express the circular dichroism per mole of bound dye. The bound dye concentration is given by

$$C_B = C_1 + C_{12} \qquad (7.3)$$

Following the definition of r, we can write the two quantities as follows:

$$r_1 = C_1/C_{DNA} \quad \text{and} \quad r_{12} = C_{12}/C_{DNA} \qquad (7.4)$$

Equation 7.1 can then be written as

$$K_2 = \frac{r_{12}}{C_F(r_1 - r_{12})} \qquad (7.5)$$

At infinite dilution of the dye into the DNA, only the intercalated dye in a monomeric form is present. If fact, its CD spectrum is similar in shape to the absorption spectrum; the position maxima of the two spectra coincide. We have also seen that the evolution of the CD spectrum with r was governed by dye-dye interactions[85,89,92-95]. That is

why the existence of only two bound species in the strong binding region enables us to express the molar circular dichroism at each wavenumber in terms of a monomeric and a dimeric contribution

$$\Delta\varepsilon(\tilde{\nu}) = \Delta\varepsilon(\tilde{\nu})_{mono} + \Delta\varepsilon(\tilde{\nu})_{dimer} \qquad (7.6)$$

In general, the expression for circular dichroism is more complex than the one for absorption[119]: not only does the intercalated dye acquire optical activity because of the perturbation of the DNA base-pairs, but so too does the non-intercalated dye of the dimer. Thus, we can write the monomeric molar circular dichroism in equation 7.6 as

$$\Delta\varepsilon(\tilde{\nu})_{mono} = \frac{r_1}{r}\Delta\varepsilon_1(\tilde{\nu}) + \frac{r_{12}}{r}\Delta\varepsilon_2(\tilde{\nu}) \qquad (7.7)$$

where $\Delta\varepsilon_1(\tilde{\nu})$ and $\Delta\varepsilon_2(\tilde{\nu})$ are the molar circular dichroism induced into the species A_1 and A_2 respectively. Because these monomeric CD spectra originate from the same electronic transition of the dye and because the same source of perturbation is responsible for the induction of optical activity in the intercalated and non-intercalated dyes, we can assume that the shape and position of these CD spectra are identical, although they may differ both in sign and magnitude. Thus, unless $\Delta\varepsilon_1(\tilde{\nu})$ is zero, we may write

$$\Delta\varepsilon_2(\tilde{\nu}) = p\Delta\varepsilon_1(\tilde{\nu}) \qquad (7.8)$$

where p is a constant. Equation 7.7 becomes

$$\Delta\varepsilon(\tilde{\nu})_{mono} = (\frac{r_1}{r} + \frac{r_{12}}{r}p)\Delta\varepsilon_1(\tilde{\nu}) \qquad (7.9)$$

According to our model, the dimeric molar circular dichroism is given by

$$\Delta\varepsilon(\tilde{\nu})_{dimer} = \frac{r_{12}}{r}\Delta\varepsilon_{12}(\tilde{\nu}) \qquad (7.10)$$

where $\Delta\varepsilon_{12}(\tilde{\nu})$ arises from degenerate exciton interactions between the two dyes in the species A_1A_2. The vibronic exciton theory described in paragraph 2.2 as well as the procedure followed in paragraph 5.5 to calculate the spectrum of APA were used to interpret the dimeric CD spectrum. It follows that $\Delta\varepsilon_{12}(\tilde{\nu})$ is composite, including the contribution by the in-phase $\Delta\varepsilon^{+}(\tilde{\nu})$ and the out-of-phase $\Delta\varepsilon^{-}(\nu)$ coupling between the transition moments of the two dyes constituting the dimer.

The optical activity observed may be expressed by the corresponding rotational strength defined in equation D.2 (appendix D) and thus permits a better comparison with theoretical calculations. In the same way as equations 7.9 and 7.10, we may write

$$\mathcal{R}_{mono} = \frac{r_1}{r}\mathcal{R}_1 + \frac{r_{12}}{r}\mathcal{R}_2$$

$$\mathcal{R}_{dimer} = \frac{r_{12}}{r}\mathcal{R}^{-} \qquad (7.11)$$

where $\mathcal{R}^{-}$ is the rotational strength corresponding to the out-of-phase coupling of the transition moments in the dimer (equation 2.17).

7.3 The Circular Dichroism of the Acridine Orange -DNA Complex

Figure 7.3 shows some CD spectra of the AO-DNA complex in 10^{-3} mol dm^{-3} NaCl solution for different values of r. These spectra are corrected for the free dye contribution. This was achieved by the use of the binding equilibrium data of Armstrong *et al.*[26] at the lowest ionic strength studied to find the concentration of the bound dye, C_B, and hence the CD per mole of bound dye, $\Delta\varepsilon$, at various values of r. Their data were later confirmed by the equilibrium dialysis

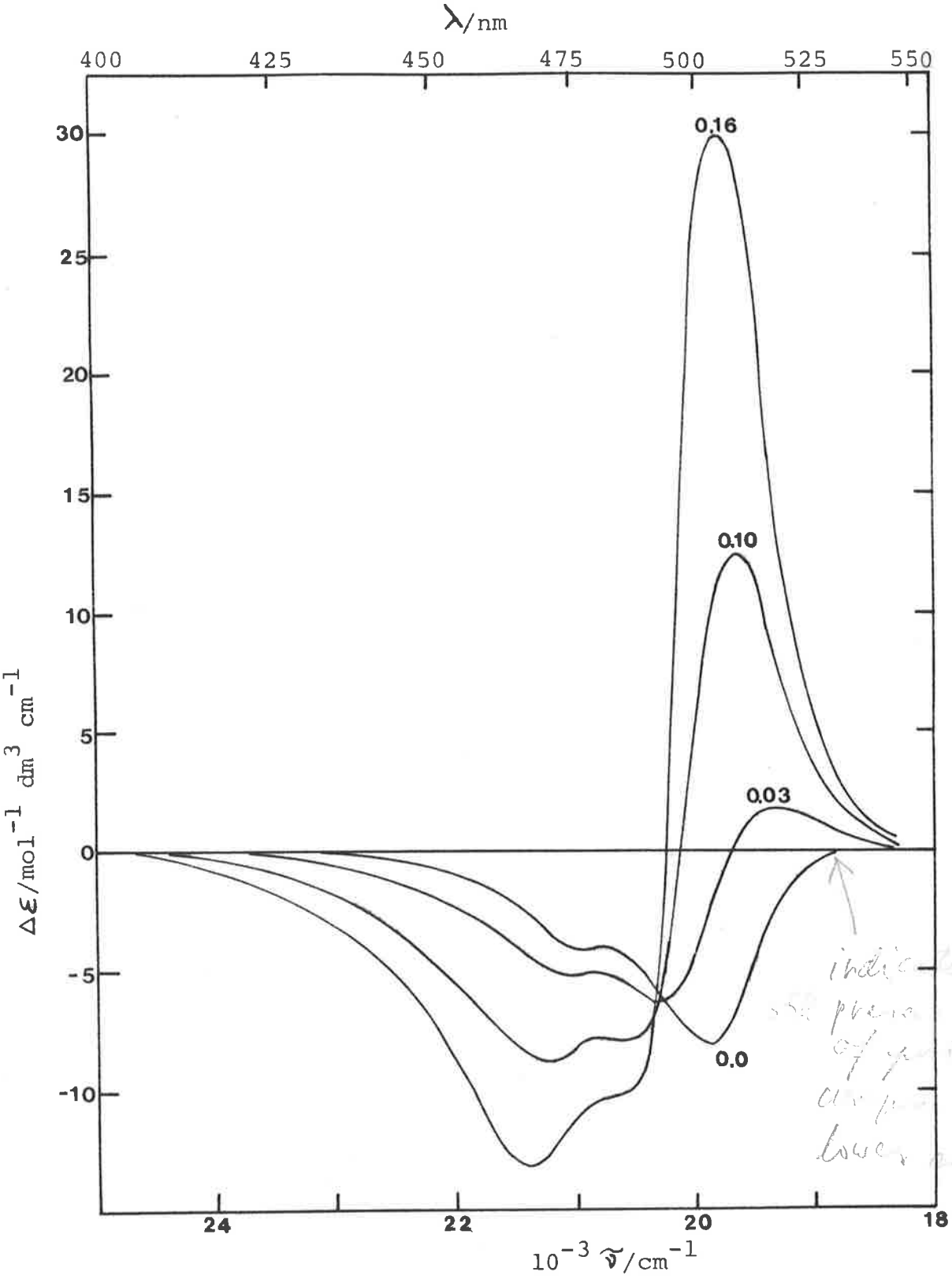

FIG.7.3 CIRCULAR DICHROISM PER MOLE OF ACRIDINE ORANGE BOUND TO DNA IN 0.001 M NACL AT THE r VALUES INDICATED.
The total dye concentration is 10^{-5} mol dm^{-3}.

measurements of Fredericq and Houssier[92] in 10^{-3} mol dm^{-3} NaCl. Figure 7.3 also includes the CD spectrum extrapolated to r = 0. Its shape and its maximum position coincide with those of the corresponding absorption spectrum, shown in figure 7.4, as predicted by theory[120,121]. The starting point for the procedure used to calculate the dimeric spectrum, is the determination of the absorption spectrum of the intercalated monomeric species, A_1, and its fit to a single harmonic progression represented in figure 7.4. The vertical lines show the positions and are proportional to the intensities of the individual vibronic bands. The results of the deconvolution of the absorbance spectrum in vibronic bands provide five parameters which are characteristic of the monomeric spectrum and are given in table 7.3. In addition to three of the fixed parameters, X, V and b_g, only one adjustable parameter, the exciton coupling parameter, which characterizes the strength of the exciton coupling between the two moieties of the dimer, is needed for the computation of the dimer spectra. A series of computed CD dimer spectra for different values of the exciton coupling parameter is shown in figure 7.5. In this figure, the positive peak maxima have been normalised to unity. As we have already noted for the CD spectrum of APA in paragraph 5.5, the vibronic character of the spectrum is responsible for producing asymmetrical positive and negative contributions to the dimeric CD spectrum, even though the spectrum is "conservative" with $\mathcal{R}^+ + \mathcal{R}^- = 0$. From our model, we assume that the geometry of the bound dimer is fixed, which also implies a constant value of the exciton coupling parameter as the amount of binding increases. The value of the exciton coupling parameter was chosen so that the spectrum

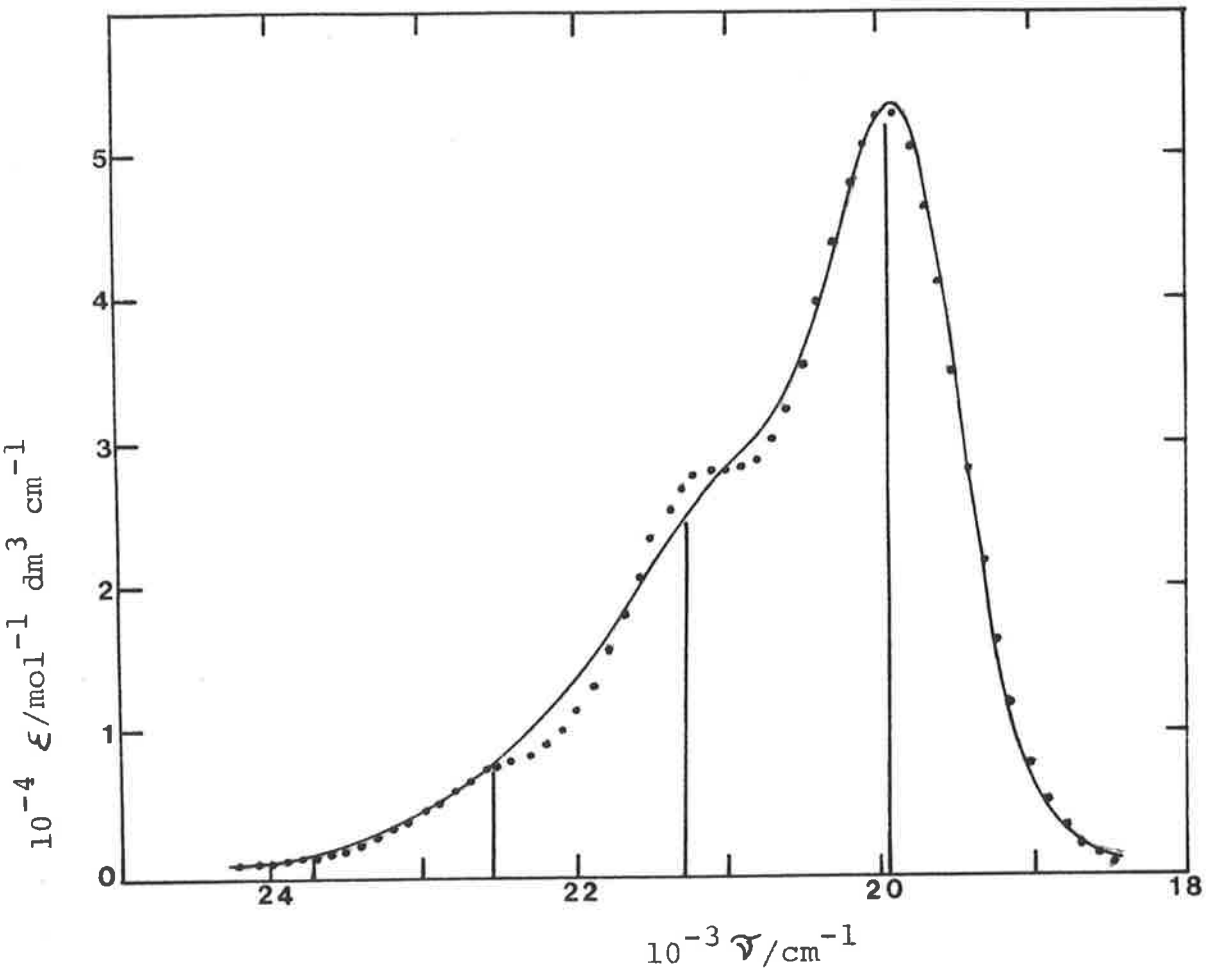

FIG.7.4 ABSORPTION SPECTRUM OF ACRIDINE ORANGE-DNA COMPLEX IN 0.001 M NACL AT r=0.002.
$C_{AO}=1.2\times10^{-6}$ mol dm^{-3}.Symbols as in fig.7.1.

Table 7.3 PARAMETERS OBTAINED FROM THE FIT OF THE ACRIDINE ORANGE-DNA SPECTRA AT r = 0.

(Figures in brackets are linear estimates of the standard deviations of the best-fit parameters.)

Parameters[a]	Absorption	Circular dichroism
$\tilde{\nu}_{oo}$ (cm^{-1})	19,940 (10)	19,960 (20)
X	0.50 (0.01)	0.46 (0.02)
V (cm^{-1})	1300 (20)	1290
b_g (cm^{-1})	1150 (20)	1050 (20)
ε_{oo}(mol^{-1} dm^3 cm^{-1})	50,900 (700)	
f	0.44_4	
$\Delta\varepsilon_{oo}$(mol^{-1} dm^3 cm^{-1})		-8.2 (0.2)

a - The parameters are defined in appendix C.

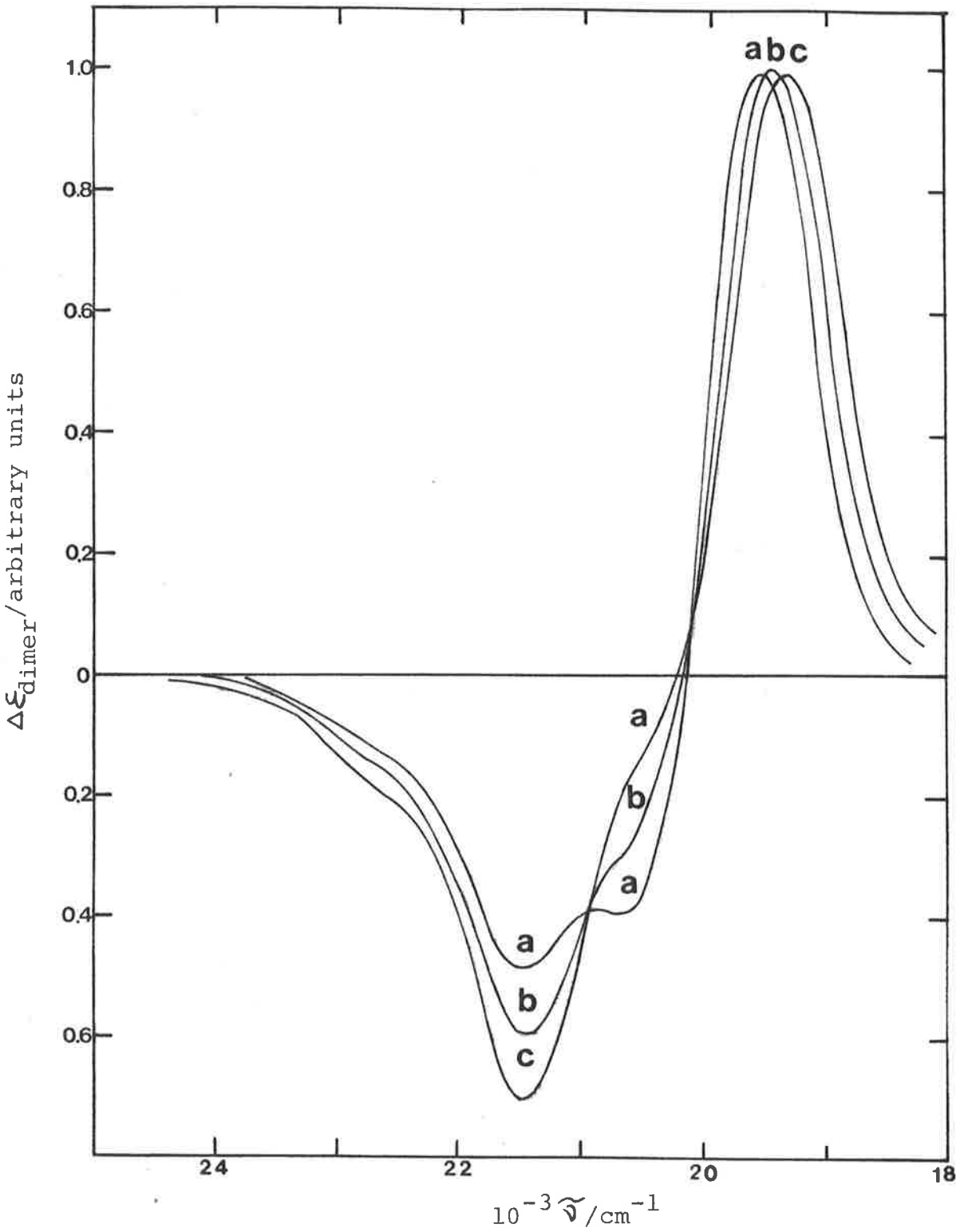

FIG.7.5 COMPUTED CIRCULAR DICHROISM DUE TO EXCITON COUPLING BETWEEN ACRIDINE ORANGE DYES.
Value of the exciton coupling parameter:(a),150 cm^{-1}; (b),450 cm^{-1};(c),650 cm^{-1}.

obtained from the superposition of a monomer CD spectrum with a computed dimer CD spectrum gives the best fit to the experimental CD spectra. The criterion for this choice has been mainly based on the shape of the CD spectrum, in particular on the ratio of the two negative lobe intensities and on the ratio of the positive to negative peak intensities. We found a value of 180 cm^{-1} for the exciton coupling parameter to be the most suitable value for the fitting of all the experimental CD spectra of the AO-DNA complex. The knowledge of the shape of both the monomeric and dimeric CD spectra enables us to separate the experimental CD spectra into monomeric and dimeric contributions in accordance with equations 7.6 and 7.11 as in figure 7.6. Figures 7.7 and 7.8 give some examples of the fit of the observed CD spectra. The full vertical lines show the positions and are proportional to the intensities of the calculated exciton bands. The broken lines are proportional to the vibronic bands of the monomeric spectrum of species A_1 and A_2. The observed spectra result from the cancellation of positive and negative bands whose actual magnitudes exceed the scale of figures 7.7 and 7.8. The value of $\mathcal{R}_1$ in equation 7.11, which corresponds to the intercalated species A_1, is determined from an extrapolation of the observed CD spectra to r = 0. The use of the value of the dimerization constant, K_2, already determined in a study of the AO-DNA complex in dilute salt[26], enables us to calculate the quantities $\frac{r_1}{r}$ and $\frac{r_{12}}{r}$ using equation 7.5. Next, the fit of the experimental monomeric and dimeric rotational strengths to equation 7.11 gives the value of $\mathcal{R}_2$ and $\mathcal{R}$ (figure 7.9). The values of the rotational strengths of AO bound to DNA are collected in table 7.4

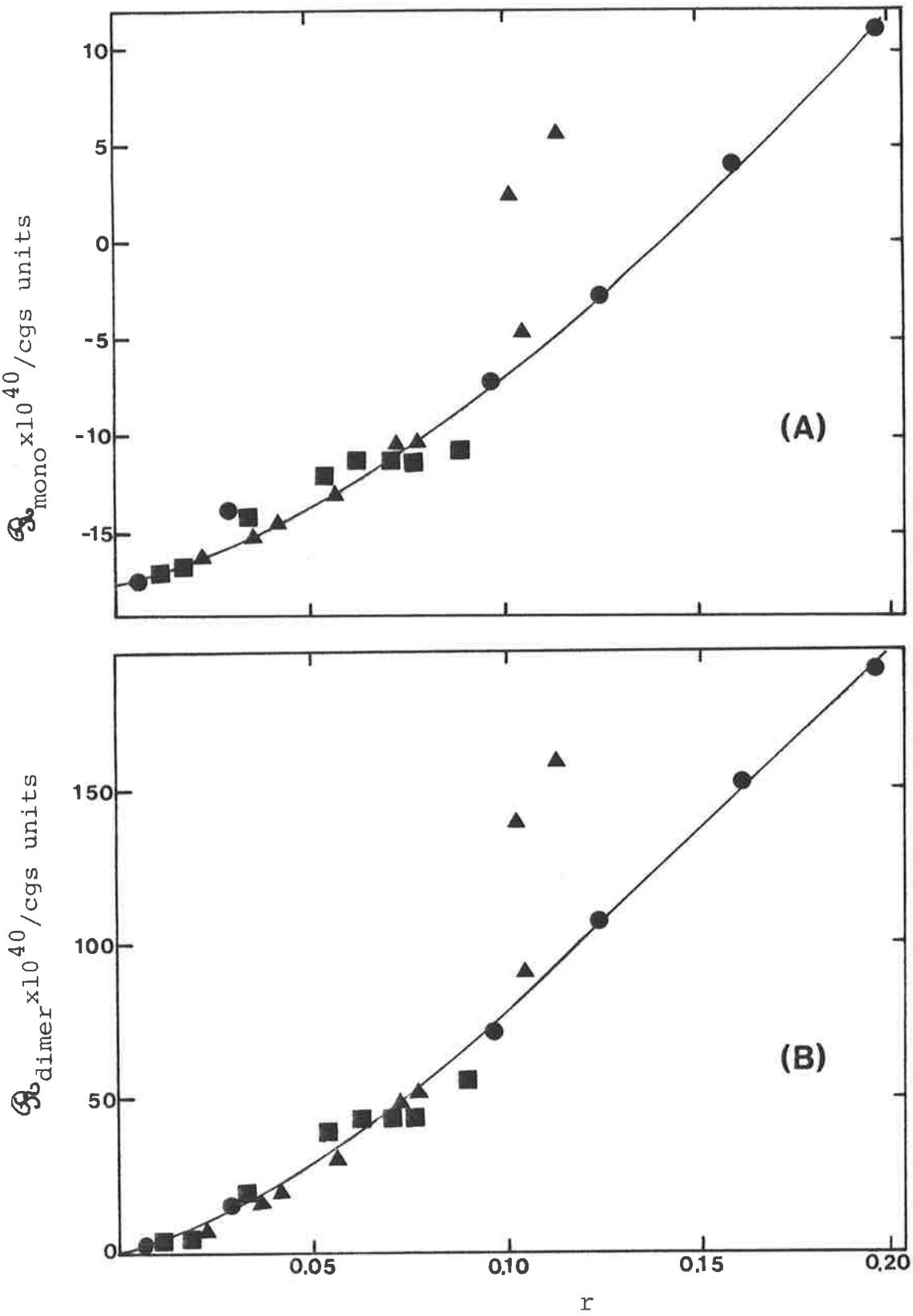

FIG.7.6 CONTRIBUTION TO THE OBSERVED ROTATIONAL STRENGTHS BY THE MONOMERIC SPECIES (A) AND BY THE DIMERIC SPECIES (B) OF THE AO-DNA COMPLEX IN 0.001 M NACL (●), IN 0.1 M NACL (▲) AND IN 1.0 M NACL (■).

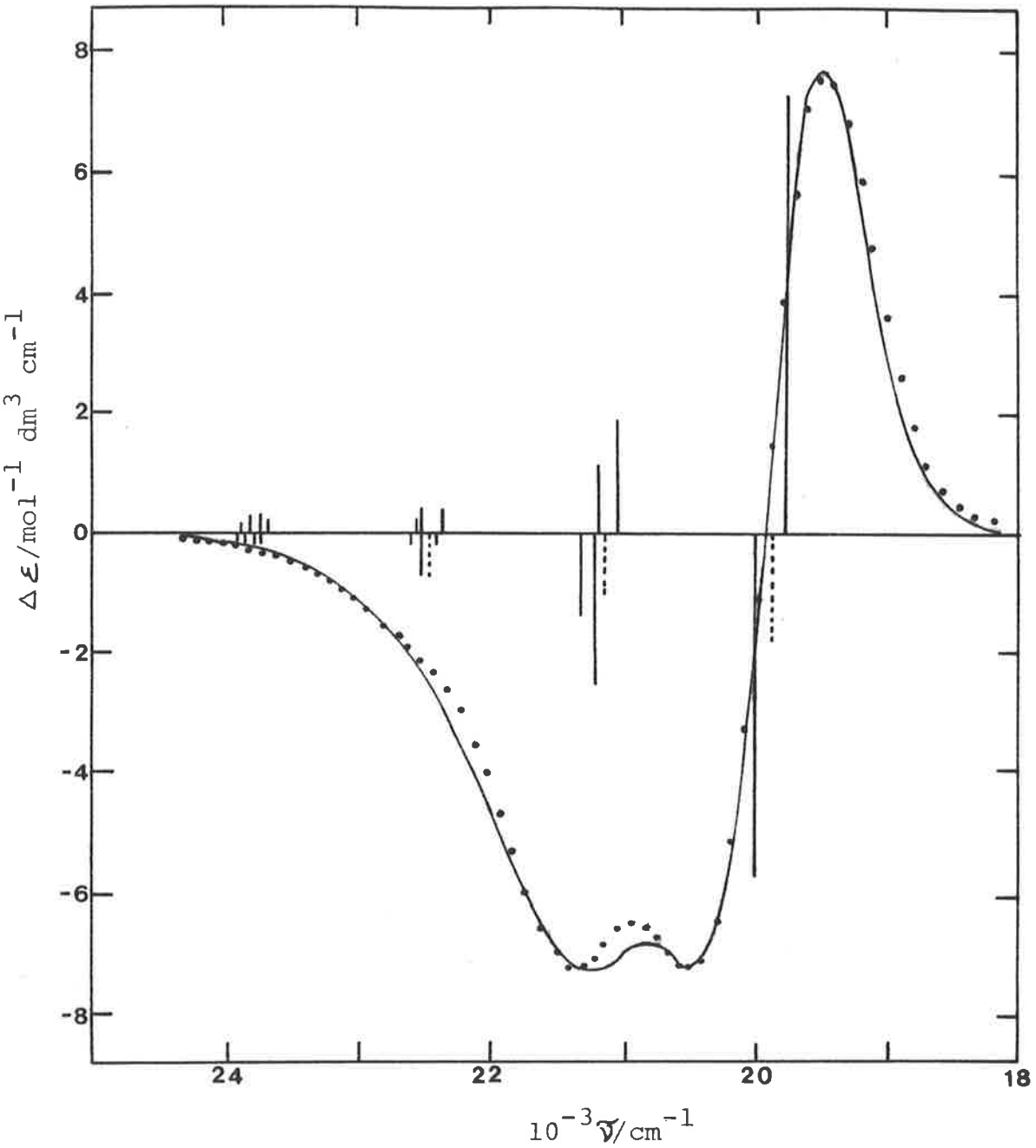

FIG.7.7 CIRCULAR DICHROISM PER MOLE OF ACRIDINE ORANGE BOUND TO DNA IN 0.001 M NACL AT r=0.07.
Full curve: experimental spectrum; dots: fitted spectrum with full vertical lines referring to the exciton bands and dotted vertical lines to the monomeric bands.

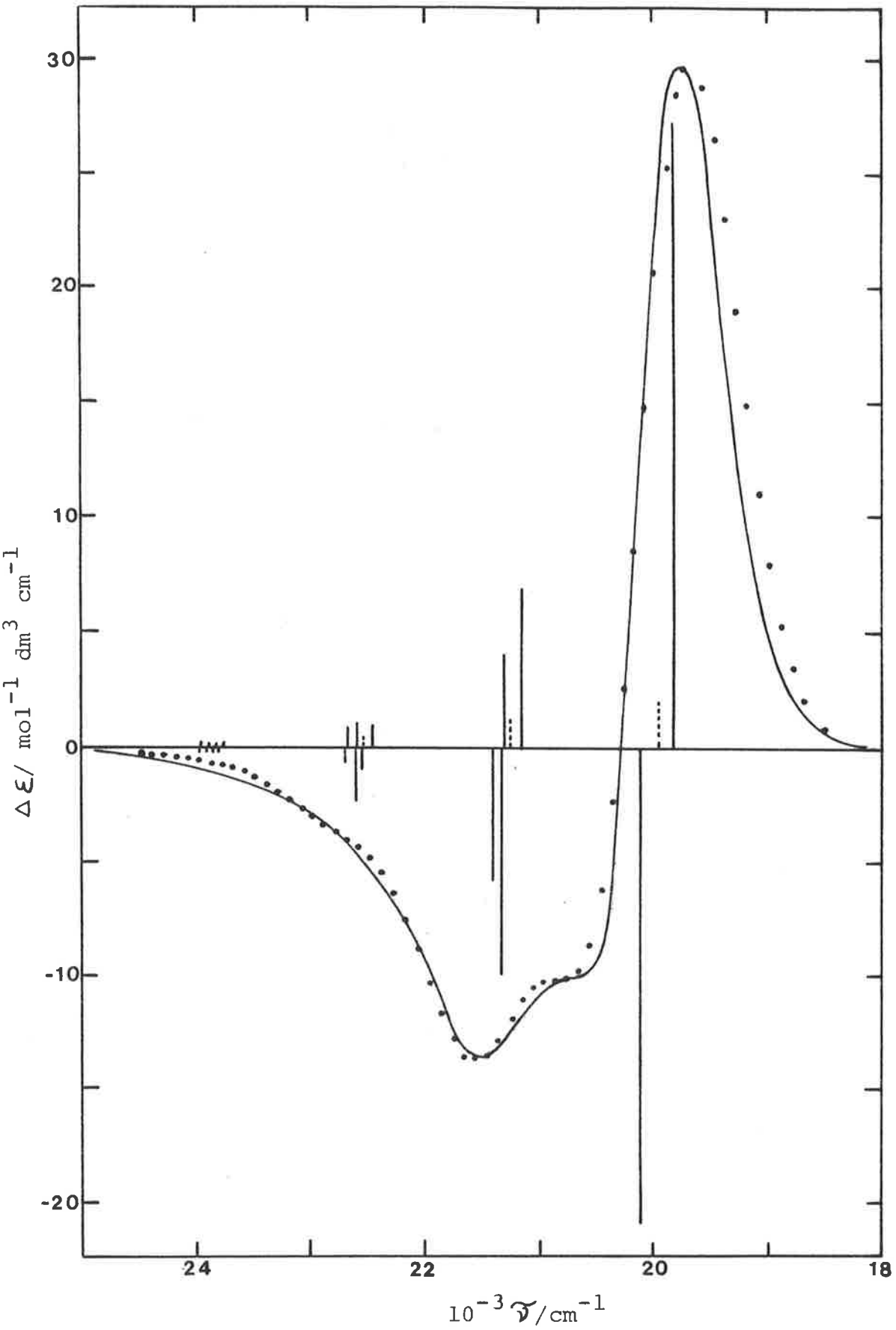

FIG .7.8 CIRCULAR DICHROISM PER MOLE OF ACRIDINE ORANGE BOUND TO DNA IN 0.001 M NACL AT r=0.16. Symbols as in fig.7.7.

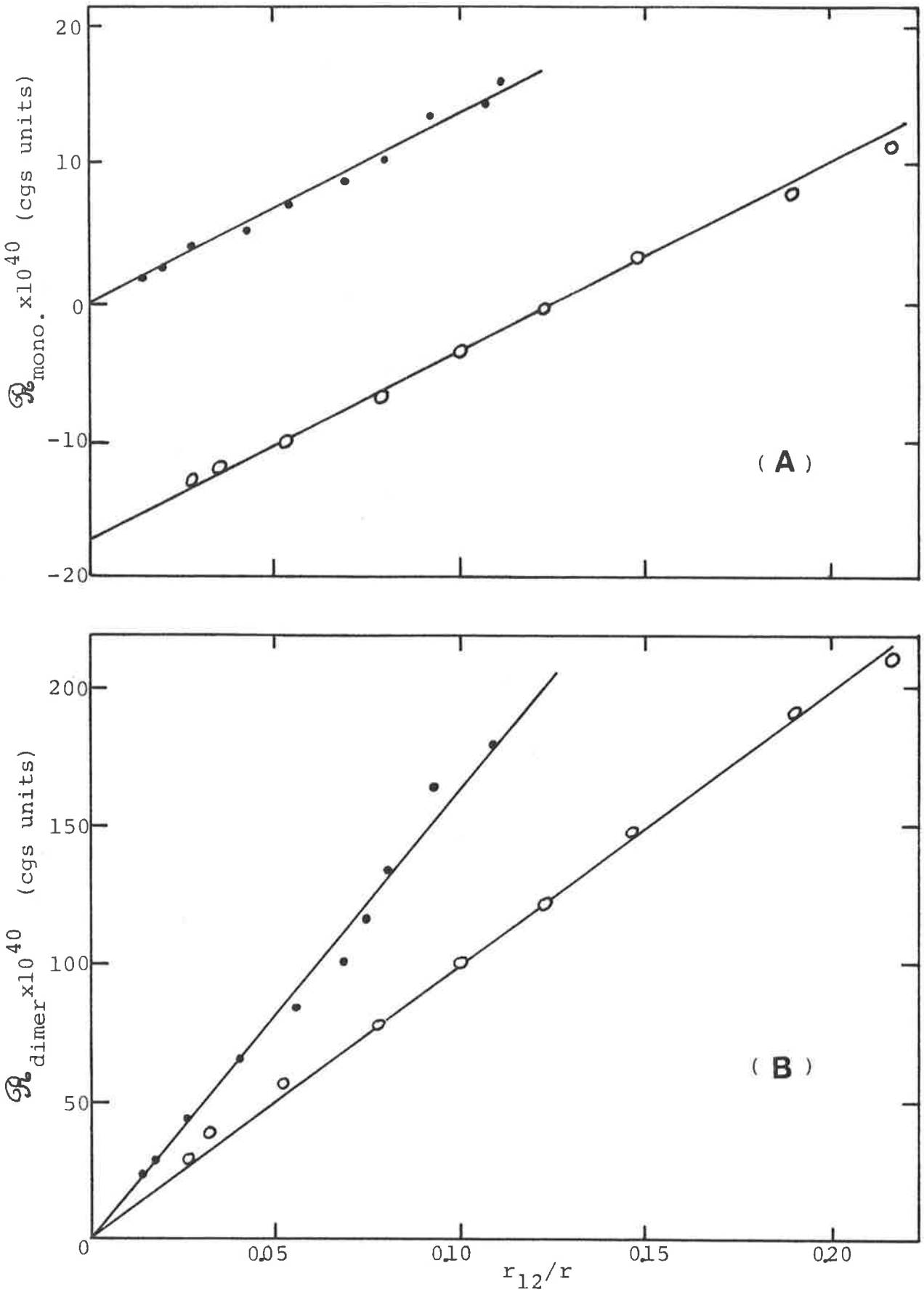

FIG.7.9 RELATION BETWEEN r_{12}/r AND THE OBSERVED MONOMERIC (A) AND DIMERIC (B) ROTATIONAL STRENGTHS OF AO-DNA (o) AND PF-DNA (•) IN 0.001 M NACL ACCORDING TO EQU.7.11.

Table 7.4 CONTRIBUTIONS TO THE ROTATIONAL STRENGTHS OF DYES BOUND TO DNA.

Concentration of NaCl (mol dm^{-3})	$\mathcal{R}_1$ x 10^{40} (cgs units)	$\mathcal{R}_2$ x 10^{40} (cgs units)	$\mathcal{R}^-$ x 10^{40} (cgs units)
	Acridine Orange		
0.001 - 1.0	-17	121	1000
	Proflavine		
0.001	0	136	1630
0.1	4.1		
1.0	9.6		

The CD spectra of the AO-DNA complex in solutions of 0.1 and 1.0 mol dm^{-3} NaCl concentrations were also studied. However, the amount of uncertainty in the values of K_2, determined previously at high ionic strengths[26], prevents their use in our study. This has led us to use a different procedure in order to extract the parameters characteristic of the binding of the dye at high salt concentrations. The evolution of the CD spectra with the amount of binding, is similar to that observed at low salt concentration. The extrapolation of the CD spectra to infinite dilution of the AO dye in DNA is found to be independent of the salt concentration, in the limits of experimental uncertainty (figure 7.6). We can assume, then, that the geometry of the non-intercalated dye in high salt concentrations is similar to that in 0.001 mol dm^{-3} NaCl solution; it follows that $\mathcal{R}_2$ and $\mathcal{T}$ are also independent of the salt concentration. From these quantities, we are able to calculate the concentrations of the species A_1, A_1A_2, the amount of bound dye C_B as a function of r and to deduce the value of the dimerization constant K_2 for the two high salt concentrations by using equation 7.1 (figure 7.10). The binding isotherms obtained by plotting r/C_F versus r are shown in figure 7.11. They were fitted to the neighbour exclusion equation 7.2, using the value of K_2 derived in figure 7.10. The values of K_1 and n determined at the different salt concentrations are collected in table 7.5.

7.4 The Circular Dichroism of the Proflavine-DNA Complex

The same procedure will be used to analyse the CD spectra of the PF-DNA complex. Figure 7.12 shows some experimental CD spectra of the complex in 0.001 mol dm^{-3} NaCl

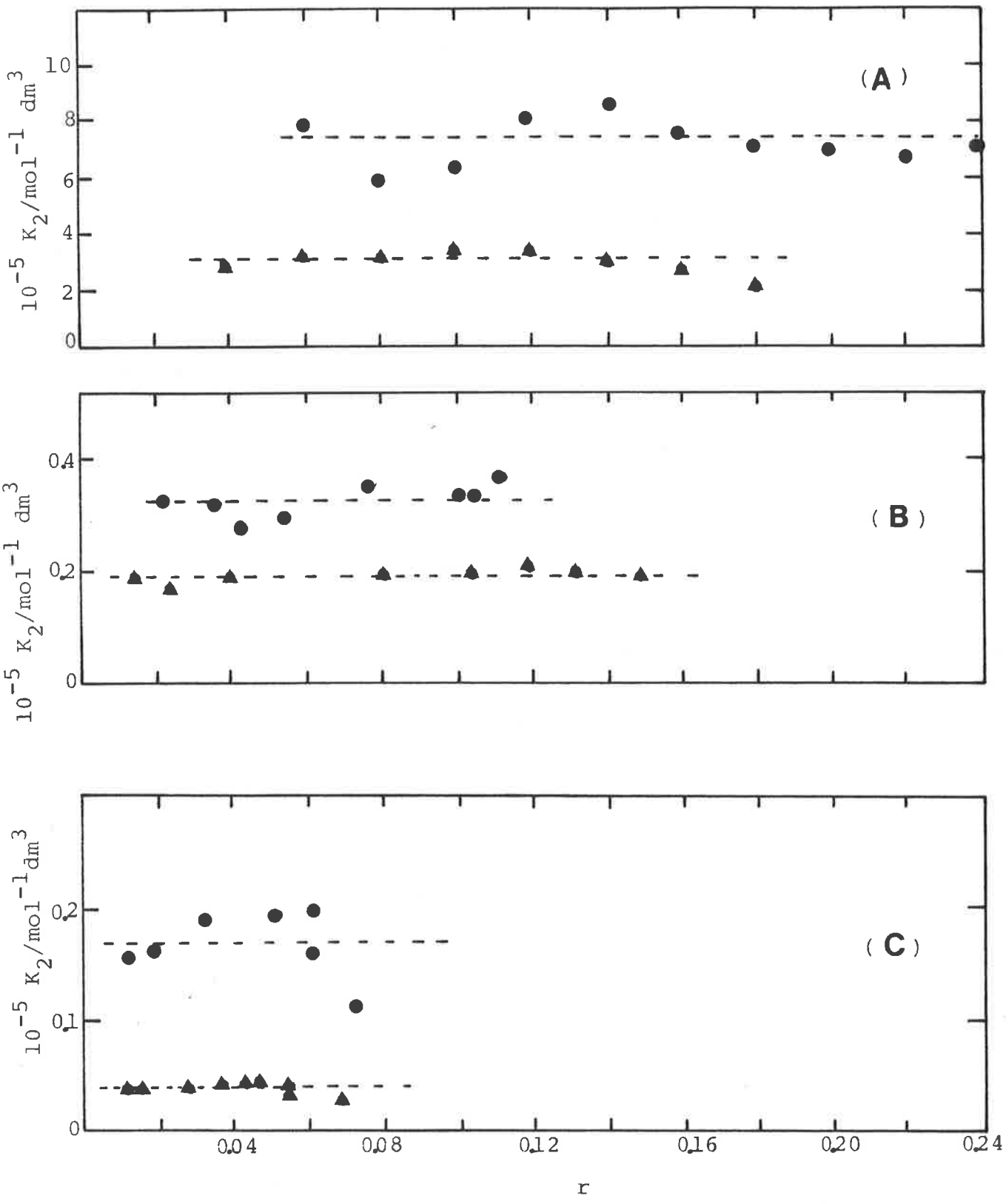

FIG.7.10 TEST PLOT FOR EQU.7.5 FOR AO-DNA (●) AND FOR PF-DNA (▲) IN 0.001 M NACL[26](A), 0.1 M NACL (B) AND 1 M NACL (C).

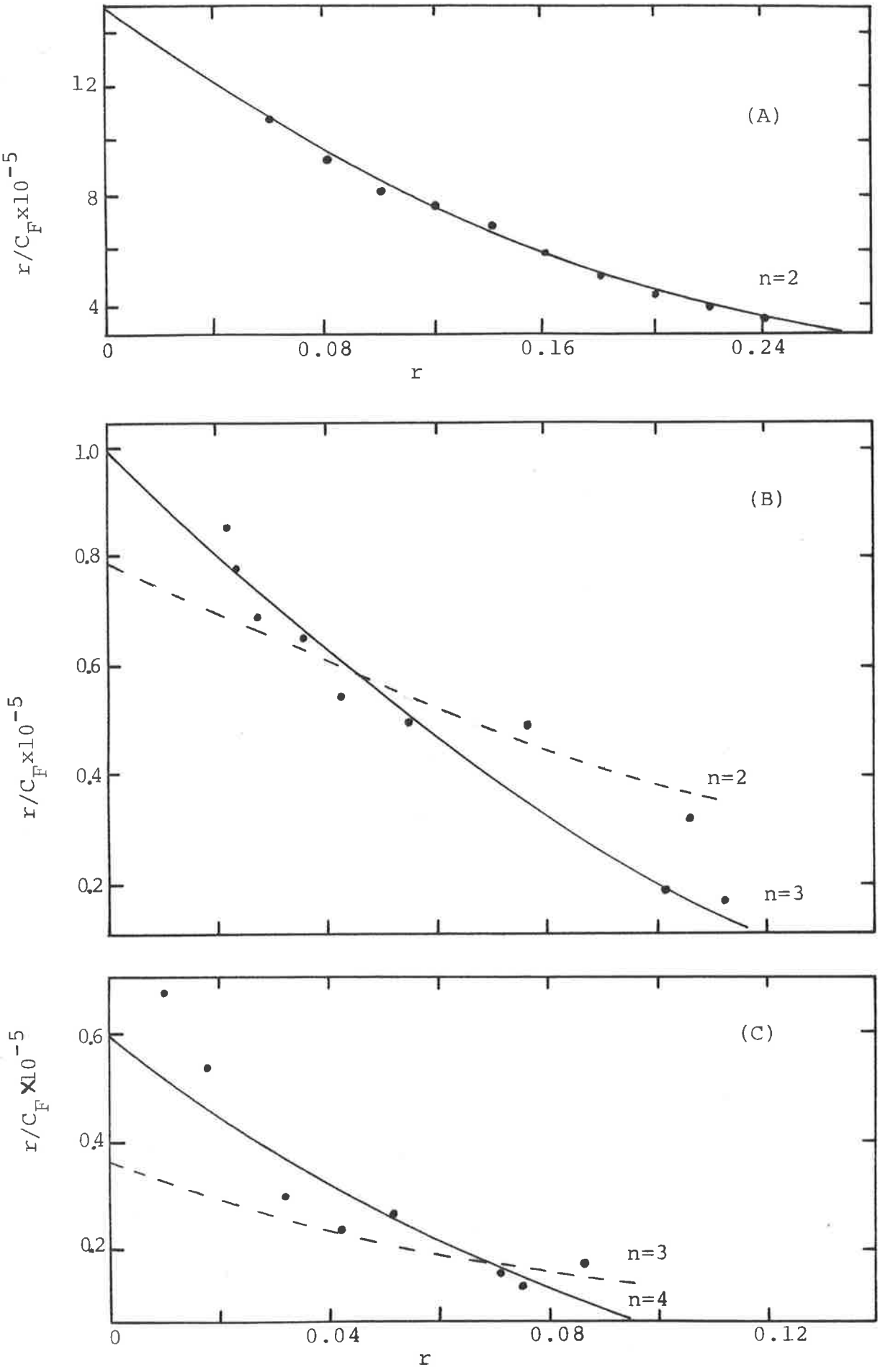

FIG.7.11 BINDING ISOTHERMS FOR ACRIDINE ORANGE IN 0.002 (A)[26], 0.1 (B) AND 1.0 M NACL (C). The curves have been calculated by mean of equ.7.2 .

Table 7.5 EQUILIBRIUM CONSTANTS OF INTERCALATION AND OF DIMERIZATION OF DYES BOUND TO DNA.

Concentration of NaCl; mol dm^{-3}	$K_2 \times 10^{-5}$ $mol^{-1}\ dm^3$	$K_1 \times 10^{-5}$ $mol^{-1}\ dm^3$	n (eq. 7.2)
	Acridine Orange		
0.001[a]	7.3 ± 1.0	30 ± 5	2
0.1	0.32 ± 0.05	2.0 ± 0.2	3
1.0	0.17 ± 0.04	1.2 ± 0.3	4
	Proflavine		
0.001[a]	1.5 ± 0.5	30 ± 5	2
0.1	0.19 ± 0.02	2.2 ± 0.3	2
1.0	0.040 ± 0.005	0.3 ± 0.1	3

a - Values taken from reference 26.

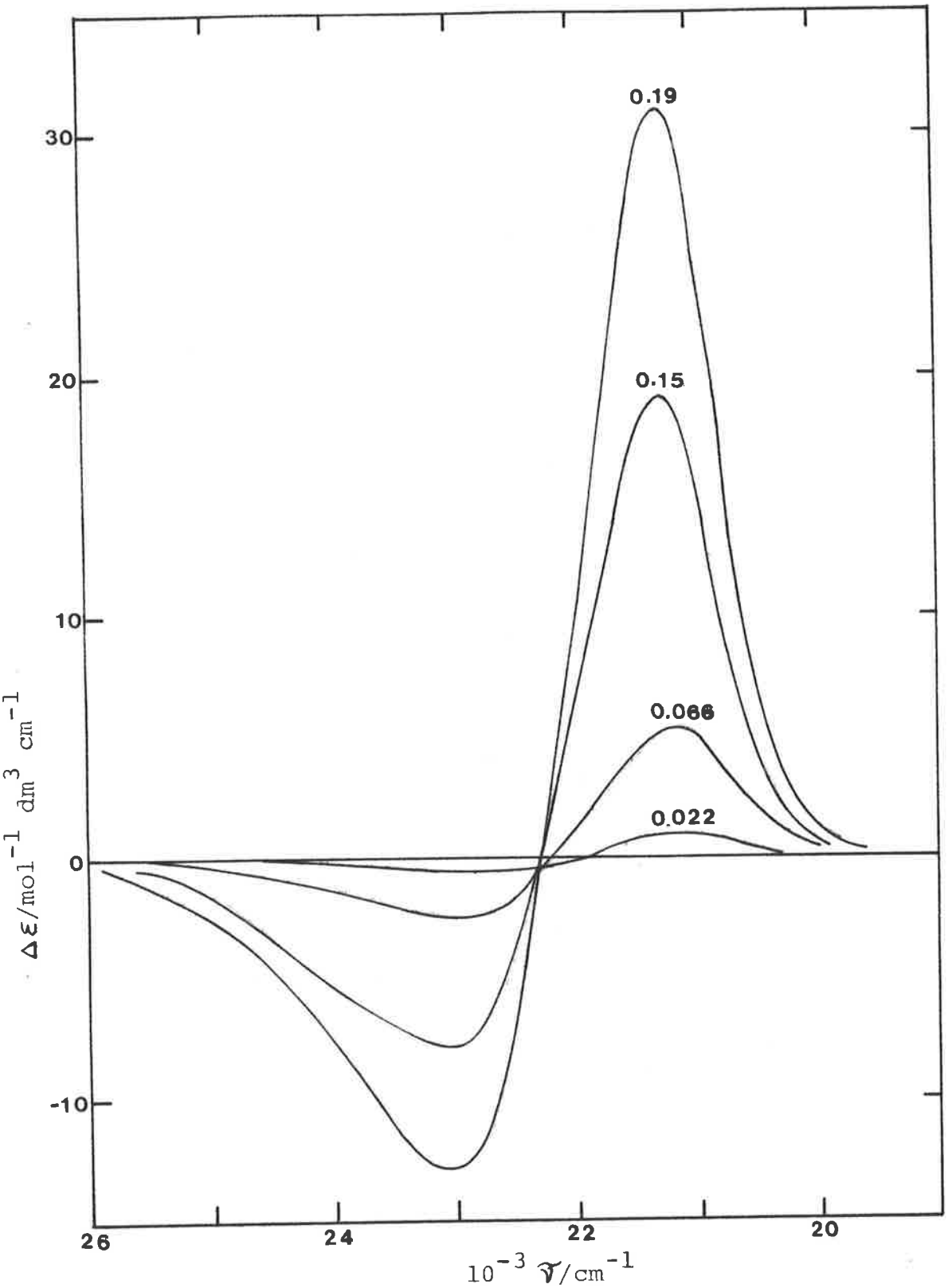

FIG.7.12 CIRCULAR DICHROISM PER MOLE OF PROFLAVINE BOUND TO DNA IN 0.001M NACL SOLUTION AT THE r VALUES INDICATED.
The total dye concentration is 10^{-5} mol dm^{-3}.

solution, corrected for the free dye contribution. It is found in figure 7.13 that the value of $\Delta\varepsilon_1(\nu)$ (or $\mathcal{R}_1$) increases with salt concentration, being nil for the 0.001 mol dm^{-3} NaCl solution. Figure 7.14 represents the extrapolated CD and absorption spectra to r = 0 and the tentative fit of these spectra to an harmonic progression whose parameters are given in table 7.6. Figure 7.15 shows an experimental CD spectrum together with the calculated one. The values of $\mathcal{R}_2$ and $\mathcal{R}^-$ are obtained through the use of equation 7.11 (figure 7.9). The fit of the binding isotherms to the neighbour exclusion equation 7.2 is represented in figure 7.16. In table 7.4 and 7.5 are collected all of the results of the analysis of the CD spectra of the PF-DNA complex in the three concentrations of NaCl solutions.

7.5 Interpretation of the Results Obtained from the Binding Study

To the methods of analysis such as equilibrium dialysis, viscosimetry, absorption and fluorescence spectroscopy[26,92], which have satisfied the requirements of the Armstrong, Kurucsev and Strauss model[26], we have to add circular dichroism spectroscopy. In fact, even though the application of the observed data was not direct, the hypotheses made in order to obtain these results were all fully justified.

7.5.1 Justification of the Method Used

The presence of only one electronic transition which dominates the visible spectrum, a key element in the justification of the procedure we used, is manifest, not only if one looks at the results of previous investigations[106]

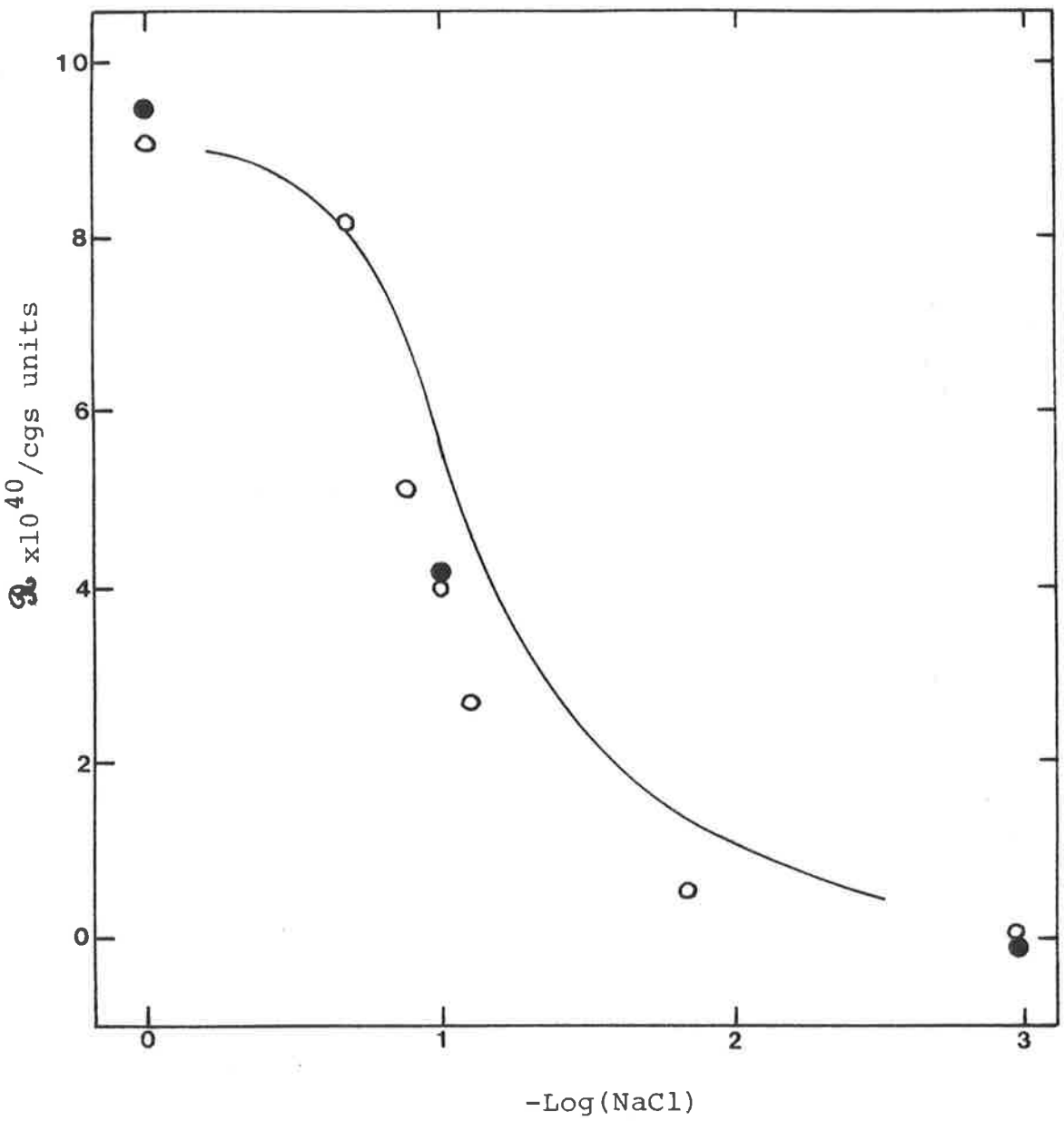

FIG.7.13 SALT CONCENTRATION DEPENDENCE OF THE ROTATIONAL STRENGTH OF THE PROFLAVINE-DNA COMPLEX EXTRAPOLATED TO r=0 .
(—),measurements of Kamiya[139] (Their data were multiplied by 2.295x10^{-39} according to equ.D.2); (o), measurements of Li and Crothers[98];(●),this study.

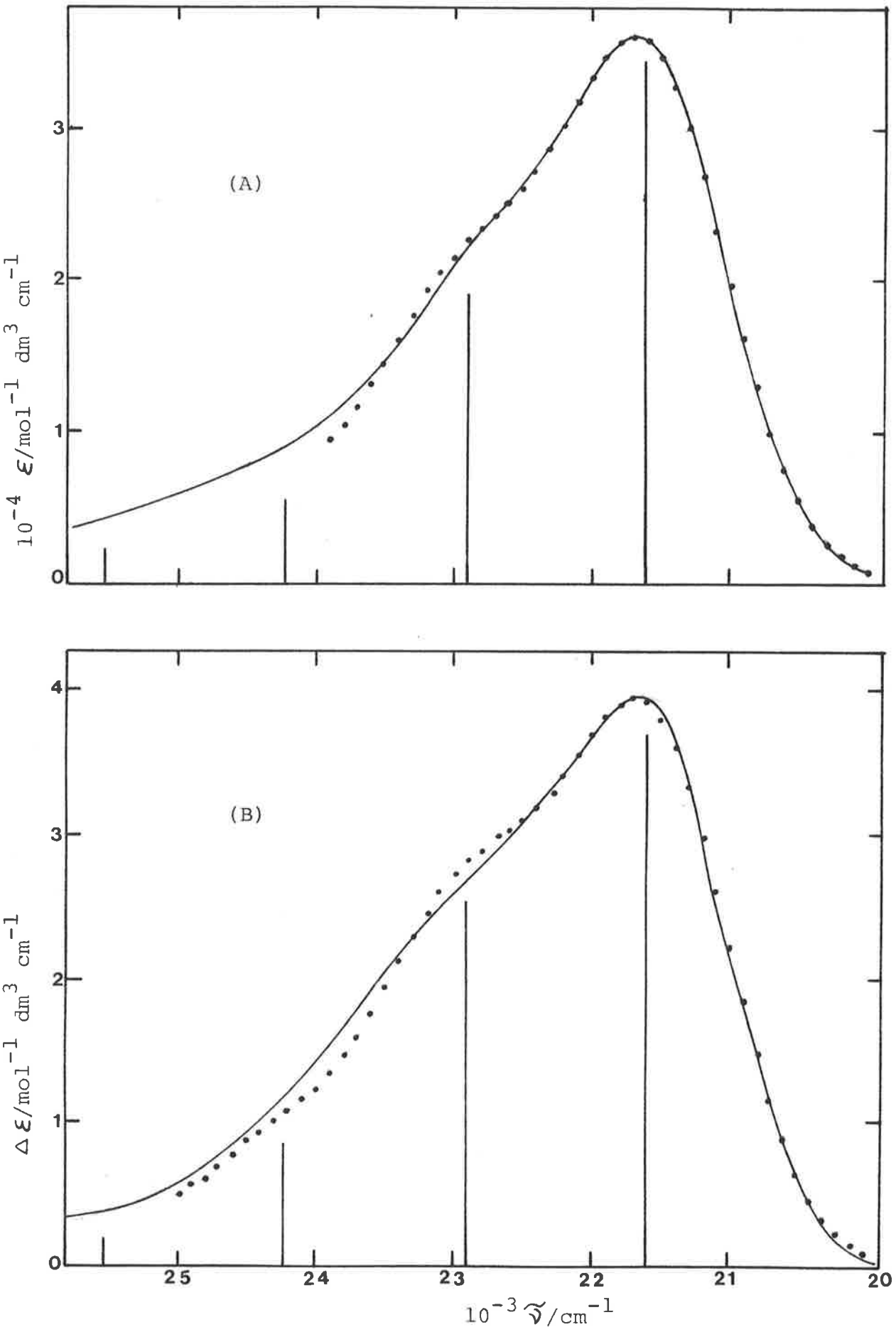

FIG.7.14 ABSORPTION (A) AND CIRCULAR DICHROISM (B) SPECTRA OF PROFLAVINE-DNA COMPLEX IN 1.0 M NACL AT r=0.001. $C_{PF}=10^{-5}$ mol dm^{-3}. Symbols as in fig.7.1 .

Table 7.6 PARAMETERS OBTAINED FROM THE FIT OF THE PROFLAVINE-DNA SPECTRA AT r = 0.

(Figures in brackets are linear estimates of the standard deviations of the best-fit parameters.)

Parameters[a]	Absorption	Circular dichroism
$\tilde{\nu}_{oo}$ (cm^{-1})	21,620 (10)	21,600 (20)
X	0.56 (0.01)	0.67 (0.02)
V (cm^{-1})	1310 (30)	1310
b_g (cm^{-1})	1390 (20)	1390 (30)
ε_{oo}(mol^{-1} dm^3 cm^{-1})	34,200 (400)	
$\Delta\varepsilon_{oo}$(mol^{-1} dm^3 cm^{-1})		3.65 (0.05)[b]
f	0.38_3	

a - The parameters are defined in Appendix C.

b - $\Delta\varepsilon_{oo}$ is given for a NaCl concentration of 1.0 mol dm^{-3}.

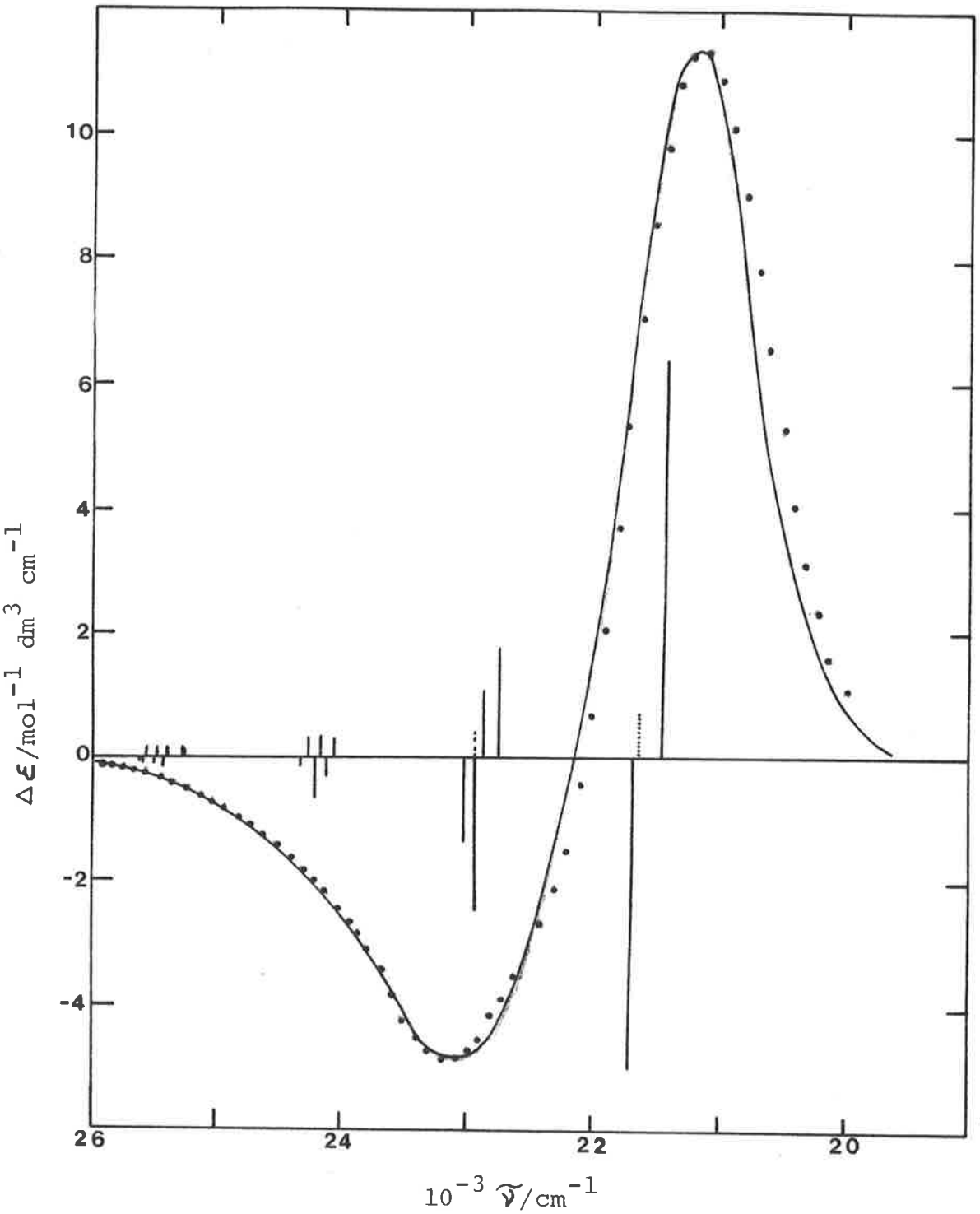

FIG.7.15 CIRCULAR DICHROISM PER MOLE OF PROFLAVINE BOUND TO DNA IN 0.001 M NACL AT r=0.10.
Symbols as in fig.7.7.

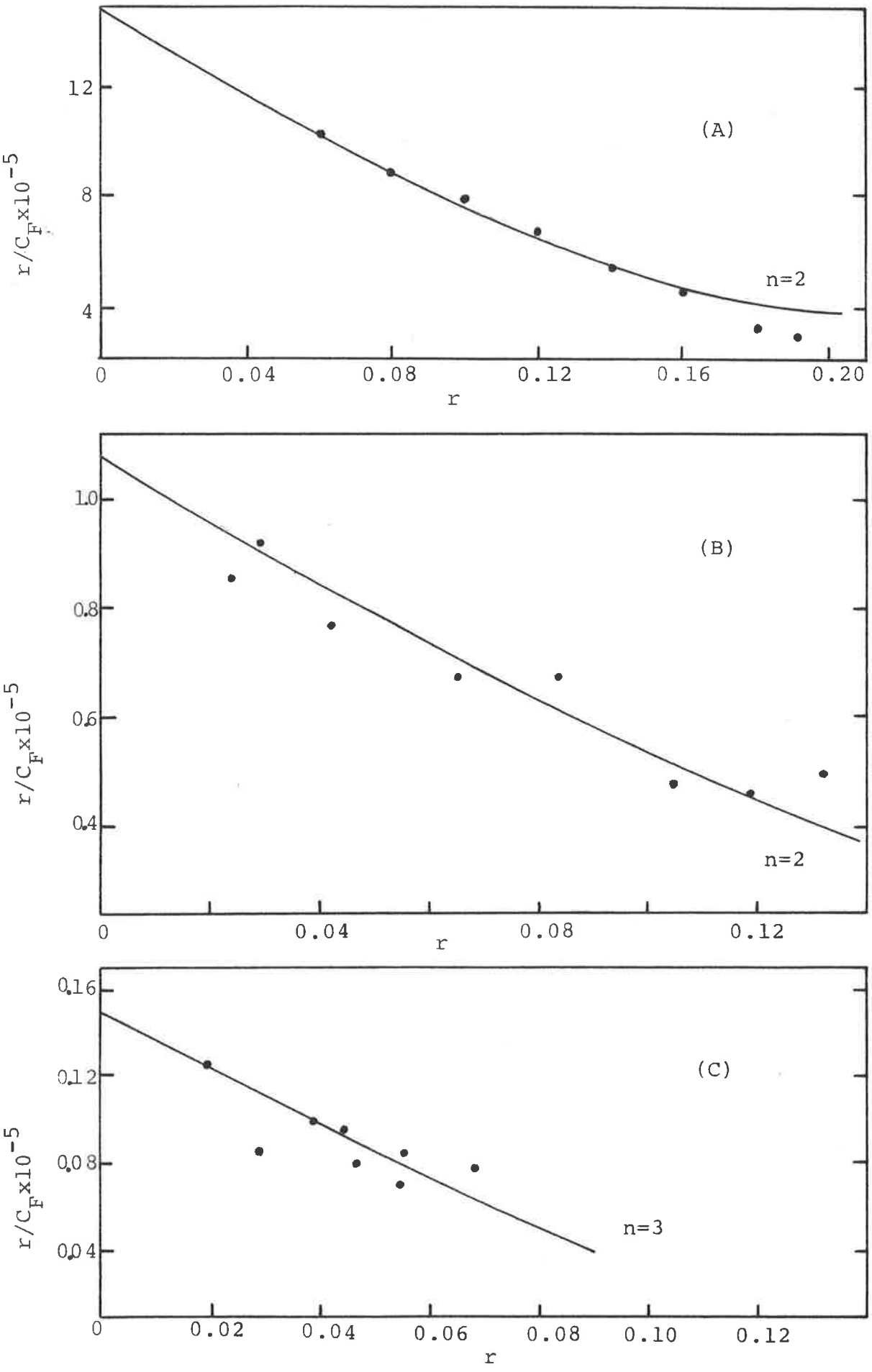

FIG.7.16 BINDING ISOTHERMS FOR PROFLAVINE IN 0.002 (A)[26], 0.1 (B) AND 1.0 M NACL.
The curves have been calculated by mean of equ.7.2.

but also if one considers the results of theoretical calculations[108,109] that deny the presence of a weak π-π^* transition on the low energy side of the strong long axis polarised transition. We have also shown that the absorption and CD spectra of the dye-DNA complexes, as well as the absorption spectrum of the dye alone, could be satisfactorily fitted to a single harmonic progression. Given the different geometrical relationships existing between the short and long axis transitions of the dyes on the one hand and the perturbation brought about by the DNA on the other, we would expect these differences to be expressed in the CD spectrum envelope (in particular a shift of the CD maximum position in relation to the absorption maximum position as was the case with adenosine in paragraph 4.3). Now, the parameters in tables 7.6 and 7.3 show the similarity between the absorption and CD spectra, which is in agreement with theoretical calculations[120,121] made on this particular problem.

Moreover, the assumption that the position and the shape of the spectrum of both the intercalated and the non-intercalated species were identical, can be amply justified, if, for example, one compares the visible absorption spectra of proflavine (figure 7.14) with its di-tert-butyl derivative (figure 2 of reference 30). Not only are their shapes identical but, above all, on binding to DNA their maximum position is shifted to the red by the same amount of energy ($\sim$ 800 cm^{-1}), even though proflavine is intercalated[22,25,26], while di-tert-butyl proflavine binds to the DNA but does not intercalate[30].

As for the computed dimeric spectrum, its validity is based on a well developed theory which has already been

applied with success in similar cases (absorption spectra of dye dimers and dinucleosides in solution[122] and CD spectra of dinucleosides in paragraph 5.) and it not only fits quite satisfactorily the experimental spectra but it also appears to resolve most of the problems previously encountered in the interpretation of the dye-DNA complex CD spectra. The "non-conservative" aspect of the CD spectra has been one of these problems[89-91,93,94,96,98], and was mainly attributed to the presence of non-degenerate interactions adding to the degenerate ones. Now, we show in figure 7.5, that only the presence of degenerate interactions is necessary to produce a "non-conservative" CD spectrum, which is a consequence of the vibronic nature of the transition considered. Another problem has been the number of bands appearing in the AO-DNA CD spectrum. Only two bands of opposite sign are predicted by the exciton theory; the presence of two negative lobes in addition to the intense positive band at lower energy has been attributed by some to the existence of two exciton interactions[89,92-94], one between monomers, the second between dimers, and by others to the existence of several electronic transitions[97-99]. However, it is evident that the difference between the CD spectra of AO and PF-DNA complexes, in figures 7.7, 7.8 and 7.15, arises only from the particular shape of their monomeric spectrum whose vibronic bands are better resolved in the case of AO than for PF (compare the absorption spectra of the two dyes in solution in figure 7.1, or in the presence of DNA in figures 7.4 and 7.14, as well as their CD spectra for r = 0 in figures 7.3 and 7.14.

From the various parameters derived, we can make several conclusions about the binding of dyes to DNA.

7.5.2 The Intercalation Process

Figures 7.11 and 7.16 show that the binding isotherm curves derived from equation 7.2 give a reasonable fit to the AO and PF binding data. Our derived values of K_1 in 0.1 and 1 mol dm^{-3} NaCl solutions (table 7.5) are of the same order of magnitude as the ones obtained with different methods[14,92,123-125], which gives further support for the validity of the model used. Although the nearest-neighbour exclusion model prevails at low salt concentrations (n = 2), with the exclusion arising from changes in local DNA structure at neighbouring base-pairs of an intercalated dye[126,127,144,145], it is shown to be unsuitable in higher salt concentrations. Indeed, figures 7.11 and 7.16 as well as table 7.5 show that the number of sites excluded (n - 1) for intercalation, increases with the salt concentration, which is in entire agreement with equilibrium dialysis results[14,42,123]. Competitive binding between intercalated dyes and cations[113,125] seems to be responsible for the dependence of both the parameters n and K_1 on salt concentration. In fact, sodium cations for example, not only bind to the phosphate groups as one would expect on electrostatic grounds, but they have also been found, using X-ray measurements, in a more "intercalated" position, either bound to a hydroxyl group of a cytidine residue[60] or to a carbonyl group of uracyl[128]. Another possible reason for the decrease in maximum intercalation with increasing concentration of salt is that the sodium cations, bound to the phosphate groups, prevent the dye from approaching the base-pairs of DNA (this effect will be more important in the small groove of DNA which has a high density in phosphates[131]). It has

also been demonstrated that, in low salt concentration, the electrostatic repulsions between the phosphate groups of DNA are strong enough to overcome the base stacking interactions[129], and therefore to increase the separation between base-pairs, which is favourable to the intercalation process[123]. Although the effects of cations have been satisfactorily analysed through their influence on the parameters n and on the binding constant K_1, a more complex isothermic model[117] should be used if one wants to give a more correct representation of the intercalation process.

7.5.3 The Dimerization Process

The decrease in the value of the dimerization constant, K_2, with an increase in salt concentration also indicates a decrease in dye binding to DNA. But, if we plot the quantity K_2C_F against r, as in figure 7.17, we can see that the experimental data, referring to the three salt concentrations used, lie approximately on the same curve. Thus K_2C_F, which is equivalent to the ratio of the bound dimer to bound monomer concentrations (equation 7.1), is independent of the salt concentration. This implies that, unlike the intercalation process, the dimerization process is rather insensitive to salt effects. Therefore, the lesser amount of dimer formed in high salt concentrations is mainly the consequence of the presence of less intercalated dyes, as we can see in figure 7.17, through the existence of a "saturation level" of bound dyes which occurs at decreasing values of r when the salt concentration increases; for example, this saturation in PF dyes binding to DNA occurs for a value of r around 0.14 in 0.1 mol dm^{-3} NaCl solution, which is in perfect agreement with the results obtained from

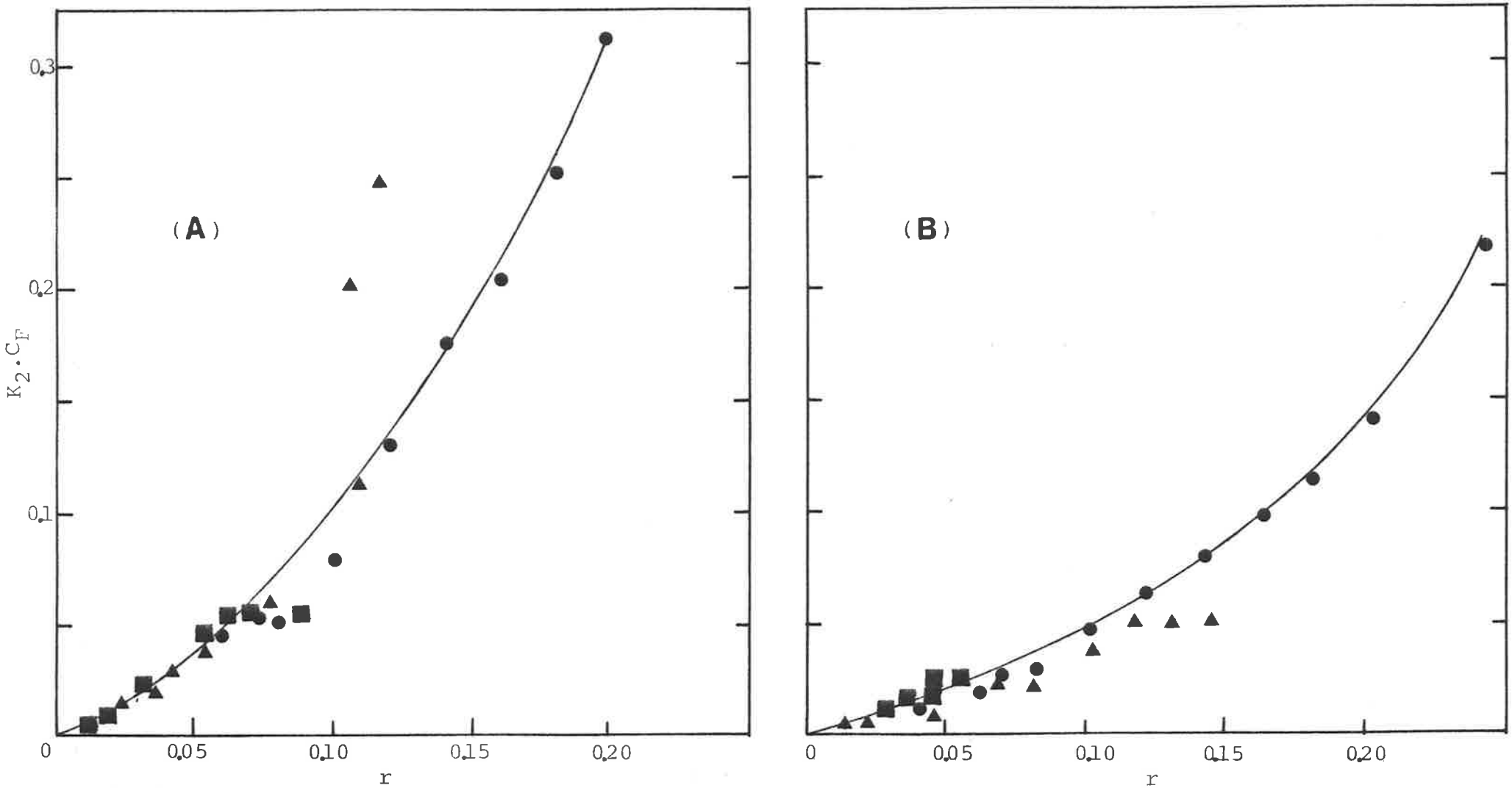

FIG.7.17 RATIO OF THE CONCENTRATIONS OF THE MONOMERIC TO DIMERIC BOUND DYE SPECIES PLOTTED AGAINST r. (A),ACRIDINE ORANGE;(B),PROFLAVINE. (●),0.001 M NaCl;(▲),0.1 M NaCl;(■),1 M NaCl. The ordinate is common to both A and B.

an electron microscope study of the PF-DNA complex in the same salt concentration[132]. Moreover, the assumption made about the non-intercalated and dimeric rotational strength independence on salt concentration, finds support in our conclusions on the insensitivity of the dimerization process to salt concentration. Furthermore, if we compare the dimerization constant of the two dyes, in table 7.5, we can conclude that the presence of a non-intercalated dye, or dimer process, depends on the tendency of the two dyes to dimerize in free solution[81,82,107,133], as was the case when these dyes bind to polymers[97,118].

As it has been established that a high ionic strength prevents electrostatic binding of the dye to the outside of the DNA[14], we want to dissociate this kind of binding, called "weak binding", mainly associated with the binding of aggregates and occurring for values of r higher than the ones we studied, from the binding of our non-intercalated species which forms a dimer with an already intercalated dye and which takes place in the strong binding region (from the inspection of the AO-DNA CD spectra, the presence of the dimeric species is already manifest at a value of r = 0.008).

7.5.4 The Geometry of the Dimeric Dye Bound to DNA

Table 7.4 informs us about the binding of the non-intercalated dye. The derived values of the induced CD of the non-intercalated bound dye are similar for AO and PF dyes and, more important, these values correspond to that of the typically non-intercalated di-tert-butyl proflavine dye[130]. A rotational strength of about 140 x 10^{-40} cgs at r = 0 was calculated from the published data (figure 3 of reference 130). This agreement is in favour of the binding

model used and shows clearly that the dyes bind to the "outside" of DNA in a rather similar way, which is not surprising for such similar dyes. The precise location of the non-intercalated dye is rather uncertain. Given the similar change in the absorption spectra of the intercalated and non-intercalated dyes on binding to DNA, we can conclude that the latter interacts also with the DNA bases, probably in one of the grooves of DNA[131]. We can also point out that a much stronger induced optical activity is associated with the long axis polarised transition of the non-intercalated dyes compared with that of the intercalated dyes[79,130].

The uncertainty in the derived values of the dimeric rotational strength do not allow us to make a comparison between the PF and AO bound dimer, but the magnitude of the exciton coupling parameter, of the order of 200 cm^{-1}, is such that interactions between the two moieties of the dimer are weak, which is in agreement with the model used in which the overlap between the two dye molecules is less than that of a dimeric dye in free solution[26]. Several intercalation models have been proposed (paragraph 6.1), but the existence of the dimer is incompatible with the Lerman model[15], for example, in which the intercalated dye is buried between two successive base-pairs, which does not allow for any contact with a non-intercalated dye. On the other hand, in the model postulated by Pritchard *et al.*[43] or that suggested by Dalgleish *et al.*[46], the intercalated dye has a portion of its structure projecting outside the DNA helix, which is a necessary condition for the formation of a dimer with a non-intercalated dye.

The finding by viscosimetry[33] and temperature-jump studies[49] of the G-C specificity of the non-intercalated dye

implies that the dimerization process is also G-C specific. From an inspection of the CD spectra of PF-polynucleotide complexes, previously published (figure 3 of reference 152), one can note the larger proportion of dimer present in PF-poly(G)-poly(C) complex than in PF-poly(A)-poly(U) complex, for example.

7.5.5 The Induced Circular Dichroism of the Intercalated Dye

The induced CD of the intercalated dye obtained for r = 0 presents certain particularities. Firstly, it is negative for AO and positive for PF, secondly it is independent of the salt concentration for AO but, for PF, its magnitude increases with salt concentration, as we can see in figure 7.13, while maintaining a similar monomeric shape spectrum.

The difference in sign reflects a difference in the intercalated dye position inside the DNA, since the CD spectrum is associated with the same long axis polarised transition of the two dyes. The fact that AO presents a positive induced CD, when intercalated in RNA[135], supports the hypothesis about the dependence of the sign of the CD spectrum on the dye-DNA complex geometry and not on the electronic properties of the dye itself. Furthermore, AO is the only dye known to show a negative CD spectrum associated with its long axis polarised transition, when it intercalates in the DNA. It should be noted that this opposite sign induced CD of AO when bound to DNA and RNA has also been found upon the intercalation of the 2,4 dinitro-aniline reporter (N,N,N-trimethyl-N',N'-dimethyl-N'-(β-2,4-dinitro-anilinoethyl)-1,3-diammoniumpropane dibromide)[134]. This change of CD sign has been correlated

with the steric hindrance between the 2'-hydroxyl group in the minor groove of the RNA and the 4-NO_2 group of the reporter molecule, which forces the latter to take a more external position; but in DNA, where the 2'-hydroxyl group is missing, the 4-NO_2 group points toward the centre of the helix[134]. This particularity of AO is not only restricted to CD; indeed, when bound to an A-T or a G-C base-pair, the AO fluorescence is enhanced, whereas for most of the dyes studied, their fluorescence is quenched when bound to a G-C base-pair[136]. Moreover, AO is the only dye studied which, with 10-methylacridinium and 9-amino-10-methylacridinium dyes, proves to be non-mutagenic[4,136,137]. These differences of behaviour between AO and PF are peculiar if one considers that they intercalate in DNA to the same extent (same K_1 and n) and do not show any particular binding specificity to any kind of base-pair[65,66]. Although the geometry of the dye intercalation is not known, the long axis of the dye is almost perpendicular to the helix axis with a value of 78° ± 3° for PF[36] and 76° ± 4° for AO. In favour of a different intercalation geometry, X-ray studies on dinucleoside-dye complexes have shown that the AO intercalation is asymmetric[57,60], whereas the PF one is symmetric[55,57].

The induced CD spectrum of the PF-DNA complex, obtained at r = 0, shows a dependence on the salt concentration (figure 7.13), unlike other dyes, such as ethidium bromide[138], AO (paragraph 7.3) and 9-AA complexed to DNA. Li and Crothers[98] and Kamiya[139] have already noticed this remarkable decrease in the magnitude of the PF-DNA CD spectrum as the salt concentration decreases. Theoretical calculations[139], based on the exciton interactions between

the intercalated dye and the DNA bases 'electronic transitions, have shown that an increase in the distance separating the intercalated dye from the DNA base-pairs or a decrease in the DNA rotation angle, lead to a decrease in the magnitude of the CD spectrum. In low salt concentrations, the electrostatic repulsions between the phosphate groups will unwind[141] and thus expand the DNA helix[129,142]. This expansion of the DNA helix, as the salt concentration decreases, manifests itself in a decrease in the sedimentation coefficient as well as in an increase in the intrinsic viscosity of DNA[129,140]. It is interesting to observe that the dependence of the DNA intrinsic viscosity on the salt concentration levels off when the value of the salt concentration is around 0.6 mol dm^{-3} which is independent of the nature of the salt (figure 3 of reference 140). In figure 7.13, we can see that the dependence of the PF-DNA induced CD on the salt concentration levels off at a similar value of the salt concentration to that found above. Even though this explanation seems satisfactory, we cannot understand why only the CD spectrum of the PF-DNA complex manifests this salt dependence, unless it is because PF is the only intercalated dye which has been found[55,57] with its two amino groups forming hydrogen bonds with the phosphate groups on opposite chains.

7.6 Conclusion

Thus, throughout this CD study, we have shown that the binding model of Armstrong, Kurucsev and Strauss[26] which has been confirmed by some[92] but criticized by others[96,143], interprets in a satisfactory manner the evolution of the CD spectra of the AO- and PF-DNA complexes with the amount of binding. But we must not forget that our CD results were

based upon and depend on the interpretation of the binding data by the neighbour exclusion equation 7.2. We have seen that its mathematical expression, although it takes into account most of the features of the binding process (site exclusion and dimerization), is a simplified one[117,146]. Hence, the need was felt for an independent method for investigating the dye to DNA binding.

8. THE 9-AMINOACRIDINE-DNA COMPLEX

The meticulous and time-demanding equilibrium dialysis measurements associated with the neighbour exclusion equation 7.2, for extracting the different quantities characteristic of the binding model postulated in paragraph 7.2, were replaced by a combination of two spectroscopic methods, absorption and circular dichroism. The advantage of this procedure lies in the simplicity and the accuracy of the spectroscopic methods.

8.1 The Electronic Properties of the 9-aminoacridine Dye

Figure 8.1 shows the visible absorption spectrum of the 9-AA dye. Two major electronic transitions can be seen in the spectrum at 25,000 and at 30,700 cm^{-1}. The dichroic ratio represented in figure 8.1 indicates their respective polarizations, as well as the presence of an additional short axis polarised transition on the high energy side of the spectrum. The increase in the value of the dichroic ratio over the intense visible transition, in going to high energy, is rather peculiar considering that it was more or less constant in the case of the AO and PF dyes (figure 7.1), which allows us to suppose the presence of a long axis transition situated in between the two visible transitions. The calculated transitions of 9-AA cation are shown in table 8.1. A satisfactory correlation is found between the experimental and theoretical positions, polarisation directions and relative intensities of the four visible transitions, except in the case of the calculated long axis polarised transition at 29,200 cm^{-1} whose intensity is too high.

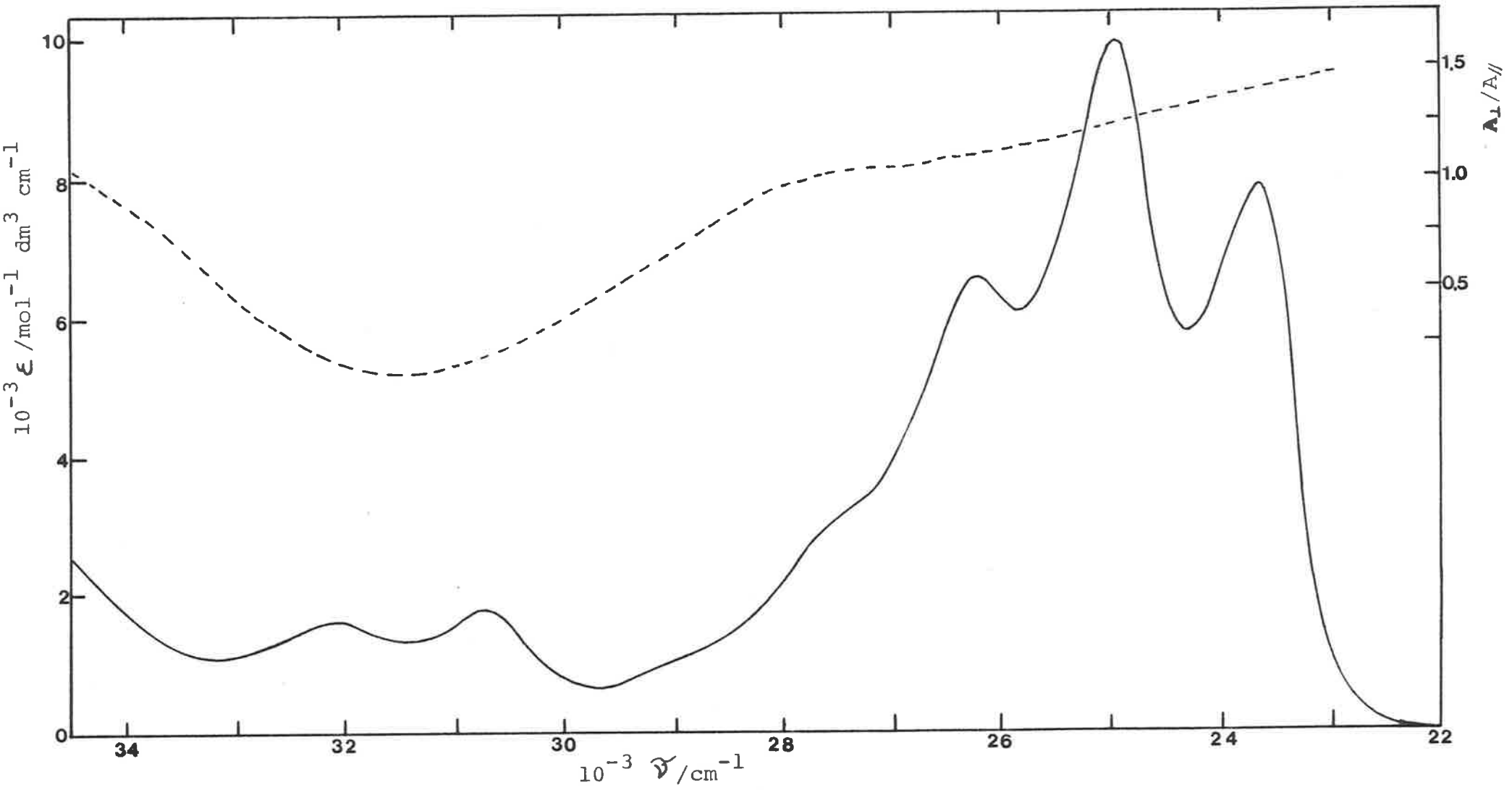

FIG.8.1 VISIBLE ABSORPTION SPECTRUM OF 9AMINOACRIDINE IN 0.001 M NACL,PH=6.6.
The reciprocal of the dichroic ratio (---) is represented instead of the dichroic ratio $A_{//}/A_\perp$

Table 8.1 CALCULATED ENERGIES, INTENSITIES AND POLARISATIONS OF 9-AMINOACRIDINE CATION.

Energy[a] of the (0,0) band in cm^{-1}	Oscillator strength f	Polarisation direction[b]
26090	0.14	Y
29290	0.70	X
30740	0.02	X
37340	0.17	Y

a - Only the transitions in the visible part of the spectrum were considered.

b - The polarisation directions X and Y correspond to the long and short molecular symmetry axes of the 9-aminoacridine, respectively.

8.2 The Binding of 9-AA to DNA as seen through the Absorption Spectra

Figure 8.2 shows the evolution with r of the visible absorption spectrum of the 9-AA-DNA complex in 0.001 mol dm^{-3} NaCl solution. No clear isosbestic point is present in the absorption spectra, which indicates the existence of more than two species. The model of binding developed for the AO and PF-DNA complexes will now be applied to the 9-AA-DNA complex.

The total molar absorptivity, $\varepsilon_T(\tilde{\nu})$, at any wavenumber, may be expressed in terms of the molar absorptivity of the free dye, $\varepsilon_F(\tilde{\nu})$, the bound monomer, $\varepsilon_1(\tilde{\nu})$, and the bound dimer, $\varepsilon_{12}(\tilde{\nu})$, by the relation

$$\varepsilon_T = \frac{C_F}{C_T}\,\varepsilon_F(\tilde{\nu}) + \frac{(C_1-C_{12})}{C_T}\,\varepsilon_1(\tilde{\nu}) + \frac{2C_{12}}{C_T}\,\varepsilon_{12}(\tilde{\nu}) \qquad (8.1)$$

All of the other quantities have been defined in paragraph 7.2. The absorption spectrum of the bound monomer is obtained by the extrapolation of $\varepsilon_T(\tilde{\nu})$ to r = 0. The only unknown absorption spectrum is that of the bound dimer. Its envelope is taken to be similar to that of the bound monomer spectrum and we may thus write

$$\varepsilon_{12}(\tilde{\nu}) = q\varepsilon_1(\tilde{\nu}) \qquad (8.2)$$

This approximation was made firstly in view of the relatively weak degenerate exciton interaction existing in the bound dimer in comparison to that found in a dimer in free solution, and in particular, because the shape of the 9-AA absorption spectrum is not very sensitive to the dimerization process, as we can see in figure 8.3 (the position of the different peaks remains practically constant when the concentration of 9-AA is increased from

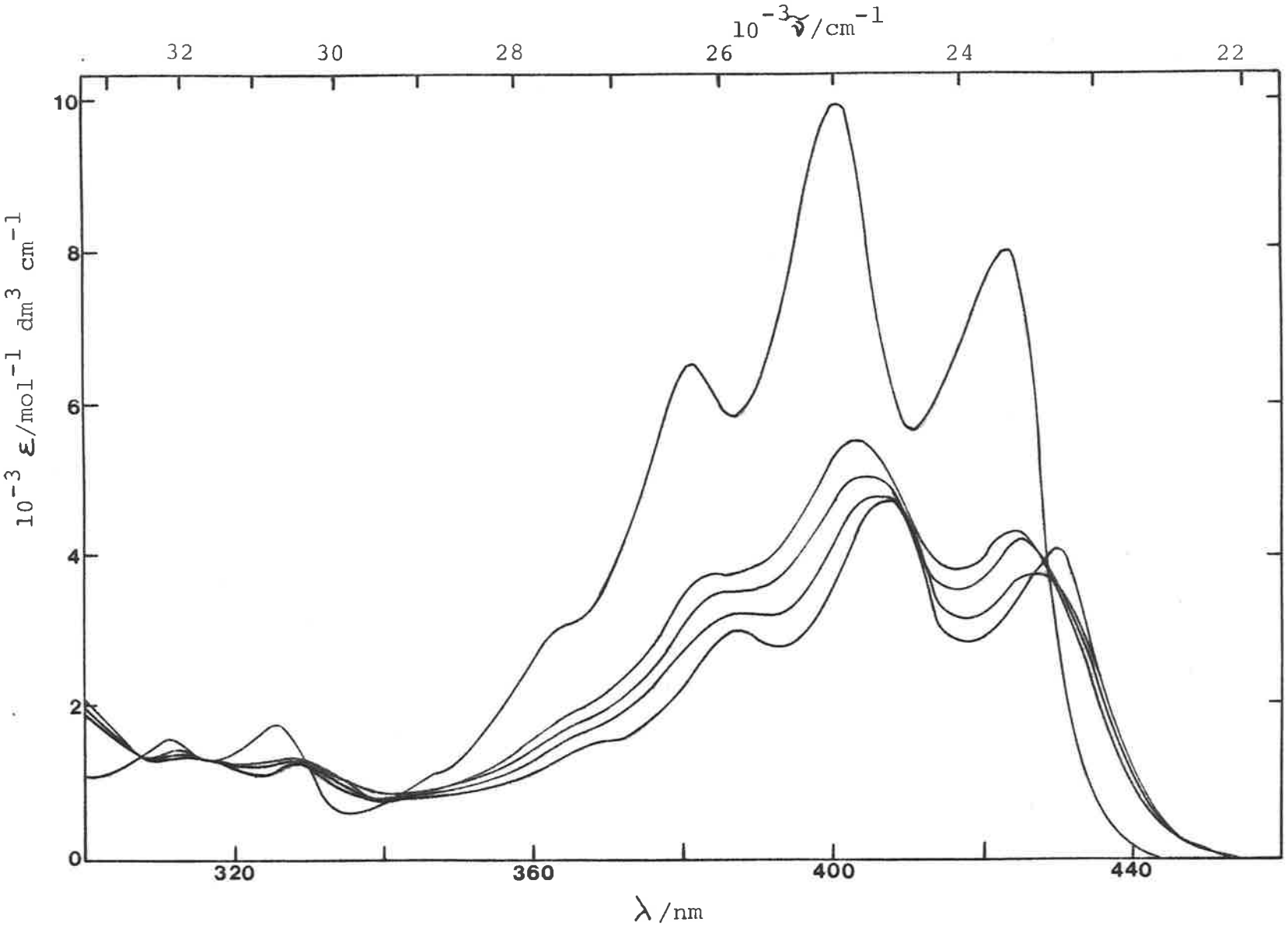

FIG.8.2 ABSORPTION SPECTRA OF 9AMINOACRIDINE-DNA IN 0.001 M NACL AT DIFFERENT 9AA TO DNA CONCENTRATION RATICS. From the top, in order: 9AA alone, 0.4, 0.32, 0.26 and 0 .

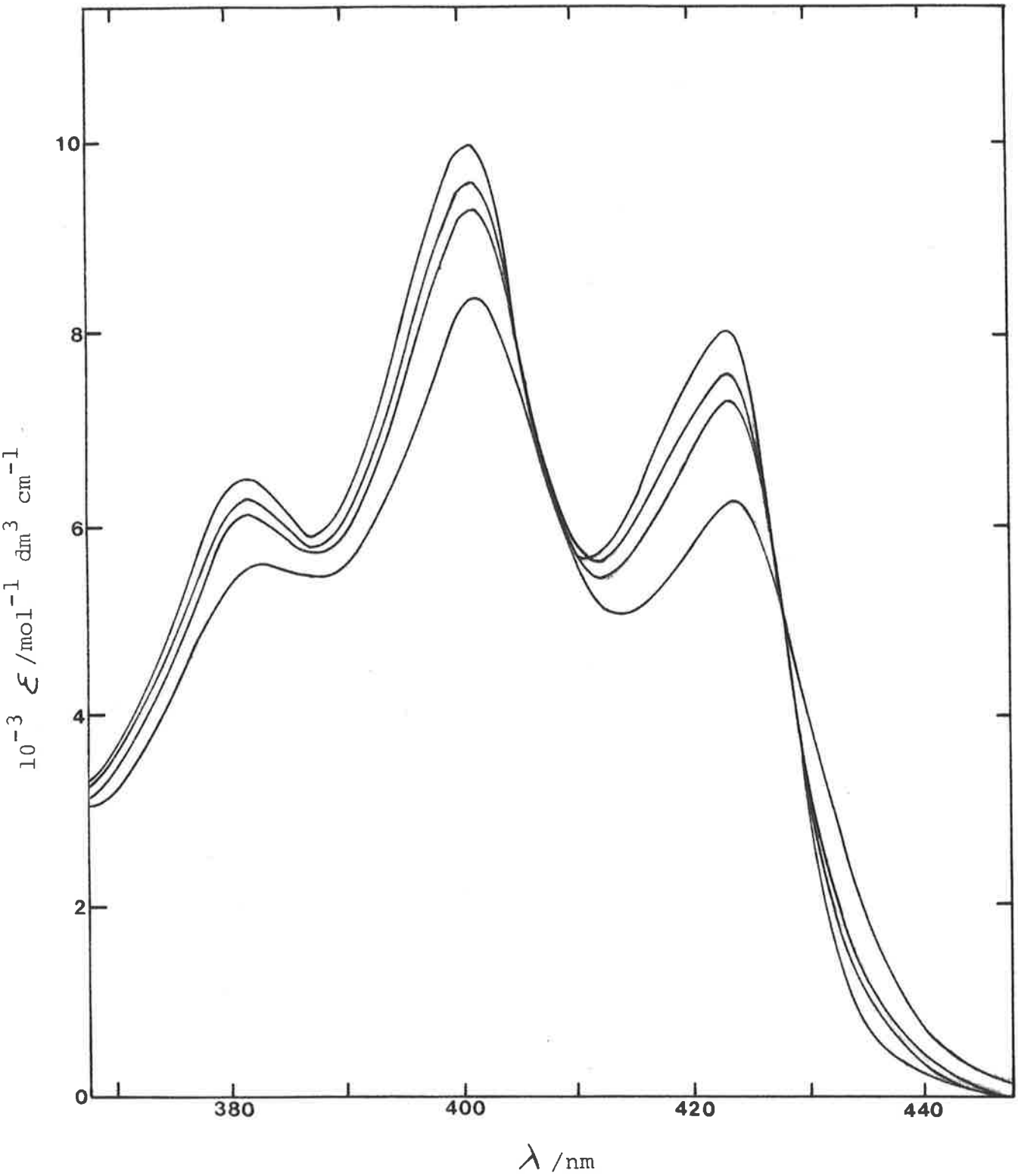

FIG.8.3 ABSORPTION SPECTRA OF 9-AMINOACRIDINE AT DIFFERENT CONCENTRATIONS IN 0.05 M NACL SOLUTION.
From the top, in order; 3.5×10^{-6} to 5×10^{-5} M, 1.8×10^{-4} M, 3.4×10^{-4} M, and 1.7×10^{-3} M.

$3.5\ 10^{-6}$ to $1.7\ 10^{-3}$ mol dm^{-3}). The weak interaction between the two moieties of the dimer and therefore the similarity in shape between the dimer and monomer absorption spectrum may be explained by the low intensity of the transition considered, which is approximately ten times less intense than in the case of the AO dye, for example; as we have already seen in equation 2.19, the exciton coupling in the dimer and therefore the splitting energy between the in-phase and out-of-phase dimeric bands are directly proportional to the intensity of the transition considered[147].

Thus, equation (8.1) may be represented as the sum of contributions from the free dye and the bound monomeric dye:

$$\varepsilon_T(\tilde{\nu}) = \frac{C_F}{C_T}\,\varepsilon_F(\tilde{\nu}) + \frac{[C_1 + C_{12}(2q-1)]}{C_T}\,\varepsilon_1(\tilde{\nu}) \qquad (8.3)$$

Equation 8.3, together with the relation $C_T = C_F + C_1 + C_{12}$ may be written in the form

$$\varepsilon_T(\tilde{\nu}) = \frac{C_F}{C_T}\,\varepsilon_F(\tilde{\nu}) + \left[1 - \frac{C_F}{C_T} - 2(1-q)\frac{C_{12}}{C_T}\right].\varepsilon_1(\tilde{\nu}) \qquad (8.4)$$

The knowledge of the quantities $\varepsilon_F(\tilde{\nu})$ and $\varepsilon_1(\tilde{\nu})$ enables us to solve equation 8.4

Eight wavenumbers between 23,100 cm^{-1} and 26,300 cm^{-1} in the spectra of figure 8.2 were chosen so as to satisfy equation 8.2. Figures 8.4 and 8.5 show the final results obtained using equation 8.4. Figure 8.6 represents the experimental binding isotherm of the 9-AA-DNA complex in 0.001 mol dm^{-3} NaCl solution as well as the tentative fit to the nearest-neighbour site exclusion model equation 7.2 (n = 2). The value of the dimerization constant K_2 was taken to be that which gives the minimum value of the standard deviation of the ratio

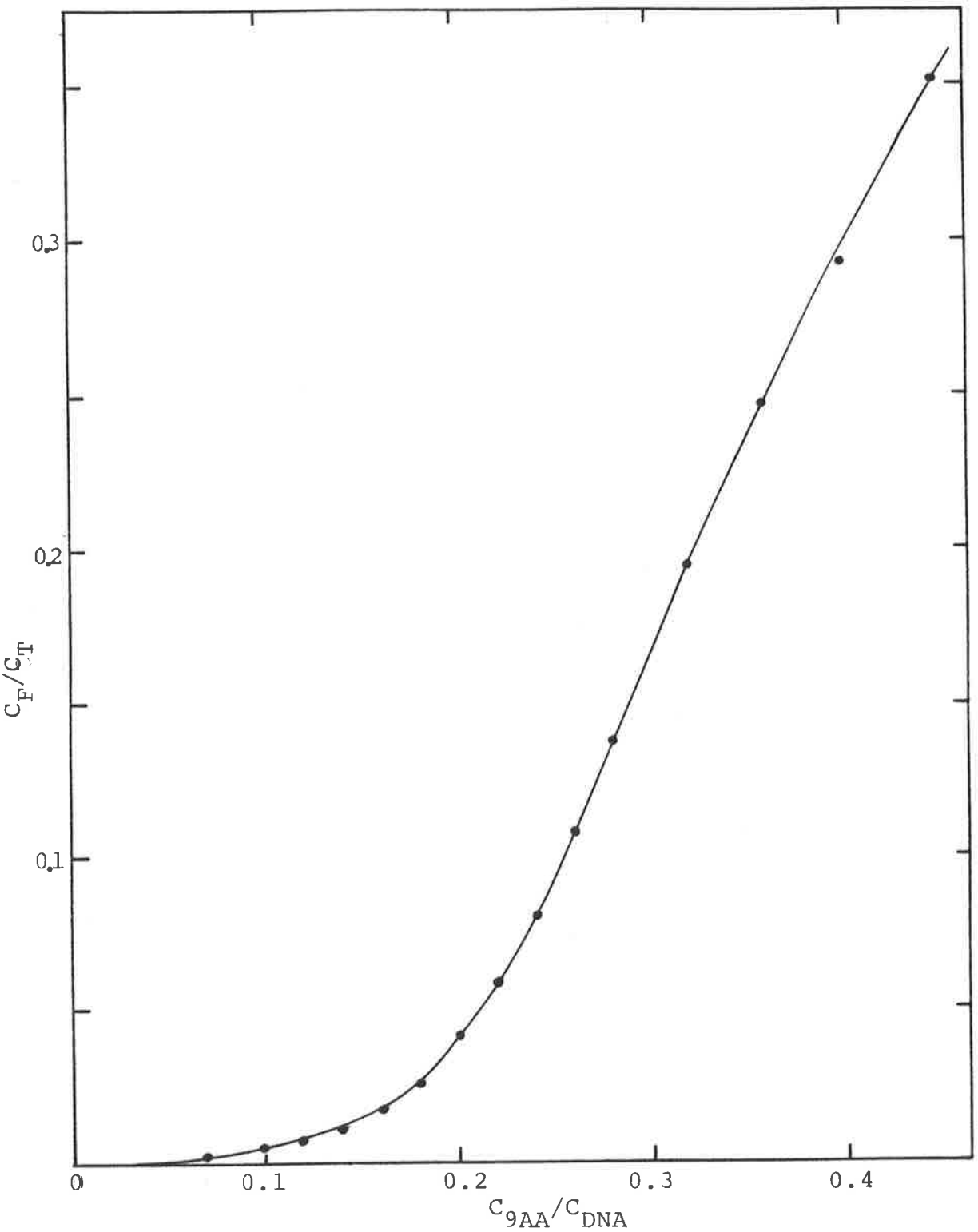

FIG.8.4 EXPERIMENTAL BINDING DATA OF 9AA OBTAINED WITH THE USE OF EQU.8.4.
$C_{9AA}=4.9\times10^{-5}$ mol dm^{-3}; $C_{NaCl}=0.001$ mol dm^{-3}.

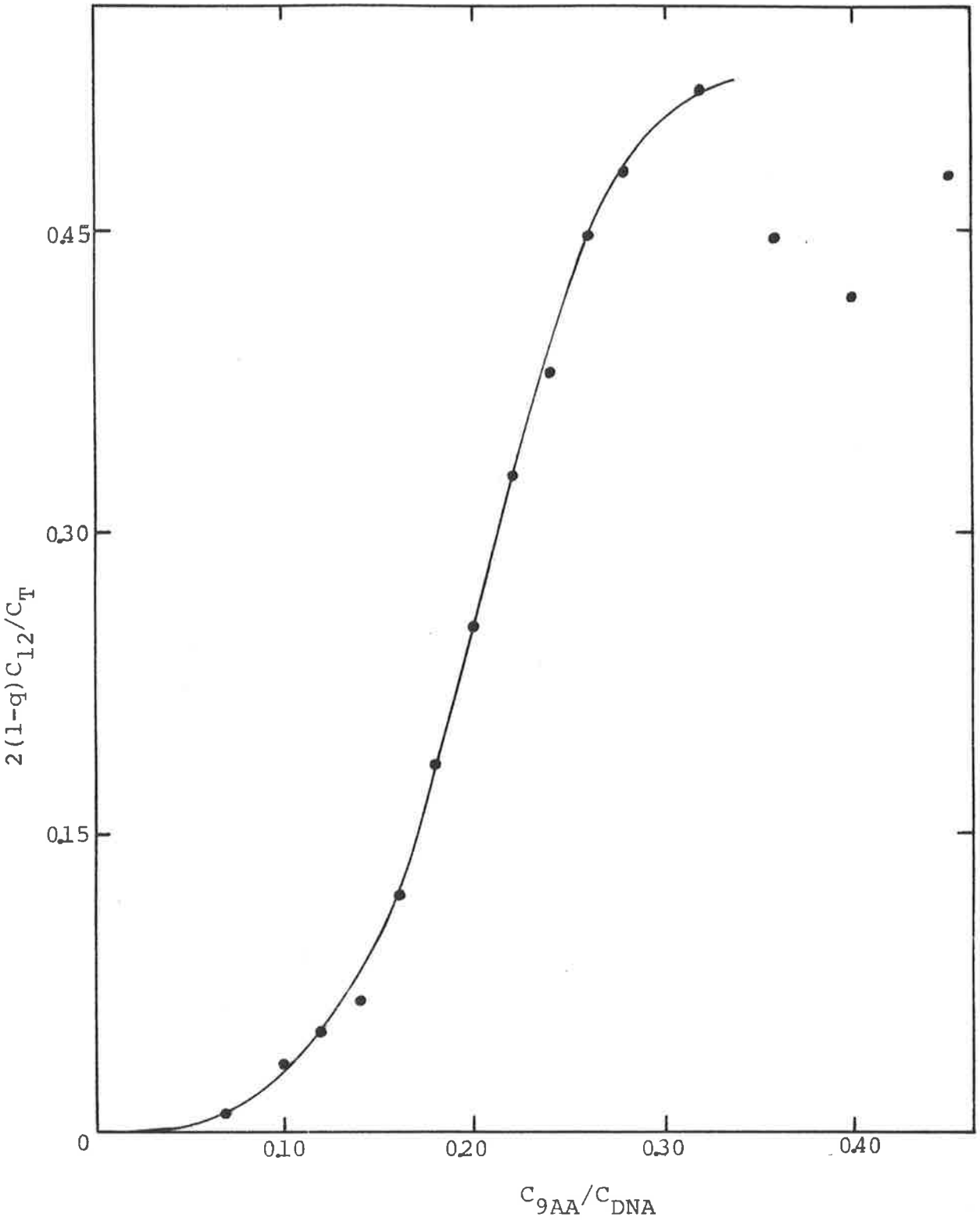

FIG.8.5 EXPERIMENTAL BINDING DATA OF 9AA-DNA COMPLEX. (see fig.8.4).

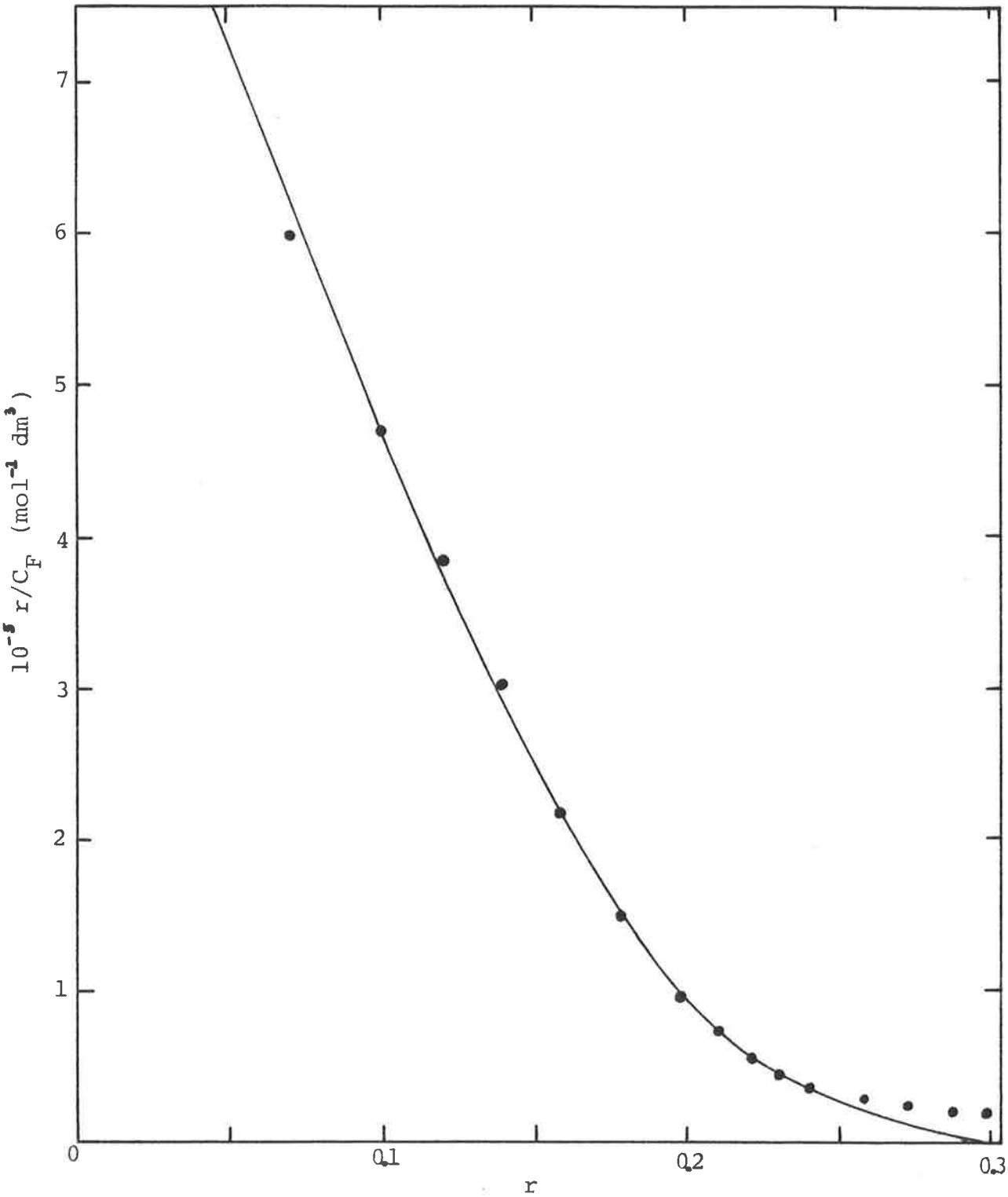

FIG.8.6 BINDING ISOTHERM OF 9AA WITH DNA IN 0.001 M NaCl.
The curve shown have been calculated by mean of equ.7.2.

$$\frac{(r/C_F)_{experimental}}{(2/K_1 . r/C_F)_{calculated}}$$

as represented in figure 8.7. A plot of

$$\frac{(r/C_F)_{experimental}}{(2/K_1 . r/C_F)_{calculated}}$$

versus r in figure 8.8 gives the limit of validity of the binding model used (this limiting value of r is found to be independent of the value of K_2). We found K_1 equal to 21×10^5 mol^{-1} dm^3 and K_2 equal to 1.55×10^4 mol^{-1} dm^3.

Equations 7.1 and 7.3, together with the quantities derived from equation 8.4, enable us to obtain the value of the constant q through the equation

$$\frac{1 - C_F/C_T}{(1-q).C_{12}/C_T} = \frac{1}{(1-q)K_2C_T} \cdot \frac{C_T}{C_F} + \frac{2}{1-q} \qquad (8.5)$$

In figure 8.9 we have represented the plot of the quantity on the left side of equation 8.5 versus $\frac{C_T}{C_F}$ for values of r up to 0.24. We find a value of q equal to 0.65 and a value of the dimerization constant, K_2, equal to 1.8×10^4 mol^{-1} dm^3 which is in agreement with that found previously.

8.3 Results Obtained from Analysis of the Circular Dichroism Spectra

Figure 8.10 shows some CD spectra of the 9-AA-DNA complex. One can note the large optical activity acquired by the long axis polarised transition at 330 nm in relation to the weak intensity of its absorption band in figure 8.2. Moreover, the existence of an additional transition situated in between the visible short and long axis polarised transitions is confirmed by the relatively high intensity obtained in this part of the CD spectrum, unlike in the absorption spectra. Due to the presence of this

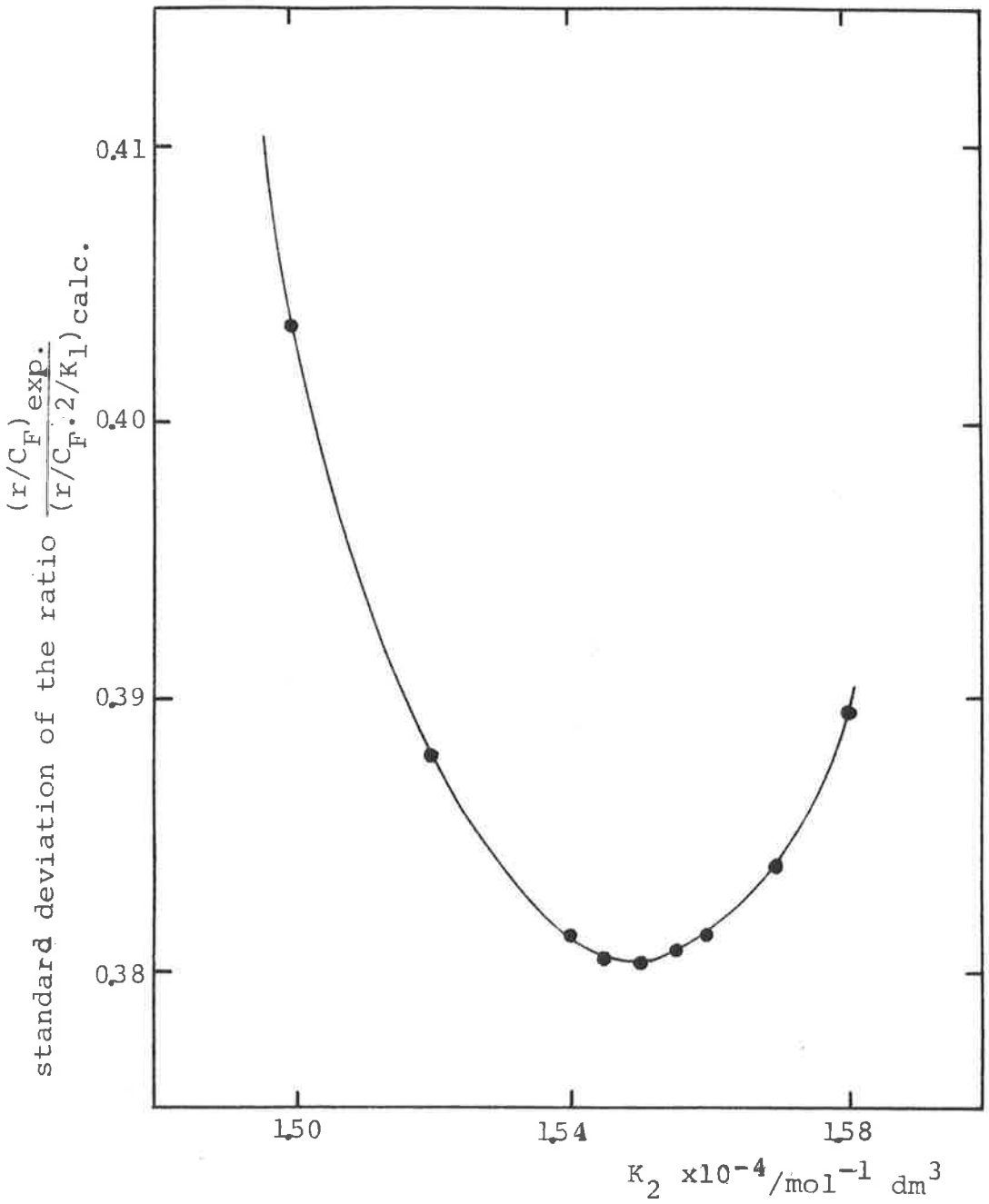

FIG.8.7 DETERMINATION OF THE DIMERIZATION CONSTANT K_2, FOR THE BEST FIT OF THE BINDING DATA OF THE 9AA-DNA COMPLEX.

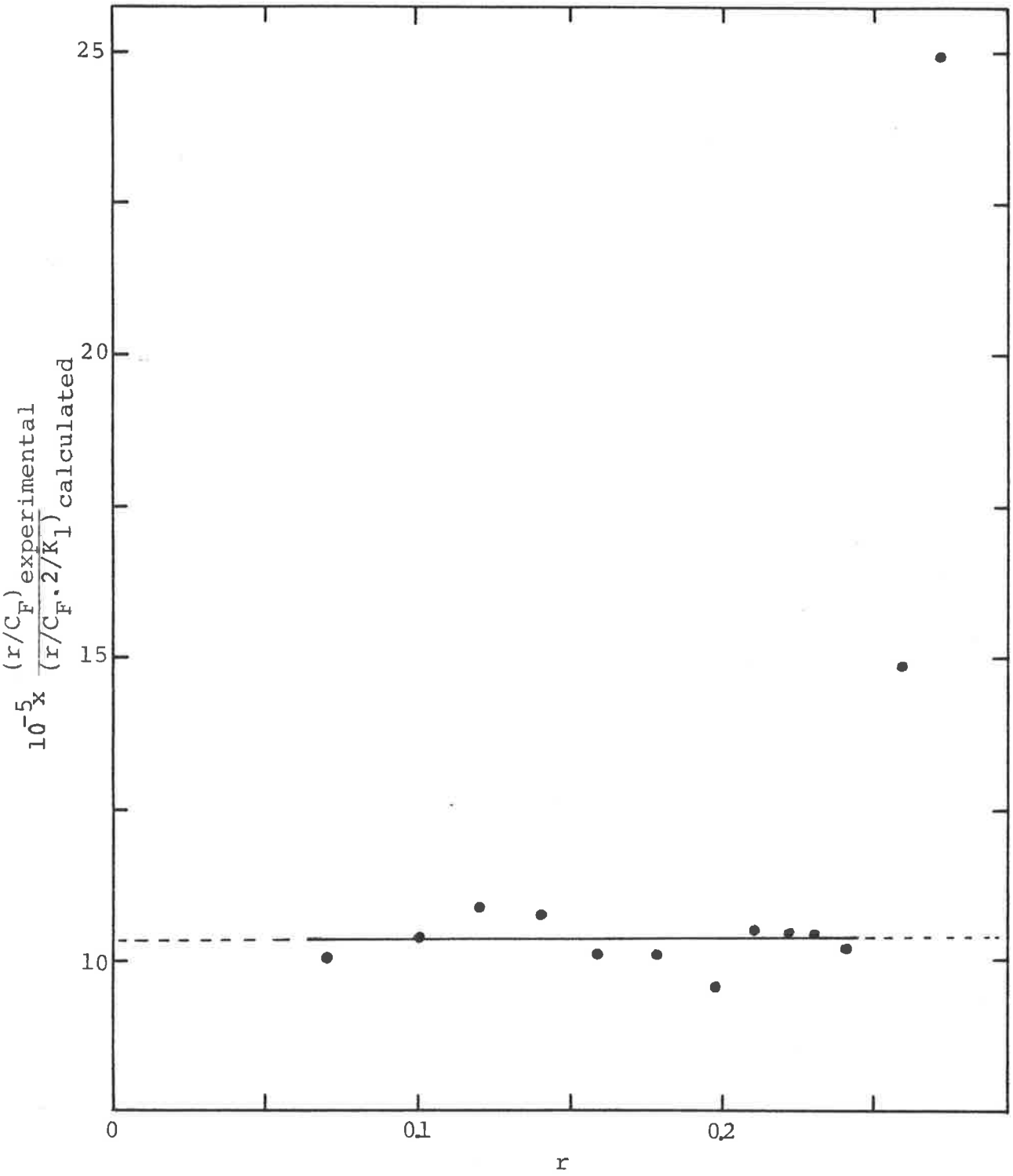

FIG.8.8 TEST PLOT FOR THE FIT OF THE BINDING DATA OF 9AA WITH EQU.7.2.

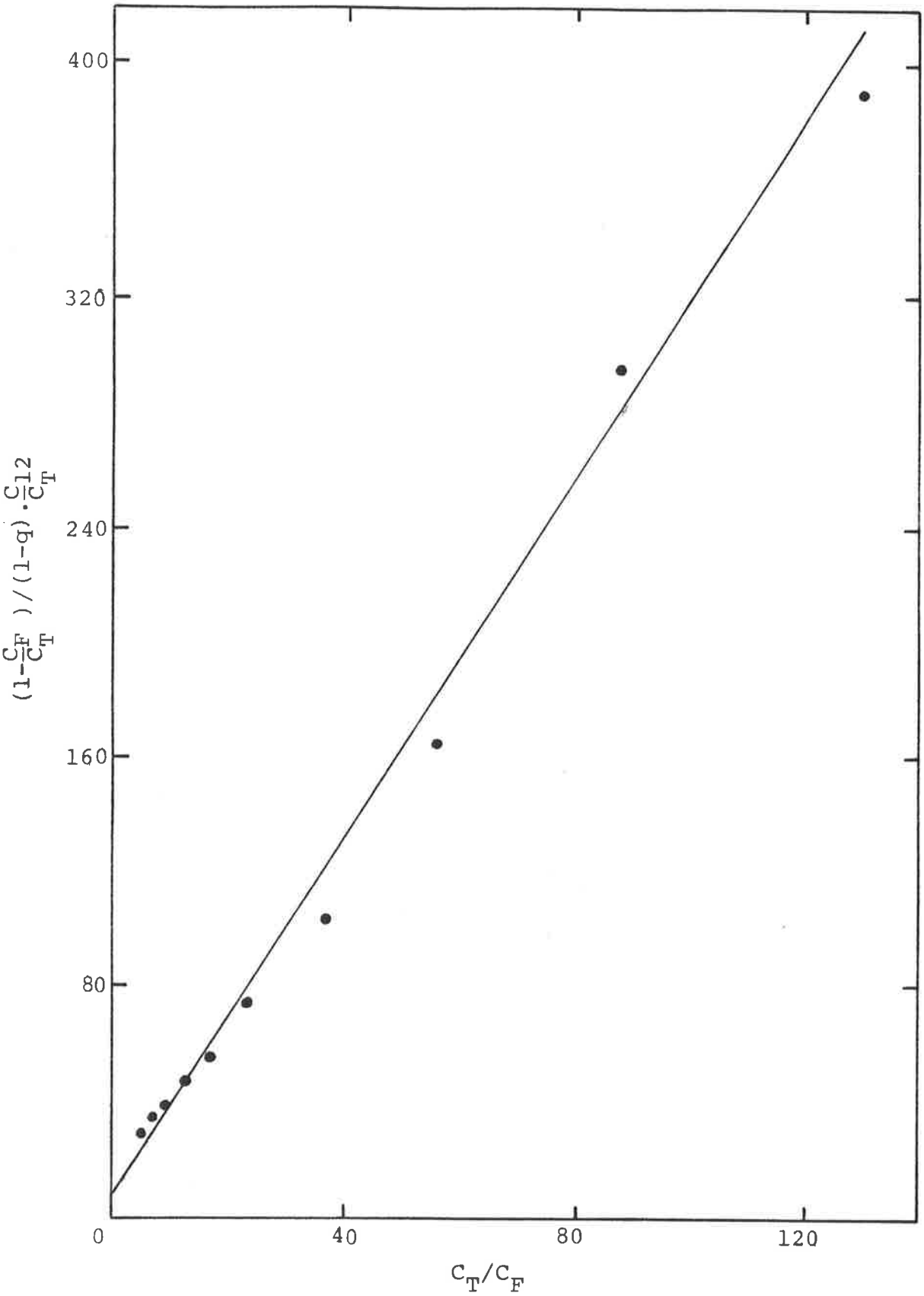

FIG.8.9 DETERMINATION OF THE BINDING PARAMETERS OF 9AA ACCORDING TO EQU.8.5.
Dots:experimental data from absorption spectra.

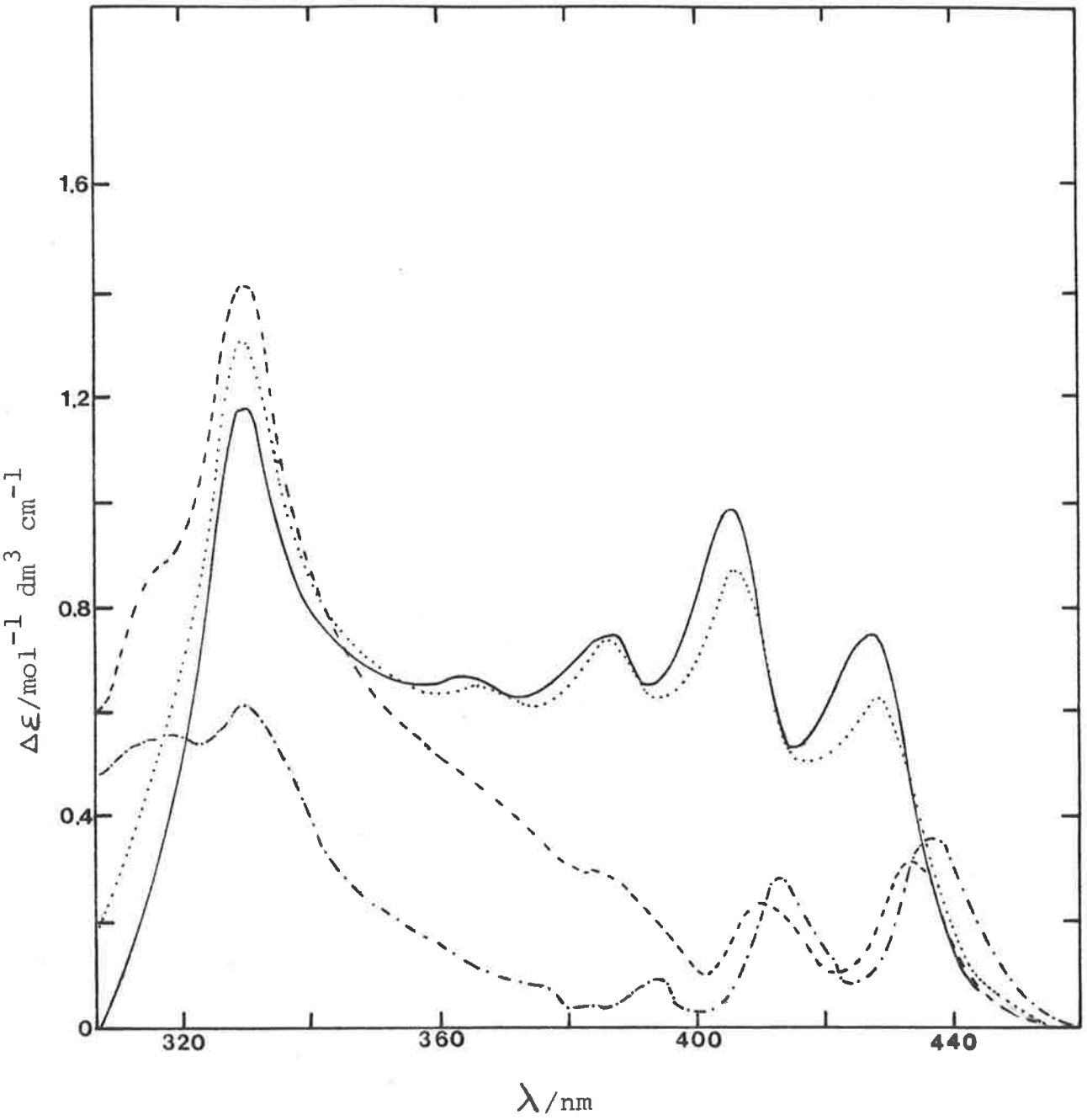

FIG.8.10 CIRCULAR DICHROISM SPECTRA OF 9AMINOACRIDINE-DNA COMPLEX IN 0.001 M NACL FOR A 9AMINOACRIDINE TO DNA CONCENTRATION RATIO OF 0.026 (—), 0.15 (··), 0.19 (---) AND 0.51 (-·-).

transition, whose envelope overlaps with that of the low energy transition (the distribution of the intensities between the vibronic bands of the CD spectra is different from that of the absorption spectra), an analysis of the CD spectra was just considered for the long axis polarised transition. The evolution of the band intensity at 330 nm with the amount of loading of the dye in the DNA is shown in figure 8.11. Combining equations 7.1, 7.3 and 7.9, we obtain the relation

$$\left[\frac{\Delta\varepsilon(\tilde{\nu})}{\frac{C_B}{C_T}\cdot\Delta\varepsilon_1(\tilde{\nu})} - 1\right]^{-1} = [C_T K_2 (p-1)]^{-1}\cdot\frac{C_T}{C_F} + \frac{2}{p-1} \qquad (8.6)$$

Because of the invariability of the maximum position of the band considered (330 nm) as the binding proceeds, it is assumed that the dimeric contribution (equation 7.10) to the overall CD spectrum is nil. This is in total agreement with the results obtained from theory which show that the dimeric CD spectrum results from the cancellation of the two CD bands of different signs; the energy separation between these two CD bands being directly proportional to the dipole strength of the transition (paragraph 2.1).

The plot, in figure 8.12, of the quantity on the left side of equation 8.6 versus $\frac{C_T}{C_F}$, enables us to obtain the value of the parameter p equal to 5.5 and the value of the dimerization constant, K_2, equal to 5×10^4 mol^{-1} dm^3.

8.4 Interpretation of the Results

Several conclusions may be drawn from the results obtained.

Although the spectrum of the dimeric species is not directly apparent in the case of the 9-AA-DNA complex, the evolution of the spectra with the amount of binding can be

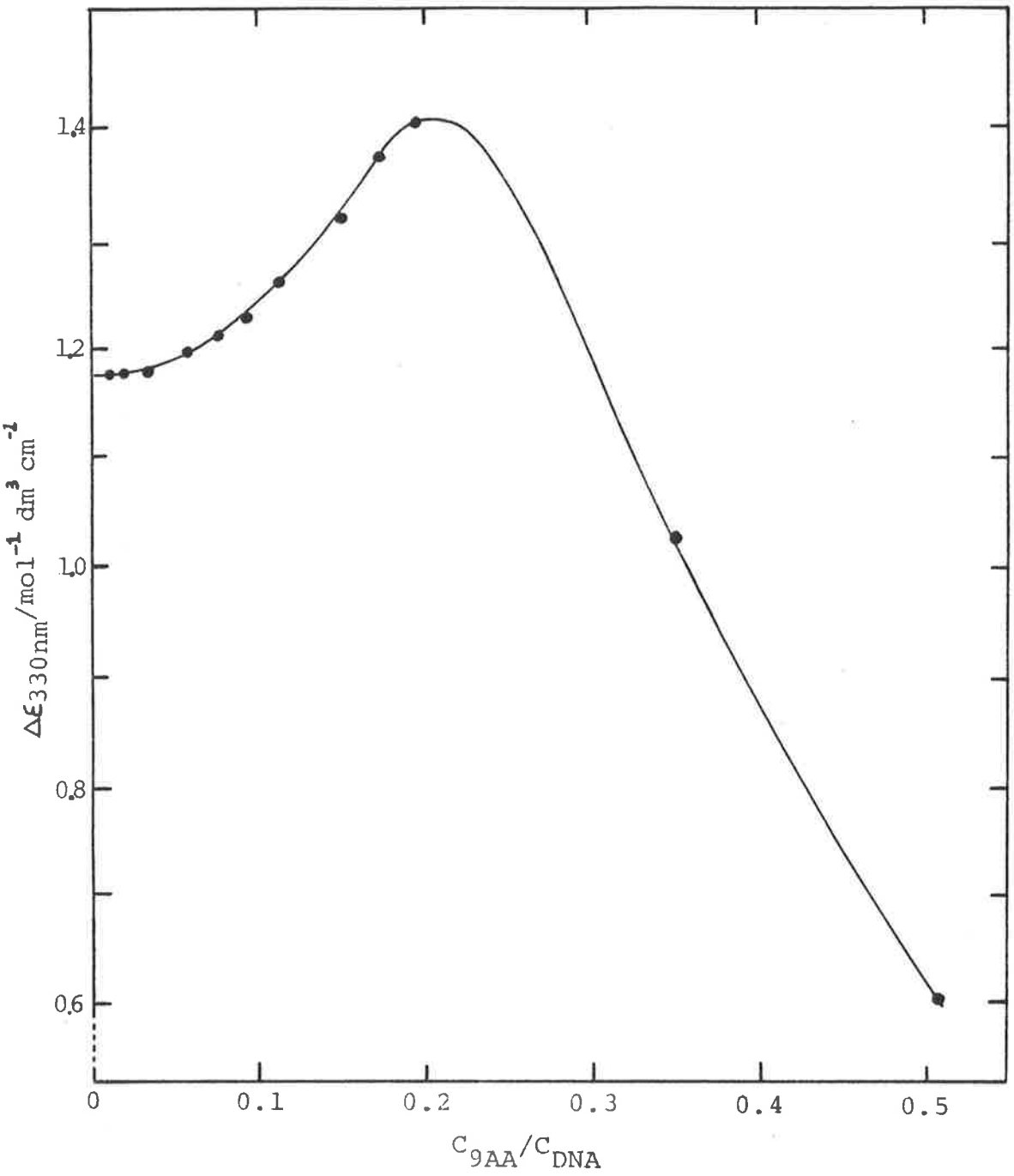

FIG.8.11 EVOLUTION OF THE MOLAR CIRCULAR DICHROISM OF 9AA-DNA COMPLEX VERSUS THE 9AA TO DNA CONCENTRATION RATIO.
$C_{9AA}=4.9\times10^{-5}$ mol dm^{-3}; $C_{NaCl}=0.001$ mol dm^{-3}.

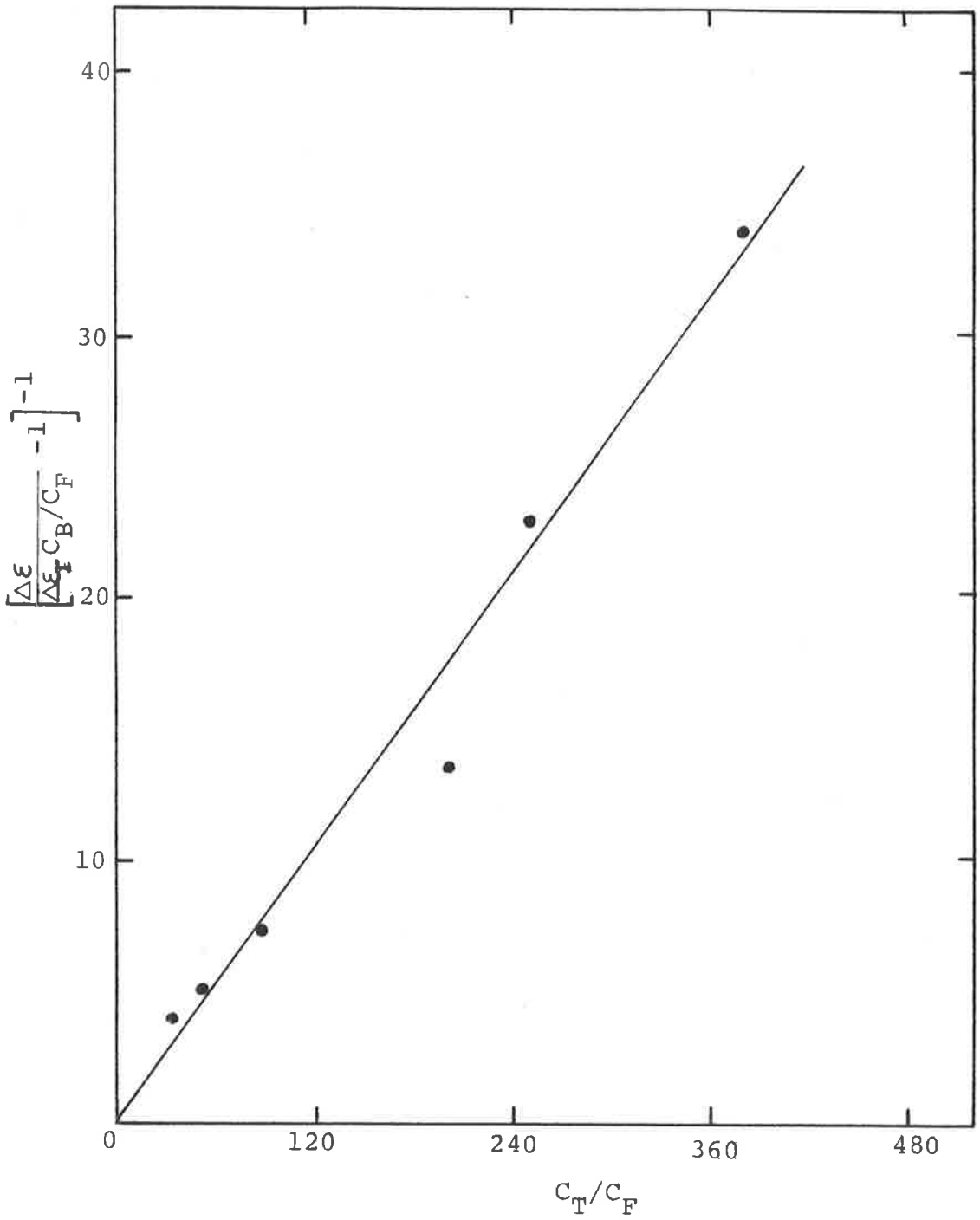

FIG.8.12 DETERMINATION OF THE BINDING PARAMETERS OF 9AA ACCORDING TO EQU.8.6.
Dots:experimental data from circular dichroism and absorption.

satisfactorily interpreted by the Armstrong, Kurucsev and Strauss model[26]. Moreover, the similarity in the values of K_2 derived from the two optical methods, provides further support for this model of binding. The magnitude of the dimerization constant, K_2, is smaller for 9-AA than for AO or PF-DNA complexes, as it is the case when these dyes are in free solution[150]. (The dimerization constant of 9-AA in 0.1 mol dm^{-3} NaCl solution is equal to 6×10^2 mol^{-1} dm^3 [151]).

The value of the binding constant, K_1, for the 9-AA-DNA complex in 0.001 mol^{-1} dm^3 NaCl solution is in agreement with that found by Kubota and Motoda[67].

The magnitude of the constant q in equation 8.2 is in conformity with a dimer model in which the coupling between the transition moments of the two moieties is weak (figure 8 of reference 26).

To be able to make a comparison between the geometry of the non-intercalated dyes, we calculated in table 8.2 the geometrical contribution to the rotational strength $\mathcal{R}_2$ (equations 4.1 and 4.2) for the dye-DNA complexes studied.

We conclude from the values obtained in table 8.2, that the orientation of the non-intercalated dye in relation to the DNA helix is similar for all the dyes studied. Therefore, we can speculate that the positively charged ring nitrogen, common in these dyes, is important for the binding of the non-intercalated dye to DNA. It would be of great interest to study the acriflavine (AC) and ethidium bromide-DNA complexes in which both dyes have substituent groups attached to the ring nitrogen; we would expect their non-intercalated dyes to have a different geometry because of the steric effect of the substituent groups. An orientation of the non-intercalated dye, such

Table 8.2 GEOMETRICAL CONTRIBUTION TO THE ROTATIONAL STRENGTH OF THE NON-INTERCALATED DYE

complex[a]	$\mathcal{R}_2$ x 10^{40} (cgs units)	$\mathcal{R}_2 / \left(\frac{\tilde{\nu}_{DNA} \cdot \tilde{\nu}_{complex}}{\tilde{\nu}^2_{DNA} - \tilde{\nu}^2_{complex}} \cdot \mu^2_{complex}\right)$
di-tert-butyl PF-DNA	140	1.7×10^{-3}
PF-DNA	136	1.8×10^{-3}
AO-DNA	121	1.5×10^{-3}
9-AA-DNA	13.6	2.3×10^{-3}

a - Only the long axis polarised visible transition was considered.

that its long axis is tangent to the DNA helix, finds support in the behaviour of the CD of the ethidium bromide and 9-AA-DNA complexes associated with the short axis polarised transition whose intensities decrease with an increase in r values, which is the opposite to what we found in the case of the long axis polarised transitions. This particular behaviour seems to indicate that the rotational strength, $\mathcal{R}_2$, for the short axis polarised transition is very small or nil. This is in agreement with the results which we obtain from the theoretical calculation of the rotational strength (equation 4.1) in which the distance vector separating the two coupled transition moments is co-linear to one of these transition moments.

9. CONCLUSION

The CD spectra of dye-DNA complexes have been successfully interpreted in terms of a monomeric CD spectrum of the intercalated and non-intercalated dyes superimposed by a dimeric CD spectrum arising from the vibronic exciton interactions between them.

This study has shown that circular dichroism is extremely sensitive to the dimerization process. In fact, we have shown that the CD of the bound dimeric species and therefore the CD of the non-intercalated dye was responsible for the variations in the observed CD with increasing values of r, because their magnitudes are much larger than that of the intercalated dye (compare $\mathcal{R}_1$ with $\mathcal{R}_2$ or $\mathcal{R}^-$ in table 7.4). On the one hand, the magnitude of these CD is directly proportional to the dipole strength of the transition considered (equation III B-22 of reference 119). The molar absorptivity of the visible transition of the 1AA-, 2AA- and 9AA-DNA complexes is less than 5×10^3 mol^{-1} dm^3 cm^{-1},[88] therefore it is not surprising that these dye-DNA complexes do not show as large a variation in their CD as that found for dyes complexed to DNA such as 3-AA[88], PF[26], AO[26], AC[148] or thionine[99] which have a much stronger visible transition ($\varepsilon_{max} > 15 \times 10^3$ mol^{-1} dm^3 cm^{-1}). On the other hand, the dimeric CD spectrum results from the cancellation of two bands of opposite signs whose energy separation is directly proportional to the dipole strength of the transition considered (paragraph 2.1). The visible transitions of AO-, PF-, AC- and thionine-DNA complexes have in common, a dimeric type of CD spectrum, but the transition of the 3AA-DNA complex which is five times weaker than that of the

above mentioned complexes, lacks the presence of this dimeric spectrum due to the total cancellation of the in-phase and out-of-phase CD bands. The explanation for the different behaviours of the CD spectrum, which we based on the magnitude of the dipole strength and not on a different intercalation geometry as was suggested by Dalgleish *et al.*[46,90], finds support in the case of the ethidium bromide-DNA complex; in fact its visible transition, which is ten times weaker than the UV transition[113], shows only a small variation in its CD with increasing r values[149], whereas the CD of the strong UV transition shows signs of a dimeric type of CD[138] and increases considerably with r[149].

It has also been shown in this study that the binding model used[26], which particularities lie in the presence of excluded intercalation sites next to an already intercalated dye and also on the presence of bound dimeric dyes, can be generalised to apply to most of the dye-DNA complexes. This similarity in the binding process is confirmed by the fact that the constant of binding, K_1, as well as the geometry of the non-intercalated dye, are similar in the three dye-DNA complexes studied.

This study has also shown that a correlation between theoretical and experimental results, enables us to obtain valuable geometrical information about the bound dye.

REFERENCES

1. E.F. Gale, E. Cundliffe, P.E. Reynolds, M.H. Richmond and M.J. Waring, *The Molecular Basis of Antibiotic Action*, John Wiley, London (1972).
2. F.H.C. Crick, L. Barret, S. Brenner and R.J. Watts-Tobin, *Nature*, 192, 1227 (1961).
3. A. Orgel and S. Brenner, *J. Mol. Biol.*, 3, 762 (1961).
4. L.S. Lerman, *J. Cell. Comp. Physiol.*, 64, 1 (1964).
5. J.W. Drake, *The Molecular Basis of Mutation*, Holden-Day, San Francisco (1970).
6. J. Hurwitz, J.J. Furth, M. Malamy and M. Alexander, *Proc. Nat. Acad. Sci. USA*, 48, 1222 (1962).
7. G. Hartman, W. Behr, K.A. Beissner, K. Honikel and A. Sippel, *Angew. Chem. Int. Ed.*, 7, 693 (1968).
8. A. Albert, *The Acridines*, Edward Arnold, London (1966).
9. T. Capersson, L. Zech, E.T. Modest, G.E. Foley, U. Wagh and E. Simonson, *Exp. Cell Res.*, 58, 120, 141 (1969).
10. R.N. Paul, *Stain Technology*, 55, 195 (1980).
11. L. Michaelis, *Cold Spring Harbor Symp. Quant. Biol.*, 12, 131 (1947).
12. G. Oster, *Trans. Faraday Soc.*, 47, 660 (1951).
13. H.G. Heilweil and Q. Van Winkle, *J. Phys. Chem.*, 59, 939 (1955).
14. A.R. Peacocke and J.N. Skerrett, *Trans. Faraday Soc.*, 52, 261 (1956).
15. L.S. Lerman, *J. Mol. Biol.*, 3, 18 (1961).
16. V. Luzzati, S.F. Mason and L.S. Lerman, *J. Mol. Biol.*, 3, 634 (1961).
17. L.S. Lerman, *Proc. Natl. Acad. Sci. USA*, 49, 94 (1963).
18. L.S. Lerman, *J. Mol. Biol.*, 10, 367 (1964).

19. For general reviews, see; A.R. Peacocke, *Studia Biophysica*, 24, 213 (1970); S. Georghiou, *Photochem. Photobiol.*, 26, 59 (1977).

20. S. Neidle, Progress in Medicinal Chem., 16, 151 (1979).

21. J. Cairns, *Cold Spring Harbor Symp. Quant. Biol.*, 27, 311 (1962).

22. D.S. Drummond, N.J. Pritchard, V.F.W. Simpson-Gildemeister and A.R. Peacocke, *Biopolymers*, 4, 971 (1966).

23. L.V. Crawford and M.J. Waring, *J. Mol. Biol.*, 25, 23 (1967).

24. W. Müller and D.M. Crothers, *J. Mol. Biol.*, 35, 251 (1968).

25. G. Cohen and H. Eisemberg, *Biopolymers*, 8, 45 (1969).

26. R.W. Armstrong, T. Kurucsev and U.P. Strauss, *J. Am. Chem. Soc.*, 92, 3174 (1970).

27. D.E.V. Schmechel and D.M. Crothers, *Biopolymers*, 10, 465 (1971).

28. J. Paoletti and J.B. Le Pecq, *J. Mol. Biol.*, 59, 43 (1971).

29. W.J. Pigram, W. Fuller and M.E. Davies, *J. Mol. Biol.*, 80, 361 (1973).

30. W. Müller, D.M. Crothers and M. Waring, *Eur. J. Biochem.*, 39, 223 (1973).

31. L.P.G. Wakelin and M.J. Waring, *Mol. Pharm.*, 9, 544 (1974).

32. M. Waring, *Progress in Molecular and Subcellular Biology*, vol. 2, p. 216, Hahn, Ed., Springer-Verlag, New York (1971).

33. J. Ramstein, M. Dourlent and M. Leng, *Biochem. Biophys. Res. Com.*, 47, 874 (1972).

34. V.A. Bloomfield, D.M. Crothers and I. Tinoco, Jr., *Physical Chemistry of Nucleic Acids*, p. 136, Harper-Row, New York (1974).

35. C. Houssier, B. Hardy and E. Fredericq, *Biopolymers*, 13, 1141 (1974).

36. G.R. Kelly and T. Kurucsev, *Biopolymers*, 15, 1481 (1976).

37. M.L. Barley, *Theoret. Chim. Acta*, 13, 56 (1969) and 16, 309 (1970).

38. N.F. Gersh and D.O. Jordan, *J. Mol. Biol.*, 13, 138 (1965).

39. V. Kleinwachter and J. Koudelka, *Biochem. Biophys. Acta*, 91, 539 (1964).

40. G. Löber, H. Schutz and V. Kleinwachter, *Biopolymers*, 11, 2439 (1972).

41. D.S. Drummond, V.F.W. Simpson-Gildemeister and A.R. Peacocke, *Biopolymers*, 3, 135 (1965).

42. A. Blake and A.R. Peacocke, *Biopolymers*, 6, 1225 (1968).

43. N.J. Pritchard, A. Blake and A.R. Peacocke, *Nature*, 212, 1360 (1966).

44. G. Löber and G. Achtert, *Biopolymers*, 8, 595 (1969).

45. W. Füller and M.J. Waring, *Ber. Bunsenges. Phys. Chem.*, 68, 805 (1964).

46. D.G. Dalgleish, A.R. Peacocke, C. Harvey and G. Fey, *Biopolymers*, 10, 1853 (1971).

47. H.J. Li and D.M. Crothers, *J. Mol. Biol.*, 39, 461 (1969).

48. M. Sakoda, K. Hiromi and A. Akasaka, *Biopolymers*, 10, 1003 (1971).

49. J. Ramstein and M. Leng, *Biophys. Chem.*, 3, 234 (1975).

50. T.D. Sakore, B.S. Reddy and H.M. Sobell, *J. Mol. Biol.*, 135, 763 (1979).

51. C.J. Alden and S. Arnott, *Nucleic Acids Res.*, 2, 1701 (1975) and 4, 3855 (1977).

52. J.E. Scott, *Histochemie*, 9, 30 (1967).

53. C.C. Tsai, S.C. Jain and H.M. Sobell, *J. Mol. Biol.*, 114, 301, 317 (1977).

54. E. Westhof and M. Sundaralingam, *Proc. Natl. Acad. Sci. USA*, 77, 1852 (1980).

55. H.M. Berman, W. Stallings, H.L. Carrell and J.P. Glusker, *Biopolymers*, 10, 2405 (1979).

56. T.D. Sakore, S.C. Jain, C.C. Tsai and H.M. Sobell, *Proc. Natl. Acad. Sci. USA*, 74, 188 (1977).

57. B.S. Reddy, T.P. Seshadri, T.D. Sakore and H.M. Sobell, *J. Mol. Biol.*, 135, 787 (1979).

58. D.M. Neville, Jr. and D.R. Davies, *J. Mol. Biol.*, 17, 57 (1966).

59. S. Neidle, A. Achari, G.L. Taylor, H.M. Berman, H.L. Carrell, J.P. Glusker and W.C. Stallings, *Nature*, 269, 304 (1977).

60. A.H.J. Wang, G.J. Quigley and A. Rich, *Nucleic Acids Res.*, 6, 3879 (1979).

61. H.S. Sielh, H.M. Berman, M. Dabrow and S. Neidle, *Nucleic Acids Res.*, 81, 85 (1980).

62. R.K. Tubbs, W.E. Ditmars, Jr. and Q. Van Winkle, *J. Mol. Biol.*, 9, 545 (1964).

63. L.M. Chan and Q. Van Winkle, *J. Mol. Biol.*, 40, 491 (1969).

64. L.M. Chan and J.H. McCarter, *Biochim. Biophys. Acta*, 204, 252 (1970).

65. G. Duportail, Y. Mauss and J. Chambron, *Biopolymers*, 16, 1396 (1977).

66. N.F. Ellerton and I. Isemberg, *Biopolymers*, 8, 767 (1969).

67. Y. Kubota and Y. Motoda, *Biochemistry*, 19, 4189 (1980).

68. G.R. Stewart, *Biopolymers*, 6, 1737 (1968).

69. V. Kleinwachter, Z. Balcarovia and J. Bohacek, *Biochim. Biophys. Acta*, 174, 188 (1969).

70. R. Bidet, J. Chambron and G. Weill, *Biopolymers*, 10, 225 (1971).

71. J.C. Thomes, G. Weill and M. Daune, *Biopolymers*, 8, 647 (1969).

72. Y. Kubota, K. Hirano and Y. Motoda, *Chem. Lett.*, 123 (1978).

73. B. Norden and T. Tjerneld, *Chemical Physics Letters*, 50, 508 (1977).

74. S. Georghiou, *Photochem. Photobiol.*, 22, 103 (1975).

75. Y. Kubota and R.F. Steiner, *Biophys. Chem.*, 6, 279 (1977).

76. M. Dourlent and J.F. Hogrel, *Biochemistry*, 15, 430 (1976).

77. J. Ramstein, M. Ehrenberg and R. Rigler, *Biochemistry*, 19, 3938 (1980).

78. G. Weill and M. Calvin, *Biopolymers*, 1, 401 (1963).

79. K. Yamaoka, *Biopolymers*, 11, 2537 (1972).

80. W. Müller and F. Gautier, *Eur. J. Biochem.*, 54, 385 (1975).

81. M.E. Lamm and D.M. Neville, *J. Phys. Chem.*, 69, 3872 (1965).

82. T. Kurucsev and U.P. Strauss, *J. Phys. Chem.*, 74, 3081 (1970).

83. V. Zanker, M. Held and H. Rammensee, *Z. Naturforsch.*, 146, 789 (1959).

84. I. Tinoco, Jr., *J. Am. Chem. Soc.*, 82, 4785 (1960).

85. D.M. Neville, Jr. and D.F. Bradley, *Biochem. Biophys. Acta*, 50, 397 (1961).

86. E.R. Blout and L. Stryer, *Proc. Natl. Acad. Sci. USA*, 45, 1591 (1959).

87. L. Stryer and E.R. Blout, *J. Am. Chem. Soc.*, 83, 1411 (1961).

88. K. Jackson and S.F. Mason, *Trans. Faraday Soc.*, 67, 966 (1971).

89. B.J. Gardner and S.F. Mason, *Biopolymers*, 5, 79 (1967).

90. D.G. Dalgleish, H. Fujita and A.R. Peacocke, *Biopolymers*, 8, 633 (1969).

91. M. Zama and S. Ichimura, *Biopolymers*, 9, 53 (1970).

92. E. Fredericq and C. Houssier, *Biopolymers*, 11, 2281 (1972).

93. C.H. Lee, C.T. Chang and J.G. Wetmur, *Biopolymers*, 12, 1099 (1973).

94. A.I. Poletayev, *FEBS Letters*, 67, 171 (1976).

95. A. Blake and A.R. Peacocke, *Biopolymers*, 4, 1091 (1966).

96. T. Imae and S. Ikeda, *Polymer J.*, 8, 531 (1976).

97. K. Yamaoka and R.A. Resnik, *J. Phys. Chem.*, 70, 4051 (1966).

98. H.J. Li and D.M. Crothers, *Biopolymers*, 8, 217 (1969).

99. Y.J. I'Haya and T. Nakamura, *Bull. Chem. Soc. Japan*, 44, 951 (1971).

100. D.F. Bradley, I. Tinoco, Jr. and R.W. Woody, *Biopolymers*, 1, 239 (1963).

101. V. Zanker, *Z. Physik. Chem. N.F.*, 2, 52 (1954).

102. V. Zanker and G. Schiefele, *Ber. Bunsenges. Phys. Chem.*, 62, 86 (1958).

103. A. Wittwer and V. Zanker, *Z. Physik. Chem. N.F.*, 22, 417 (1959).

104. V. Zanker and A. Wittwer, *Z. Physik. Chem. N.F.*, 24, 183 (1960).

105. J.R. Platt, *J. Chem. Phys.*, 17, 484 (1949).

106. Y. Matsuoka and K. Yamaoka, *Bull. Chem. Soc. Japan*, 52, 3163 (1979).

107. G.R. Haugen and W.H. Melhuish, *Trans. Faraday Soc.*, 60, 386 (1964).

108. L.L. Ingraham and H. Johansen, *Arch. Biochem. Biophys.*, 132, 205 (1969).

109. H. Ito and Y.J. I'Haya, *Int. J. Quant. Chem.*, 2, 5 (1968).

110. Gift from Mrs. K.A. Rye.

111. D.M. Crothers, *Biopolymers*, 6, 575 (1968).

112. W. Bauer and J. Vinograd, *J. Mol. Biol.*, 47, 419 (1970).

113. J. Pauluhn and H.W. Zimmermann, *Ber. Bunsenges, Phys. Chem.*, 82, 1265 (1978).

114. Z. Balcarova, V. Kleinwachter, J. Koudelka, G. Löber, K.E. Reinert, L.P.G. Wakelin and M.J. Waring, *Biophys. Chem.*, 8, 27 (1978).

115. A. Andreoni, S. Cova, G. Bottiroli and G. Prenna, *Photochem. Photobiol.*, 29, 951 (1979).

116. J.A. Shellman, *Isr. J. Chem.*, 12, 219 (1974).

117. J.D. McGhee and P.H. Von Hippel, *J. Mol. Biol.*, 86, 469 (1974).

118. K. Yamaoka and R.A. Resnik, *Nature*, 213, 1031 (1967).

119. I. Tinoco, Jr., *Adv. Chem. Phys.*, 4, 113 (1962).

120. W. Moffit and A. Moscowitz, *J. Chem. Phys.*, 30, 648 (1959).

121. S.E. Harnung, E.G. Ong and O.E. Weigang, Jr., *J. Chem. Phys.*, 55, 5711 (1971).

122. M.E. Gal, G.R. Kelly and T. Kurucsev, *J. Chem. Soc. II*, 69, 395 (1973); D.E. Joyce and T. Kurucsev, *Biophys. Chem.*, 2, 273 (1974); L.P. Gianneschi, Ph.D. Thesis, University of Adelaide (1977); L.P. Gianneschi, A. Cant and T. Kurucsev, *J. Chem. Soc. II*, 73, 664 (1977).

123. J. Chambron, M. Daune and C. Sadron, *Biochim. Biophys. Acta*, 123, 306 (1966).

124. Y. Kubota, Y. Eguchi, K. Hashimoto, M. Wakita, Y. Honda and Y. Fujisaki, *Bull. Chem. Soc. Japan*, 49, 2424 (1976).

125. S.C. Riemer and V.A. Bloomfield, *Biopolymers*, 18, 1695 (1979).

126. D.S. Millar, R.J. Robbins and A.H. Zewail, *Proc. Natl. Acad. Sci. USA*, 77, 5593 (1980).

127. V.A. Bloomfield, D.M. Crothers and I. Tinoco, Jr., *Physical Chemistry of Nucleic Acids*, p. 415, Harper-Row, New York (1974).

128. N.C. Seeman, J.M. Rosemberg, F.L. Suddath, J.J.P. Kim and A. Rich, *J. Mol. Biol.*, 104, 109 (1976).

129. V.A. Bloomfield, D.M. Crothers and I. Tinoco, Jr., *Physical Chemistry of Nucleic Acids*, Chapter 7, paragraph II, Harper-Row, New York (1974).

130. D.G. Dalgleish, M.C. Feil and A.R. Peacocke, *Biopolymers*, 11, 2415 (1972).

131. G.V. Gurskii, *Biofizika*, 11, 737 (1966).

132. S. Dasgupta, D.N. Misra and N.N. Dasgupta, *Biochim. Biophys. Acta*, 294, 38 (1973).

133. V. Zanker, *Z. Phys. Chem. (Leipzig)*, 199, 225 (1952).

134. E.J. Gabbay, *J. Am. Chem. Soc.*, 90, 6574 (1968); E.J. Gabbay, *J. Am. Chem. Soc.*, 91, 5136 (1969).

135. M. Zama and S. Ichimura, *Biopolymers*, 15, 1693 (1976).

136. J.P. Schreiber and M. Daune, *J. Mol. Biol.*, 83, 487 (1974).

137. R.B. Webb and H.E. Kubitschek, *Biochem. Biophys. Res. Commun.*, 13, 90 (1963).

138. S. Aktipis and A. Kindelis, *Biochemistry*, 12, 1213 (1973).

139. M. Kamiya, *Biochim. Biophys. Acta*, 562, 70 (1979).

140. P.D. Ross and R.L. Scruggs, *Biopolymers*, 6, 1005 (1968).

141. J.C. Wang, *J. Mol. Biol.*, 43, 25 (1969).

142. R.E. Harrington, *Biopolymers*, 17, 919 (1978).

143. J. Ramstein, M. Leng and N.R. Kallenbach, *Biophys. Chem.*, 5, 319 (1976).

144. H.M. Sobell, C.C. Tsai, S.G. Gilbert, S.C. Jain and T.D. Sakore, *Proc. Natl. Acad. Sci. USA*, 73, 3068 (1976).

145. H.M. Sobell, C.C. Tsai, S.C. Jain and S.G. Gilbert, *J. Mol. Biol.*, 114, 333 (1977).

146. A.S. Zasedatelov, G.V. Gurskii and M.V. Vol'kenshtein, *Mol. Biol.*, 5, 245 (1971).

147. McClure, *Can. J. Chem.*, 36, 59 (1958).

148. G. Symonds, Honours Report, University of Adelaide (1979).

149. C. Houssier, B. Hardy and E. Fredericq, *Biopolymers*, 13, 1141 (1974).

150. T. Kurucsev and U.P. Strauss, *J. Phys. Chem.*, 74, 3081 (1970).

151. G.E. Boehm, personal communication.

152. V. Deubel and M. Leng, *Biochimie*, 56, 641 (1974).

Appendices

APPENDIX A: MATERIALS AND METHODS

A.1 Nucleosides and Dinucleosides

Adenosine, adenosine 5'-monophosphoric acid (AMP), deoxyadenosine (dA), adenylyl-(3'-5')-adenosine (APA), 2'-deoxyadenylyl-(3'-5')-2'-deoxyadenosine (dApdA), guanosine and guanylyl-(3'-5')-guanosine (GPG) were all obtained from Sigma and used without any further purification. The diammine dichloro platinum(II) *cis* and *trans* were a gift of Dr. I.A. Roos and were recrystallised from hydrochloride acid[5,6]. Complexes with adenosine were obtained by dissolving the corresponding platinum (Pt) in a solution of 10^{-2} mol dm^{-3}, sodium perchlorate. The solution was kept at 37°C for a period of 14 days[7].

All solutions were initially prepared by dissolving the appropriate compound in a cacodylic acid-sodium cacodylate buffer which gave a pH of 6.9 at 20°C[1]. The buffer was prepared as follows: 7.5 cm^{-1} of 1 M cacodylic acid + 50 cm^3 of 1 M sodium cacodylate diluted to 1 dm^3 with distilled water.

The Lambert-Beer law was obeyed for the monomers studied in the concentration range used (less than 10^{-4} mol dm^{-3}). For guanosine and GPG, a concentration of 6×10^{-5} mol dm^{-3} was used to prevent aggregation[2,3,4]. Concentrations were determined spectrophotometrically; optical parameters are given in terms of the molar concentration of residues. The molar absorptivities of all the compounds are given in Table A.1.

A.2 Dye-DNA Complexes

Proflavine (PF) was obtained from B.D.H. Chemicals Ltd., Poole, England and was purified as the free base[9,10]. Acridine

Table A.1 U-V AND VISIBLE ABSORPTION DATA[a]

Compound	λ_{max}	$\varepsilon_{max} \times 10^{-3}$	Reference
Adenosine (A)	260	14.9	29
AMP	259	15.4	29
cis-Pt adenosine	265.5	8.75	30
trans-Pt adenosine	269	8.90	30
Deoxyadenosine (dA)	259	15.3	31
Guanosine (G)	253	13.6	31
ApA	260	13.9 (at 20°C)	32
dApdA	258	12.7 (at 28°C)	33
GpG	253	12.7[b]	36
Calf-thymus DNA	260	6.6	34
Acridine orange (AO)	492	59.0	11
Proflavine (PF)	444	41.0	35
9-aminoacridine (9-AA)	400	9.98	this study

a - The maximum wavelength (λ_{max}) is given in nanometers and the maximum molar absorptivity (ε_{max}) is given in mol^{-1} dm^3 cm^{-1}.

b - Calculated from the hypochromicity and from the molar absorptivity of guanosine.

Orange (AO) was purified[11] and both PF and AO free bases were converted to the hydrochloride form[11]. 9-aminoacridine hydrochloride was obtained from A.G. Fluka and was recrystallised twice from ethanol and dried under vacuum. Calf thymus DNA was prepared by the anionic detergent procedure[8]. The DNA sample was stored dry at 0°C. In all the experiments, we adjusted the ionic strength with NaCl and all the solutions were filtered twice. A concentrated stock solution of calf thymus DNA (0.2 g in 100 cm^3) in 10^{-3} M NaCl was prepared and left in the cold (0 - 4°C), with continual stirring over a seven day period. The DNA solution was centrifuged at 10,000 RPM for forty-five minutes in a Sorwall superspeed RC-B automatic refrigerated centrifuge.

For the AO and PF dyes, their adsorption on soft glass vessel walls was significant and photolytic degradation of the dyes after light exposure was noticeable. That is why special precautions were taken. Although our rule was to prepare fresh solutions, all flasks containing dye solutions were wrapped with aluminium paper to protect them from light and stored at 4°C. The concentration of the dye in the flask only remained constant approximately one day after preparation due to the saturation of the vessel walls with the dye. Pipettes used to transfer the dye solutions were also saturated with the dye prior to use.

The stock DNA solution was diluted with a NaCl solution so as to obtain the desired ionic strength and concentration. The dye-DNA solutions were prepared by weight in spectroscopic silica cells. The dye solution was added to the DNA solution drop by drop with rapid stirring to prevent any precipitation of the complex formed,

especially at high dye to DNA ratios. It was found that the absorbance of the dye-DNA complexes were changing over a period of approximately one hour after the mixing. To assume complete equilibrium between dye and DNA, the solutions were kept overnight at 4°C in the dark. The pH of the solutions was measured with a digital pH meter (Orion Research, model 701A) and found to vary between 6.3 and 6.7.

A.3 Preparation of Films

A.3.1 Dye Films

Polyvinyl-alcohol (PVA) films were cast from a solution of PVA (J.T. Baker Chemical Co.) in water (5% w:v). The film was immersed in an aqueous solution of the required solute, then left to dry on a glass plate and was clamped in a stretching device[12]. The film was stretched at a slow rate over a water bath at 50°C[13] until a stretched ratio (ratio of a distance between two marks after and before stretching) of 4.5 was obtained. Although it was possible to obtain higher stretched ratios, a value of 4.5 was found to give higher reproducibility. The contribution from the absorbance of PVA was determined by the use of "blank" films prepared under similar conditions but without the solute.

A.3.2 Dye-DNA Films

Dye-DNA solutions with a dye to DNA concentration ratio between 0.002 and 0.008 were prepared by slow addition of the dye to a 1% DNA solution with constant stirring and were then poured into the holes of a perspex tray. The solution took approximately one week to dry. The dye-DNA film thus obtained is progressively adhered to a supporting polyethylene

film above a water bath maintained at 40°C and is rolled flat with a teflon rod. The use of a polyethylene film as the support instead of a PVA film used previously[12] enables us to avoid the use of an intermediate layer of DNA between the dye-DNA film and the support necessary to prevent the dye from penetrating into the support. The film was then stretched very slowly with the stretching device to 2.8 times its original length under a water bath maintained at 40°C. The film was then mounted inside a humidity cell[12] maintained at 93% relative humidity with sodium sulphate and was left for a period of two days before measurement (time necessary to reach an equilibrium[12]). This new procedure of using a polyethylene film instead of a PVA film for the support has the advantage of using far less DNA and allowing us to measure the contribution of the polyethylene film to the total absorbance. In fact, after the stretched film had been maintained under running water, the dye-DNA film could be easily peeled off from the polyethylene film. Then by measuring the absorbance spectrum of the polyethylene film, it was verified that no dye had penetrated into it.

A.4 Temperature Studies

The cell holder temperature was regulated with a cooling and thermostating bath combination built in this laboratory. The temperature of the solution was measured in the cell with a copper thermocouple previously calibrated and inserted in a thin glass sheath going through the teflon stopper of the cell. Measurements were taken at each temperature after a ten minutes equilibration time and the temperature during the measurement was kept

constant to within ± 0.1°C. At low temperature, dry nitrogen gas was introduced through the cell compartment to prevent condensation. Absorbance readings were corrected for volume expansion.

APPENDIX B: OPTICAL MEASUREMENTS

B.1 Linear Dichroism

A Zeiss PMQII spectrophotometer with a wide window photomultiplier detector was used to eliminate the scattering contribution to the measured absorbance of the films studied[12,14]. The sample film mounted inside the cell could be positioned as close as 4 mm from the front window of the photomultiplier. A Glan-Taylor calcite polarising prism was mounted in such a way as to allow it to be rotated through 90°, thus enabling us to change the plane of polarization of the light while keeping the same part of the film in the light path. (An important precaution due to the non-uniformity in the thickness of the film). The wavenumber calibration of the monochromator showed that no correction was needed in the ultra-violet and visible regions of the spectrum. (In fact, a deviation of only -20 cm^{-1} was found in the visible part of the spectrum; this correction was not considered necessary in view of the resolution limit of the instrument.) The standard deviation in the transmittance scale was found to be better than 0.2%. A resolution of 200 cm^{-1} or better was possible with a judicious choice of slit widths. The molar absorptivity (ε) is given in mol^{-1} dm^3 cm^{-1}.

B.2 Circular Dichroism

Circular dichroism measurements were done on a Jasco J-40CS automatic recording spectropolarimeter. The wavelengths calibration was done with the use of (+)-camphor-10-sulphonic acid monohydrate from Fluka (MW = 232.30, $[\alpha]_D^{20}$ = +20 ± 1) having a molar

ellipticity [θ] = +7260 at 290.5 nm[15] and with the use of a holmium oxide filter producing peaks at 279.4, 287.5, 360.9, 460 and 536.2 nm, if we record the photomultiplier voltage (as it is proportional to the absorbance) instead of the ellipticity. No correlation was necessary until 350 nm, but a correction of -0.5 nm between 350 nm and 500 nm as well as a correction of -1.2 nm between 500 nm and 600 nm was necessary. The recorded ellipticity was adjusted to correspond to a molecular ellipticity [θ] of 7260 mol dm^{-3} m^{-1} at 290.5 nm for D-10 camphot sulfonic acid[15]. Cells of 0.1 to 5 cm pathlength were used to maintain the optical density of the solution studied at a value less than 2. Optimum conditions of measurement can be achieved with a judicious compromise between wavelength scanning, chart speed, slit width, time constant and optical density. All the solvents and solutions studied were filtered if possible to eliminate any impurity that could increase the noise level and this, therefore, enabled us to use smaller bandwidths. As a measure of precaution, all the measurements were repeated at least twice, or more if the recorded spectra were not identical within the limits of precision of the spectropolarimeter and they were then averaged. The cell blanks containing the solvent were measured before and after any recording of the sample. Although the scale of the Jasco is in ellipticity, we used in this thesis the molar circular dichroism Δε in mol dm^{-3} cm^{-1}, which is related to molar ellipticity according to the relation $[\theta]^{\lambda} = 3300\ \Delta\varepsilon^{\lambda}$. No refractive index correction has been applied to the CD data.

To this spectropolarimeter, was added a microprocessor (MC-85) based on Intel 8085 which was

assembled and expanded by Mr. Snigg and programmed by Dr. M. Dwyer and Mr. G.E. Boehm. The microprocessor controlled the operations of the spectropolarimeter, that is to say the wavelength step size, the range of wavelength to be scanned and above all the accumulation of user-specified number of points (in multiples of 2^8 with 20 μsec. per point) in 32-bit precision followed by signal averaging. For the nucleoside study, due to the low CD signal obtained, it was necessary to accumulate $2^7 \times 2^{12}$ points to be averaged at each wavelength. This procedure was carried out three times for each sample and averaged. The data points were collected on paper tape.

B.3 Ultra-Violet and Visible Absorption

U-V and visible absorption measurements were done on a Zeiss DMR10 spectrophotometer equipped by Mr. G.E. Boehm with an Intel 8080 microprocessor similar to the one attached to the Jasco spectropolarimeter. The wavelength calibration shows a maximum deviation of less than 0.05 nm for the two emission peaks of the deuterium lamp at 486.00 nm and 656.10 nm. The photometric accuracy in the absorbance scale was found to be better than 0.3%. To obtain the maximum accuracy in the measurements, the following procedure was adopted: A baseline was recorded initially with the buffer solution to allow for the mismatching of the cell. The cells were left in their positions, the solution was removed by suction, then the empty cells were rinsed and filled with the next solution to be analysed. The spectrum of each solution was recorded twice.

APPENDIX C: COMPUTATIONAL METHODS

All the computations were carried out on a CDC Cyber 173 computer.

The computer program PISCF[21] for the PPP-CI calculations of 9-aminoacridine and proflavine uses the method of Bailey[16,17] and incorporates the calculation of the core integrals on protonated nitrogen heterocyclics[18].

Monomer spectra have been analysed in terms of their vibronic bands and were fitted by the use of a weighted, non-linear least-squares program BANDFIT[21] to a five parameters equation[19,20].

$$I(\tilde{\nu}) = (I_{oo})_{max} \sum_m \frac{X^m}{m!} \left(1 + \frac{mV}{(\tilde{\nu}_{oo})}\right) \exp\left[-(\tilde{\nu} - \tilde{\nu}_{oo} - mV)^2 \frac{4\ln 2}{b_g^2}\right] \qquad (C.1)$$

where each vibronic band is assumed to have a gaussian shape. $I(\tilde{\nu})$ is the total intensity; $\tilde{\nu}_{oo}$ is the position of the (0,0) band in cm^{-1} which has an intensity maximum I_{oo}; V is the separation between successive bands maxima; b_g is the bandwidth at half maximal intensity; X is the (1,0) to (0,0) band intensity ratio (X is related to the difference in equilibrium nuclear conformation of the ground and excited state).

The program EXCITON[21] calculates the theoretical dimeric spectra using the model of Fulton and Gouterman[22,23] which has been described in the introduction. This program uses the monomeric parameters, V, b_g and X determined in fitting the monomeric spectrum of each moiety constituting the dimer and includes two extra parameters, the exciton coupling parameter and the angle θ between the two monomers[19,24,25]. The program has an option to calculate the absorption or the circular dichroism spectrum.

The absorption and circular dichroism data were analysed using a modified version of the program DMR10 written by Mr. G.E. Boehm. This program calculates, for each wavelength, the mean actual absorbance and the molar absorptivity or the difference in absorbance ΔA and the molar circular dichroism $\Delta\varepsilon$.

The optical data of the thermal denaturation study of APA and dApdA were analysed by the use of a non-linear weighted least-squares program APAFIT[21] and were fitted to a four parameters equation

$$\ln K_{(T)} = \ln \frac{\alpha_u - \alpha_{(T)}}{\alpha_{(T)} - \alpha_s} = \frac{\Delta S^\circ}{R} - \frac{\Delta H^\circ}{RT} \qquad (C.2)$$

All the quantities are defined in paragraph 5.4.3 of chapter II.

APPENDIX D: DERIVATION OF THE EXPRESSION OF THE DIPOLE STRENGTH AND THE ROTATIONAL STRENGTH

The expression for the dipole strength[27] is given by

$$\mathcal{D} = \mu^2 = \frac{(2303)3hc}{8\pi^3 N} \int \frac{\varepsilon d\tilde{\nu}}{\tilde{\nu}} = 9.18 \times 10^{-39} \int \frac{\varepsilon d\tilde{\nu}}{\tilde{\nu}} \qquad (D.1)$$

where μ is the electric dipole moment for the transition and h, c, N, ε represent respectively the Planck's constant, the velocity of the light, the Avogadro's number and the molar absorptivity of the transition considered. In the same way, the expression for the rotational strength can be written as

$$\mathcal{R} = \frac{6909\ hc}{32\pi^3 N} \int \frac{\Delta\varepsilon d\tilde{\nu}}{\tilde{\nu}} = 2.295 \times 10^{-39} \int \frac{\Delta\varepsilon d\tilde{\nu}}{\tilde{\nu}} \qquad (D.2)$$

where $\Delta\varepsilon$ is the molar circular dichroism for left and right circularly polarised light in $dm^3\ mol^{-1}\ cm^{-1}$.

From the use of the five parameters equation (C.1) described in the appendix C which gives the value of the total intensity of the band as a function of the wavenumber, equation (D.1) becomes:

$$\mathcal{D} = 9.18 \times 10^{-39} \int (\varepsilon_{oo})_{max} \sum_m \frac{X^m}{m!} \left(1 + \frac{mV}{\tilde{\nu}_{oo}}\right) \exp$$

$$\left\{-(\tilde{\nu} - \tilde{\nu}_{oo} - mV)^2 \frac{4\ln 2}{b_g^{\,2}}\right\} \frac{d\tilde{\nu}}{\tilde{\nu}}$$

and we obtain a similar expression for the rotational strength $\mathcal{R}$.

Following the method given by Gal *et al.*[48] for deriving the oscillator strength we can write the expression of the dipole strength as

$$\mathcal{D} = 9.18 \times 10^{-39} (\varepsilon_{oo})_{max} \frac{b_g \pi^{1/2}}{2(\ln 2)^{1/2}} \sum_m \left[\frac{X^m}{m!} \frac{1}{(\tilde{\nu}_{oo} + mV)}\right]$$

or $$\mathcal{D} = 9.772 \times 10^{-39} (\varepsilon_{oo})_{max} b_g \sum_m \left[\frac{X^m}{m!} \frac{1}{(\tilde{\nu}_{oo} + mV)}\right] \qquad (D.3)$$

Similarly the expression for the rotational strength is

$$\mathcal{R} = 2.443 \times 10^{-39} (\Delta\varepsilon_{oo})_{max} b_g \sum_m \left[\frac{X^m}{m!} \frac{1}{(\tilde{\nu}_{oo} + mV)}\right] \qquad (D.4)$$

where $(\varepsilon_{oo})_{max}$ and $(\Delta\varepsilon_{oo})_{max}$ represent respectively the value of the molar absorptivity and the molar circular dichroism of the (0,0) band.

A parameter of considerable importance in the study of a given transition is the Kuhn's anisotropy factor g defined as

$$g = 4 \frac{\mathcal{R}}{\mathcal{D}} \qquad (D.5)$$

Let us consider two interacting transition moments μ_A and μ_B. Their rotational strength[27] can be expressed if we use a first order approximation as:

$$\mathcal{R}_A = \frac{2\pi}{hc} V_{AB} \frac{\tilde{\nu}_A \tilde{\nu}_B}{\tilde{\nu}_A^2 - \tilde{\nu}_B^2} \vec{R}_{AB} (\vec{\mu}_B \times \vec{\mu}_A) \qquad (D.6)$$

where $\tilde{\nu}_A$ and $\tilde{\nu}_B$ are the frequencies of transition, $\vec{R}_{AB} = \vec{R}_B - \vec{R}_A$ is the vector distance from group A to group B and V_{AB} is the potential energy interaction which, if we make the point dipole approximation, can be written as

$$V_{AB} = \frac{\vec{\mu}_A \vec{\mu}_B}{R_{AB}^3} - 3 \frac{(\vec{\mu}_A . \vec{R}_{AB})(\vec{\mu}_B . \vec{R}_{AB})}{R_{AB}^5} \qquad (D.7)$$

following the development of Caldwell and Eyring[28], the expression of the rotational strengths can be written as

$$\mathcal{R}_A = \frac{2\pi}{hc} \frac{\tilde{\nu}_A \tilde{\nu}_B}{\tilde{\nu}_A^2 - \tilde{\nu}_B^2} \vec{\mu}_A \times \vec{R}_{AB} . \vec{\mu}_B \vec{\mu}_B . T . \vec{\mu}_A$$

with $$T = \frac{1}{R_{AB}^3} \left(1 - \frac{\vec{R}_{AB}\vec{R}_{AB}}{R_{AB}^2}\right) \qquad (D.8)$$

or if we use the polarizability tensor $\alpha_B(\tilde{\nu}_B)$ of groups B at the frequency $\tilde{\nu}_A$

$$\mathcal{R}_A = \frac{\pi}{h} [\vec{R}_{AB} \times \vec{e}_A \cdot \alpha_B(\tilde{\nu}_A) . T . \vec{e}_A] \tilde{\nu}_A \mu_A^2 \qquad (D.9)$$

with $\vec{e}_A$ representing a unit vector along the direction of the transition of group A. We can see in the last equation that the rotational strength is proportional to the dipole strength. The factor in brackets as well as the ratio $\frac{\mathcal{R}_A}{\mathcal{D}_B}$ depend only on the molecular geometry and the polarizability of the group B.

APPENDIX E: CALCULATION OF THE "GEOMETRICAL FACTOR" OF THE CD SPECTRUM OF ADENOSINE WITH THE USE OF THE COUPLED OSCILLATOR THEORY

Figure E.1 gives a shcematic representation of the adenosine nucleoside. The C1´ atom is chosen to represent the origin of our system. We define four angles:

θ_B, the angle between the transition moment direction e_B in the base and the axis Y.

θ_C, the angle between the vector R_{AB} and the axis Y.

θ_A, the angle between the induced moment direction e_A in the sugar and the axis Z.

θ, the angle of rotation that makes the projection of e_A on the plane YX around the glycosyl bond N9-C1´.

The angle θ is set to zero when the projection of e_A on the plane XY coincides with the axis Y.

The use of these angles allows us to write equation 4.2 (in paragraph 4.4.1), which represents the geometric factor dependence of the rotational strength, such as:

$$V_{AB}R_{AB}.(\vec{e}_A \times \vec{e}_B) = \sin\theta_A\sin\theta\sin(\theta_B-\theta_C)[\cos\theta_B\sin\theta_A\cos\theta+ \sin\theta_B\cos\theta_A-3\cos(\theta_B-\theta_C).(\sin\theta_A\cos\theta\cos\theta_C+\sin\theta_C\cos\theta_A)]$$

The angle θ_C was fixed to a value of 78° in relation with X-ray data[26]. The directions of the two transitions in the adenine base were taken to be perpendicular to one another. Although the two transitions are more or less oriented along the short and long axis of the base, the angle they make with the C4-C5 bond is not accurately known. Therefore, we fixed a value of 90° ± 10° for the angle between the long axis polarised transition and the C4-C5 bond of adenine.

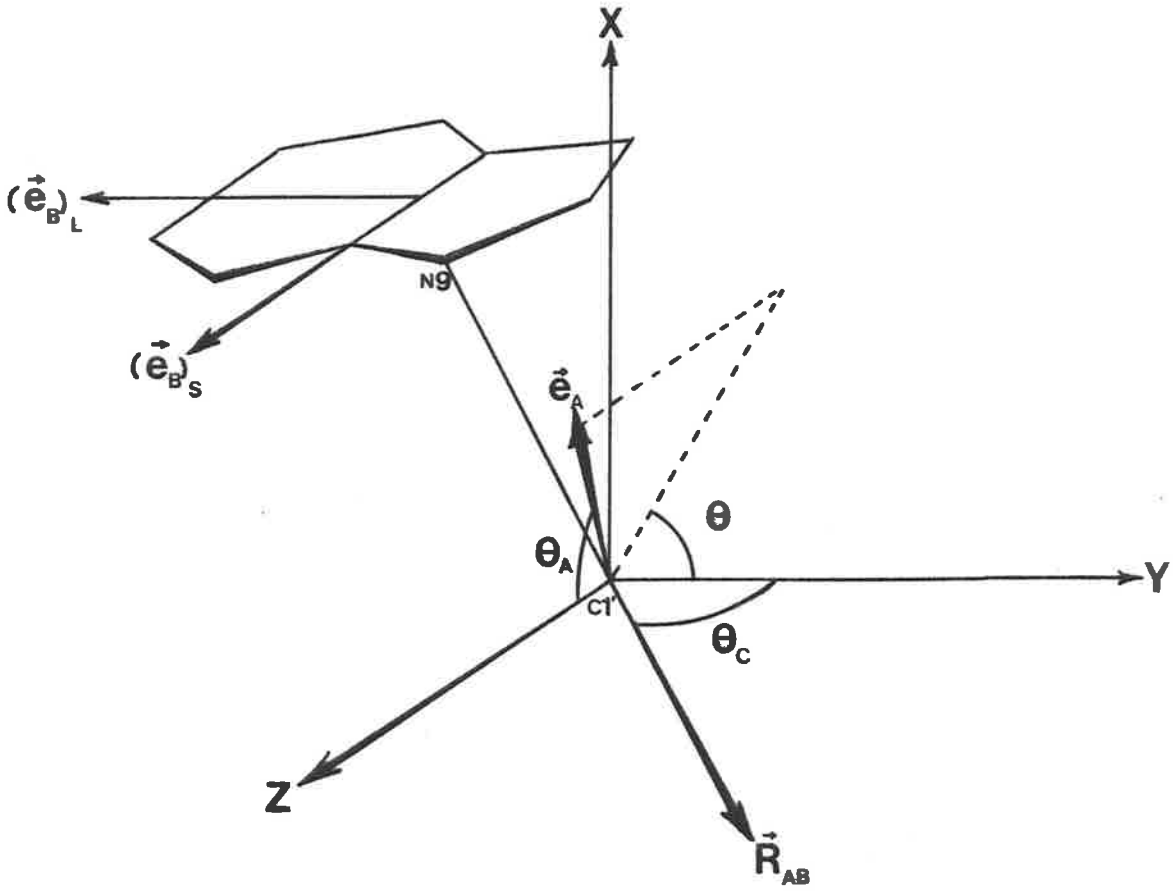

FIG.E.1 SCHEMATIC DIAGRAM SHOWING THE GEOMETRY USED IN CALCULATING THE GEOMETRICAL FACTOR (see text for discussion).

The angle θ is increased in 20° increments. Different values of θ_A are used until the trend in figure 4.10 (paragraph 4.3.4) is reproduced.

The optimum results are given below.

Angles of +100° and +10° are found between the transition moments of the base and the C4-5 bond. The projection in the YX plane (or sugar plane) of the induced moment forms an angle of 107° with the C1′ - O1′ bond. The induced moment also makes an angle, out of the plane of the sugar and on the same side as the C1′ - N9 bond, of 40° for the β configuration and of 20° for the α configuration (figure 4.11).

APPENDIX F: ABBREVIATIONS

Angstrom	Å
Centigrade	C
Centimeter	cm
Cm-g-s unit system	cgs
Decimeter	dm
Electrostatic unit	esu
Gramme	g
Kelvin	K
Kilocalorie	Kcal
Mole	mol
Nanometer	nm
Revolution per minute	RPM
Second	s
Temperature	T
Weight per volume	w:v
Configuration interaction	CI
Configuration mixing	CM
Linear combination of atomic orbitals	LCAO
Molecular orbitals	MO
Pariser-Parr-Pople	PPP
Self-consistent field	SCF

REFERENCES

1. Biochemists' Handbook, C. Long, E.J. King and W.M. Sperry edit., E.C.F.N. Spon Ltd., London (1961).
2. S.R. Jaskunas, C.R. Cantor and I. Tinoco, Jr., *Biochemistry*, 7, 3164 (1968).
3. J.F. Chantot and W. Guschlbauer, *Jerusalem Symp. Quant. Chem. Biochem.*, 4, 205 (1972).
4. J.M. Delabar and W. Guschlbauer, *J. Amer. Chem. Soc.*, 95, 5729 (1973).
5. J. Kleinberg, *Inorg. Synth.*, 7, 236 (1963).
6. S.C. Dara, *Indian J. Chem.*, 8, 193 (1970).
7. I.A.G. Roos, A.J. Thomson and S. Mansy, *J. Amer. Chem. Soc.*, 96, 6484 (1974).
8. R.F. Steiner and R.F. Beers, *Polynucleotides*, Elsevier Publishing Company, appendix B, p. 348 (1961).
9. G. Weill and M. Calvin, *Biopolymers*, 1, 401 (1963).
10. N.F. Ellerton and J. Isemberg, *Biopolymers*, 8, 767 (1969).
11. R.V. Armstrong, T. Kurucsev and U.P. Strauss, *J. Amer. Chem. Soc.*, 92, 3174 (1970).
12. G.R. Kelly, Ph.D. Thesis, University of Adelaide (1974).
13. C.C. Bott, Ph.D. Thesis, University of Adelaide (1977).
14. L.P. Gianneschi and T. Kurucsev, *J. Chem. Soc. Faraday II*, 70, 1334 (1974).
15. J.Y. Cassim and J.T. Yang, *Biochemistry*, 8, 1947 (1969).
16. M.L. Bailey, *Theoret. Chim. Acta*, 13, 56 (1969).
17. M.L. Bailey, *Theoret. Chim. Acta*, 16, 309 (1970).
18. S. Mataga and N. Mataga, *Z. Phys. Chem. N.F.*, 19, 231 (1959).
19. M.E. Gal, G.R. Kelly and T. Kurucsev, *J. Chem. Soc. Faraday II*, 69, 395 (1973).

20. T. Kurucsev, *J. Chem. Education*, 55, 128 (1978) and references therein.

21. Computer program written in Fortran by T. Kurucsev.

22. R.L. Fulton and M. Gouterman, *J. Chem. Phys.*, 35, 1059 (1961).

23. R.L. Fulton and M. Gouterman, *J. Chem. Phys.*, 41, 2280 (1964).

24. L.P. Gianneschi, A. Cant and T. Kurucsev, *J. Chem. Soc. Faraday II*, 73, 664 (1977).

25. D.E. Joyce and T. Kurucsev, *Biophys. Chem.*, 2, 273 (1974).

26. M. Sundaralingam and L.H. Jensen, *J. Mol. Biol.*, 13, 914 (1965).

27. V.A. Bloomfield, D.M. Crothers and I. Tinoco, Jr., *Physical Chemistry of Nucleic Acids*, p. 36, 39, Harper-Row Publ., New York (1974).

28. D.J. Caldwell and H. Eyring, *The Theory of Optical Activity*, p. 104, Wiley, New York (1971).

29. G.D. Fasman (Ed.), *Handbook of Biochemistry and Molecular Biology*, Nucleic Acids, 3rd Ed., C.R.C. Press Inc. (1975).

30. V. Kleinwächter and R. Zaludova, *Chem. Biol. Interactions*, 16, 207 (1977).

31. C.A. Sprecher and W.C. Johnson, Jr., *Biopolymers*, 16, 2243 (1977).

32. J.T. Powell, E.G. Richards and W.B. Gratzer, *Biopolymers*, 11, 235 (1972).

33. P.S. Miller, K.N. Fang, N.S. Kondo and P.O.P. Ts'o, *J. Amer. Chem. Soc.*, 93, 6647 (1971).

34. H.P. Mahler, B. Kline and B.D. Mehrota, *J. Mol. Biol.*, 9, 801 (1964).

35. G.R. Hangen and W.H. Melhuish, *Trans. Farad. Soc.*, 60 386 (1964).

36. M.M. Warshaw and I. Tinoco, Jr., *J. Mol. Biol.*, 20, 29 (1966).

Fornasiero, D. & Kurucsev, T. (1981). Circular dichroism spectra and the interaction between acridine dyes and deoxyribonucleic acid. *The Journal of physical chemistry, 85*(5), 463-618.